



GEOLOGICAL SURVEY OF CANADA  
BULLETIN 550

## BETTS COVE OPHIOLITE AND ITS COVER ROCKS, NEWFOUNDLAND

J.H. Bédard, K. Lauzière, A. Tremblay, A. Sangster,  
S.L. Douma, and T. Dec



2000



Natural Resources  
Canada

Ressources naturelles  
Canada

Canada

**COOPERATION**

**COOPERATION  
AGREEMENT ON  
MINERAL DEVELOPMENT**

**ENTENTE DE  
COOPÉRATION SUR  
L'EXPLOITATION MINÉRALE**

Contribution to Canada-Newfoundland Cooperation Agreement on Mineral Development (1990-1994), a subsidiary agreement under the Canada-Newfoundland Economic and Regional Development Agreement.

Contribution à l'Entente de coopération Canada-Terre-Neuve sur l'exploitation minérale (1990-1994), entente auxiliaire négociée en vertu de l'Entente Canada-Terre-Neuve de développement économique et régional.

Contribution to Canada-Newfoundland Agreement on Mineral Development (1994-1995), a subsidiary agreement under the Economic and Regional Development Agreement.

Contribution à l'Entente Canada-Terre-Neuve sur l'exploitation minérale (1994-1995), entente auxiliaire négociée en vertu de l'Entente Canada-Terre-Neuve de développement économique et régional.

**Canada**



**Newfoundland  
Terre-Neuve**

GEOLOGICAL SURVEY OF CANADA  
BULLETIN 550

**BETTS COVE OPHIOLITE AND ITS  
COVER ROCKS, NEWFOUNDLAND**

J.H. Bédard, K. Lauzière, A. Tremblay,  
A. Sangster, S.L. Douma, and T. Dec

2000

©Her Majesty the Queen in Right of Canada, 2000  
Catalogue No. M42-550E  
ISBN 0-660-18115-0

Available in Canada from  
Geological Survey of Canada offices:

601 Booth Street  
Ottawa, Ontario K1A 0E8

3303-33rd Street N.W.  
Calgary, Alberta T2L 2A7

101-605 Robson Street  
Vancouver, B.C. V6B 5J3

A deposit copy of this publication is also available for reference  
in selected public libraries across Canada

Price subject to change without notice

***Cover description***

View looking north from Betts Cove at the sheeted dyke unit. The dykes are disrupted by several fault zones. The Mount Misery massive sulphide showing outcrops in the saddle at the top. Photograph by J. Bédard. GSC 2000-006

***Critical reviewers***

***G.A. Jenner***

***R.A. Coish***

***Authors' addresses***

***J.H. Bédard***

***K. Lauzière***

Geological Survey of Canada  
Centre Géoscientifique de Québec  
CP 7500  
Ste-Foy, Quebec G1V 4C7

***A. Tremblay***

Institut National de la Recherche Scientifique  
Centre Géoscientifique de Québec  
CP 7500  
Ste-Foy, Quebec G1V 4C7

***A. Sangster***

***S.L. Douma***

Geological Survey of Canada  
Mineral Resources Division  
601 Booth Street  
Ottawa, Ontario K1A 0E8

***T. Dec***

Petroleum Consulting  
#2604, 609 - 8th Street SW  
Calgary, Alberta T2P 2A6

*Original manuscript submitted: 26-04-1999*

*Final version approved for publication: 17-02-2000*

## CONTENTS

1	Abstract/Résumé
2	Summary/Sommaire
6	Introduction and geological framework
7	Acknowledgments
8	Methodology and revised stratigraphy
8	Field and petrological description of units
8	Betts Cove ophiolite
8	Serpentinite and talc-magnesite-carbonate schist
10	Layered cumulate rocks
15	Late intrusive suite
17	Sheeted dykes
18	Dyke-lava transition zone
18	Betts Head Formation boninitic lavas
20	Snooks Arm Group
20	Mount Misery Formation tholeiitic lavas
22	Scrape Point Formation, Sedimentary Member
24	Scrape Point Formation, Volcanic Member
25	Bobby Cove Formation, Basal Member (tuff)
27	Bobby Cove Formation, Upper Member (turbidite)
27	Venam's Bight Formation
29	Balsam Bud Cove Formation, Basal Member
29	Balsam Bud Cove Formation, Upper Member (debrite)
33	Round Harbour Formation
33	Mafic sills
34	Adjoining ophiolitic rocks
34	Undifferentiated Snooks Arm Group rocks
34	Nippers Harbour ophiolitic massif
34	Post-Ordovician rocks
34	Cape St. John Group
35	Quartz-feldspar-mica porphyry
35	Burlington granodiorite and Cape Brulé granite porphyry
36	Deformation history
36	Preobduction structures
36	Obduction-related structures
36	Silurian structures
37	Compressional structures and regional folds and thrusts
37	Mineral chemistry, geochemistry, and petrogenesis
37	Mineral chemistry
42	Geochemistry and petrogenesis
43	Impact of hydrothermal metamorphism
43	Betts Head Formation and the sheeted dyke complex
51	Layered cumulate rocks, trondhjemite, and the late intrusive suite
53	Snooks Arm Group magmas
58	Nippers Harbour ophiolitic massif
62	Cape St. John Group
63	Silurian granitoid rocks

63	Tectonic models
63	Seafloor spreading in a marginal fore-arc, and the transition to a mixed arc–back-arc volcanic association
64	Silurian extensional and ‘Acadian’ compressional events
65	Mineral deposits
65	Copper and copper-gold occurrences
65	Tilt Cove mine
66	Betts Cove mine
69	Mount Misery and Foot Pond occurrences
70	Nudulama occurrence
70	Burton’s Pond occurrence
70	Gold deposits
70	Nugget Pond mine and Nugget Pond horizon
71	Long Pond East occurrence
72	Castle Rock occurrence
72	Talc-carbonate schist-hosted occurrences from the base of the ophiolite
72	Disseminated pyrite-quartz vein occurrences
72	Hematite-quartz vein occurrences
72	Carbonate-hosted occurrences
72	Talc-carbonate-hosted occurrences
72	Origin of the gold mineralization
73	Conclusions
73	References

## Figures

7	1. Tectonostratigraphic division of Newfoundland Appalachians
9	2. Geological map of Betts Cove complex
10	3. Stratigraphic column
11	4. Geological map of the Betts Cove mine and Mount Misery area
12	5. Geological map of the Red Cliff Pond–Long Pond area
13	6. Geological map of the Tilt Cove area
14	7. Geological map of the area between Betts Cove and West Pond
16	8. Photomicrograph of quartz-Fe-Ti-oxide-gabbro-norite
17	9. Photomicrograph of high-grade ductile shear zone
18	10. Photomicrograph of zoned amphibole phenocryst from a dyke injected into a fault beneath the Betts Cove graben
20	11. Photograph of talus breccia with a boninititic igneous matrix at Tilt Cove
21	12. Talus breccia in Mount Misery Formation
23	13. Photomicrograph of Scrape Point basal ironstone
25	14. Typical subaqueous blocky welded Bobby Cove tuff
26	15. Photomicrograph of welded subaqueous tuff of the Bobby Cove Formation
26	16. Photomicrograph of welded mafic subaqueous tuff of the Bobby Cove Formation
27	17. Photomicrograph of dacitic tuff of the Bobby Cove Formation
28	18. Detailed section measured from the upper member of the Bobby Cove Formation
29	19. Photomicrograph of a rhyolitic tuff of the Balsam Bud Cove Formation
30	20. Representative section showing the base of the Upper Member (debrite) of the Balsam Bud Cove Formation
32	21. Representative section from the middle of the Upper Member (debrite) of the Balsam Bud Cove Formation
33	22. Matrix of volcanoclastic debrite of Balsam Bud Cove Formation
35	23. Photomicrograph of a quartz-feldspar-mica-porphyrific dyke from Tilt Cove
41	24. Cr/(Cr+Al) versus $Fe^{+2}/(Mg+Fe^{+2})$ in Cr-spinel phenocrysts from Betts Cove cumulate rocks and dykes

- 43 25. Enstatite-wollastonite-ferrosilite in clinopyroxene from Betts Cove cumulate  
rocks and lavas and dykes
- 50 26. Major and trace element variation diagrams for Betts Head Formation lavas,  
Betts Cove sheeted dykes, Nippers Harbour Massif dykes and lavas,  
and Mount Misery Formation lavas
- 51 27. Extended trace element plots normalized to N-MORB for rocks of the  
Betts Head and Mount Misery formations
- 52 28. Major and trace element variation diagrams for fractionation, melting,  
and source mixing models
- 52 29. La/Nd versus La (ppm) showing fractionation and melting vectors compared  
to field of data of Betts Cove boninitic rocks
- 53 30. Ba/La versus La/Sm (normalized to N-MORB) ratio plot
- 53 31. Extended trace element profiles for model melts coexisting with Betts  
Cove cumulate rocks
- 54 32. Na<sub>2</sub>O+K<sub>2</sub>O-FeO\*-MgO (AFM) diagrams for Betts Cove basalt
- 55 33. Ti versus Zr tectonic discriminant diagram for Betts Cove basalt
- 56 34. Ti/100-Zr-Y\*3 tectonic discriminant diagram for Betts Cove basalt
- 57 35. Log Ti versus log Cr tectonic discriminant diagram for Betts Cove basalt
- 57 36. Log Zr/Y versus log Zr tectonic discriminant diagram for Betts Cove basalt
- 58 37. MnO\*10-TiO<sub>2</sub>-P<sub>2</sub>O<sub>5</sub>\*10 tectonic discriminant diagram for Betts Cove basalt
- 58 38. V versus Ti tectonic discriminant diagram for Betts Cove basalt
- 59 39. Major and trace element variation diagrams for Snooks Arm Group upper  
tholeiitic lavas and dykes
- 59 40. Major and trace element variation diagrams for Snooks Arm Group  
calc-alkaline magmas and various tuffs and sedimentary rocks
- 60 41. Extended trace element plots normalized to N-MORB of  
Snooks Arm Group tholeiitic lavas and dykes
- 61 42. Extended trace element plots normalized to N-MORB of  
Snooks Arm Group calc-alkaline lavas, pyroclastic rocks, and tuffs
- 61 43. Log Nb versus log Y, and log Rb versus log Y+Nb tectonic discriminants  
for felsic and granitoid rocks from Betts Cove and environs
- 62 44. Extended trace element plots normalized to N-MORB of Cape St. John  
Group mafic and felsic lavas, dykes, and tuffs
- 62 45. Major and trace element variation diagrams for Silurian igneous rocks
- 64 46. Schematic cross-section illustrating the evolution of the Betts Cove  
ophiolite and its cover rocks
- 66 47. Geological plan and section from the main Tilt Cove mine
- 69 48. Distribution of mineralized shear zones and associated airphoto linear  
features, Betts Cove mine
- 71 49. Geological drill and assay section, Nugget Pond gold mine

### Tables

- 38 1. Spinel analyses
- 39 2. Clinopyroxene analyses
- 42 3. Amphibole analyses
- 44 4. Average geochemical data for Betts Cove lavas, sills, tuffs, and sedimentary rocks
- 48 5. Average geochemical data for Betts Cove cumulate rocks
- 67 6. Element and trace element analyses of mineral occurrences from the Betts  
Cove ophiolite





---

# BETTS COVE OPHIOLITE AND ITS COVER ROCKS, NEWFOUNDLAND

---

## **Abstract**

*The Betts Cove ophiolite formed through seafloor spreading in an Ordovician fore-arc marginal basin, since dykes of the sheeted dyke complex, the lower lavas (the Betts Head Formation), and the cumulate rocks all have boninitic affinities; and recent boninitic lavas are only found in fore-arc environments. Synmagmatic extensional faults dissect the lavas and dykes into horst-and-graben structures. The faults localized hydrothermal flow and controlled sulphide deposition. The lowermost unit of the overlying Snooks Arm Group, the Mount Misery Formation, is composed of arc tholeiitic rocks. They are overlain by thick sequences of evolved tholeiitic rocks (Scrape Point Volcanic Member; Venam's Bight, Round Harbour formations) and feeder sills, calc-alkaline pyroclastic rocks (lower Bobby Cove, lower Balsam Bud Cove formations), and sedimentary rocks derived through erosion of the different types of volcanic rocks (Scrape Point sedimentary rocks, upper Bobby Cove, upper Balsam Bud Cove formations). During obduction, the ophiolite and its cover rocks were thrust above a talc-serpentinite unit. Chloritized synoceanic faults formed during seafloor spreading were reactivated at this time.*

*In the Silurian, granitoid batholiths (Burlington and Cape Brulé) intruded the Laurentian basement and the overthrust oceanic terranes. The Silurian Cape St. John Group unconformably overlies the tilted ophiolite. It consists of subaerial fluvial sedimentary rocks, basalt, and felsic pyroclastic rocks, that probably represent ejecta from the granitoid batholith (Cape Brulé). Quartz-feldspar-porphry dykes intruded along active north- and east-dipping normal faults, and may represent feeders for Cape St. John Group felsic pyroclastic rocks. Subsequently, the entire package was affected by northeast-dipping thrusts and associated folds, which probably record the effects of the Acadian Orogeny.*

## **Résumé**

*L'ophiolite de Betts Cove s'est formée par suite de l'expansion du fond océanique dans un bassin marginal d'avant-arc de l'Ordovicien, car les dykes du complexe filonien, les laves inférieures (Formation de Betts Head) et les cumulats ont tous des affinités boninitiques, et qu'on ne rencontre les laves boninitiques modernes que dans des environnements d'avant-arc. Des failles de distension synmagmatiques découpent les laves et les dykes en des structures en horst et graben. Ces failles ont canalisé l'écoulement hydrothermal et ont contrôlé le dépôt des sulfures. L'unité basale du Groupe de Snooks Arm sus-jacent, la Formation de Mount Misery, se compose de roches tholéiitiques d'arc que recouvrent des séquences épaisses de roches tholéiitiques évoluées (Membre volcanique de la Formation de Scrape Point, formations de Venam's Bight et de Round Harbour) et de filons-couches, des roches pyroclastiques calco-alkalines (parties inférieures des formations de Bobby Cove et de Balsam Bud Cove), et des roches sédimentaires produites par l'érosion de divers types de roches volcaniques (roches sédimentaires de la Formation de Scrape Point, parties supérieures des formations de Bobby Cove et de Balsam Bud Cove). Pendant leur obduction, l'ophiolite et les roches qui la recouvraient ont été charriées au-dessus d'une unité de talc-serpentinite. Des failles chloritisées formées au moment de l'expansion du fond océanique ont été réactivées à cette époque.*

*Au Silurien, des batholites granitoïdes (Burlington et Cape Brulé) ont fait intrusion dans le socle Laurentien et dans les terranes océaniques chevauchants. Le Groupe de Cape St. John, du Silurien, recouvre en discordance l'ophiolite basculée. Il est constitué de roches sédimentaires fluviales subaériennes, de basaltes et de roches pyroclastiques felsiques qui représentent probablement des produits extrusifs associés au batholite granitoïde (Cape Brulé). Des dykes de porphyre quartzofeldspathique ont fait intrusion le long de failles normales actives à pendage nord et est; ils pourraient représenter les filons nourriciers des roches pyroclastiques felsiques du Groupe de Cape St. John. Plus tard, tout l'assemblage a été déformé par des failles de chevauchement à pendage nord-est et par des plis associés, qui témoignent probablement des effets de l'orogénèse acadienne.*

## SUMMARY

The Betts Cove ophiolite massif and its cover rocks belong to the Notre Dame Subzone of the Dunnage Zone of the Newfoundland Appalachians. The ophiolite is a relic of Ordovician marginal oceanic crust, and records the initiation of seafloor spreading in a fore-arc marginal basin, since dykes of the sheeted dyke complex, the lower lavas (the Betts Head Formation), and the cumulate rocks all have boninitic affinities; and recent boninitic lavas are only found in fore-arc environments. The cover sequence, known as the Snooks Arm Group, represents maturation of the marginal basin spreading system, and the development of an island-arc system.

Layered cumulate rocks form steeply dipping homoclinal sections up to 1 km thick, separated by sheared serpentinite and/or peridotitic breccia zones, some of which are synoceanic faults associated with seafloor spreading. Cyclic sequences range from peridotite to pyroxenite and gabbro-norite. Geochemical modelling implies they formed from boninitic lavas with trace element signatures similar to those of overlying dykes and lavas. Layered cumulate rocks are at an angle of 44° from the plane defined by intralava sedimentary rocks. Intrusions of massive, pink-weathering, quartz-Fe-Ti-oxide-gabbro-norite (commonly with interstitial granophyre), gabbro, and trondhjemite are commonly present along faults or at the interface between layered cumulate rocks and sheeted dykes.

Basal and upper contacts of the sheeted dyke complex are either gradational, characterized by a progressive decrease in the proportion of dykes, have been injected by intrusions of gabbro-norite, or are faulted. Some of the fault-breccia units are impregnated with magma. Dykes can be subdivided into four subtypes. Low-Ti boninitic dykes contain spinel+olivine+orthopyroxene phenocrysts (1–5%), and are compositionally identical to the low-Ti Betts Head boninite lavas. Dykes of “perknite” are porphyritic equivalents. Diabasic and microgabbroic dykes are dominated by clinopyroxene and feldspar, and most represent differentiation products of these same boninitic magmas. A subpopulation of intermediate-Ti dykes contain small phenocrysts of clinopyroxene and feldspar

The Betts Head Formation constitutes the autochthonous lavas of the oceanic crust. This unit is composed of spherulitic, sparsely porphyritic, sparsely amygdaloidal, low-Ti and intermediate-Ti boninite pillow lavas and flow tubes. Thick (5–20 m) pillow-breccia layers are common. Low-Ti and intermediate-Ti lava series are interbedded. Low-Ti lavas carry olivine+orthopyroxene+chromite phenocrysts. Intermediate-Ti lavas have clinopyroxene±plagioclase±olivine phenocrysts, and are gradational to the arc tholeiitic rocks of the subconformably overlying Mount Misery Formation. North-west- to southwest-trending corridors of breccia, 1–10 m

## SOMMAIRE

L'ophiolite de Betts Cove et ses roches de couverture font partie de la sous-zone de Notre-Dame de la zone de Dunnage des Appalaches de Terre-Neuve. L'ophiolite est un lambeau de croûte océanique marginale ordovicienne et témoigne du début de l'expansion du fond océanique dans un bassin marginal d'avant-arc, car les dykes du complexe filonien, les laves inférieures (Formation de Betts Head) et les roches à cumulats ont tous des affinités boninitiques; et qu'on ne rencontre les laves boninitiques modernes que dans des environnements d'avant-arc. La séquence de couverture, appelée «Groupe de Snooks Arm», témoigne de la maturation du système d'expansion du bassin marginal et de la mise en place d'un système d'arc insulaire.

Les cumulats stratifiés forment des sections homoclinales à pendage abrupt jusqu'à 1 km d'épaisseur, séparées par des zones de serpentinite cisailée et/ou de brèche à péridotite, dont certaines sont des failles synocéaniques associées à l'expansion du fond océanique. Les séquences cycliques passent de la péridotite à la pyroxénite et à la gabbro-norite. La modélisation géochimique laisse supposer qu'elles sont issues de laves boninitiques dont les signatures en éléments traces sont similaires à celles des laves et dykes sus-jacents. Les cumulats stratifiés forment un angle de 44° par rapport au plan défini par les roches sédimentaires présentes entre les laves. Des intrusions de gabbro-norite à quartz et oxydes de Fe-Ti (souvent avec du granophyre interstitiel) massive à couleure d'altération rose, de gabbro et de trondhjemite se rencontrent le long des failles ou à l'interface entre les cumulats stratifiés et le complexe filonien.

Les contacts inférieur et supérieur du complexe filonien sont soit transitionnels, caractérisés par une diminution progressive de la proportion de dykes, ou ont été injectés par des intrusions de gabbro-norite, ou encore sont faillés. Certaines unités de brèche de faille sont imprégnées de magma. On peut répartir les dykes en quatre sous-groupes. Les dykes boninitiques à faible teneur en Ti contiennent de 1 à 5 p. 100 de phénocristaux de spinelle+olivine+orthopyroxène et ont une composition identique à celle des laves boninitiques à faible teneur en Ti de la Formation de Betts Head. Les dykes de «perknite» en sont des équivalents porphyriques. Les dykes diabasiques et microgabbroïques se composent surtout de clinopyroxène et de feldspath, et la plupart représentent des produits de différenciation de ces mêmes magmas boninitiques. Une sous-population de dykes à teneur intermédiaire en Ti contient de petits phénocristaux de clinopyroxène et de feldspath.

La Formation de Betts Head représente les laves autochtones de la croûte océanique. Cette unité se compose de laves en coussins et de tubes de lave à texture sphérolitique, peu porphyriques et peu amygdaloïdes, de composition boninitique, à teneur faible et intermédiaire en Ti. Des couches épaisses (de 5 à 20 m) de brèche de coussins abondent. Les séquences de laves à faible teneur en Ti et à teneur intermédiaire en Ti sont interlitées. Les laves à faible teneur en Ti contiennent des phénocristaux d'olivine+orthopyroxène+chromite. Les laves à teneur intermédiaire en Ti ont des phénocristaux de clinopyroxène±plagioclase±olivine et évoluent vers les roches tholéiitiques d'arc de la Formation de Mount Misery subconcordante

wide, represent synoceanic faults or fissures. Axial mafic dykes are common in these breccia corridors, confirming their synoceanic origin.

Synmagmatic extensional faults dissect the lavas and dykes into horst-and-graben structures. The faults localized hydrothermal flow and so controlled deposition of sulphide minerals at the Betts Cove mine. Late gabbro-norite intrusions appear to have provided the localized heat sources needed to drive intense hydrothermal circulation. The mineralized breccia zones of the Tilt Cove mine appear to be a mixture of primary hyaloclastite, fault and/or talus breccia, and hydraulic breccia, cemented by quartz+calcite+hématite+epidote and locally abundant sulphide minerals. The mineralization is mostly located at or near the interface between the Betts Head and Mount Misery formations, and may originally have formed as a conformable volcanogenic massive sulphide deposit, subsequently reworked by multiple intrusive and/or faulting and/or hydrothermal events. In places, chalcopyrite-bearing massive sulphide layers, red chert, and ironstone occur at conformable boninite-tholeiite contacts. In places, breccia contains fragments of gabbro and basalt that are injected and impregnated by boninitic magma. Elsewhere, 10 m sized pillow basalt olistoliths appear suspended in an epiclastic matrix. We infer an origin for many of these breccia zones as oceanic fault-talus deposits developed during seafloor spreading. Some were reworked by later extensional faults during eruption of Snooks Arm Group basaltic lavas.

The lowermost unit of the overlying Snooks Arm Group, the Mount Misery Formation, is composed of arc tholeiitic rocks. The basal Mount Misery lavas are spherulitic, olivine-phyric pillow lavas and flow tubes, grading up to plagioclase+clinopyroxene-phyric basaltic and ferrobasaltic lavas at the summit. Thick (5–20 m) pillow-breccia layers are common. Northwest- to southwest-trending corridors of breccia (2–40 m wide), commonly with axial mafic dykes, represent synoceanic normal faults. Some breccia zones are transformed to chlorite+albite-rich greenschist-facies assemblages, suggesting considerable hydrothermal throughflow. Pillow lavas between closely spaced breccia corridors have a crackled appearance, with red-weathering oxidized cores and green-weathering reduced rims. The uppermost Mount Misery lava flows are commonly magnetic. The magnetic lavas are spatially associated with ironstone of the overlying Scrape Point Formation. We interpret most of the breccia domains to be fault-talus deposits; but some of them appear conglomeratic, containing rounded clasts of basalt and peridotite in an epiclastic matrix with detrital chromite grains. This suggests exhumation of mantle and/or deep crustal rocks along major extensional faults.

sus-jacente. Des corridors de brèche de 1 à 10 m de largeur, à orientation nord-ouest à sud-ouest, représentent des failles ou fissures synocéaniques. Des dykes mafiques axiaux sont nombreux dans ces corridors de brèche, ce qui confirme leur origine synocéanique.

Des failles de distension synmagmatiques découpent les laves et les dykes en structures en horst et graben. Ces failles ont canalisé l'écoulement hydrothermal et ont ainsi contrôlé le dépôt des sulfures à la mine Betts Cove. Des intrusions tardives de gabbro-norite semblent avoir été les sources de chaleur locales nécessaires à la circulation intense de fluides hydrothermaux. Les zones de brèche minéralisée de la mine Tilt Cove semblent être composées d'un mélange d'hyaloclastite primaire, de brèche de faille et/ou de brèche de talus et de brèche hydraulique, le tout cimenté par une association de quartz+calcite+hématite+épidote avec, par endroits, des sulfures en abondance. La minéralisation est surtout localisée à l'interface (ou près de celle-ci) entre les formations de Betts Head et de Mount Misery et pourrait avoir été à l'origine un gisement de sulfures massifs volcanogènes concordant, remanié par la suite par de multiples événements intrusifs, tectoniques ou hydrothermaux. Par endroits, on trouve des couches de sulfures massifs à chalcopyrite, des cherts rouges et des roches ferrugineuses le long des contacts conformes entre les laves boninitiques et tholéiitiques. À certains endroits, la brèche contient des fragments de gabbro et de basalte injectés et imprégnés de magma boninitique. Ailleurs, des olistolithes de basalte en coussins de 10 m de diamètre semblent flotter dans une matrice épicalastique. Nous concluons que plusieurs des zones de brèche sont des dépôts de talus de faille océanique mis en place durant l'expansion du fond océanique. Certains ont ensuite été remaniés par des failles de distension tardives pendant l'éruption des laves basaltiques du Groupe de Snooks Arm.

L'unité de base du Groupe de Snooks Arm sus-jacent, la Formation de Mount Misery, se compose de roches tholéiitiques d'arc. Les laves inférieures de la Formation de Mount Misery sont des tubes de lave et des laves en coussins à phénocristaux d'olivine et à texture sphérolitique, qui se transforment progressivement vers le sommet en laves basaltiques et ferro-basaltiques à phénocristaux de plagioclase+clinopyroxène. Des couches épaisses (de 5 à 20 m) de brèche de coussins sont nombreuses. Des corridors de brèche de 2 à 40 m de largeur, à orientation nord-ouest à sud-ouest, que recoupent souvent des dykes mafiques axiaux, représentent des failles normales synocéaniques. Certaines zones de brèche ont été transformées en associations riches en chlorite+albite du faciès des schistes verts, ce qui indiquerait une forte circulation de fluides hydrothermaux. Les laves en coussins entre des corridors de brèche étroitement espacés ont un aspect fendillé; les coeurs des coussins sont oxydés et ont une couleur d'altération rouge alors que les bordures sont réduites et ont une couleur d'altération verte. Les coulées de laves sommitales de la Formation de Mount Misery sont souvent magnétiques. Les laves magnétiques sont associées spatialement à des roches ferrugineuses de la Formation de Scrape Point sus-jacente. Selon notre interprétation, la plupart des domaines de brèche sont des dépôts de talus de faille. Cependant, certains d'entre eux ont un aspect conglomératique et contiennent des fragments arrondis de basalte et de péridotite dans une matrice épicalastique avec des grains de chromite détritique. Cela suppose que des roches du manteau ou de la croûte profonde ont été exhumées le long des principales failles de distension.

Rocks of the Mount Misery Formation are overlain by evolved tholeiitic basalt and sedimentary rocks of the Scrape Point Formation. In the southern part of the map area, the sedimentary member is thin and appears to be restricted to the base of the formation. North of East Pond, sedimentary rocks are more abundant and are not restricted to the base of the unit. The base of the formation is an erosional unconformity that bevels a series of tilted fault blocks. A laterally discontinuous boulder conglomerate or pebbly sandstone grades up into iron-formation, and then into tuffaceous, sandstone-siltstone turbidite beds. The conglomerate contains fragments of basaltic lava and red chert up to 0.5 m derived from basaltic lavas of the underlying Mount Misery Formation. The clasts are either veined and cemented by nearly pure magnetite+hematite, or they sit in a sandy matrix rich in euhedral magnetite. Dark brown to black magnetic ironstone beds contain up to 80% euhedral magnetite, associated with hematite, acicular stilpnomelane, quartz, and sericite. The magnetite is not detrital, and probably records volcanogenic exhalations. Locally, coarse cubic auriferous pyrite is developed (Nugget Pond mine). The faults that cut the Mount Misery lavas also offset Scrape Point sedimentary rocks, though with lesser throws, implying that these are syndepositional normal growth faults. Chaotic slump folds and small growth faults are common in Scrape Point sedimentary rocks. Swarms of medium- to coarse-grained, mafic sills commonly split the sedimentary rocks into thinner packages. Contact metamorphic effects produced black slate and purple-silver phyllite. North of East Pond, the sedimentary member is interbedded with lavas throughout. It is composed of green turbiditic and tuffaceous sandstone and siltstone, red mudstone, and locally pyritiferous, stilpnomelane-bearing ironstone. Green tuffaceous sandstone beds, some welded, may have 1–2 cm sized lapilli of amygdaloidal, plagioclase-porphyrific andesite, petrologically and geochemically similar to tuffs of the Bobby Cove Formation. Tuffaceous sandstone and siltstone record eruption and erosion of a calc-alkaline volcano, the paroxysmal eruption of which constitutes the overlying Bobby Cove Formation.

Scrape Point lavas are amygdaloidal, sparsely plagioclase+clinopyroxene-phyric, Fe-Ti-rich, tholeiitic pillow lavas and massive flows. Massive flows have thin, lobed or pillowed tops and bases. Plagioclase-porphyrific facies may contain up to 50% plagioclase phenocrysts (up to 2 cm). These lavas represent eruptions of evolved back-arc tholeiitic rocks originating from undepleted sources, with only minor addition of subducted components.

The base of the Bobby Cove Formation is an accumulation of calc-alkaline pyroclastic rocks. Thick-bedded, coarse blocky tuffs are composed of abundant andesitic clasts in a crystal-lithic-vitric matrix. These are very proximal to their

Les roches de la Formation de Mount Misery sont recouvertes de basalte tholéiitique évolué et de roches sédimentaires de la Formation de Scrape Point. Dans la partie méridionale de la région cartographique, le membre sédimentaire est mince et semble se limiter à la base de la formation. Au nord du lac East Pond, les roches sédimentaires sont plus abondantes et ne se limitent pas à la partie inférieure de l'unité. La base de la formation est une discordance d'érosion qui biseaute une série de blocs faillés inclinés. Un conglomérat à blocs ou grès caillouteux latéralement discontinu passe progressivement à une formation de fer, puis à des lits tufacés de turbidite gréseux et silteux. Le conglomérat contient des fragments de lave basaltique et de chert rouge dont la taille atteint 0.5 m, qui sont issus des laves basaltiques de la Formation de Mount Misery sous-jacente. Les clastes sont soit veinés et cimentés par de la magnétique+hématite presque pure, ou logés dans une matrice sableuse riche en magnétite automorphe. Des lits brun foncé à noirs de roche ferrugineuse magnétique contiennent jusqu'à 80 p. 100 de magnétite automorphe associée à de l'hématite, à du stilpnomélane aciculaire, à du quartz et à de la séricite. La magnétite n'est pas détritique et témoigne probablement d'exhalations volcanogènes. De la pyrite aurifère cubique à grain grossier se rencontre par endroits (mine Nugget Pond). Les failles qui recoupent les laves de la Formation de Mount Misery décalent également les roches sédimentaires de la Formation de Scrape Point, mais les rejets verticaux y sont plus faibles, ce qui signifie que ces failles sont des failles normales synsédimentaires. Des plis de glissement chaotiques et de petites failles synsédimentaires abondent dans les roches sédimentaires de la Formation de Scrape Point. Des essaims de filons-couches mafiques à grain moyen à grossier divisent souvent les roches sédimentaires en ensembles plus minces. Des phénomènes de métamorphisme de contact ont formé des schistes ardoisiers noirs et des phyllades pourpres-argentées. Au nord du lac East Pond, le membre sédimentaire est interlité avec des laves sur toute son épaisseur. Il se compose de grès et de siltstones tufacés à turbiditiques verts, de mudstones rouges et de roches ferrugineuses à stilpnomélane (localement pyriteuses). Les lits de grès tufacés verts, certains soudés, peuvent contenir des lapillis de 1 à 2 cm d'andésite à phénocristaux de plagioclase et à texture amygdaloïde pétrologiquement et géochimiquement similaires aux tufs de la Formation de Bobby Cove. Ces grès et siltstones tufacés témoignent de l'éruption et de l'érosion d'un volcan calco-alkalin. À son paroxysme, l'éruption a produit la Formation de Bobby Cove sus-jacente.

Les laves de la Formation de Scrape Point sont constituées de laves en coussins et de coulées massives. Elles sont d'affinité tholéiitique, riches en Fe-Ti, à texture amygdaloïde et contiennent peu de phénocristaux de plagioclase+clinopyroxène. Les sommets et les bases des coulées massives ont de minces zones lobées ou en coussins. Les faciès à phénocristaux de plagioclase peuvent contenir jusqu'à 50 p. 100 de phénocristaux (jusqu'à 2 cm) de plagioclase. Ces laves témoignent d'éruptions de roches tholéiitiques évoluées d'arrière-arc qui proviennent de sources non appauvries, contenant une fraction minimale de composantes ajoutées lors de la subduction.

La base de la Formation de Bobby Cove est une accumulation de roches pyroclastiques calco-alkalines. Les tufs à blocs à lits épais et à grain grossier contiennent une forte proportion de fragments d'andésite dans une matrice cristallo-lithique et cristallo-vitreuse. Ils sont très proches de leur source; la plupart représentent des

source and most represent subaqueous debris flows, some of which were pyroclastic eruptions. The amalgamated conglomerate flow units can be more than 100 m thick and can be traced along strike for several kilometres. Significant erosion and truncation of underlying deposits is observed. These alternate with bedded tuffs, and represent welded, subaqueous pyroclastic flows. Poorly bedded dacitic crystal tuffs containing abundant (10–15%) small (1–2 cm) xenoliths are locally prominent. Thin (<3 m), felsic tuffs are subordinate, and may represent subaqueously deposited ashfalls. Subordinate flows and dykes of clinopyroxene±plagioclase-phyric andesite and basalt are also present. The lavas and juvenile clasts belong to two series, one composed of arc tholeiitic rocks similar to the Mount Misery Formation lavas, the other being more purely calc-alkaline.

The upper part of the Bobby Cove Formation is composed of volcanogenic to tuffaceous turbidite sequences, and is cut by numerous diabasic sills that fed the overlying basaltic lavas of the Venam's Bight Formation. The latter is composed of pillow lavas that are nearly indistinguishable from basaltic lavas of the Scrape Point Formation.

The base of the overlying Balsam Bud Cove Formation is composed of interbedded turbidite units, black shale, basaltic lavas, and rhyolitic to dacitic tuffs with calc-alkaline signatures that may record eruptions of the same magma chambers that produced the Bobby Cove flows. Above these are volcanoclastic debris and turbidite units derived principally from erosion of basaltic lavas similar to the underlying Venam's Bight Formation. The uppermost unit of the Snooks Arm Group is the Round Harbour Formation, which is composed of basaltic lavas that closely resemble the Venam's Bight lavas. These basaltic lavas are cut by felsic dykes of calc-alkaline affinity.

The Snooks Arm Group records alternations of tholeiitic and calc-alkaline volcanism, both proximal, suggesting that different types of sources were available beneath this Ordovician marginal basin. The gradation from depleted boninitic lavas and dykes, to less depleted arc tholeiitic rocks, to undepleted back-arc basin basalt units suggests that undepleted mantle sources were drawn up into the melting zone by the extension associated with seafloor spreading. The persistence of arc magmatism throughout this progression suggests that subduction was ongoing.

The nearby Nippers Harbour ophiolitic massif is composed of gabbro, sheeted dykes, and lavas. It is separated from the Betts Cove ophiolite by a prominent fault, lined by serpentinite. Preliminary data suggest that the Nippers Harbour lavas and dykes are similar to the more evolved boninitic magmas from the Betts Cove massif, suggesting that the two may be lateral equivalents.

coulées de débris subaquatiques dont certaines étaient des éruptions pyroclastiques. Les unités de coulées de débris conglomératiques amalgamées peuvent avoir plus de 100 m d'épaisseur, et on peut les suivre sur plusieurs kilomètres parallèlement à la direction. On peut observer que les unités sous-jacentes ont été fortement érodées et tronquées. Ces dépôts alternent avec des tufs lités et représentent des coulées pyroclastiques subaquatiques soudées. Par endroits, dominant des tufs cristallins dacitiques mal lités contenant d'abondants (de 10 à 15 p. 100) petits (de 1 à 2 cm) xénolites. Des tufs felsiques minces (< 3 m) moins volumineux représentent probablement des dépôts subaquatiques de cendres volcaniques. On rencontre également une petite quantité de coulées et de dykes d'andésite et de basalte à phénocristaux de clinopyroxène±plagioclase. Les laves et les clastes juvéniles appartiennent à deux séries, une composée de roches tholéiitiques d'arc similaires aux laves de la Formation de Mount Misery, et une autre étant d'affinité plus calco-alkaline.

La partie supérieure de la Formation de Bobby Cove comporte des séquences de turbidites volcanogènes à tufacées et est recoupée par de nombreux filons-couches de diabase qui ont alimenté les laves basaltiques sus-jacentes de la Formation de Venam's Bight. Cette dernière se compose de laves en coussins qui sont presque identiques aux laves basaltiques de la Formation de Scrape Point.

La base de la Formation de Balsam Bud Cove sus-jacente comporte des unités interlitées de turbidites, de shales noirs, de laves basaltiques et de tufs rhyolitiques à dacitiques. Leurs signatures calco-alkalines pourraient indiquer des éruptions provenant des mêmes chambres magmatiques qui sont à l'origine des coulées de la Formation de Bobby Cove. Recouvrant ces derniers, on retrouve des unités de fragments volcanoclastiques et de turbidites dérivés principalement de l'érosion de laves basaltiques semblables à celles que l'on retrouve dans la Formation de Venam's Bight sous-jacente. L'unité sommitale du Groupe de Snooks Arm est la Formation de Round Harbour, qui se compose de laves basaltiques très similaires à celles de la Formation de Venam's Bight. Ces laves basaltiques sont recoupées par des dykes felsiques d'affinité calco-alkaline.

Le Groupe de Snooks Arm montre une alternance de roches volcaniques tholéiitiques et calco-alkalines de faciès proximal, laissant supposer que deux sources magmatiques étaient présentes sous ce bassin marginal ordovicien. Le passage des dykes et des laves boninitiques appauvries à des roches tholéiitiques d'arc moins appauvries, puis à des basaltes non appauvris de bassin d'arrière-arc, indique que les forces associées à l'expansion du fond océanique ont remonté des sources mantelliques non appauvries dans la zone de fusion. La persistance du magmatisme d'arc pendant cette évolution porte à croire que la subduction se poursuivait au même moment.

L'ophiolite voisine de Nippers Harbour se compose de gabbro, d'un complexe filonien de dykes et de laves. Une faille importante, bordée de serpentinite, la sépare de l'ophiolite de Betts Cove. Les données provisoires indiquent que les laves et les dykes de l'ophiolite de Nippers Harbour sont semblables aux magmas boninitiques plus évolués de l'ophiolite de Betts Cove, ce qui incite à conclure que les deux ophiolites sont probablement des équivalents latéraux.

During obduction onto North America, the ophiolite and its cover rocks were thrust above a talc-serpentinite unit. Talc-magnesite-carbonate schist domains commonly occur as diffuse haloes around shear zones and faults in serpentinite. They typically contain rusty-weathering iron-carbonate, cubic pyrite, and euhedral magnetite bi-pyramids, some of which have relict holly-leaf chromite cores with lower Cr/Al than is typical of chromite from the layered cumulate rocks. Some of these may represent relict mantle peridotite. In places, the Snooks Arm Group rocks slid over the underlying ophiolite along east-dipping thrust faults. Chloritized synoceanic faults were reactivated at this time.

In the Silurian, granitoid batholiths (Burlington and Cape Brulé) intruded the Laurentian basement and the overthrust oceanic terranes. The Silurian Cape St. John Group unconformably overlies tilted rocks of the ophiolite. It consists of boulder conglomerate, subaerial fluviatile sedimentary rocks, basaltic lavas, and felsic pyroclastic rocks that probably represent a caldera-fill associated with the granitoid batholith (Cape Brulé). Quartz-feldspar-porphry dykes intrude the ophiolite along a system of active north- and east-dipping normal faults, and may represent feeders for Cape St. John Group felsic pyroclastic rocks. Subsequently, the entire package was affected by northeast-dipping thrusts and associated folds, which probably record the effects of the Acadian Orogeny.

Pendant leur obduction sur le continent nord-américain, l'ophiolite et les roches qui la recouvraient ont été charriées au-dessus d'une unité de talc-serpentinite. Des domaines de schistes à talc, magnésite et carbonates forment couramment des auréoles diffuses autour des zones de cisaillement et des failles dans la serpentinite. Généralement, ils sont constitués de carbonates de fer, bipyramidaux à surface d'altération rouillée de pyrite cubique et de magnétite euhédrique, dont certaines ont des coeurs avec des reliques de chromite en forme de houx et un rapport Cr/Al plus bas que celui qui est typique des chromites des cumulats stratifiés. Certains d'entre eux pourraient être des reliques de péridotites mantelliques. À certains endroits, les roches du Groupe de Snooks Arm ont glissé par-dessus l'ophiolite sous-jacente le long de failles de chevauchement à pendage est. Les failles chloritisées formées au moment de l'expansion du fond océanique ont été réactivées à cette époque.

Au Silurien, des batholites granitoïdes (Burlington et Cape Brulé) ont fait intrusion dans le socle Laurentien et dans les terranes océaniques chevauchants. Le Groupe de Cape St. John, du Silurien, recouvre en discordance des roches basculées de l'ophiolite. Il est constitué de conglomérat à blocs, de roches sédimentaires fluviatiles subaériennes, de laves basaltiques et de roches pyroclastiques felsiques qui témoignent probablement d'un remplissage de caldeira associé au batholite granitoïde (Cape Brulé). Des dykes de porphyre quartzofeldspathique recoupent l'ophiolite le long d'un système de failles normales actives à pendage nord et est, et ils pourraient représenter les filons nourriciers des roches pyroclastiques felsiques du Groupe de Cape St. John. Plus tard, tout l'assemblage a été déformé par des failles de chevauchement à pendage nord-est et par des plis associés, qui témoignent probablement des effets de l'orogénèse acadienne.

---

## INTRODUCTION AND GEOLOGICAL FRAMEWORK

The Baie Verte Peninsula, Newfoundland (Fig. 1), has played an important role in the development of concepts related to the Wilson cycle (e.g. Dewey, 1969; *see review in* Hibbard (1983)). The Betts Cove area is of particular interest for the mineral exploration industry, since it hosts a producing gold mine and two historic volcanogenic copper-sulphide mines. Although the Betts Cove ophiolitic complex has been intensively investigated before the present study was initiated, substantive problems remained with regard to the stratigraphy of its supracrustal sequence, the magmatic affinity of the plutonic section, and the geological controls on ore deposition. The present study attempts to resolve some of these issues, and to provide a stratigraphic framework that may be applicable to other, potentially correlative, Ordovician supracrustal sequences of the Baie Verte Peninsula. A 1:20 000 scale map (Bédard et al., 1999) that complements this memoir has been published separately. The complete digital data file that underpins the map and report, together with sample locations and the complete analytical and structural data file are available as an Open File CD-ROM (Bédard et al., in press).

The Baie Verte Peninsula is underlain by rocks of the Laurentian continental margin (the Humber Zone), which are in tectonic contact with a collage of accreted oceanic terranes known as the Dunnage Zone (Williams, 1979; Hibbard, 1983; Williams et al., 1988). The Betts Cove ophiolitic complex (Bédard et al., 1999) constitutes one of these accreted terranes, and provides a record of marginal basin evolution and accretion during the Ordovician Taconian Orogeny, extension in the Silurian, followed by compression in the Upper Silurian to Lower Devonian Acadian Orogeny.

An exhaustive review of previous work in the Baie Verte Peninsula, and on the Betts Cove ophiolitic complex can be found in Hibbard (1983). The following capsule summary is meant only to provide a broad regional framework for the detailed study of the Betts Cove ophiolitic complex that follows. In the Baie Verte Peninsula, Precambrian to Lower Paleozoic rocks of the Humber Zone comprise a structural basement of eclogite, gneiss, and migmatitic rocks (e.g. the East Pond metamorphic suite); a cover sequence of metaclastic schist, marble, amphibolite, and greenschist (notably the Fleur de Lys Supergroup); and a granitoid intrusive suite (e.g. the Wild Cove igneous suite; Hibbard, 1983). These rocks are characterized by polyphase deformation and

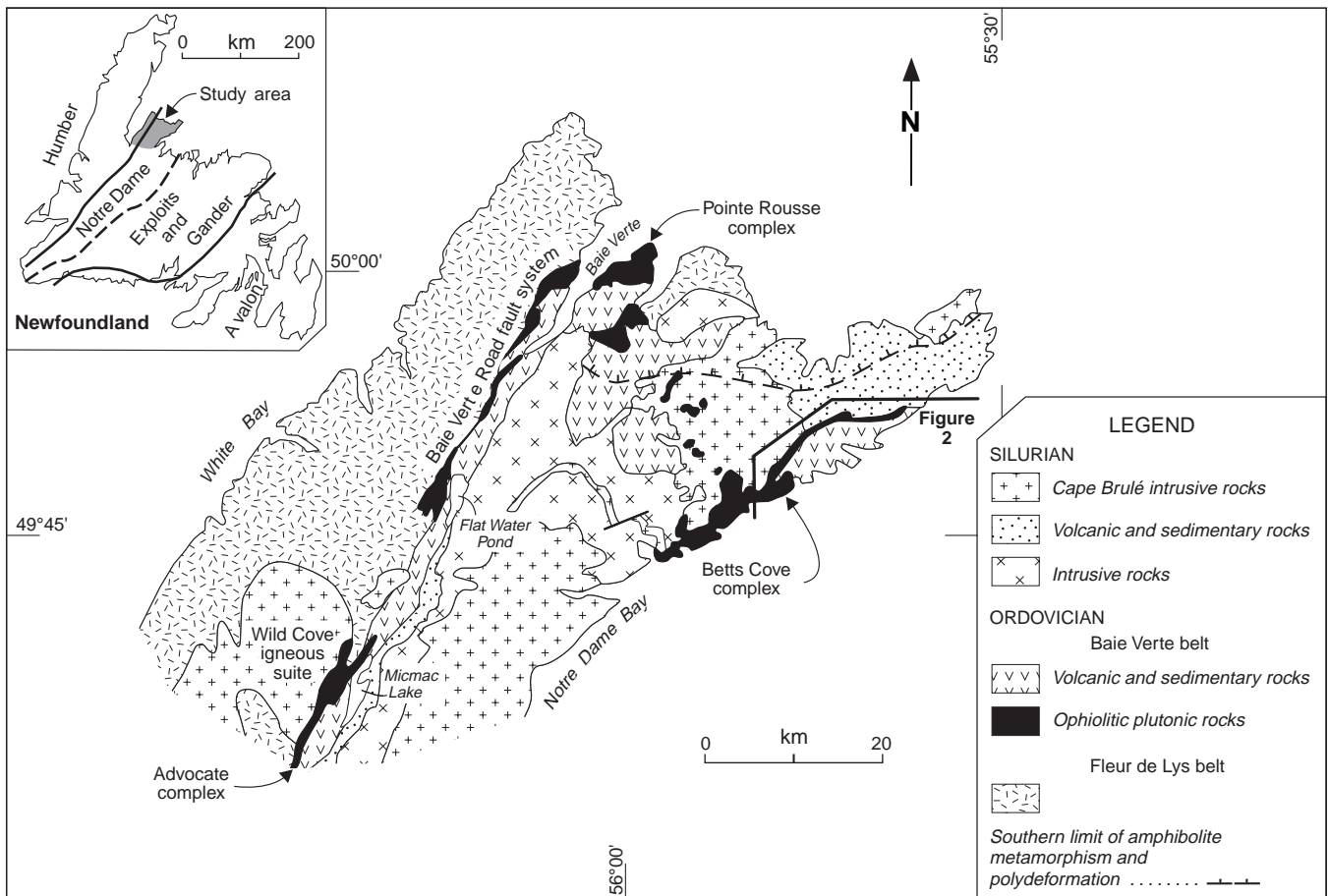


**Figure 1.** Tectonostratigraphic division of Newfoundland Appalachians focusing on the Baie Verte Peninsula (modified from Hibbard, 1983; Tremblay et al., 1997).

metamorphism traditionally ascribed to the Taconic Orogeny (Williams, 1979; Hibbard, 1983); but which have been reinterpreted as belonging to the Silurian Salinian Orogeny (Dunning et al., 1990; Cawood et al., 1994).

Humber and Dunnage zone rocks are separated by the Baie Verte fault zone (Fig. 1), part of the Baie Verte–Brompton Line. The Baie Verte–Brompton Line is a suture formed by overthrusting of continental margin rocks (Humber Zone) by oceanic terranes of the Dunnage Zone (Fig. 1). The Baie Verte–Brompton Line records ductile and brittle-ductile dip-slip and strike-slip shear from the Ordovician through to the Devonian (Goodwin and Williams, 1996).

Southeast of the Baie Verte–Brompton Line, the Baie Verte Peninsula comprises the following four principal associations.

- 1) A window of basement rocks correlative with the Humber Zone (Hibbard, 1982, 1983) known as the Ming’s Bight inlier.
- 2) Ordovician ophiolitic rocks and cover rocks (the Pointe Rousse, Nipper’s Harbour, Advocate, and Betts Cove ophiolitic complexes, and the Pacquet Harbour Group,

Fig. 1) that were accreted to North America during the Taconic Orogeny (Hibbard, 1983; Tremblay et al., 1997; Swinden et al., 1997).

- 3) Silurian fluvial conglomerate and sandstone, basaltic lavas, and felsic tuffs of the Cape St. John and MicMac Lake groups (Fig. 1) that unconformably overlie the different ophiolitic complexes, and which have been folded along northeast-trending axes in the Acadian Orogeny (Neale et al., 1975; Hibbard, 1983; Tremblay et al., 1997; Bédard et al., 1999).
- 4) Silurian and Devonian granitoid intrusions include the Burlington granodiorite, the Dunamagon granite, the Cape Brulé porphyry, and the LaScie intrusive suite (Hibbard, 1983; Cawood and Dunning, 1993; Kerr, 1997).

### Acknowledgments

Many people provided assistance in this study. Al Sangster’s initial involvement was via a GSC-Bitech Industrial Partners Project with the collaboration of Bill Hamilton and Jim Wade of Bitech. The 1994–1995 field seasons and analyses were financed through a Federal-Provincial Mineral Development

Agreement. The 1996 field season and analyses were financed through an Industrial Partenariat program between the Geological Survey of Canada and Noveder Inc., Sulliden Exploration Inc., and Ressources Dianor Inc.

A follow-up campaign in 1997 was funded through NSERC grants to Pierre Cousineau (UQAC) and by Marathon Oil through Giff Kessler. Scott Swinden, then of the Geological Survey of Newfoundland and Labrador (GSNL) provided much advice and documentation. The GSNL furnished some much appreciated logistical aid. Real Gosselin, Marc-Antoine Dion, Jean-Pierre Ricbourg, Isabelle Bélanger, and Marc Greendale produced the geochemical data. Jean-Claude Bérubé made the thin sections. Éric Boisvert and Christine Deblonde assisted with some much needed computer wizardry. Jean Dougherty provided advice on formation names. We also wish to acknowledge discussions and collaboration with the company personnel carrying out exploration and mining in the area, in particular we wish to thank Alain Morissette, Vincent Jourdain, and Pearce Bradley (Noveder Inc.); Robert Sansfaçon, Kirsten Oravec, Alain Berclaz, and David Morin (Groupe Conseil GesplAur); Jacques Trottier (Sulliden Exploration Inc.); and Steve McAlpine, Kevin Regular, and Alan Cram (Richmont Mines Inc.). Ray Coish, George Jenner, Benoit Dubé, Greg Lynch, and Michel Malo provided valuable comments. Charles Langmuir supplied software. Ginger Rogers, Peter Frampton, Joel Hickey, Barbara Fortin, Mark Piasecki, Maxime Tellier, and Kirsten Oravec assisted in the field. We also wish to thank the people of Tilt Cove, Snooks Arm, LaScie, and Nippers Harbour, who provided invaluable assistance as boatmen, woodsmen, and in recounting recollections and stories of early mining in the Tilt Cove area. In particular, we wish to thank Terry Rideout and Don Collins of Tilt Cove, Ray Wimbledon and Bob Jacobs of Snooks Arm, Ralph and Vida Short of LaScie, and Tanya and Paul Winsor of Nippers Harbour, who made our stay particularly memorable.

## METHODOLOGY AND REVISED STRATIGRAPHY

Field data were collected during the summers of 1994 to 1997, complemented by data from the literature (Snelgrove, 1931; Riccio, 1972; Upadhyay, 1973; DeGrace et al., 1976; Beischer et al., 1988), and air-photo interpretation, and by geochemical and petrographic correlations. Geochemical and mineralogical data were also compiled (*see below*).

The results of the new mapping and geochemical interpretation have forced us to revise the existing stratigraphy of the Betts Cove ophiolitic complex (Fig. 2, 3). Specifically, the supracrustal rocks that immediately overlie the plutonic section of the Betts Cove ophiolite are attributed to three new formations. The “Lower Lavas” of Coish (1977a, 1989; *see also* Coish and Church, 1979; Coish et al., 1982) are separated into two formations. The lowermost is directly associated with the oceanic crust, and we propose it be called the Betts Head Formation. Snelgrove (1931) used this name to refer to components of the sheeted dyke complex at Betts Cove. Since these dykes fed the overlying lavas and are strictly comagmatic with them (*see below*), we have extended

the name to the lavas themselves. We propose that the uppermost component of the “Lower Lavas” be called the Mount Misery Formation, and that this formation should be included in the Snooks Arm Group. We also include the “Upper Lavas” (and associated sedimentary rocks) of Coish (1977a, 1989) in the Snooks Arm Group, and we propose that these rocks should constitute the Scrape Point Formation. We now proceed with a systematic description of all the units of the ophiolitic complex and immediately adjoining rocks, after which we will present the geochemical data upon which the new tectonostratigraphic interpretations are based.

## FIELD AND PETROLOGICAL DESCRIPTIONS OF UNITS

The Betts Cove ophiolitic complex is constituted of the Betts Cove ophiolite, a relic of Ordovician oceanic crust (Riccio, 1972; Upadhyay, 1973; Dunning and Krogh, 1985), and its conformably overlying volcano-sedimentary cover sequence, the Snooks Arm Group (Hibbard, 1983).

### *Betts Cove ophiolite*

The preserved oceanic crustal section measures 4320 m (maximum stratigraphic thickness, Fig. 2, 3), though the apparent thickness is much less due to erosion of tilted fault blocks, and to superimposed extensional and compressional deformation. Six map units are recognized (Bédard et al., 1999; Fig. 4–7), 1) a zone of marginal serpentinite and talc-magnesite-carbonate schist, 2) layered cumulate rocks, 3) a late intrusive suite, 4) sheeted dykes, 5) a mixed lava-dyke unit, and 6) the Betts Head Formation lavas.

### **Serpentinite and talc-magnesite-carbonate schist**

A band composed of serpentinite and talc-magnesite-carbonate schist and mylonite extends along most of the northern margin of the massif (Fig. 2, 4–7). The rocks in the southeast appear to record several deformation episodes.

The serpentinitic rocks are phacoidally cleaved, are rusty-weathering, and are green or blue on fresh surfaces. They are dominated by serpentine, with minor magnetite and talc. Locally, they grade into peridotite or serpentinite mélange that contains lenses of less deformed metaperidotite.

Massive talc+magnesite+carbonate-rich metaperidotite lenses range from fist-sized knobs to domains hundreds of metres in size (e.g. east shore of Red Cliff Pond, Fig. 5), and are dominated by felty or prismatic pale blue talc. Euhedral magnetite octahedra (3–8%, 0.5–2 mm) may contain relict chromite cores. Euhedral, rhombic, honey-brown ankerite (10–30%, ~2 mm) may contain aggregates of fine-grained pyrrhotite. Ankerite is concentrated in and around veins, which also appear to have controlled the formation of minor cubic pyrite (up to 3 mm). Pyrite may contain blebs of chalcopyrite, and is rimmed by magnetite or hematite. Rarely, stubby prismatic orthopyroxene (30–60%, 2–8 mm) is pseudomorphed by fibrous bastite dusted with magnetite.



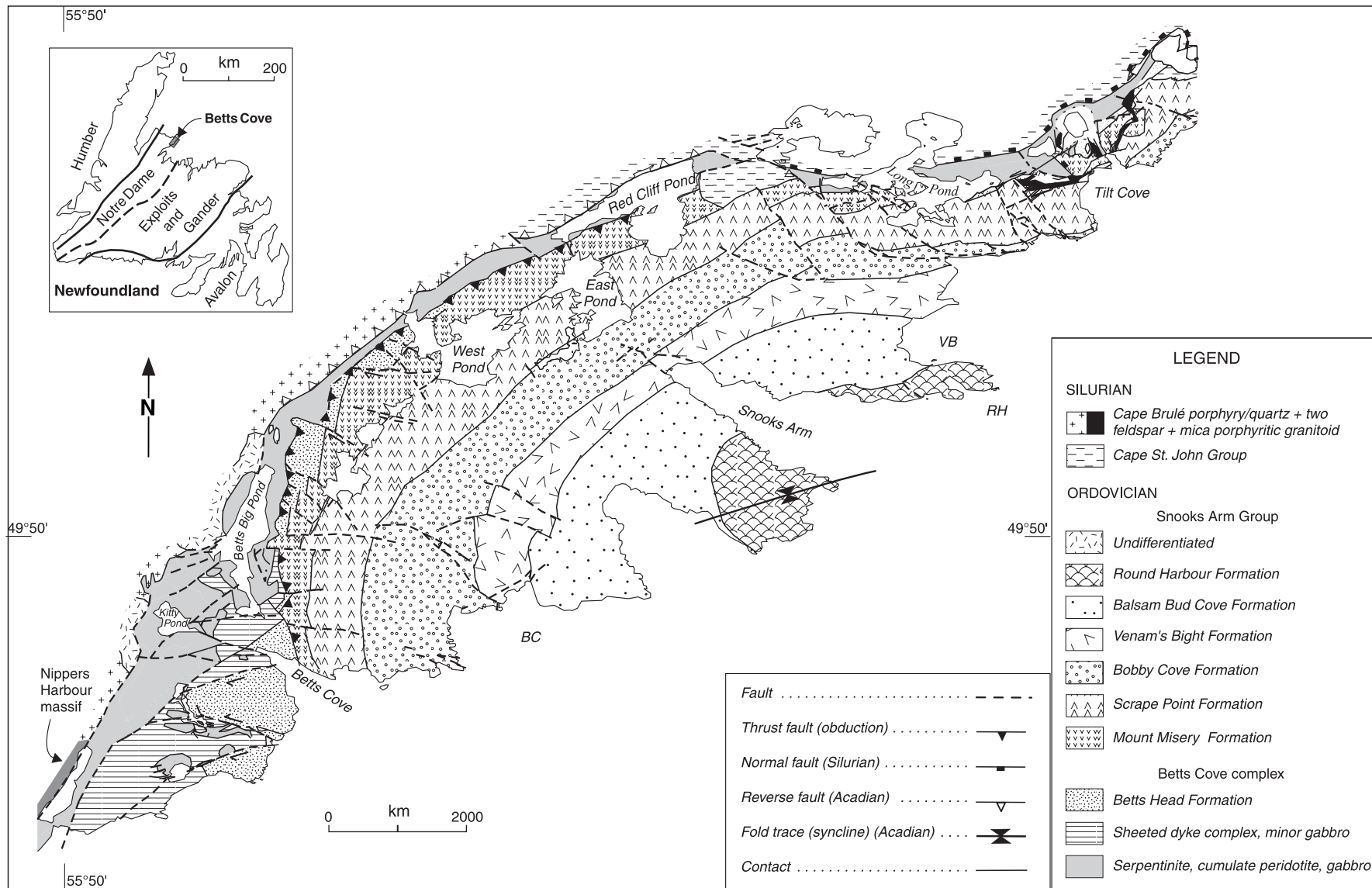


**Figure 2.** Simplified geological map of Betts Cove complex (modified from Fig. 1, Bédard et al., 1999). 'VB' is Venam's Bight, 'BC' is Bobby's Cove, 'RH' is Round Harbour.

Hydraulic breccia units on the shores of Long Pond (Fig. 5) contain angular fragments of serpentinized or massive metaperidotite, veined by carbonate-rich assemblages. Serpentinized olivine, relict poikilitic pyroxene (altered to carbonate), and minor (~3%) holly-leaf spinel with magnetite rims can be recognized.

### Layered cumulate rocks

Layered medium- to coarse-grained cumulate rocks form homoclinal sections up to 1 km thick (Fig. 4; Upadhyay, 1973), which are separated by sheared serpentinite and/or

peridotitic breccia zones. Bedding in cumulate rocks is inclined about 44° from bedding and flow contacts in overlying sedimentary rocks and lavas. The layered cumulate rocks that are adjacent to the sheeted dyke complex are typically intruded by Fe-Ti-oxide-bearing gabbronorite of the late intrusive suite. Rocks of both units are cut in turn by swarms of fine-grained dykes of the sheeted dyke complex (cf. Church and Riccio, 1974).

The cumulate rocks are organized into cyclic and rhythmic sequences (10–100 m thick, Upadhyay (1973)) that range from peridotite, to pyroxenite, to gabbronorite. Cumulate bedding in peridotite-dominated sections is typically 0.2–3 m

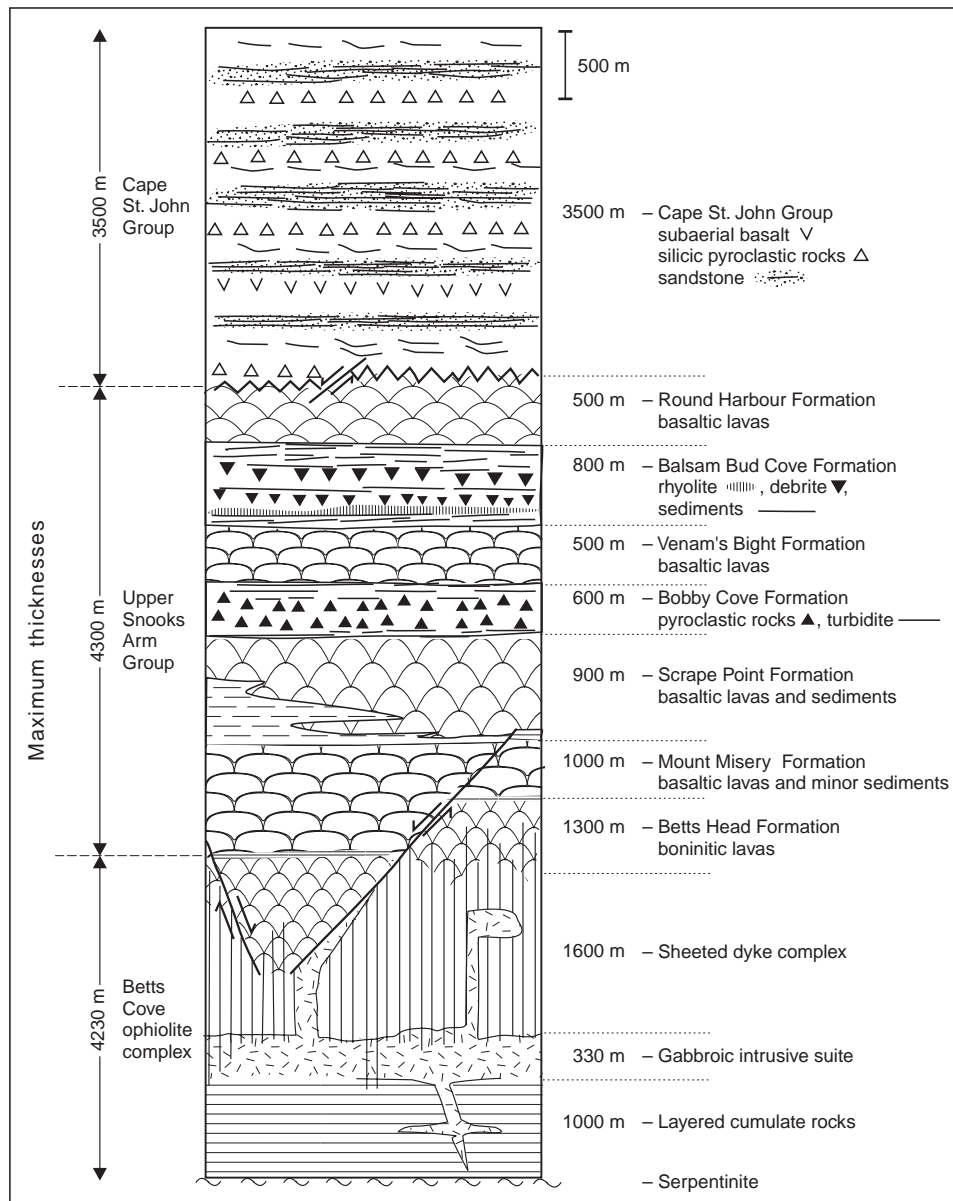


**Figure 3.** Schematic stratigraphic column through rocks of the Betts Cove ophiolitic complex, Snooks Arm Group, and Cape St. John Group (modified from Kessler and Bédard, 2000).

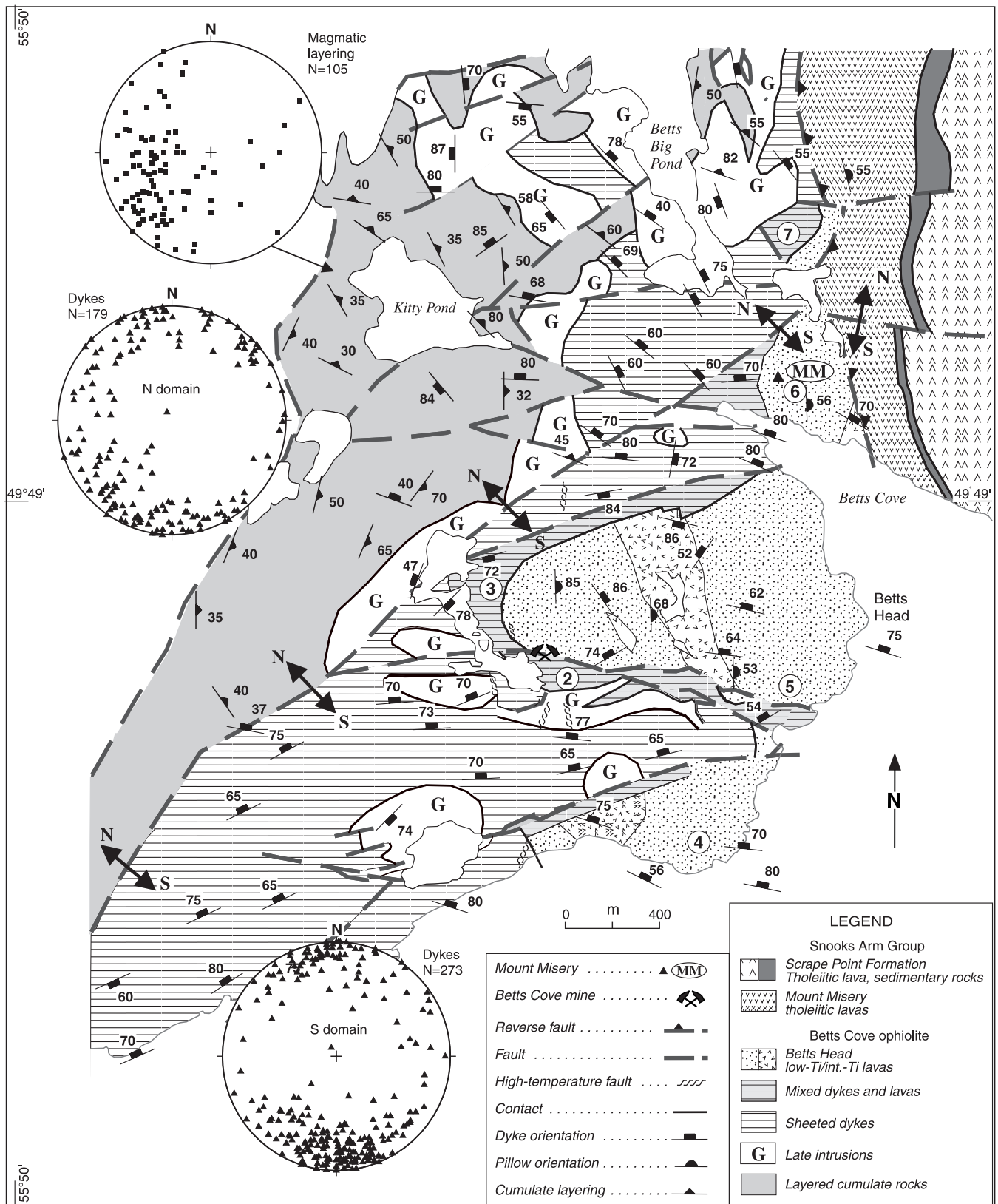


**Figure 4.** Simplified geological map of the Betts Cove mine and Mount Misery area (modified from Bédard et al., 1999). Equal-area stereographs show orientations of cumulate bedding and of dykes on both sides of the inferred décollement. Double-ended arrows point to northern and southern structural domains, respectively. Showings or mines: 2 = Betts Cove mine, 3 = Joey's Pond, 4 = Betts Head, 5 = Dolphin Cove, 6 = Mount Misery, 7 = Foot Pond. The Burton's Pond showing is immediately off the southwest part of the map.

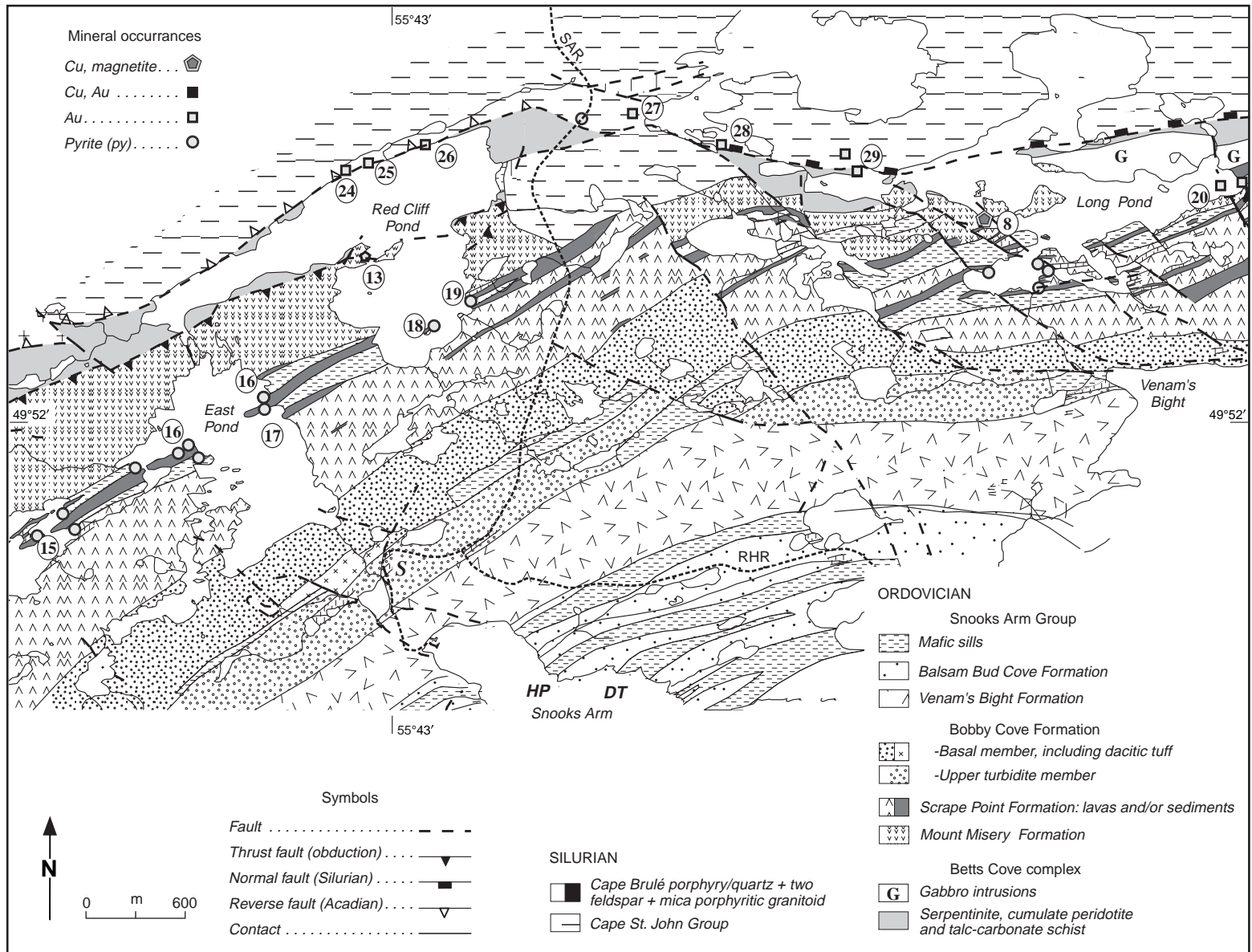


**Figure 5.** Simplified geological map of the Red Cliff Pond–Long Pond area (modified from Bédard et al., 1999). ‘S’ is the location of the section shown in Figure 18. ‘HP’ and ‘DT’ are the Haggis Point (Fig. 20) and Devil’s Splitting Table sections, respectively. SAR = Snooks Arm road; RHR is the Round Harbour road. Showings or mines: 8 = Nudulama; 13, 18 = Red Cliff Pond; 15 = West Pond; 16, 17 = East Pond; 19 = Low Water, 20 = Long Pond East, 24 = George, 25 = George Extension, 26 = Melange, 27 = Boneyard, 28 = Tom, 29 = Long Pond and Long Pond West.

thick. Rare dunite beds grade up to lherzolite. Beds composed of lherzolite (the most common type of peridotite) grade up into olivine pyroxenite and orthopyroxenite. The proportion of pyroxenite increases upwards in the section. Near the top of the unit, cumulate orthopyroxenite forms the base of 5 cm

to 3 m beds that commonly grade up through websterite to clinopyroxene-rich websterite, and locally to foliated gabbronorite near the top of the section. Beds are graded with respect to grain size and mode, and may display basal loading structures (up to 10 cm amplitude, 30 cm wavelength) that deform

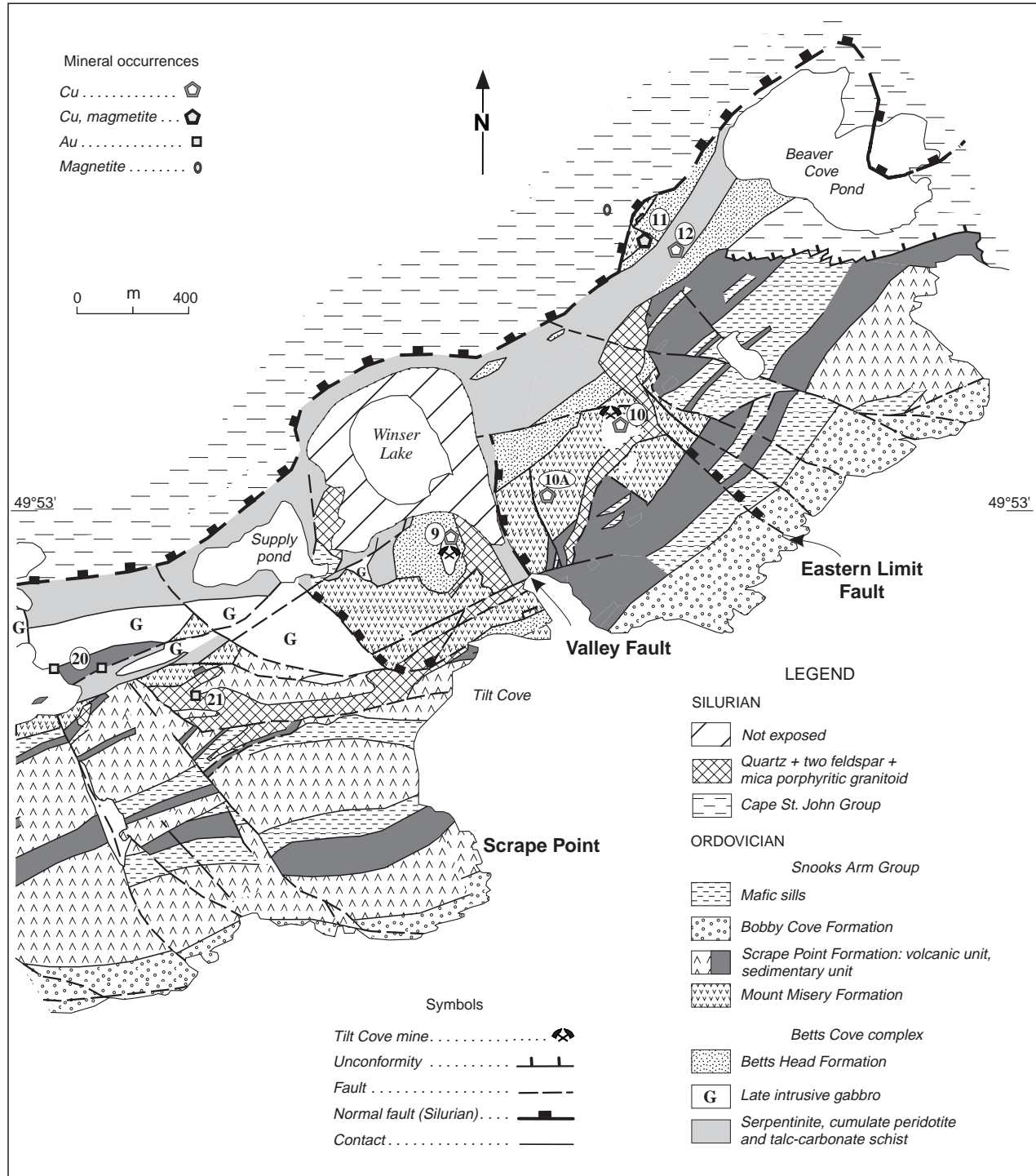


**Figure 6.** Simplified geological map of the Tilt Cove area (modified from Bédard et al., 1999). Showings or mines: 9 = Tilt Cove West mine, 10 = Tilt Cove East mine, 10A = A or Cliff zone, 11 = Beaver Cove, 12 = Mud Pond or Scrape, 20 = Long Pond East, 21 = Castle Rock.

the foliation of underlying gabbronorite. Clinopyroxene-rich websterite beds are commonly layered on a centimetre scale, with layering being defined by variations of grain size or mode. Some of the thicker gabbronorite layers contain orthopyroxenitic lenses of problematic origin.

Peridotite weathers orange to pale red. Orthopyroxenite units weather chocolate brown, brick red, or ivory, depending on the pseudomorphic phase that is present. Clinopyroxenite weathers green, whereas gabbroic rocks weather white or pale pink. Olivine is replaced by serpentine± talc. Orthopyroxene is replaced by talc-rich bastite or serpentine. Clinopyroxene is

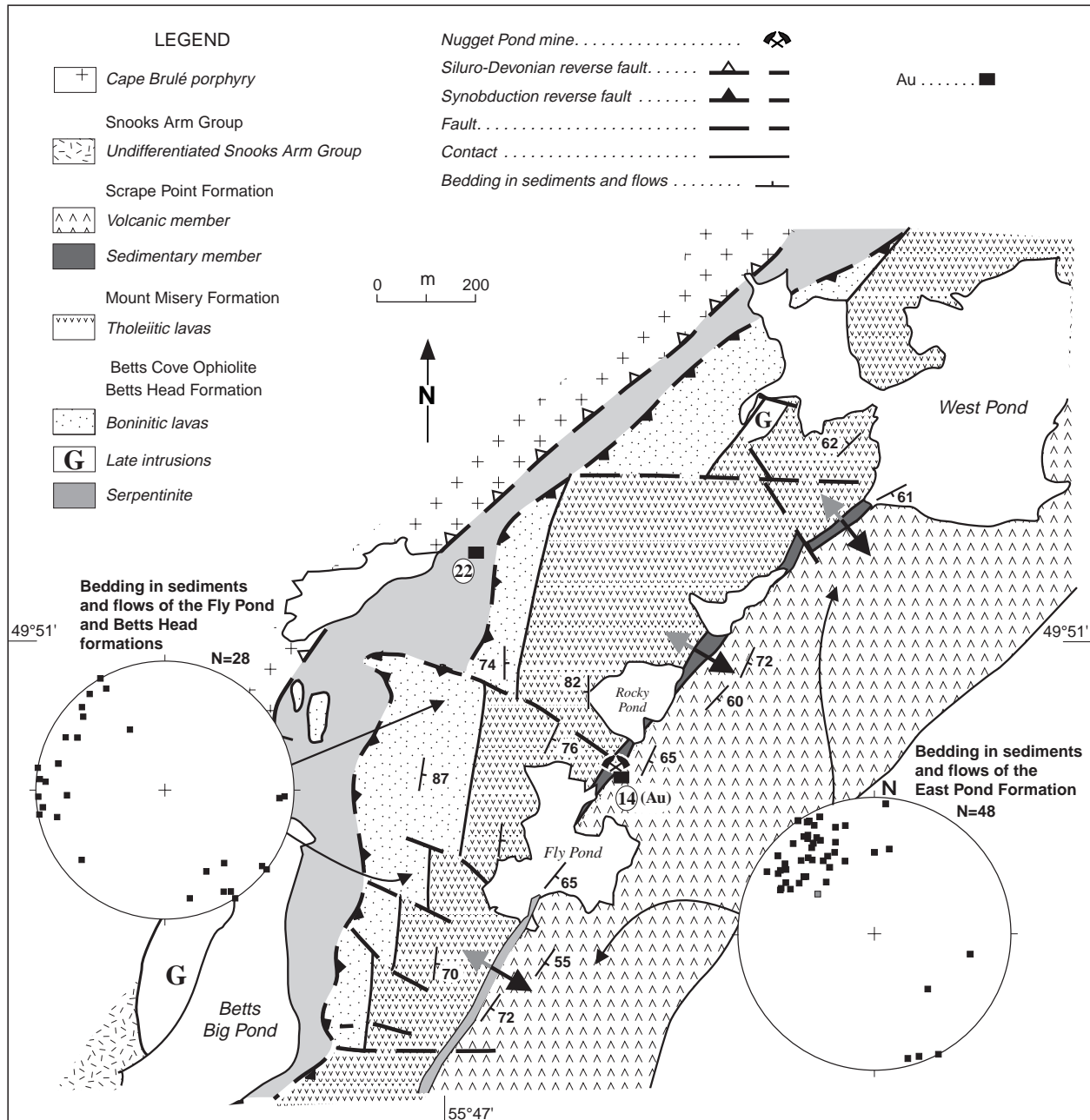


**Figure 7.** Simplified geological map of the area between Betts Cove and West Pond, illustrating how tilted fault blocks were eroded flat before deposition of Scrape Point Formation sedimentary rocks, and how the throw on normal faults decreases upsection (modified from Bédard et al., 1999). Equal area stereographs illustrate how bedding in Betts Head and Mount Misery Formation lavas are rotated relative to the paleohorizontal surface defined by bedding in the Scrape Point Formation. Showings or mines: 14 = Nugget Pond mine, 22 = Betts Big Pond.

commonly fresh, or is replaced by actinolite and chlorite. Feldspar is saussuritized or sericitized. Iron-titanium-oxide minerals are partly replaced by leucoxene. Euhedral chromite commonly has thin magnetite rims. Minor (~1%) disseminated pyrite±chalcopyrite is common.

Dunitic rocks range from true dunite to dunitic harzburgite. Cumulus olivine is equant (75–92%, 1–8 mm). Chromite (1–5%, ≤ 0.5 mm) is euhedral. Interstitial material (5–20%) is a mixture of serpentine and talc after (?) olivine and (?) orthopyroxene, with rare (?) clinopyroxene pseudomorphs.

Lherzolite contains 50–60% anhedral to subhedral cumulus olivine. Chromite (1–3%, <1 mm) is included in all other phases. Orthopyroxene (25–35%) commonly has a cumulus habit, with equant rectangular shapes (1–3 cm), but may also be interstitial or (rarely) be included in olivine. Cumulus orthopyroxene is typically crowded with olivine inclusions. Clinopyroxene (10–40%) is interstitial (<10 mm) or poikilitic (1–6 cm). Minor (1–3%) brown hornblende is common, and may be abundant (15%).

Olivine orthopyroxenite is dominated (20–60%) by coarse (1–5 cm) orthopyroxene pseudomorphs. Some also contain a few, distinctly larger, orthopyroxene grains that may represent accumulated megacrysts. Cumulus orthopyroxene is subhedral, equant or rectangular, and is aligned parallel to bedding. Oikocrystic to interstitial orthopyroxene is less common. Serpentinized cumulus olivine (10–50%) may be included in cumulus orthopyroxene. Clinopyroxene is interstitial or oikocrystic (~10–30%, 1 mm to 4 cm). Rare euhedral clinopyroxene (1–2 cm) may be present. Minor (1–2%, <1 mm) chromite is included in orthopyroxene.

Orthopyroxenite layers are similar to olivine pyroxenite units, differing by having less olivine (<10%) and more orthopyroxene (70–85%, 1 mm to 1 cm). Clinopyroxene is generally interstitial (10–25%, ≤ 1 mm), but up to 10% cumulus clinopyroxene (4–5 mm) may be present.

Typical websterite contains both cumulus orthopyroxene (50–75%, 0.5–4 mm) and cumulus clinopyroxene (25–50%, 0.2–1 mm). Clinopyroxene becomes increasingly euhedral and prismatic as its abundance increases. Larger cumulus clinopyroxene grains (2–5%) may contain inclusions of orthopyroxene. A few (3–20%) larger (2 mm to 1 cm) orthopyroxene phenocrysts containing inclusions of clinopyroxene may also be present. A well developed bedding-parallel mineral foliation is commonly present. Minor amounts of quartz (5%, <1 mm), brown hornblende (~1%) with green hornblende rims, and chromite (<1%) may be present.

Clinopyroxene-rich websterite layers are dominated by rounded to subhedral, weakly foliated clinopyroxene (50–65%; 0.1–0.5 mm, locally 1 mm), and have granoblastic or adcumulate textures. Cumulus orthopyroxene constitutes less than 50% (0.3–0.5 mm, locally 1 mm) of the rock. Minor (2%) feldspar may be present.

Interbedded cumulate gabbro-norite layers are dominantly composed of saussuritized plagioclase laths (50–70%, 1–2 mm). Some contain two feldspar populations — large, subrounded grains (3–4 mm), and smaller laths (1 mm). Equant to euhedral, prismatic, cumulus clinopyroxene (25–40% 0.1–5 mm) may be fresh. Subhedral to anhedral orthopyroxene (5–30%, 1 mm) is serpentinized. There are trace amounts of sulphide minerals, ilmenite, or leucoxene.

The layered cumulate rocks are cut by pyroxenitic, gabbroic, gabbro-noritic, and trondhjemitic dykes and sills that may coalesce into intrusive breccia (cf. Riccio, 1972). When traced along strike, conformable pyroxenite layers commonly jog up- or down-section by several metres, or join with discordant pyroxenitic intrusions.

Some graded beds have a different paragenesis (olivine+clinopyroxene) from the dominant series (olivine+orthopyroxene clinopyroxene) described above, and may represent intrusions derived from a different magma. One such bed has a base containing phenocrysts of olivine (20%, 2–8 mm) and clinopyroxene (<5%, 5–6 mm) in a fine-grained olivine websterite matrix, which grades up into a websterite with cumulus clinopyroxene (60%, 1 mm) and orthopyroxene (40%, <1 mm).

Clinopyroxenitic dykes contain abundant (75–90%) fresh, twinned, anhedral (interpenetration boundaries) to euhedral clinopyroxene (2–7 mm) and subordinate (15%) orthopyroxene. Wehrlitic dykes, some pegmatitic, are present locally. Gabbro-norite sills contain orthopyroxene phenocrysts (10–20%, 1–15 mm), in a finer grained gabbro-norite matrix containing minor quartz (5%) and Fe-Ti-oxide minerals. Trondhjemite dykes and sills are dominated by pale green aggregates of quartz and epidotized plagioclase, with partly altered, pale green clinopyroxene phenocrysts (5–10%, <0.5–3 mm), and minor Fe-Ti-oxide pseudomorphs.

## Late intrusive suite

### *Betts Cove area*

A series of intrusions in the Betts Cove area (Fig. 4) are composed of gabbro-norite to quartz-Fe-Ti-oxide gabbro-norite, with subordinate gabbro, olivine gabbro, hornblende diorite, and trondhjemite. Intrusive contacts with pyroxenite hosts are observed locally, and basaltic or pyroxenitic xenoliths may be present. These intrusions typically occupy the junction between the layered cumulate rocks and the sheeted dykes. Presumably the magmas from which they crystallized exploited the mechanical and density contrast represented by this interface. Dykes of wehrlite, clinopyroxene-rich pyroxenite, and gabbro-norite that cut layered cumulate rocks may also belong to this suite. A few feldspar-phyric gabbro-norite intrusions injected originally vertical breccia and shear zones that are discordant to layering in the cumulate rocks.

A high-level fault zone near Betts Head contains slivers (<100 m) of sheared websterite and peridotite that are petrographically similar to the layered cumulate rocks. Field

evidence is consistent with an origin either as tectonic slivers of layered cumulate rocks, or as intrusions emplaced along the faults.

Gabbroic intrusions attributed to the late intrusive suite were injected into the overlying sheeted dyke and lava units in places (Fig. 4). Most are 100–200 m wide (up to 400 m) anastomosing, originally steeply dipping sheets. Others are more plug-like. Gabbroic sheets envelop slivers of pillow lavas and fine-grained dykes, yet are themselves cut by dykes of the sheeted dyke complex. Crosscutting dykes become more abundant as the intrusion margins are approached, with a cutoff of 50% dykes being used to define the map units. Thin septa of gabbro within the sheeted dykes probably represent slivers detached from gabbroic intrusions by later dykes.

Porphyritic facies are common near intrusion margins. Common, square-sectioned, prismatic plagioclase phenocrysts (5–30%, 1–8 mm) are saussuritized, epidotized, sericitized, or silicified. Common, euhedral, prismatic clinopyroxene phenocrysts (1–10%, 1–3 mm) may be replaced by fibrous chlorite, actinolite, or hornblende. Coarser pyroxene+feldspar glomerocrysts (<2 cm), orthopyroxene phenocryst pseudomorphs, and Fe-Ti-oxide phenocrysts (1–3 mm) may also be present. The groundmass ranges from material indistinguishable from the common, red-weathering dykes of the sheeted dyke complex (*see* below), to gabbroic textures identical to those found in the cores of intrusions.

The cores of these late gabbroic intrusions contain prismatic, euhedral to interstitial clinopyroxene (30–50%, 0.5–4 mm, Fig. 8) and orthopyroxene (clinopyroxene: orthopyroxene ~35:15) or their pseudomorphs. Saussuritized plagioclase (40–60%, 1–5 mm) is interstitial or lath-like. Interstitial quartz and granophyric-textured quartz+(?)albite intergrowths (Fig. 8) are locally abundant (5–20%, 2–6 mm). Minor (1–2%, 1 mm) leucoxene after Fe-Ti-oxide minerals is ubiquitous; and some rocks contain as much as 15–20% of

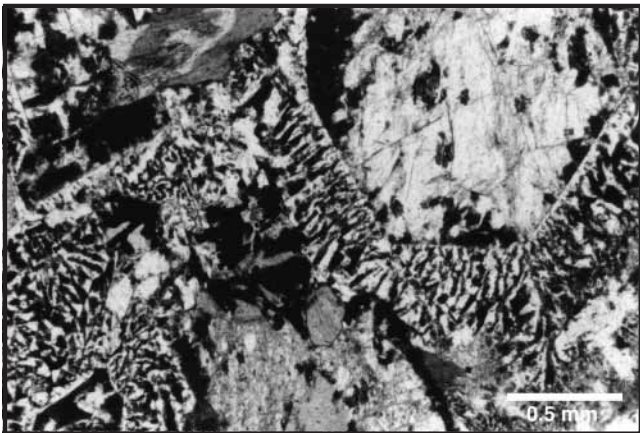


**Figure 8.** Plane light photomicrograph of a quartz-Fe-Ti-oxide-gabbroic rock (sample BC-96-297) sampled just north of Betts Cove. Note the abundant granophyric-textured interstitial quartz surrounding an euhedral clinopyroxene pseudomorph. Note also the relict magnetite-ilmenite grain, now a trellis-textured leucoxene.

such pseudomorphs. Minor (1–3%) disseminated pyrite, chalcopyrite, and pyrrhotite are common. Sulphide minerals are also associated with hydrothermal quartz veins. Minor secondary hematite may be present. Interstitial hornblende is generally related to hydrothermal alteration, but may also be igneous. Prismatic apatite may also be present.

#### *Intrusions near Long Pond and Tilt Cove*

A large, texturally variable body of gabbro is exposed along the north shore of Long Pond (Fig. 5), extending to the south of Supply pond (Fig. 6). This gabbro was dated by Dunning and Krogh (1985) at 488.6±3.1/-1.8 Ma. The dominant facies is a massive medium-grained gabbro containing stubby laths of sericitized plagioclase (average 1 mm); rare (<5%) plagioclase phenocrysts (4–5 mm); subophitic to intersertal clinopyroxene, replaced by chlorite+actinolite, or by pleochroic green-brown hornblende; rare prismatic pseudomorphs after (?)orthopyroxene; fine-grained interstitial leucoxene after Fe-Ti-oxide minerals (5–10%, 1–2 mm); and minor pyrite.

The massive gabbro facies give way locally to rhythmically interlayered (1–10 cm scale) medium-grained foliated leucogabbro, and coarser grained ferro-gabbro to feldspathic websterite. The leucogabbro contains crowded, foliated laths of plagioclase (60%, 3–4 mm) and about 35% interstitial clinopyroxene and orthopyroxene. The pyroxenitic layers contain less than 20% plagioclase and abundant, prismatic, euhedral orthopyroxene and clinopyroxene (1–10 mm).

Domains of igneous breccia are prominent south of Supply pond (Fig. 6). Clasts are composed of gabbro, websterite, or plagioclase±clinopyroxene-phyric basalt; the matrix is typical massive gabbro.

Crosscutting clinopyroxene+plagioclase-porphyritic basaltic dykes are common throughout the gabbroic rocks of the Long Pond area. Clinopyroxene phenocryst pseudomorphs (fibrous green hornblende) are euhedral prisms (4–10%; <7 mm, average 1–3 mm). Saussuritized plagioclase phenocrysts (5–20%, 1–3 mm) are euhedral laths, and may have sieved cores. The microdiabasic groundmass contains disseminated granular leucoxene (1–3%, <0.5 mm) with a few larger skeletal pseudomorphs (3 mm). Carbonate alteration products are locally abundant.

Hydrothermal vein systems cut both gabbro units and dykes. The oldest system contains hornblende+albite ±prehnite. These are cut by successively younger sets of prehnite+chlorite+(?)albite veins, albite±epidote veins, and then by a set of quartz veins. Locally, there are prominent hydrothermal breccia zones, with matrices of chlorite+prehnite, or hematite+calcite+epidote+quartz±sulphide minerals.

Discontinuous lenses of metagabbro embedded in the serpentinite mélange between Supply pond and Beaver Cove Pond (Fig. 6) probably represent tectonic slivers of the Long Pond gabbro. They are massive to weakly foliated, medium-grained (2–6 mm) gabbro and olivine gabbro, which are composed of plagioclase laths (60%, replaced by calcite



or saussurite), and interstitial, subophitic or euhedral clinopyroxene pseudomorphs (20–40%). Dark green to black, chlorite-rich pseudomorphs after olivine or orthopyroxene may also be present (5–15%). Minor leucosiderite after Fe-Ti-oxide minerals, interstitial quartz, and veinlets of siderite+cubic pyrite may also be present.

### Sheeted dykes

The sheeted dyke unit is very well developed in the Betts Cove mine area (Fig. 4), where it is about 1.6 km thick (stratigraphically) and 4.5 km wide (perpendicular to the dykes). Along most of its length, the contact between the sheeted dyke and cumulate units is a prominent north-east-trending lineament. Shear zones are observed locally along this northeast-trending lineament, which is interpreted to represent a ductile décollement structure. Parasitic shear zones with conjugate orientations occur higher in the stratigraphy, where they cut the sheeted dykes and late gabbroic intrusions, and appear to have controlled emplacement of amphibole-phyric and felsic dykes. The parasitic shear zones contain clinopyroxene and brown amphibole porphyroclasts (Fig. 9), indicating high-temperature, ductile deformation; however, most of this lineament (or décollement) is now occupied by plutons of the late intrusive suite.

East-trending dykes dominate south of the décollement (stratigraphically above it). North of the décollement (stratigraphically below it), dykes are harder to recognize, the sheeted complex is thinner, and dyke trends are more dispersed. Dykes intrude underlying layered cumulate rocks, indicating that the dyke complex is rooted in the plutonic section.

Unambiguous occurrences of sheeted dykes have not been recognized in the Tilt Cove area (Fig. 6), although locally abundant dykes within the Betts Head Formation lavas there may preserve portions of the dyke-lava transition zone.

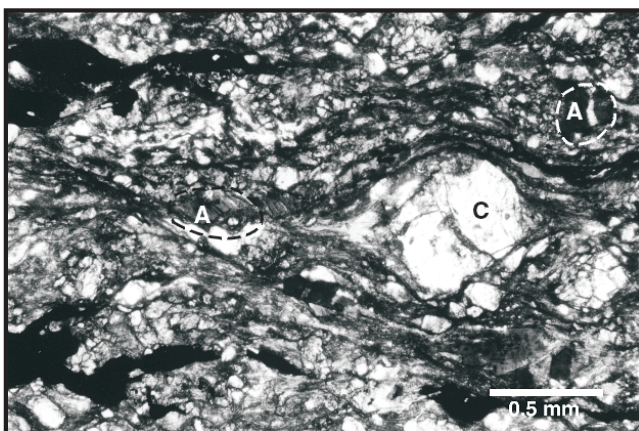


**Figure 9.** Plane light photomicrograph of a high-grade ductile shear zone (sample BC-95-508) from within the sheeted dyke complex on the south shore of Betts Head. The shear zone has a shallow paleodip. Note the clinopyroxene (C) and brown hornblende (A) porphyroclasts (apparent dextral movement indicated), and the ribbon-textured matrix.

The main sheeted dyke body south of Betts Cove (Fig. 4) is typically composed of 100%, 30–80 cm wide, planar to anastomosing dykes. Most dykes are pervasively transformed to greenschist-facies assemblages (chlorite+actinolite+epidote+titanite±quartz±sulphide minerals), but clinopyroxene and chromite relics may be present. Several locally dominant dyke types are recognized, but there is no consistency in the crosscutting relationships.

The most common dykes weather black or brick red, and are bright olive green to black-green on a fresh surface. Geochemical data (*see* below) imply that they are boninite, and we will refer to them as boninite dykes henceforth. They contain 1–10% of small phenocrysts (<5 mm). Sparse euhedral chromite phenocrysts (1–2%, 0.1–1 mm) are included in other phenocryst phases. Ovoid olivine phenocrysts are replaced by serpentine±calcite. Euhedral orthopyroxene phenocrysts are replaced by bastite, or serpentine after bastite. The dyke matrix has prismatic pyroxene (>60%, 0.2–1.5 mm) and interstitial feldspar+quartz (<30%). Calcium-rich clinopyroxene (pseudomorphed by actinolite) and orthopyroxene (talc, serpentine, and bastite pseudomorphs) prisms are both present.

Porphyritic dykes, referred to as “perknite” in the older literature, contain larger (1–10 mm) and more abundant (10–50%) phenocrysts of the same type as those found in the boninite dykes. Phenocrysts are generally concentrated into the centre of the dykes, and may define a flow lineation. Coish and Church (1979) proposed that the phenocrysts accumulated by flow differentiation. We consider the perknite to be a phenocryst-rich facies of the boninite dykes.

Some orange- to red-weathering dykes also contain plagioclase and clinopyroxene phenocrysts (<10%, 1 mm). Both the pyroxene prisms and the feldspar laths may be oriented parallel to dyke walls. Groundmass pyroxene prisms are embedded in anhedral and/or interstitial, lath-shaped or swallowtail plagioclase (≤ 1 mm) and minor (?) primary quartz (~3–5%). Minor pyrite is common.

Pink-weathering microgabbroic and ferro-gabbroic dykes represent the fine-grained margins of the intrusive gabbros described previously. Blue-green-weathering, sparsely phyric diabase dykes are dominated by clinopyroxene and feldspar. Some contain stubby octagonal prismatic clinopyroxene phenocrysts (~5%, 1–3 mm). Saussuritized plagioclase laths (~40%, 1 mm) can be randomly oriented or foliated parallel to dyke walls. Groundmass clinopyroxene (~40%, 1 mm) can be prismatic, interstitial, subophitic, or ophitic. Prismatic bastite pseudomorphs after (?) orthopyroxene are subordinate (~20%). Gabbroic or harzburgitic xenoliths (<1–4 mm) may be present. A few composite dykes have red-weathering olivine-phyric chilled margins and diabasic cores, suggesting a genetic link.

Rare, discordant, northeast-trending felsic and mafic dykes (2 m wide) have shallow paleodips relative to previously horizontal (determined on the basis of the orientation of sedimentary interbeds and lava channels in the overlying supracrustal rocks). The felsic dykes weather white or very pale green, with dark, waxy green or khaki fresh surfaces, and blackened or bleached alteration veins. They contain stubby,

pale green or white phenocrysts of carbonated feldspar (~2–25%, <1–3 mm); square- or oval-sectioned grey recrystallized phenocrysts of quartz (~2–10%, 1–3 mm); black, prismatic, recrystallized mafic (?) phenocrysts (~2%, 1–3 mm); and tiny oxide microphenocrysts (<1%).

Mafic dykes with shallow paleodips contain prismatic chlorite+calcite pseudomorphs after olivine and/or (?) orthopyroxene (~5–10%, 1–3 mm); glomeroporphyritic (?) plagioclase phenocrysts, pseudomorphed by calcite+epidote (5–6%, 1–3 mm); and euhedral, acicular, brown pleochroic hornblende phenocrysts (5–10%, 0.5–2 mm), with ovoid, brown hornblende cores (Fig. 10). The groundmass is panidiomorphic, with euhedral acicular brown hornblende in an anhedral quartz+feldspar matrix. Rare anhedral magnetite may be present. Groundmass hornblende swirls and wraps around clasts, but the crystals are not themselves deformed, implying an origin through magmatic flow. There are prominent (2–5%, 1–3 mm) euhedral pyrite cubes containing abundant silicate and rare chalcopyrite inclusions. Fine-grained chalcopyrite (~3%) is disseminated in the matrix. About 10–15% of the groundmass is composed of feldspathic ocelli, mineralogically similar to the normal groundmass, though coarser and richer in feldspar, and also containing alkali feldspar and euhedral pyrite.

#### Dyke-lava transition zone

Basal and upper contacts of the sheeted dyke complex south of Betts Cove are locally gradational. The gradational upper contact is a 50–200 m wide transition zone characterized by alternating dyke swarms (10–20 m wide) and septa of spherulitic pillows (2–5 m wide), and demonstrates that the overlying lavas are rooted in the sheeted dyke complex.

Just as commonly, however, the contact between the dykes and lavas is tectonic, consisting of low-temperature faults with steep paleodips. Lithological offsets imply normal

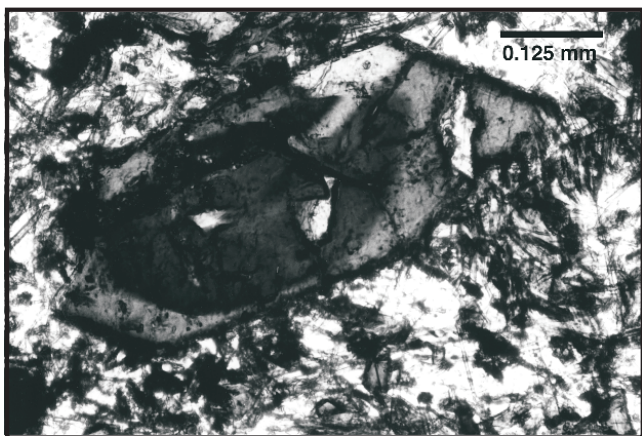


**Figure 10.** Photomicrograph, partially crossed nicols, of a zoned amphibole phenocryst with an ovoid, Fe-rich core, in a panidiomorphic groundmass rich in acicular amphibole. From a 1 m intrusion (sample BC-95-526) injected into a (paleo-) shallowly dipping fault beneath the Betts Cove graben.

paleomotions on these faults, and these high-level faults dissect the sheeted dykes and lavas into a horst-and-graben system (Fig. 4). Prominent fault-breccia zones are developed locally, and in places fault breccia is impregnated by igneous matrices, which implies that the faults predate obduction.

A magmatic impregnation in a fault breccia from the Betts Cove area that was examined in thin section, contains bastite pseudomorphs after (?) orthopyroxene phenocrysts (~3%, 1 mm), fresh clinopyroxene microphenocrysts (2–3%, 0.5 mm), and may also contain olivine phenocrysts, now pseudomorphed by chlorite. Its groundmass is composed of acicular to swallow-tail plagioclase, and prismatic orthopyroxene pseudomorphs in a turbid chlorite+epidote+actinolite-rich matrix, with minor disseminated magnetite and chalcopyrite. Thus, the impregnating magma was petrologically identical to typical sheeted dyke magmas, suggesting that faulting was synchronous with seafloor spreading.

Commonly, the fault zones are chloritized and contain minor sulphide minerals. The Betts Cove mine (mineral occurrence 2, Fig. 4) contains the largest amount of Cu-Zn-Au sulphide mineralization (Upadhyay and Strong, 1973; Saunders and Strong, 1986; Sangster et al., 1995) and is surrounded by a prominent albite-sericite alteration halo. The chloritized fault zones are commonly reworked by anastomosing, metre-wide, brittle-ductile, chloritic shear zones. The steeply dipping fibres in these structures imply reverse motions, a conclusion at odds with the apparent motion deduced from lithological offsets.

#### Betts Head Formation boninitic lavas

Along the spine and shores of Betts Head (the proposed type section), 1.3 km (stratigraphic height) of Betts Head Formation lavas are superbly exposed (Fig. 4). These lavas form the autochthonous cover of the ophiolite *sensu stricto*.

Betts Head Formation pillow lavas and flow tubes (10 cm to ~1 m) are hemispherical or round and most are spherulitic and sparsely phyrlic (2–10%, 0.5–3 mm). On fresh surfaces, devitrified pillow rims are black-green, with pale green spherulites (1 mm to 4 cm) appearing within 1–2 cm of the edge. The spherulites are characterized by dendritic clinopyroxene (now chlorite) and feldspar, suggesting a quench origin (Saunders, 1985). Internal drainage features are rare. Interpillow red chert is common. Thick bands (5–20 m) of pillow breccia are common, but whether individual occurrences represent hyaloclastite breccia, fault talus deposits, debris flows, or tectonic breccia is rarely evident.

The Betts Head Formation lavas can be divided into two petrological subtypes, a dominant olivine+orthopyroxene+chromite±clinopyroxene-phyric facies, and a locally prominent plagioclase+clinopyroxene-phyric facies. This petrological division corresponds exactly to the division into low-Ti and intermediate-Ti boninitic rocks defined by Coish and Church (1979) and Coish (1989, *see below*). In the interest of clarity and simplicity, we will henceforth refer to these Betts Head subtypes as low-Ti (olivine+orthopyroxene+chromite±clinopyroxene-phyric) and intermediate-Ti (plagioclase+clinopyroxene-phyric) boninitic rocks.

Geochemistry is the most reliable discriminant, since the two subtypes are almost indistinguishable in the field. Low-Ti boninitic rocks weather dark green to black. Intermediate-Ti boninite lavas weather slightly more orange-brown, and tend to form larger (up to ~1.5 m), more flattened pillows.

Among the low-Ti boninite lavas, olivine phenocrysts (chlorite±quartz±epidote pseudomorphs) dominate. Rectangular phenocrysts pseudomorphed by bastite with parallel extinction are interpreted to be after orthopyroxene. Rare clinopyroxene phenocrysts (Coish, 1977a) are partly or completely replaced by chlorite+epidote+actinolite. Euhedral chromite microphenocrysts occur as inclusions in other phenocrysts. Sparse amygdals have chlorite- or calcite-rich infills. The lava groundmass is generally rich in pale green prismatic or dendritic clinopyroxene (pseudomorphed by chlorite with actinolite overgrowths), prismatic (?)orthopyroxene pseudomorphs, interstitial plagioclase (albitized or epidotized), and quartz.

Among the intermediate-Ti boninite lavas, plagioclase and clinopyroxene phenocrysts and microphenocrysts (<10%, 0.5–3 mm) are common. Olivine phenocryst pseudomorphs and amygdals (<5%, <5 mm) may also be present. The groundmass is microdiabasic, with feldspar microlites and minor leucoxene+epidote granules (5–10%).

In the core of the Betts Head graben, intermediate-Ti boninite lavas form a coherent layer about 200 m thick (Fig. 4) sandwiched between thicker sections of low-Ti boninite lava, confirming that the intermediate-Ti lavas represent an integral part of the Betts Head Formation. At Mount Misery, an obduction-related fault has decapitated the section, which grades from low-Ti boninite at the base to intermediate-Ti boninite at the summit. The two subtypes are finely interbedded in the section northwest of Fly Pond (Fig. 7).

Corridors of breccia that originally had subvertical inclinations 1–10 m wide are common within the Betts Head lavas. They represent either synoceanic faults, or oceanic fissures infilled by debris. Some breccia corridors have hydrothermal matrices (epidote+chlorite), but axial low-Ti or intermediate-Ti boninite dykes and magmatic impregnations within breccia corridors are also common. A single occurrence of a tholeiitic intrabreccia dyke (assigned to the Mount Misery Formation) from Betts Head was discovered.

In contrast to the rather coherent packages of Betts Head lavas found in the western half of the ophiolite (Fig. 4, 7), occurrences of these rocks in the eastern half of the ophiolite (Fig. 5, 6) are extremely disrupted by several generations of faults, and are difficult to interpret as a consequence.

Two small, unmappable occurrences of Betts Head lavas in the Long Pond area are of the intermediate-Ti subtype. One is a 10 m wide domain of pillow lavas located on a small island in the middle of Long Pond (Fig. 5). This domain is embedded within a breccia zone which contains clasts and

(?)flows of tholeiitic basalt belonging to the overlying Mount Misery Formation. We interpret this isolated Betts Head pillow lava domain to be an olistolith.

A second occurrence is found within an igneous and tectonic breccia exposed along the extreme eastern shore of Long Pond (near mineral occurrence 20, Fig. 6). This breccia occurs stratigraphically above gabbro, although the contact itself is not exposed, and beneath sedimentary rocks of the Scrape Point Formation. The breccia is affected by intense chlorite+quartz+calcite±sulphide alteration. The breccia contains several types of clasts, including one with an Scrape Point Formation affinity, implying that these rocks were reworked during or after deposition of the Scrape Point Formation. Nevertheless, one of the clasts in this breccia has an intermediate-Ti boninite composition, and is veined by slightly coarser grained igneous material with a nearly identical composition, implying an initial stage of synmagmatic brecciation synchronous with Betts Head volcanism.

At Tilt Cove (Fig. 6), thin slivers of both low- and intermediate-Ti Betts Head lavas subtypes, as well as slivers of Mount Misery lavas, are caught up in the talc-serpentinite shear zone that bounds the Betts Cove ophiolite to the north. Pillow shapes, spherulites, and amygdals are recognizable, despite intense chloritization. Intermediate-Ti Betts Head lavas are interbedded with Mount Misery Formation lavas on the cliffside north of the Tilt Cove road (Hurley, 1982). At this location (mineral occurrence 11, Fig. 6) a thin band (~1 m) of red chert±magnetite-rich ironstone±massive sulphide minerals separates the Betts Head and Mount Misery lavas. The (?)marcasite+quartz+chalcopyrite-bearing sulphide beds are up to 15 cm thick. These relationships imply that sulphide exhalite deposits are associated with the transition from Betts Head to Mount Misery volcanism.

There is a fairly coherent block of massive low-Ti and intermediate-Ti Betts Head Formation lavas (possibly pillows and sheet flows) and rare dykes situated immediately beneath (stratigraphically) the main eastern and western lobes of the Tilt Cove copper-sulphide orebody (mineral occurrences 9, 10, and 10A on Fig. 6). The sulphide orebodies occur as replacements of breccia, which appear to represent a mixture of primary hyaloclastite, fault and talus breccia, and hydraulic breccia, all of which are cemented by quartz+calcite+hematite+epidote and locally, abundant sulphide minerals. The adjacent host rocks are intensely chloritized and carbonatized, and are cut by brittle chlorite±sulphide-bearing shear zones.

The rocks immediately underlying the West Pit orebody (mineral occurrence 9, Fig. 6) are heterolithic breccia units. Clasts of intermediate-Ti boninite dominate, but fragments of gabbro are also present, suggesting an origin as a fault talus deposit. This particular breccia was injected and impregnated by intermediate-Ti boninite magma (Fig. 11) that chilled at the clast contacts. Plagioclase microphenocrysts in the impregnations are aligned parallel to the contact and get coarser and more abundant away from it.



**Figure 11.** Talus breccia with an igneous matrix (intermediate-Ti boninite suite) at Tilt Cove. Photograph by J. Bédard. GSC 2000-005A

The East Pit orebodies (mineral occurrences 10, 10A on Fig. 6) are situated very close to the Betts Head–Mount Misery transition, but most of the clasts in the wall rocks have chemical signatures characteristic of the Mount Misery Formation, with one diabasic clast having a composition more similar to typical Scrape Point Formation lavas (*see below*).

The situation is equally problematic for the West Pit orebodies, since the upper contact is a steeply dipping fault, now occupied by sheared and chloritized bodies of Silurian quartz-feldspar porphyry. This fault separates the mineralized breccia of the West Pit from an overlying band (~200 m thick) of Mount Misery Formation tholeiitic lavas, which are also dissected by the quartz-feldspar porphyry intrusions and faults. Upsection, immediately to the south, a thin band (~3 m) of sheared red mudstone and green sandstone separates the tholeiitic lavas from another sequence (~100 m thick) of Betts Head intermediate-Ti lavas. Above this is yet another complex breccia zone that contains both tholeiitic and boninitic clasts. A spectacular outcrop of this breccia is visible by boat about 200 m west of the Tilt Cove dock. Here, there are large (1–10 m) olistoliths of pillow basalt with interpillow red chert, embedded in an epiclastic matrix.

Due to the lack of way-up criteria and structural complexity of the Tilt Cove area, we cannot ascertain if this complicated succession of tholeiitic and boninitic lavas is due to successive eruptions of different lava types, whether it is a structural repetition, or whether we are simply looking at unusually large clasts of diverse affinity in a very thick talus deposit.

### **Snooks Arm Group**

The Snooks Arm Group (Hibbard, 1983) is subdivided into six formations (Fig. 3), the first two of which are new and documented here. These are the Mount Misery (1 km), Scrape Point (900 m), Bobby Cove (600 m), Venam's Bight (500 m), Balsam Bud Cove (800 m), and Round Harbour (500 m) formations.

### **Mount Misery Formation tholeiitic lavas**

The proposed type section for the formation is the prominent barren ridge that extends north from Mount Misery towards Fly Pond (Fig. 2, 4, 7). In the field, the lavas of the Mount Misery Formation are difficult to distinguish from Betts Head Formation lavas. Geochemistry is the most reliable method. In the Mount Misery area (Fig. 4), the base of the section is an east-dipping thrust fault that Tremblay et al. (1997) attributed to ophiolite obduction. In the section northwest of Fly Pond (Fig. 7), the contact zone with the underlying Betts Head lavas is a breccia of uncertain origin (possibly fault or hyaloclastite). In the Tilt Cove area (Fig. 6), Mount Misery lavas are interbedded with Betts Head lavas, demonstrating a subconformable depositional relationship.

#### *Southwestern area*

In the southwestern half of the map area, Mount Misery Formation lavas consist of well formed spherulitic pillow lavas and flow tubes, intercalated with thick (5–20 m) pillow-breccia layers. Thin bands of laminated green chert contain minor sulphide minerals. Northwest- to southwest-trending corridors of breccia (2–40 m wide) commonly contain axial mafic dykes, and may correspond to marked offsets in the stratigraphy, indicating that they are synoceanic normal faults. The faults separate a series of tilted (30° from inferred previously horizontal) blocks (Fig. 7). Most breccia fragments in the fault zones are angular, but some clasts display conspicuous flattening parallel to the walls of the fault zones. Some fault zones are transformed to chlorite+albite -rich greenschist-facies assemblages, suggesting considerable hydrothermal throughflow. Pillow lavas between closely spaced breccia corridors have a cracked appearance, with red-weathering oxidized cores and green-weathering reduced rims.

Basal Mount Misery Formation lavas are composed of primitive olivine+clinopyroxene-phyric basalt. Olivine phenocrysts (<10%, 1–3 mm) are pseudomorphed by chlorite. Euhedral clinopyroxene phenocrysts (<1–3%, 3 mm) are partly replaced by chlorite+epidote±quartz. Amygdales (<1–10%, 3–5 mm) are filled with calcite+epidote+ quartz+chlorite+hematite. The groundmass is composed of actinolite after clinopyroxene in a chlorite+epidote-rich devitrified glass matrix. Minor disseminated pyrite (less than about 5%, up to 1 mm) may have hematite rims.

The primitive basal Mount Misery Formation lavas grade up to more evolved, iron-rich, sparsely amygdaloidal (<1–5%, 1 mm), plagioclase+clinopyroxene-phyric lavas. Euhedral, lath-shaped plagioclase phenocrysts (1–15% 0.5–4 mm) are sericitized, carbonated, epidotized, or silicified and/or hematized. Euhedral prismatic clinopyroxene phenocrysts (2–10%, 0.5–3 mm) are partly replaced by chlorite+actinolite. The groundmass is commonly microdiabasic, with plagioclase laths and interstitial to prismatic clinopyroxene (partly replaced by chlorite+actinolite). Heavily altered samples are composed of chlorite+actinolite+epidote+calcite+titanite+hematite+quartz+(?)albite assemblages.

Euhedral to interstitial, fine-grained, magnetite-ilmenite intergrowths (~10–15%) are partly replaced by leucoxene+epidote. Minor (less than about 2%, 1–2 mm) anhedral disseminated pyrite and/or pyrrhotite is rimmed by magnetite.

Interpillow and intrapillow epidosite and related alterations comprise mixtures of quartz+calcite+chlorite+epidote+pyrite as replacements or veins. There are also zones of diffuse replacement by aggregates of quartz+calcite+muscovite+albite+chalcopryrite+pyrrhotite.

The uppermost Mount Misery Formation lava flows are commonly magnetic, with a characteristic dark grey to black colour on the fresh surface, very dark brick red on the weathered surface, and may be interbedded with red chert and ironstone. They contain up to 20% magnetite-ilmenite, and may be associated with magnetite+hematite-filled breccia.

Near Mount Misery, the magnetic lavas grade into a zone of pervasive hematization 50 m thick and 1 km long that is surrounded by a halo of hematite-rich veins that variably replace the epidote-rich pillow lavas. The core of the hematized zone is massive, brick red metamorphosed lava, in which it is still possible to recognize small chlorite+epidote-filled amygdalites (5%, ~1 mm), laths of calcite+quartz+sericite+epidote after plagioclase phenocrysts (~5%, 1–2 mm), pseudomorphs after (?)clinopyroxene phenocrysts (~5%, 1–2 mm), and microdiabasic groundmass textures. Concentrations of hematite form against calcite+quartz veins. Minor malachite and muscovite may also be present.

An intrabreccia dyke sampled from within Betts Head Formation lavas on Betts Head has a Mount Misery affinity. This dyke contains subhedral pseudomorphs after feldspar phenocrysts and glomerocrysts (~3%, 2 mm) and fresh euhedral clinopyroxene microphenocrysts (5%, 0.5–1 mm, *see* Table 2), some of which are sector zoned. The microdiabasic groundmass of this dyke contains brownish clinopyroxene, interstitial plagioclase, and rare opaque granules.

#### *Northeastern area*

Northeast of East Pond, the Mount Misery Formation is thinner (Fig. 2, 5, 6), and the well formed pillows give way to a complex of altered massive flows, breccia zones, rare pillows, and sill-like intrusions. Pillows have spherulitic margins that grade into cores with randomly oriented feathery dendrite (~1mm long) or square-sectioned plagioclase grains. The more massive lavas may represent granular-textured sheet flows (1–2 m thick), or possibly subvolcanic sills. Massive lavas can be aphyric, olivine-phyric, or plagioclase+clinopyroxene-phyric, and are locally amygdaloidal. Plagioclase phenocrysts and glomerocrysts (5–15%, 1–4 mm) are euhedral and intensely sericitized. Microphenocrysts (~2–3%, <0.3 mm) of (?)clinopyroxene are chloritized. The groundmass is typically diabasic, with plagioclase laths (<1 mm), interstitial to subophitic pyroxene

(chlorite or actinolite pseudomorphs), and equant oxide microphenocrysts (<3%, partially replaced by leucoxene). Flecks of pale leucoxene (<0.5–5%, 0.1–0.3 mm) are common, as is minor pyrite (2–5%).

Where alteration is particularly severe, the igneous assemblages are completely replaced by carbonate or chlorite, with abundant veinlets of grey microcrystalline quartz+calcite. Larger veins of chlorite+calcite, epidote, pyrite, and hematite are common. Some rocks contain platy specular hematite (~3%), which is coarser in chlorite-rich veins. The most iron-rich lavas have as much as 80% opaque minerals (magnetite+hematite mostly), partly concentrated into veinlets.

In many places, these massive and pillowed lavas are embedded in breccia, and in some places massive lava appears to entirely surround irregular lensoid breccia pods. It is not clear if these are foundered flow-top breccia, or whether the massive ‘flows’ were injected into the breccia and represent subvolcanic sills. Some domains are heterolithic, containing boninitic olistoliths. Other domains resemble conglomerate with rounded to angular cobbles of metaperidotite and metabasalt (Fig. 12), in what appears to be a pebbly sandstone matrix which includes chromite grains. The presence of detrital chromite and metaperidotite clasts implies that ultramafic cumulate or perhaps mantle rocks were exposed on the seafloor, presumably by major extensional faults similar to the northeast-trending décollement exposed in the Betts Cove area (Fig. 4). We therefore interpret most of the breccia and conglomerate of the Mount Misery Formation in the Long Pond area (Fig. 5) to be synvolcanic fault-talus deposits, with eruption of Mount Misery lavas occurring synchronously with movement along the faults and mass wasting. Essentially all of the complex breccia exposed on the cliffs east of Winsor Lake (Fig. 6) are of Mount Misery affinity also, and we attribute the same fault talus deposit origin to them.



**Figure 12.** Talus breccia in Mount Misery Formation containing basalt and peridotite clasts in a sandy matrix; from an island in Long Pond. Photograph by J. Bédard. GSC 2000-005B

## Scrape Point Formation, Sedimentary Member

In the southwestern part of the map area, the Sedimentary Member is thin and is restricted to the base of the formation. Northeast of East Pond, the proportion of the Sedimentary Member increases markedly and sedimentary rocks are not restricted to the formation's base.

### *Southwestern area*

Southwest of East Pond, the Sedimentary Member forms a single, thin basal package deposited on an shallowly dipping erosional unconformity. Locally, coarse cubic auriferous pyrite is abundant (*see below*, Nugget Pond mine, *see also* Swinden et al., 1990; Sangster et al., 1994). The outcrop pattern of the sedimentary rocks is very linear between West Pond and Betts Cove, bevelling a series of tilted fault blocks (Fig. 7). These faults offset the Mount Misery–Scrape Point formation contact (<30 m) substantially less than they do the Betts Head–Mount Misery formation contact (~100 m, Fig. 7). Both of these mapped offsets are very much less than the inferred throw along the normal faults separating the Betts Head lavas from the sheeted dykes (>1 km, Fig. 5). The upwardly decreasing throws along the same structures imply that these are syndepositional growth faults. In places, there are tight intraformational folds in the sedimentary rocks. Some of these may be slumps. Others might have developed as fault blocks tilted during extension and sedimentation. Alternatively, the folds may be related to Acadian orogenic compression, with strain being absorbed by the thin metasedimentary unit sandwiched between the relatively rigid masses of pillow lava to either side. Purple-silver or black phyllitic schist composed of mixtures of quartz, sericite, magnetite, chlorite, and stilpnomelane form adjacent to gabbroic sills, probably by contact metamorphism.

The sedimentary package is divisible into lower red and upper green clastic units. The red clastic unit is, in turn, divisible into a laterally discontinuous lower basal breccia or conglomerate (subunit a), a magnetic sandy to conglomeratic subunit (b), a brick red clastic subunit (c), and an upper interlaminated brick red and green clastic subunit (d) transitional into the upper green clastic unit. The last commonly contains a basal, dark green sulphidic horizon (subunit e) that is overlain by medium to light green, finely laminated and graded sets of turbiditic and/or tuffaceous sandstone and siltstone (f). Not all of these subunits are present everywhere, and there are marked facies changes along strike, particularly in the basal subunits.

The base of the sedimentary sequence is very complex and is commonly referred to as an iron-formation for the sake of simplicity. Near the Nugget Pond mine it is 3–5 m thick though it can reach 18 m elsewhere. The chaotic basal breccia or conglomerate (subunit a) contains clasts of Mount Misery Formation pillow basalt and chert that are cemented by magnetite-hematite ironstone and cherty quartz. The second subunit (b) ranges from sandstone to conglomerate. It contains clasts of bedded sedimentary rocks cemented by chert and quartz, locally with abundant euhedral magnetite. The lack of lateral continuity of these two subunits suggests sedimentation

took place in small, fault-bounded subbasins. The third subunit (c) is a very fine-grained, dark red siltstone that contains abundant, very fine-grained magnetite, typically concentrated into laminae. The lowest part of the fourth subunit (d) consists of an aphanitic, red, massive to very thinly laminated mudstone composed of quartz and chlorite with feldspar and sericite (XRD analysis) and an evenly distributed hematite matrix that is only moderately magnetic. The proportion of sandy beds increases upwards. The sandstone beds may contain millimetre- to centimetre-scale clasts, mainly of basalt. Near the top of the red succession, the coarser sand-sized sediment component is mainly green, resulting in a banded red and green sequence. The reddish mudstone interbeds are locally enriched in magnetite.

Near the Nugget Pond mine, the upper green metasedimentary unit consists of two subunits (e and f). The rocks directly overlying the red clastic rocks (subunit e) are distinctive in that there are abundant layer-parallel bands of sieve-textured pyrite and pyrrhotite (~15% to locally submassive sulphide). There are local concentrations of magnetite. The sedimentary rocks are typically dark green, commonly weakly to moderately foliated, with small-scale deformation structures, and are composed of chlorite, muscovite, quartz, and carbonate.

The upper and thickest portion of the green clastic unit (subunit f) is a sequence of grey-green-weathering tuffaceous sandstone-siltstone-mudstone turbidite units forming Bouma A or B to E(t) sequences. Individual beds range up to about 0.5 m in thickness. The pebbly volcaniclastic sandstone beds are generally normally graded and massive, whereas the siltstone units exhibit fine laminations. The colour of individual sedimentary beds is principally a function of grain size, with sandstone being darker green, siltstone lighter green, with a transition to tan or sometimes red in the finest mudstone. The coarser clasts in the sandy facies indicate derivation from a basaltic protolith. The pyrite content is always much less than 1%. The contact between the green sedimentary rocks and the overlying basalt may be slightly sheared, with an associated increase in the proportion of secondary pyrite, epidote, and magnetite.

Immediately southwest of Fly Pond (Fig. 7), magnetic pillow lavas and pillow breccia of the Mount Misery Formation are overlain by a 30 cm thick sequence (subunit a) containing angular cobbles of basalt, red chert, and ironstone, all of which are cemented by veins (1–5 cm) of massive, breccia-textured, colloform, or laminated magnetite+hematite. Goethite laminae (1–3mm wide) and spherules are contorted. Stilpnomelane needles and quartz+epidote veins are also present. Above the conglomerate is more than 3 m of thinly laminated, silicified red mudstone or chert containing magnetite-rich laminae (subunit c). Locally, the chert is brecciated, with a breccia fill of chert or magnetite. The basal ironstone and chert units are succeeded upsection by sequences of grey-green laminated to massive siltstone (subunit f).

Further to the southwest, the base of the member is well exposed in only a few places. Here, altered magnetic pillow lavas of the Mount Misery Formation are directly overlain by thin-bedded tuffaceous green siltstone and sandstone, and

magnetite-rich red chert and ironstone interlaminated on a 1–5 cm scale (subunit d). This contact is offset by small normal faults, oriented parallel to the main block faults, and with the same sense of motion.

East of the Nugget Pond mine as far as East Pond (Fig. 5, 7), the basal sedimentary sequence is characterized by a relative paucity of the brick red siltstone that hosts the Nugget Pond deposit. Maroon siltstone is more common instead.

A coarse basal conglomerate (subunit a) is exposed on a small island near the western shore of West Pond (Fig. 7). Here there are rounded cobbles (10–60 cm) of pillow lava, some with fragments of red chert still attached, in a magnetite-rich matrix. The dark green metabasalt clasts contain silicified plagioclase phenocryst pseudomorphs (~15%, 1 mm), euhedral prismatic clinopyroxene phenocrysts (~10%, 1 mm, replaced by chlorite+epidote), and rare amygdals, in a carbonated groundmass with abundant (10–15%) fine-grained euhedral magnetite. Petrographically, these cobbles resemble the upper, Fe-rich facies of the Mount Misery Formation.

Pyrite, with minor associated stilpnomelane, is abundant between the west end of West Pond and the Low Water occurrence (mineral occurrence 19, Fig. 5) on the east shore of Red Cliff Pond. The pyrite occurs both as irregular grains and as 0.5–1 cm cubic crystals similar to pyrite at the Nugget Pond mine, although they are not auriferous. In the area between West Pond and the East Pond peninsula the pyrite is spatially associated with filamentous quartz+feldspar veins, except on the south shore of the northwest arm of East Pond, where massive bull quartz veins are present (mineral occurrence 16, Fig. 5).

Along the eastern shore of East Pond, Mount Misery Formation pillow lavas are sharply truncated by the basal Scrape Point Formation unconformity. The first sediment deposited here is a massive (50 cm bed), dark brown, magnetite-rich, conglomeratic sandstone (subunit b). Depressions in the irregular pillow lava substrate are occupied by 1–10 cm sized red chert cobbles, probably interpillow material derived from the underlying Mount Misery Formation. Overlying magnetite-rich sandstone beds are laminated or banded on a millimetre to centimetre scale. Other beds are massive or graded. Magnetite-rich layers (up to 80%) are dark brown. Pale pink layers contain as little as 5% magnetite. Magnetite is euhedral (0.1–1 mm), and is separated by yellow-red stilpnomelane prisms and needles (10–80%, 0.1–2 mm), intergrown with chlorite and sericite (Fig. 13). The magnetite-rich bands are irregular and anastomosing, and locally form discordant veins. Magnetite-rich veinlets are composed of faceted crystals of magnetite±(?)ilmenite, associated with concentrations of sulphide minerals, stilpnomelane needles, and chlorite clots. Other layer-parallel veins contain stilpnomelane +quartz+sericite. There are several other vein types containing mixtures of quartz, platy to fine-grained sericite, calcite, chalcopyrite, a low-reflectance anhedral (?)magnetite with chalcopyrite inclusions, dusty anhedral pyrite (0.1–1 mm), prismatic stilpnomelane, a white mica, and (?)hematite. Some samples have been affected by late sulphidation, with the formation of pyrite rims on magnetite crystals. Others

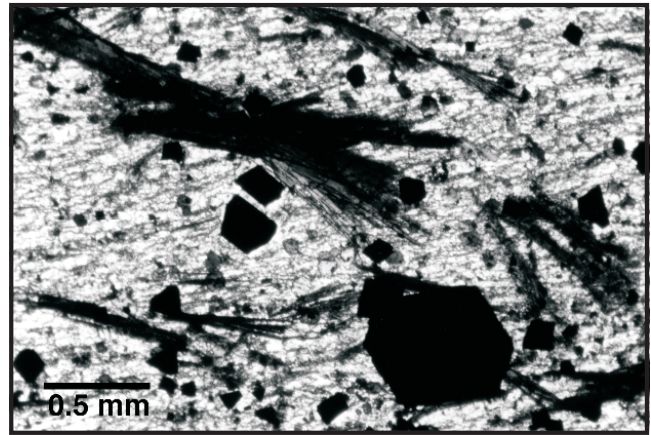


**Figure 13.** Plane light photomicrograph of Scrape Point Sedimentary Member, basal ironstone at East Pond (stratigraphically below showing 16, Fig. 5). Note the euhedral magnetite grains (black), and the prominent stilpnomelane needles in a sericite-rich groundmass.

have unusual concentrations of hematite (50–70%), with isolated, larger, euhedral grains of hematite that contain small pyrite inclusions. Abundant (~15–20%) randomly oriented needles of well cleaved, colourless, low-birefringence (?)actinolite may be present.

Interbedded shale (subunit c) and massive laminated quartz-hematite-rich mudstone contain minor groundmass magnetite, and are cut by quartz+epidote reduction veins along which euhedral pyrite cubes (5–8%, 1–8 mm) are developed. The pyrite contains euhedral epidote prisms and chalcopyrite as inclusions, and has magnetite+hematite rims, testifying to a subsequent oxidation event. These relationships indicate the action of superimposed oxidation-sulphidation events, and a porosity control on pyrite deposition.

The morphology of magnetite, and the common occurrence of Fe-oxide veins and breccia fills, appears inconsistent with a detrital origin for the ironstone of the Scrape Point Formation. A volcanogenic exhalite origin seems more probable. This also suggests that the iron-rich magnetic upper facies of the Mount Misery Formation may have been enriched in iron by reaction with the exhalite, and does not represent a primary ferrotholeiite magma.

#### *Northeastern area*

Northeast of East Pond, the Sedimentary Member is not restricted to the base of the formation (Fig. 5, 6). Sedimentary rocks may occur anywhere in the sequence as thick packages (>10 m), or as thin interbeds (<1 m) intercalated among lavas and sills. The metasedimentary packages thicken and become more numerous northeastwards. East of Tilt Cove (Fig. 6) the Sedimentary Member predominates over the Volcanic Member. Intra-formational folds are common. Folds are well exposed on an ephemeral island (low water only) on the south shore of Long Pond (Fig. 5). The fold axes are injected by ferrodolerite intrusions, which appear to be synkinematic,

suggesting that at least some of the folds are responses to block rotation and the concentration of slip in the weaker sedimentary members.

To the northeast of East Pond, the Scrape Point Sedimentary Member is principally composed of green turbiditic to tuffaceous sandstone and laminated siliceous siltstone, with minor conglomerate and ironstone. The green laminated siltstone units may contain round pyritic spherules (0–30%, 1 mm). Conglomerate lenses are up to 3 m thick, and contain angular clasts (up to 70% clasts, 3–30 cm, angular to ovoid). Most clasts are composed of sandstone, with subordinate proportions of red or white chert, green or oxidized metamorphosed lava, and fragments of foliated tuffaceous siltstone (4–5 cm), all in a feldspar-rich tuffaceous sandy matrix. The green sandstone occurs as massive beds (5 cm to 1 m), locally with pebbly bases that grade up into finer grained laminated sandstone and siltstone, and then into mudstone. Some of the mudstone is red and/or purple and/or black and rich in magnetite. The sandstone commonly contains grains of bright red (?) chert, volcanic lithic fragments (some with euhedral hornblende inclusions), flattened glass shards, fragments of sericitized or saussuritized plagioclase, partly altered clinopyroxene and hornblende, and with minor quartz and magnetite. Some of these sedimentary rocks are tuffaceous, others are more conventional epiclastic turbidite units. Grains commonly show a good bedding-parallel foliation and some look flattened.

Some of the green sedimentary rocks are clearly tuffaceous. In one case a massive bed of lapilli tuff (15 cm thick) is interbedded with normally graded green sandstone (1–20 cm thick), and thin-bedded, laminated (2 mm to 1 cm), waxy-green siltstone. The lapilli tuff bed contains a bimodal clast population, with 30% of 1 cm round lapilli, and 30% of compositionally identical 1–3 mm lapilli. The rounded lapilli are composed of amygdaloidal porphyritic andesitic rocks and contain both abundant, randomly oriented, sericitized, lath-shaped plagioclase microphenocrysts (0.5 mm), and rare equant chlorite prisms pseudomorphous after (?) clinopyroxene microphenocrysts. These clasts closely resemble typical Bobby Cove Formation juvenile pyroclasts (*see below*), both petrographically and geochemically. The foliated (bedding-parallel) leucocratic tuffaceous matrix of this bed is rich in prismatic chlorite+epidote pseudomorphs after crystal fragments of (?) clinopyroxene, turbid pseudomorphs after crystal fragments of plagioclase, and small andesite fragments.

As in the southwestern half of the study area, the base of the Sedimentary Member in the north is commonly composed of red mudstone and siltstone (locally pyritiferous and auriferous), magnetite and stilpnomelane-bearing sandstone, and massive hematite+magnetite ironstone. Interbedded lavas are commonly Fe-rich and magnetic. However, the northern magnetic-metalliferous sedimentary rocks may be found anywhere in the sequence, and the regular progression of subunits (a to f) breaks down completely. Some of these magnetic sandstone beds are normally graded, with the proportion of stilpnomelane needles increasing upwards (to ~10%, 0.5–1 mm) as the proportion of clasts decreases. East of Tilt Cove, secondary stilpnomelane is common in all

facies, including lavas and gabbroic intrusions. Pyrite is fairly common but is rarely auriferous, except at the outlet bay of Long Pond (Long Pond East showing, mineral occurrence 20, Fig. 6), and in the Castle Rock showing (mineral occurrence 21, Fig. 6), which are described in the 'Mineral deposits' section.

### Scrape Point Formation, Volcanic Member

Scrape Point lavas are commonly amygdaloidal and plagioclase-porphyritic, have pale groundmass colours, and generally do not contain prominent hyaloclastite or breccia corridors. They are Fe-Ti-rich tholeiitic basalt which is very different from the underlying Mount Misery lavas.

Northeast of East Pond, the lower half of the formation is dominated by interbedded metasedimentary rocks and massive sheet flows (2–5 m thick), which commonly have pillowed or gently lobed tops or bases. These flows are easily misidentified as sills or tuffs in the field. Most contain clinopyroxene phenocrysts (2–5%). Fresh clinopyroxene phenocrysts are euhedral, concentrically zoned, pale brown in thin section, with darker rims. Clinopyroxene may be replaced by chlorite+calcite, or actinolite±pyrite±epidote. Plagioclase phenocrysts (<3–5%, up to 20%; 1–4 mm, up to 1 cm) are euhedral, may be aligned, can have sieved cores, and are commonly glomeroporphyritic, locally being intergrown with clinopyroxene. Plagioclase may be replaced by chlorite with quartz rims, by albite+epidote, or sericite+calcite+quartz, rimmed by epidote and pyrite. One flow contains (~20%) oval to round clasts of granular (?) leucogabbro. Amygdaloids are common (2–5%, 3–4 mm), and contain chlorite±calcite±quartz±epidote±pyrite infills. The microdiabasic groundmass is pale grey-green and crammed with acicular to lath-shaped plagioclase pseudomorphs (~45–60%, 0.5–1 mm). Interstitial, subophitic or prismatic groundmass clinopyroxene (40–45%) is generally replaced by chlorite+epidote. Fresh groundmass clinopyroxene is zoned, pale brown, and pleochroic. Fine-grained Fe-Ti-oxide minerals are ubiquitous (5–10%) and are typically replaced by leucoxene. Some flows are magnetic and contain more Fe-Ti-oxide minerals (15–20%, 0.5 mm), both interstitially and as euhedral microphenocrysts, locally with well preserved trellis ilmenite-magnetite exsolutions. Magnetic flows are typically dark grey and are commonly associated with sedimentary ironstone. Interstitial pyrite (1–3%) may be sieved and platy, or rimmed by magnetite, and is commonly associated with veins and pools of quartz+chlorite+epidote+calcite.

Northeast of East Pond, the basal sheet flows grade up into a section dominated by pillow lavas, although rare sheet flows do occur among the pillows. Southwest of East Pond, the basal sheet flows are essentially absent and the entire section is composed of pillow lavas. Typically, pillows are hemispherical, about 0.5 m in diameter, with rare drainage channels. Some areas have pillows that are significantly smaller (0.2 m) or larger (2 m). Pillows may be extremely difficult to recognize in lichen-covered outcrops because of the thinness of their hyaloclastite rims. Most pillows are slightly plagioclase+clinopyroxene-phyric and amygdaloidal, but



plagioclase-porphyritic facies containing up to 50% plagioclase phenocrysts (up to 2 cm) are prominent locally. The lowermost pillow lavas south of East Pond tend to be slightly spherulitic, and may contain small proportions of olivine phenocryst pseudomorphs (2–15%, 1–3 mm) replaced by chlorite+calcite. Euhedral, lath-shaped plagioclase phenocrysts (2–20%, 1–4 mm) are commonly glomerocrystic, and may be intergrown with clinopyroxene or (?)olivine phenocrysts. Some plagioclase phenocrysts are concentrically zoned with epidote or pyrite inclusions in their core. Clinopyroxene phenocrysts are less abundant (~1–5%, 0.5–4 mm), occurring as stubby euhedral sector-zoned prisms, partially to completely replaced by epidote+chlorite. The groundmass is generally pale grey-green (locally charcoal grey) and aphanitic, with numerous small dendrite crystals. Pillow margins are almost entirely composed of devitrified glass, with rare microlites and small amygdales. Plagioclase microlites are the most common, but clinopyroxene microlites (some fresh, pale brown), and skeletal chains of Fe-Ti-oxide granules (5–10%, replaced by leucoxene), are also common in some lavas. Pillow cores are commonly microdiabasic. Amygdales (1–3%, 1–3 mm) and veins are filled with mixtures of chlorite, pyrite, pyrrhotite, chalcopyrite, calcite, epidote, hematite, quartz, and rare actinolite. Some pillows contain more and larger amygdales (~20%, 1–10 mm). Some pillowed flows contain a few gabbroic or spherulitic basalt clasts (<6 mm).

### **Bobby Cove Formation, Basal Member (tuff)**

The Basal Member of the Bobby Cove Formation is composed of sequences of interbedded, tuffaceous volcanoclastic conglomerate and tuff-breccia flow, mafic to felsic lapilli and ash tuff-turbidite units, and rare basaltic to andesitic lava flows. These rocks were deposited on an erosional unconformity with minor relief. Synsedimentary growth faults are ubiquitous. Feeder dykes are present locally. Sedimentological aspects are described in more detail in Cousineau and Bédard (1998, 2000).

The tuffaceous conglomerate and tuff breccia form compound flow units more than 100 m thick which extend more than 1 km along strike. Individual flow units are generally less than 5 m thick, but some of them are at least 50 m thick. Individual tuffaceous conglomerate beds may have reverse-graded bases, with up to 60% boulder-sized fragments in the centre of the flow unit. Clast imbrication is common (Fig. 14), indicating flow towards the south. The upper part of conglomeratic flow units commonly grade up into lapilli tuffs with similar clast types, and then into finer tuffaceous turbidite deposits.

The tuff-breccia flow units are nearly monogenic, being dominated by clasts of porphyritic basalt, basaltic andesite, and andesite (Fig. 14). Some clasts were still soft when they were deposited, and are moulded against the shapes of underlying clasts. Many have well defined chilled crusts surrounding amygdaloidal-porphyritic cores. In places, these crusts are stretched into contorted tails, suggesting that the clasts were once volcanic bombs. In some beds most of the crusts have been partly shattered, giving the false impression of a bimodal clast population, and making clasts look more

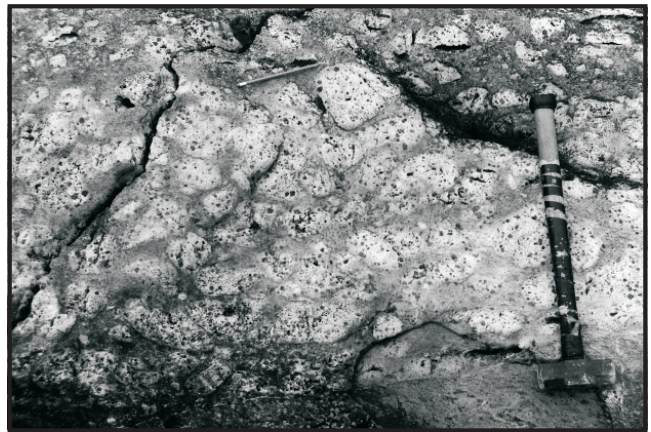


**Figure 14.** Typical subaqueous blocky welded tuff from the Bobby Cove Basal Member. All of the clasts are pyroxene+amphibole+plagioclase-phyric vesicular andesite. The matrix is a crystal tuff containing the same types of crystals, together with flattened devitrified glass shards. Sledgehammer handle is perpendicular to bedding, pencil shows orientation of imbricated clasts. Photograph by J. Bédard. GSC 2000-005C

angular. The matrix is a crystal-lithic-vitric tuffaceous sandstone composed of the same material that makes up the clasts. We interpret these deposits to be pyroclastic debris flows.

The dominant lava clast type is an amygdaloidal clinopyroxene+hornblende+plagioclase-porphyritic basaltic andesite (Fig. 14). Coarse, euhedral, prismatic clinopyroxene phenocrysts (10–15%; 3–5 mm, up to 1 cm) are partly replaced by actinolite+chlorite±calcite. Pyroxene phenocrysts are commonly intergrown with oxide phenocrysts (replaced by leucoxene) and may contain fine-grained disseminated sulphide minerals. Euhedral, diamond-shaped hornblende phenocrysts (<10%, 1–10 mm) are commonly aligned, and may also be intergrown with oxide phenocrysts. Amphibole is brown-black on a fresh surface, pleochroic and khaki-brown or tan in thin section. Igneous hornblende is partially replaced and overgrown by mixtures of actinolite, epidote, calcite, and titanite. Sericitized plagioclase phenocrysts (~10–15% 0.5–4 mm) occur as euhedral laths. Amygdales are common, variable in abundance (0–30%, 1–3 mm), and are filled with mixtures of quartz, chlorite, calcite, sericite, epidote, pyrite, and albite. Amygdales in some lapilli become more flattened and smaller towards the margin of clasts, with concentric fabrics, suggesting that the clasts were still hot and plastic when they were deposited. The igneous groundmass of these andesitic clasts is massive, pale grey-green, with small amygdales (5–50%, 0.5–1 mm), and microphenocrysts of plagioclase, (?)clinopyroxene, and leucoxene.

Other tuffaceous conglomerate sequences appear to be more epiclastic in character. These contain a much more diverse clast population, including porphyritic andesite, microlitic andesite pumice, hornblende+plagioclase+clinopyroxene+magnetite-phyric dacite, red siltstone or chert, schistose feldspathic hornblendite, hornblende

pyroxenite, and epidotized metabasalt. One deposit contains extremely large (>2 m) tabular to convoluted rafts of bedded crystal tuff (10–30 cm thick), which may represent rip-up clasts. Metre-sized basaltic clasts locally disrupt underlying bedded tuffs and appear to record ballistic impacts.

Dacitic clasts are locally prominent, and weather white, pale pink, or pale green. Fresh surfaces are waxy dark brown or green, bleached to white during hydrothermal alteration. Dacite can occur in both tuffaceous-textured (resedimented) and igneous-textured (massive plutonic or subvolcanic) variants. One spectacular deposit contains large (<2 m), composite basalt+dacite clasts. In these, the igneous-textured dacite forms angular jigsaw-puzzle breccia cemented by porphyritic basalt.

Igneous-textured dacite has stubby, square-sectioned, concentrically zoned, euhedral plagioclase microphenocryst and glomerocryst pseudomorphs (5–20%, 1–3 mm). Euhedral wedge-shaped to acicular hornblende phenocrysts (~10%, ~2 mm) are dark brown on a fresh surface, dark brown-tan-green pleochroic in thin section. They are partly altered to green actinolitic amphibole and may contain clinopyroxene cores. Leucoxene microphenocrysts (1–2%, <1 mm) also occur as inclusions in amphibole. The groundmass is very fine grained. Euhedral cubes of pyrite (1–2%, <1 mm) are associated with quartz+epidote veinlets. Tuffaceous dacite clasts resemble the dacite tuff described below.

The tuffaceous conglomerate units are interbedded with sequences (up to 100 m) of tuff-turbidite. These range from sets of massive, normally size-graded, medium-grained, thickly bedded (10 cm to 2 m) volcanogenic, tuffaceous sandstone (Fig. 15, 16), to packages (~10 cm to 1 m) of laminated (1–5 cm) volcanoclastic siltstone-ash deposits. The medium-grained tuffs may form loading structures in the underlying, finer grained ash deposits. The thinly laminated ash deposits may disaggregate in response, forming a population of fine-grained clasts in the overlying sandstone beds. Imbrication of these rip-up clasts is common. Globular devitrification structures are locally prominent.

The tuffaceous sandstone beds contain a mixture of lithic fragments (15–20%), crystal fragments (20–60%), and flattened lenses (10–25%) of turbid brown material (white in hand specimen) which are interpreted to represent devitrified glass shards. Some glass shards have multiple prongs and contain euhedral plagioclase or clinopyroxene microphenocrysts (Fig. 15, 16). The presence of glass shards and devitrification structures imply a pyroclastic origin for many of the tuff-turbidite sequences.

Lithic fragments can be subrounded, angular, or platy. The most common are amygdaloidal basaltic to andesitic metamorphosed lava clasts (10–50%) and scoria (Fig. 16). These can be aphyric or porphyritic, with sericitized or saussuritized plagioclase laths (<50%), euhedral clinopyroxene prisms (partly replaced by chlorite+ actinolite), feldspar microlites, and brown-green hornblende. Other lithic clast types include silicified red siltstone; fuchsite (<4 mm); foliated plagioclase-pyroxene-rich crystal-lithic tuffs (1–3mm grain size) which are indented by adjoining

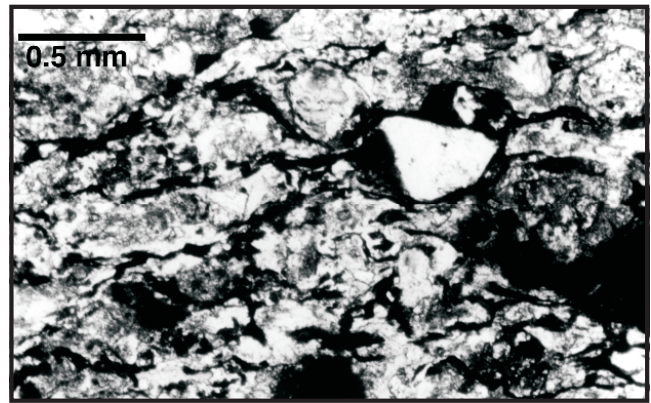


**Figure 15.** Plane light photomicrograph of welded subaqueous tuff of the Bobby Cove Basal Member (sample BC-95-89). Note the flattened devitrified glass shards (dark), some with enclosed euhedral feldspar crystals (white).

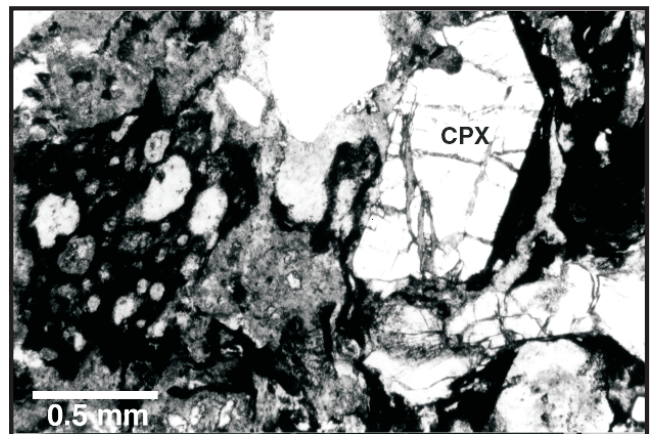


**Figure 16.** Plane light photomicrograph of welded mafic subaqueous tuff of the Bobby Cove Basal Member (sample BC-95-389). Note the devitrified glass (dark) that coats the euhedral clinopyroxene (CPX). On the left is a feldspar-phyric scoria fragment.

pyroxenite clasts; clinopyroxenite (<5%, 1–4 mm); and hornblendite with euhedral, rhombic-prismatic, tan-pale brown pleochroic hornblende.

The most mafic of the tuff-turbidite sandstone sequences contain abundant fragments of angular to platy clinopyroxene (10–20%, 0.2–3 mm) (Fig. 16), either fresh or partly altered (chlorite and/or actinolite). More leucocratic tuff-turbidite sequences are dominated by angular, rounded, or euhedral plagioclase pseudomorphs (10–30%, 0.5–3 mm). Quartz (<5%), rare opaque grains (oxide or sulphide minerals), and rare green hornblende crystal fragments may also be present.

Thin (<3 m), pink- or green-weathering, graded felsic tuffs are subordinate, and may represent subaqueously deposited ashfalls of felsic eruptions. They contain square or embayed phenocrysts of quartz (1–20%, 0.5–7 mm); plagioclase; and alkali feldspar (0.5–5%, 0.5–4 mm), some euhedral with

carlsbad twins; and altered mafic crystals. Rare (1–5%) oxide grains, and prismatic, pale brown clinopyroxene are preserved in some examples. The groundmass is a mixture of very fine-grained quartz, (?)feldspar, sericite, and calcite, with a few hematized- or magnetite-rimmed pyrite cubes. Sulphide minerals are associated with quartz+epidote veins.

A thick (~150 m) lenticular body of dacitic tuff caps the Basal Member south of East Pond (Fig. 5). These dacite tuffs are massive or thick bedded, but bedding is difficult to recognize in the field. They have a distinctive salt-and-pepper appearance, with ubiquitous (15%, 1–2 cm) angular to rounded xenoliths of basalt, microgabbro, and feldspathic hornblende. Crowded, euhedral to ovoid, partly to completely sericitized plagioclase crystals dominate (40–80%, 1–3 mm; Fig. 17). Some grains preserve concentric growth zoning or sieved cores. Euhedral, prismatic to acicular hornblende (10–25%; 1–3 mm, rare ~1 cm; Fig. 17) is commonly aligned parallel to bedding. Hornblende is black on fresh surfaces, pleochroic green to brown in thin section, with normal or reverse zoning, and may contain clinopyroxene cores. Subordinate rounded magnetite and quartz grains are also present. The very fine-grained clastic groundmass (~20%) is pale grey-green and quartzofeldspathic.

Basaltic to andesitic lava flows, pillows, and shallowly discordant dykes are present locally, though they constitute less than 10% of the section. Petrographically and geochemically (*see below*), these lavas are very similar to the dominant porphyritic basalt and/or andesite clasts of the lapilli tuff-breccia units. Dykes contain fewer amygdaloids than the clasts, however, and may have lobed margins, suggesting emplacement into hot material. Amygdaloidal basaltic lavas may contain sericitized plagioclase phenocrysts (1%, 0.5–3 mm), or prismatic chloritized (?)olivine or (?)clinopyroxene phenocrysts. The groundmass is microdiabasic, with bladed to acicular (0.3 mm) plagioclase laths and interstitial patches of chlorite+epidote, granular titanite and Fe-Ti oxide minerals (~5%), and minor disseminated pyrite.

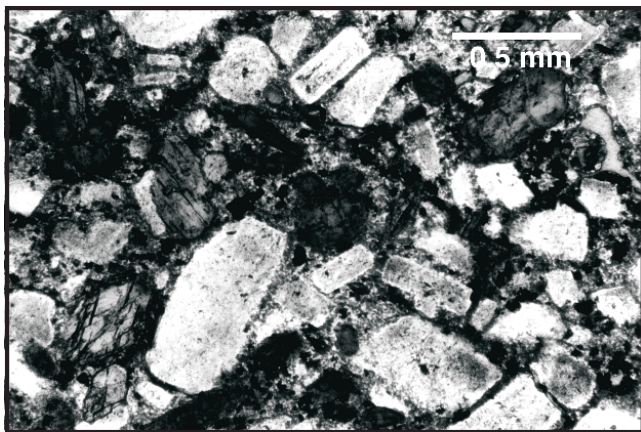


**Figure 17.** Plane light photomicrograph of a dacitic tuff of the Bobby Cove Basal Member (sample BC-95-193). Note the euhedral hornblende (dark), and the abundant feldspar grains (clear).

More primitive basaltic lavas occur near Bobby’s Cove, and at the mouth of Tilt Cove. One flow is clinopyroxene porphyritic (~40%; 1–3mm average, maximum 12 mm). Another contains a small (?)harzburgite xenolith, which is composed of olivine cumulate grains in an (?)orthopyroxene oikocryst.

A series of mafic to felsic dykes cutting the Long Pond gabbro and talus breccia units also appear to belong to the Bobby Cove suite. The chilled margin of one of these mafic dykes contains pseudomorphs after clinopyroxene (~15%, 0.5 mm).

### **Bobby Cove Formation, Upper Member (turbidite)**

The conformably overlying Upper Member of the Bobby Cove Formation is composed of sheet-like, epiclastic, volcanogenic turbidite beds with a significant feldspathic component, interbedded with purplish pelagic siliceous mudstone (sedimentological aspects are discussed *in Cousineau and Bédard, 2000*). The first appearance of thick, undisturbed mudstone marks the base of the member. Most turbidite beds are normally graded. Some show loading and flame structures. A detailed section was measured along the Snooks Arm road (Fig. 18). Thin-bedded felsic tuffs occur at the base and near the top of the unit. Typically, these are laminated on a 1–3 cm scale, and contain angular quartz, plagioclase laths, plagioclase and chert fragments, and devitrified glass fragments, all in a groundmass rich in sericite+epidote+quartz.

### **Venam’s Bight Formation**

The Venam’s Bight Formation is dominated by pillow lavas and thin (1–2 m) sheet flows. Hyaloclastite or agglomerate layers, and interlava layers of red siliceous mudstone or ironstone occur locally, and may be cut by quartz+pyrite reduction veins.

Lavas may be aphyric, but sparsely porphyritic lavas are more common. Clinopyroxene is partly replaced by chlorite or epidote, whereas plagioclase is epidotized, sericitized, or saussuritized. Zoned, euhedral, lath-shaped, plagioclase phenocryst pseudomorphs (1–10%, 1–10 mm) may be glomerocrystic. Some flows are plagioclase-porphyritic (<35%). Clinopyroxene microphenocrysts are generally subordinate (<1%, <1 mm), but a few flows are pyroxene-porphyritic (10%, <7 mm). Clinopyroxene phenocrysts may contain euhedral plagioclase inclusions. Some flows also contain microphenocrysts of Fe-Ti-oxide minerals (<10%), partly replaced by leucoxene. Most flows are slightly amygdaloidal (1–5%, 1–3 mm); but some have up to 15% of larger (<10 mm) amygdaloids. Amygdaloids are filled with mixtures of calcite, epidote, pyrite, quartz, pyrrhotite, chalcopyrite, and chlorite. Some lava flows contain pipe vesicles at their base. The groundmass may be aphanitic dark grey, purplish, pale or dark green, or brick red, depending on the dominant alteration assemblage. Many flows and pillows have orbicular, hematized hyaloclastite rims that grade in to a dark, turbid, chloritized, devitrified groundmass with randomly oriented needles (~10%) of plagioclase and clinopyroxene prisms. In

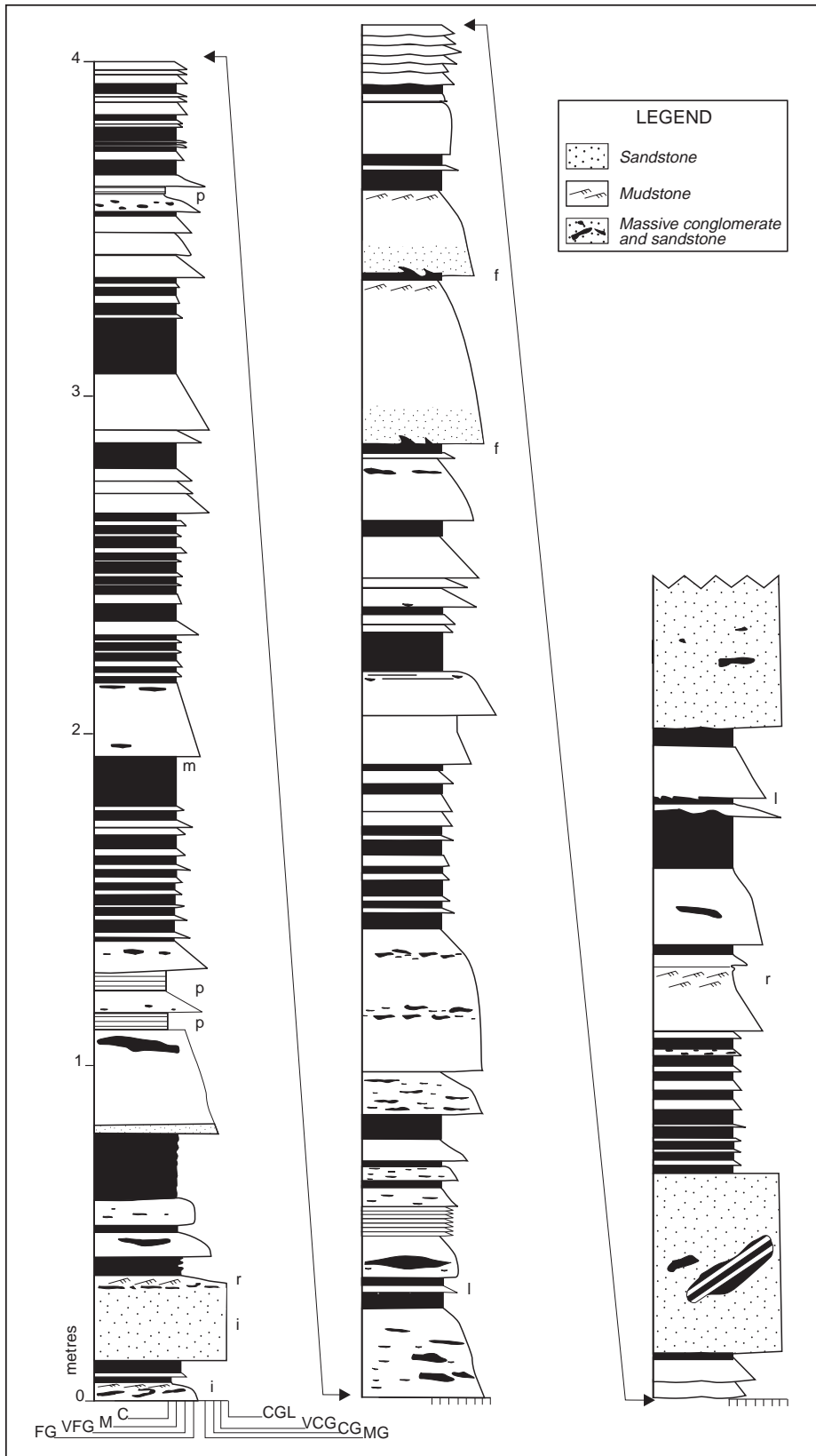


**Figure 18.**

Detailed sections measured from the Bobby Cove Upper (turbidite) Member, Snooks Arm road ('SAR' on Fig. 5). It depicts outer-fan to fan-fringe turbiditic sandstone and mudstone. Note characteristic beds of cohesive flows (stippled pattern), many of which resemble the volcanoclastic mass-flow beds described from the Balsam Bud Cove Formation (Fig. 20, 21). *p* = pelagic claystone and siltstone, *f* = flame structures, *i* = isoclinally slump-folded intraclasts, *l* = load casts, *m* = distinctive rusty sulphidic mudstone, *r* = ripple marks. Grain-size key: C = clay, M = mudstone; sandstone units: VFG = very fine grained, FG = fine grained, MG = medium grained, CG = coarse grained, VCG = very coarse grained, CGL = conglomerate.

the cores of flow units, the groundmass may be granular (~0.4 mm), with equant clinopyroxene and interstitial plagioclase, but more commonly, the groundmass is microdiabasic to subophitic, with plagioclase laths (40–50%, <1 mm), and partly altered, pale brown, pleochroic clinopyroxene (~50%). Common, interstitial Fe-Ti-oxide minerals with skeletal and/or trellis exsolutions (5–10%) are partly converted to leucoxene. Some samples contain 1–3% platy hematite. Common minor disseminated (1–2%, 0.2–0.5 mm) pyrite and lesser chalcopyrite are locally rimmed by magnetite and hematite. More abundant disseminations (up to 3%) of coarser pyrite and chalcopyrite are associated with veinlets of epidote, chlorite, and calcite. Some veins also contain pyrrhotite and chalcopyrite.

### Balsam Bud Cove Formation, Basal Member

The first 100 m of the Basal Member are poorly exposed, consisting of interbedded pelagic sediments, volcanoclastic turbidite, tuffaceous sandstone, and basaltic lavas. Basaltic lavas are sparsely amygdaloidal (<1%), fine grained, dark green, with dendritic leucoxene (~5%), and resemble Venam's Bight Formation basaltic lavas. Pelagic sedimentary rocks are composed of bright green or red siltstone and mudstone, interbedded with subordinate green volcanoclastic sandstone beds. The sandstone beds contain lava fragments (black, dark green, or red) and saussuritized plagioclase crystal fragments. They closely resemble typical sandstone of the Upper Member (debrite).

These basal sedimentary rocks and mafic lavas are succeeded by a sequence (~150–200 m) of interbedded felsic tuffs and black shale, well exposed along the Round Harbour road. The felsic tuffs weather white to grey-blue. The more massive beds (or possibly flows) are 1–4 m thick, are perlitic to brecciated, waxy grey on a fresh surface, and are principally composed of very fine-grained cherty rhyolite. They contain variable proportions (10–20%, 0.5–1 mm) of clastic plagioclase and quartz. Mafic crystals are rare. The groundmass may be weakly foliated, and is mostly composed of quartz and altered plagioclase. Secondary (?) actinolite-rich clots or concretions (3–4 mm) are prominent locally.

The massive tuffs grade to crystal-rich, thin-bedded (1–10 cm), normally graded, felsic to intermediate tuffs. Clast populations and grain sizes vary from bed to bed. Some beds are thinner equivalents of the crystal-poor tuffs described above. Others contain 20–80% of angular, pale green, sericitized plagioclase, generally euhedral to angular (Fig. 19), and subordinate ovoid quartz (0.3–1 mm), with rare clinopyroxene grains and subordinate centimetre-sized lithic fragments. Other beds are dominated (>20%) by lithic fragments, which include feldspar-phyric rhyolitic tuff, locally with sulphide minerals in the core of phenocrysts; pyroxene-phyric andesitic tuff; fine-grained epidotized (?) basalt; black basalt; and rare (?) pumice grains. Commonly, crystal and lithic fragments are aligned parallel to bedding. Small normal microfaults were observed in some samples, associated with sulphide minerals. Pyrite+minor chalcopyrite are ubiquitous, either as thin veins, or as concentrations along bedding planes.

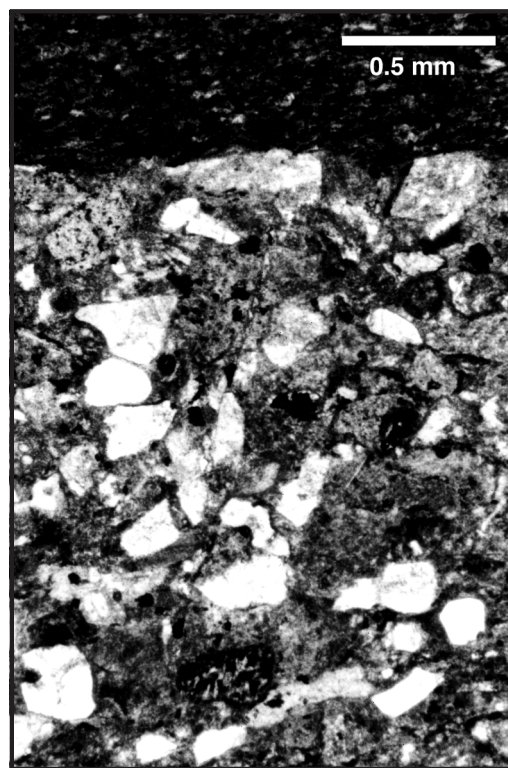


**Figure 19.** Plane light photomicrograph of a rhyolitic tuff of the Balsam Bud Cove Formation (sample BC-96-161). Note the angular quartz (clear) and feldspar (turbid) fragments, and the sharp contact with a finer grained tuffaceous bed.

The interbedded, black, sulphidic, graptolitic shale contains the fossils dated by Snelgrove (1931) and Williams (1992), of probable lower *Didymograptus bifidus* Zone age (early Llanvirn, ca. 477 Ma).

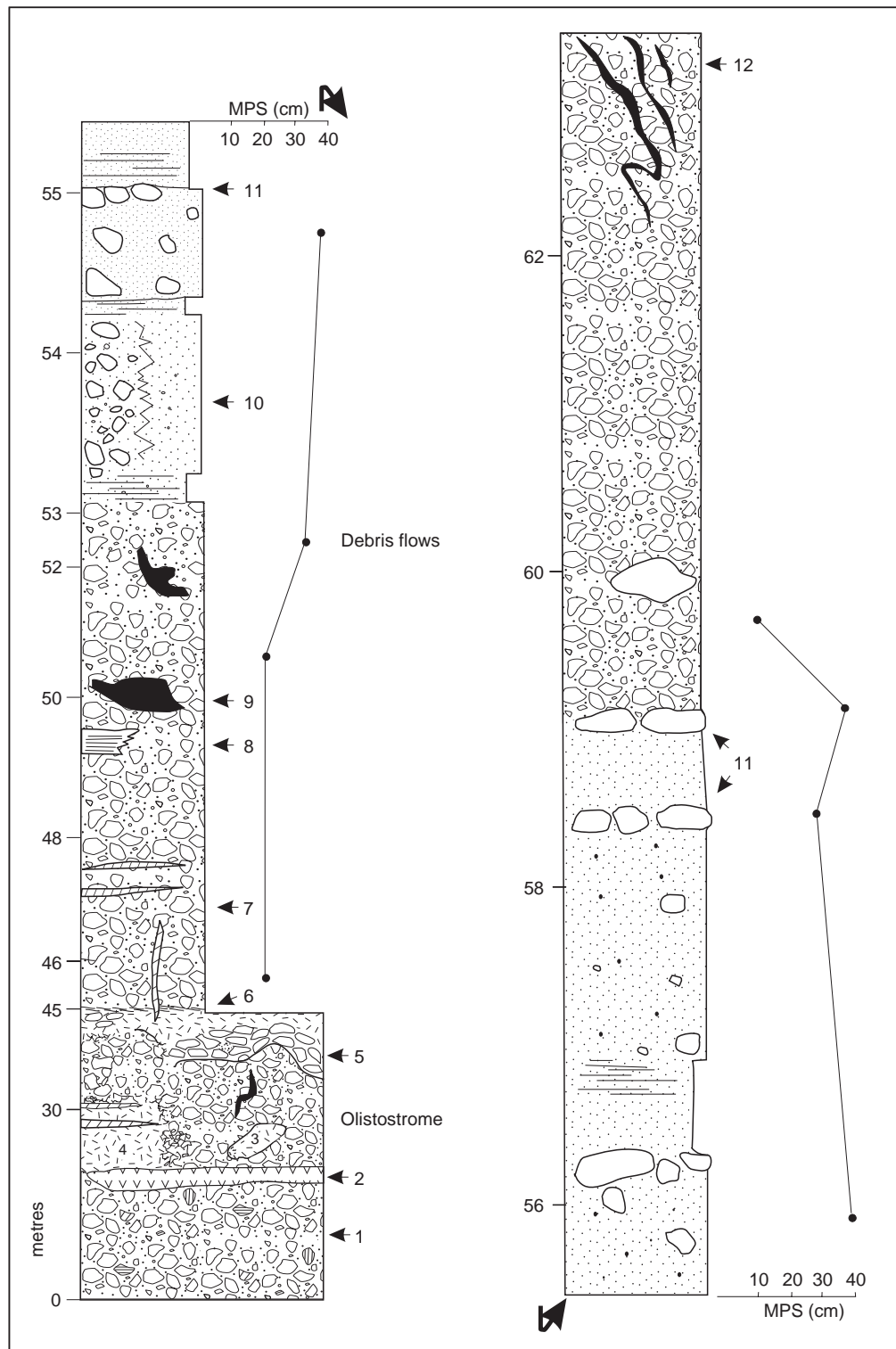
Commonly, the thin-bedded pelagic rocks, rhyolitic tuffs, and black shale of the Basal Member are tightly folded. Some of these may be primary flow folds (in the rhyolitic rocks) or slumps, but others appear to have a tectonic origin. Perhaps Acadian or Taconic deformation was absorbed by the relatively weak shale and pelagic rocks of the Balsam Bud Cove Formation Basal Member, which separate the massive Venam's Bight lavas from the almost equally massive Balsam Bud Cove Formation Upper Member.

### Balsam Bud Cove Formation, Upper Member (debrite)

The base of the Upper (or debrite) Member is defined as the first thick-bedded mass-flow deposit and is related to the development of a proximal volcanoclastic apron. Sedimentological aspects are discussed in more detail in Kessler and Bédard (2000). Detailed sections were measured on the shores of Snooks Arm at Haggis Point (HP on Fig. 5, Fig. 20). The official type section at Balsam Bud Cove is less accessible, since it is open to easterly winds and there are shallow rocks immediately offshore.

In the Snooks Arm section, a basal mass flow (Haggis Point, Fig. 20; *see also* Kessler and Bédard, 1998, 2000) is about 45 m thick and contains large fragments (up to 20 m) of massive and pillowed basalt, leucoxene-rich diabase, basalt breccia, polymictic breccia, and felsic tuff. Felsic tuff clasts are very similar to felsic tuffs of the Balsam Bud Cove

Formation Basal Member or to dacitic tuffs of the Bobby Cove Formation. The larger basaltic clasts (>10 m x 30 m) are pillowed and grade out through monomict basaltic breccia, to a polymict conglomerate. Lava clasts are cut by narrow (1–2 cm) dykes of pebbly sandstone.



This basal debrite (Haggis Point) is overlain by about 50 m of amalgamated, coarse, channelled debris-flow conglomerate or debrite (Devil's Splitting Table, DT on Fig. 5; Kessler and Bédard, 2000), with individual beds ranging from 0.9 m to 9 m. Most clasts are basaltic or andesitic. At the top of the Devil's Splitting Table section, a set of horizontally stratified and low-angle cross-stratified sandstone flow units appear, followed by sequences of thin-bedded turbiditic mudstone and pelagic mudstone.

The clasts in these first debrite units (Haggis Point and Devil's Splitting Table sections) are principally aphyric amygdaloidal and porphyritic mafic lavas. Some are spherulitic. Aphyric lavas are dark green, fine grained, and strongly magnetic, with amygdales (2–3%, 1 mm to 1.5 cm) filled with chlorite+pyrrhotite+quartz or calcite+epidote. Pyrrhotite also occurs in discontinuous veinlets and as nodules. Some porphyritic lavas contain euhedral, concentrically zoned, prismatic clinopyroxene phenocrysts (5–15%, 1–8 mm), partly replaced by actinolite+chlorite+calcite+epidote. Pyroxene phenocrysts are commonly intergrown with phenocrysts of plagioclase and Fe-Ti-oxide minerals (3–5%, partly replaced by leucoxene). Weakly aligned, euhedral, sericitized plagioclase phenocrysts (<40% 0.5–3 mm) may have scalloped edges. Rare, euhedral to anhedral, brown, pleochroic hornblende (~5%, 0.5–3 mm) may have inclusions of sericitized plagioclase, and oxide-rich rims. Rare, 1 cm microgabbro xenoliths are also present in the basalt. These xenoliths contain very fine-grained, equant, anhedral, fresh, clinopyroxene in a plagioclase-rich groundmass (~50%). One gabbroic xenolith has a large (2 mm) skeletal clinopyroxene with abundant oxide exsolutions. The groundmass of the lava clasts is very fine grained and generally completely altered to greenschist

assemblages. Turbid granules after Fe-Ti-oxide minerals are visible locally. Minor disseminated pyrite or chalcopyrite may also be present.

Clasts of feldspar+hornblende+olivine-pyroxenite are also present in places. These are composed of cumulus (?)olivine(~40–45%, ~1 mm) replaced by talc+actinolite, oikocrysts of plagioclase and/or clinopyroxene (replaced by saussurite, epidote, actinolite), and black blades and poikiloblasts of brown hornblende (~15%, 2–4 mm).

Tuffaceous sandstone clasts, which become more common higher in the section, contain variable proportions (<70%, 1 mm) of euhedral epidotized, zoned plagioclase and/or basalt. Clinopyroxene, replaced by chlorite, is subordinate (5–10%, <3 mm) and may be intergrown with Fe-Ti-oxide pseudomorphs (~5%) in a fine-grained matrix (20–50%) rich in epidote and chlorite.

Microgabbro clasts are also common. They may contain clinopyroxene and/or hornblende phenocrysts (~15%, <1–5 mm). Some of these are intergrown with leucoxene, sulphide minerals, and plagioclase. The groundmass contains ghostly pyroxene pseudomorphs, epidotized plagioclase, and leucoxene (5%, 0.3–1.5 mm).

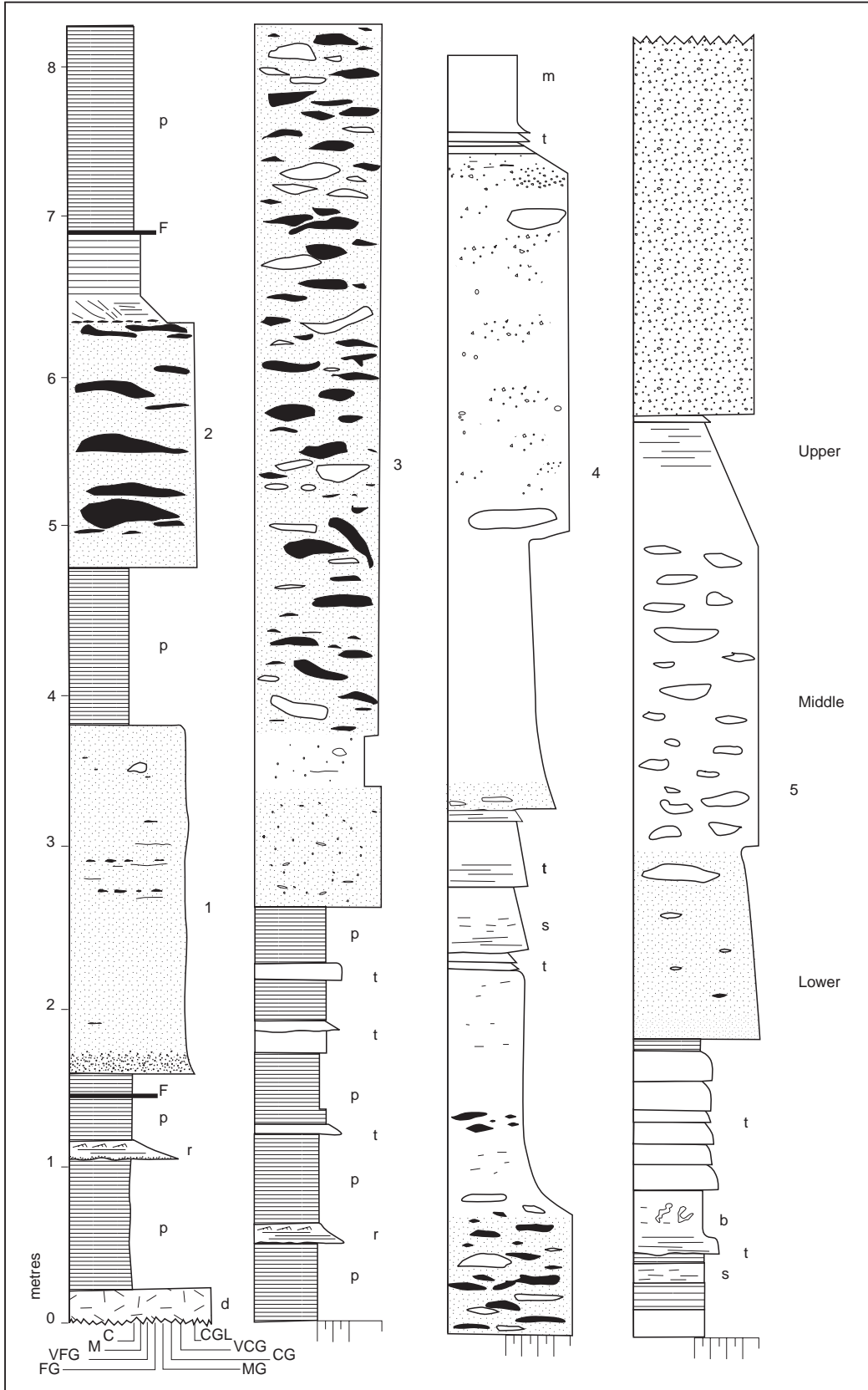
Typically, the debrite matrix contains fragments of clinopyroxene (~15%, 1–2 mm) and saussuritized plagioclase (~15% <1–2 mm), with turbid basalt fragments (~15%), in a fine-grained, turbid chlorite+epidote matrix. Minor pyrite is present.

Above the Devil's Splitting Table section, there follows a sequence (~100 m) of cohesive, channelled debris-flow deposits belonging to a distal volcanoclastic apron (Fig. 21). Within individual debris flows (0.7–8 m thick), clast populations may vary from volcanic-dominated fragments at the base to a dominance of sedimentary fragments at the top (e.g. Fig. 21, 22). Large (~1 m) platy siltstone or sandstone megaclasts are aligned parallel to bedding. They are typically concentrated at the interface between a massive, weakly graded conglomeratic sandy base, and a laminated fine sandstone or siltstone summit. Typical volcanogenic sandstone units are dark green, immature, and poorly sorted. Clast sizes and proportions vary from bed to bed. The dominant lithic populations include light green, epidotized siltstone or basalt; black plagioclase-phyric and amygdaloidal basalt; hematized basalt; and tuffaceous or epiclastic sandstone. Variably saussuritized plagioclase and chlorite+epidote pseudomorphs after clinopyroxene are the most common crystal fragments. Fragments are subangular to subrounded, and some are very irregular shaped (Fig. 22), suggesting short transport distances. Carbonate+sulphide concretions are locally prominent.

Further up in the section, these debrite units are interbedded with and succeeded by basin-plain turbidite units, pelagic rocks, and rare rhyolitic tuffs. The high proportion of pelagic mudstone at the top of the sequence suggests that the influx of clastic material decreased with time, with fewer and smaller debris flows appearing.

←

**Figure 20.** Representative section showing the base of the Balsam Bud Cove Upper (debrite) Member, showing typical features of the proximal volcanoclastic apron (Haggis Point, 'HP' on Fig. 5). Note the variations in the vertical scale. 1 = polymictic breccia or angular conglomerate, 2 = parallel-laminated felsic tuff, 3 = fractured basalt boulders surrounded by monomict basaltic breccia (transitions from the monomict breccia to the polymictic conglomerate are gradational), 4 = locally fractured, massive basaltic lava olistolith cut by neptunitic sandstone dykes, 5 = pillow lava olistolith, grading out to monomict basaltic breccia, and cut by sandstone dykes, 6 = sheared contact between large olistolith and the rest of the debris flow, 7 = conglomeratic dykes and sills cutting debrite conglomerate, 8 = lenticular interbedding of volcanoclastic sandstone, 9 = soft rafts of fine-grained sediment, 10 = lateral transition from massive conglomerate into pebbly sandstone, 11 = outsize boulders concentrated at the summit of the massive base of debris flow, topped by thin-bedded sandstone, 12 = mafic dykes and sills. MPS = maximum particle size (average of five largest)





A set of well bedded rhyolitic tuffs near the top of the formation are fine grained, light grey to slightly greenish, cherty, and have a conchoidal fracture. They contain angular quartz and feldspar grains (<15–20%). Hydrothermal concretions up to 7mm wide have calcite and chalcopyrite in their core, with pyrite or (?)marcasite as concentric overgrowths.

### Round Harbour Formation

These lavas were deposited on, and are locally interbedded with the uppermost mudstone beds of the Balsam Bud Cove Formation. They are pillow lavas and sheet flows (up to 4 m thick) that closely resemble Venam's Bight basaltic lavas. Thin (<1 m) red siliceous mudstone beds are present locally.

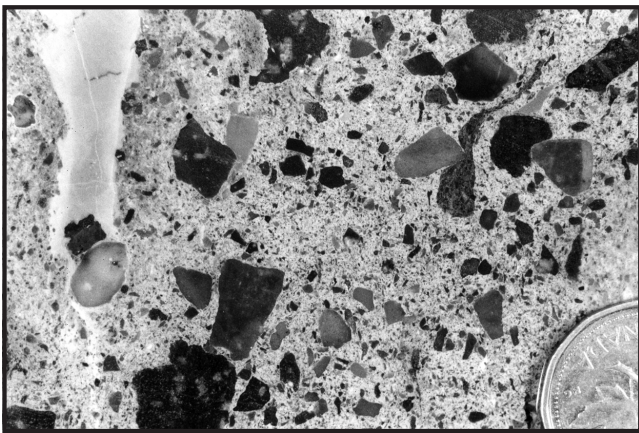


**Figure 22.** Matrix of volcanoclastic debris of Balsam Bud Cove Formation (sample BC-94-882). Clasts include basalt (black) and various types of fine-grained sedimentary rocks, some of which seem to still have been soft when deposited. The matrix is a volcanogenic sand, cemented by epidote and calcite. Photograph by J. Bédard. GSC 2000-005D

**Figure 21.** Representative section from the middle Balsam Bud Cove Upper (debrite) Member, showing typical features of the distal volcanoclastic apron. Thick-bedded cohesive debris units are interbedded with basin-plain pelagic and turbidite units. Grey and/or red intraclasts are shown in black. Key: *p* = pelagite, *r* = ripple crosslamination ( $T_c$ ), *t* = turbidite units ( $T_{a-d}$ ), *s* = extensional disruption of laminae, sedimentary shearing and boudinage, *b* = possible bioturbations, *d* = diabase sill, *F* = minor, bedding-parallel fault, *m* = massive siltstone, 1 to 5 = cohesive debris units. Three main members of the composite debris units are marked in debris 5. Grain-size key: *C* = clay, *M* = mudstone; sandstone units: *VFG* = very fine grained, *FG* = fine grained, *MG* = medium grained, *CG* = coarse grained, *VCG* = very coarse grained, *CGL* = conglomerate.

Round Harbour lavas range from aphyric to porphyritic. Plagioclase phenocrysts (5–20%, 2mm to 1 cm) are generally replaced by epidote+albite±chlorite. Clinopyroxene phenocrysts (5–15%) are euhedral and may be fresh or replaced by chlorite+actinolite. Serpentinized (?)olivine phenocrysts may be present. There are rare calcite-filled amygdales (~1 mm). The groundmass is either granular, microdiabasic or subophitic, with equant to interstitial Fe-Ti-oxide minerals (~5–15%, ~0.5 mm) partly replaced by leucoxene. Minor disseminated ragged or cubic pyrite and chalcopyrite may be present. Vein assemblages are mixtures of calcite, epidote, chlorite, quartz, pyrite, and hematite. Diabasic dykes cut the lavas in a few places. These are massive, dark green, very fine grained, and plagioclase-phyric (~5–15%, 0.5–1 mm).

A prominent corridor (>40 m wide) characterized by fissuring, intense brecciation, and epidotization is exposed along the Round Harbour road. Anastomosing epidosite locally composes 50% of the rock. Narrow (~1 m) fissures are filled by polymictic breccia, with clasts that record multiple brecciation events. Clasts include leucogabbros; quenched basaltic lavas with abundant dendrite; microdiabase and ferro-diabase; chert; metamorphosed lava containing phenocrysts of plagioclase, Fe-Ti-oxide minerals, and green to tan pleochroic hornblende in a trachytoid groundmass; felsic lava with aligned phenocrysts of quartz, plagioclase, (?) alkali feldspar, hornblende, and Fe-Ti-oxide minerals, in a trachytoid groundmass that also contains minor pyrite; and fine-grained, tan to reddish laminated siltstone and chert clasts surrounded by concentrations of anhedral to euhedral hematite, pyrite, and minor chalcopyrite. The hydrothermal matrix of this breccia is dominated by quartz and epidote, but also contains disseminations and veinlets of pyrite, either turbid and framboidal, or as large cubes (locally replaced by magnetite), together with minor disseminated chalcopyrite and (?)bornite.

The lavas and breccia are crosscut by strongly epidotized and hematized felsic dykes (2–3 m wide) that contain euhedral plagioclase phenocryst pseudomorphs (20–30%, 1–4 mm). Plagioclase may be intergrown with euhedral (?)hornblende pseudomorphs, now composed of epidote+chlorite+calcite±apatite. Rounded and embayed quartz phenocrysts (~5%, 1–3 mm) are also present, together with (?)phenocrysts of leucoxene+apatite (2–3%, 1 mm). The groundmass is dominated by plagioclase microlites aligned parallel to the dyke contacts, and by granules (5–10%) of (?)leucoxene after (?)Fe-Ti-oxide minerals, in a quartz+plagioclase-rich matrix. These dykes have chemical signatures (*see below*) similar to those of Bobby Cove dacite and rhyolite.

### Mafic sills

Mafic sills are up to 250 m thick, with shallowly discordant or brecciated contacts, and may be composite. Most sills occupy prominent discontinuities, such as lava-metasediment interfaces (Fig. 4–7), but the emplacement of others appears to be structurally controlled, either by the presence of prominent breccia zones, or by the existence of pre-existing brittle shear zones. Pyroxene is partly replaced by chlorite, epidote, and

actinolite. Feldspar is either epidotized, carbonatized, silicified, sericitized, or saussuritized. Magnetite-ilmenite intergrowths are partly converted to leucoxene. Quartz, calcite, pyrite, and titanite are common secondary phases.

Sill margins are commonly amygdaloidal (indicating shallow emplacement) and microporphyrific. Plagioclase microphenocrysts and phenocrysts are common (<1–15%, <1–8 mm) and increase in size away from the chilled margin. Clinopyroxene microphenocrysts are locally abundant (1–15%, 1–2 mm), showing concentric and sector zoning. Amygdales are typically sparse (<5%, ~1 mm), but local concentrations (up to 10%) of larger amygdales (5–10 mm), flattened parallel to contacts, may be present. Amygdales are filled with quartz, calcite, epidote, chlorite, and sulphide minerals. Near sill margins, the groundmass may be microdiabasic, with plagioclase laths (~40%, 0.5–1 mm) and subophitic clinopyroxene. Granular textured or basaltic groundmass textures are also common, with tiny Fe-Ti-oxide granules (pseudomorphed by leucoxene). In places the groundmass appears chilled and contains feldspar microlites.

The central portions of sills are coarser, with diabasic, subophitic, ophitic, or porphyritic textures. The proportion and size of phenocrysts can vary within a given sill. Rare pyroxene-phyric sills contain euhedral clinopyroxene phenocrysts (~5–15%, 3 mm). A few sills contain lozenge-shaped pools of chlorite+epidote (10%) which may represent olivine phenocrysts, amygdales, or simply patchy alteration. The more common plagioclase-phyric sills have less than 10% phenocrysts (1–10 mm), but crowded porphyritic sills may contain up to 45% phenocrysts that attain 2 cm in size (3–7 mm is more typical). Plagioclase phenocrysts are euhedral to ovoid. They are commonly sieved and/or glomeroporphyritic with clinopyroxene phenocrysts.

Aphyric sills and the groundmass of porphyritic sills typically have diabasic textures, with randomly oriented or clustered plagioclase laths (1–2 mm) and subophitic to ophitic clinopyroxene (1–3 mm). Interstitial plates of brown igneous hornblende (2%) are found locally. Skeletal to interstitial Fe-Ti-oxide minerals (2–10%, 1–3 mm) and minor sulphide minerals (2–5%) are almost ubiquitous, except in the pyroxene-phyric sills, where Fe-Ti-oxide minerals make up less than 1%. Iron-titanium oxide minerals are locally abundant (up to 20%), and can also occur as phenocrysts. Oxide minerals are commonly associated with minor sulphide minerals, and both tend to be concentrated in coarser diabasic patches. Sulphide minerals are also concentrated around hydrothermal veins. Cubic to anhedral pyrite and minor chalcopyrite and pyrrotite are common. Chalcopyrite may be intergrown with an unidentified reddish-tinted sulphide.

### ***Adjoining ophiolitic rocks***

#### **Undifferentiated Snooks Arm Group rocks**

In the Kitty Pond and Betts Big Pond area, immediately to the northwest of the layered cumulate peridotite units (Fig. 2), there are two domains composed of rocks that closely resemble upper Snooks Arm Group lithologies. These include andesitic conglomeratic and lapilli tuffs analogous to those of the

Bobby Cove Formation, volcanogenic sandstone and pelagite similar to those of the Balsam Bud Cove Formation, and pillow lavas that could belong to any of the lava-dominated formations of the Snooks Arm Group. These isolated Snooks Arm Group domains are in fault contact with the main body of the Betts Cove ophiolite. We infer a normal (northwest side down) movement for this fault. These rocks are intruded by quartz+feldspar porphyry dykes.

#### **Nippers Harbour ophiolitic massif**

The Nippers Harbour massif (Schröeter, 1971) outcrops to the southwest of the Betts Cove massif, from which it is separated by a prominent serpentinite fault zone. It is composed of massive to pegmatitic gabbro (cut by numerous dykes), sheeted dykes, and strongly altered lavas.

### ***Post-Ordovician rocks***

#### **Cape St. John Group**

The Cape St. John Group includes fluvial sandstone and conglomerate, felsic tuff and lava, and mafic to intermediate lava (Hibbard, 1983; Coyle, 1990). The felsic pyroclastic rocks were interpreted to be correlative to the Cape Brulé granite porphyry (DeGrace et al., 1976; Hibbard (1983) p. 121, quoting an unpublished report by E.R.W. Neale). An unconformable depositional contact against the ophiolitic rocks is preserved just to the east of the Snooks Arm road (Fig. 5), on the coast near Beaver Cove Pond, and in the cliffside north of Beaver Cove Pond (Neale et al., 1975). The unconformable contact is commonly overprinted by shear zones, however, with fabrics indicating either normal (north side down) or reverse motion (north side up) (Tremblay et al., 1997). The reverse faults are associated with the major fold structure in the area, which we infer to be Acadian (Tremblay et al., 1997). The normal faults are refolded by the Acadian event, as can be seen immediately northeast of Beaver Cove Pond (Fig. 6).

In many places where the Cape St. John Group rocks are in fault contact with the ophiolite (Fig. 6), there are prominent intrusions of quartz+feldspar porphyry, many of which are also affected by intense shearing and hydrothermal alteration. The faults and intrusions are inferred to be roughly synchronous (Tremblay et al., 1997), which implies that the normal faults are Silurian. Large (1–3 m) rusty-weathering Fe-carbonate veins and magnetite ironstone are commonly associated with the contact zones.

The lowermost exposed rocks of the Cape St. John Group are dark green or brown boulder conglomerate units, containing numerous clasts of quartz, red chert, fuchsite, and basalt. Interbedded sandstone and conglomerate commonly show prominent channels and crossbeds. Associated mudstone may exhibit mudcracks, implying subaerial conditions. In places, the well bedded metasedimentary rocks are cut by narrow andesitic dykelets, and by hybrid felsic+mafic dykes.

Mafic lavas are interbedded with the lowermost metasedimentary rocks. These are massive to rubbly sheet flows, generally strongly hematized and carbonatized. Large

flattened amygdales (2–10%, 3–40 mm) contain buff iron-carbonate+chlorite+quartz+hematite, and are cut by calcite+quartz crossveins. Euhedral, concentrically and sector zoned rhombs (5–30% 0.5–4 mm) of buff Fe-rich carbonate are common, and appear entirely newly formed. There is no indication that they are replacements of plagioclase phenocrysts. Prismatic grey-green, epidotized plagioclase glomerocrysts (~5%, 2–5 mm) and pyroxene phenocrysts (3–4%, 0.5–3 mm, replaced by chlorite+calcite) are recognizable in rare cases. Black, anhedral, aphanitic, (?) rip-up clasts (5%, <1 cm) of sediment or lava may be present. The groundmass is altered to chlorite+carbonate+quartz+epidote+platy hematite or hematite+(?)ilmenite. Minor disseminated pyrite and chalcopyrite, and possible (?)bornite may also be present. Less altered domains preserve plagioclase-rich microgabbroic or microdiabasic textures, and may contain up to 20% leucoxene. Common alteration veins have fibrous quartz+chlorite margins and carbonate-rich cores.

The basal sedimentary rocks and mafic lavas are overlain by thick accumulations of felsic lavas and tuffs. A felsic ignimbrite from the Snooks Arm road was dated at  $429 \pm 50$  Ma by Pringle (1978), and at  $427 \pm 2$  Ma by Coyle (1990). In places, basaltic fiamme in rhyolite record mingling events. The felsic rocks are laminated to flinty, weather pale green or salmon, and are dark blue-grey to brown on a fresh surface. Most are significantly flattened. Pale green intraclasts with platy shapes (up to 10 x 10 cm), are as little as 2mm thick. Grey and blue quartz phenocrasts (~5%, 0.5–2 mm) are stretched parallel to the foliation. Local alkali feldspar phenocrasts may also be present. Feldspar grains generally dominate. Fragments of red chert and fuchsite are present locally.

### Quartz-feldspar-mica porphyry

Quartz+two feldspar+biotite-porphyrific dykes and sills occur throughout the Betts Cove ophiolite. Inclusions of fuchsite are locally abundant in the quartz+two feldspar+biotite-porphyrific dykes, proving that these magmas traversed ultramafic basement rocks. Petrological similarities (identical phenocryst types, chert, and fuchsite fragments) suggest that the Cape St. John felsic volcanic rocks may be cogenetic, the quartz+two feldspar+biotite-porphyrific dykes representing feeders. The dykes are commonly sheared, suggesting emplacement into active faults, which would have provided a favourable channelway for their ascent (Tremblay et al., 1997). Locally, the dykes have a very chaotic, brecciated appearance, with mixed clast populations. We interpret these to represent subvolcanic breccia or phreatomagmatic deposits. Many quartz+two feldspar+biotite-porphyrific dykes are completely massive, however, with slight decreases in grain size towards the margins.

Quartz phenocrysts and glomerocrysts (2–15%, 2–7 mm; Fig. 23) are ovoid to euhedral, typically embayed, and commonly intergrown with feldspar phenocrysts. One tuffaceous quartz+two feldspar+biotite-porphyrific dyke has about 20% quartz phenocrasts, some euhedral, but many others showing evidence of cataclasis. Feldspar phenocrysts (<25%,

1–10 mm) are typically euhedral to subhedral (Fig. 23), may be glomerocrystic, and are completely bleached, hematized, or sericitized. Both plagioclase and alkali feldspar pseudomorphs are present. Aligned phenocrysts were observed in some quartz+two feldspar+biotite-porphyrific dykes. Mica phenocrysts (~5–10% 0.5–6 mm) are converted to chlorite±calcite± titanite (Fig. 23). They may have hematite rims and coronas. Some quartz+two feldspar+biotite-porphyrific dykes contain amygdales (~5%) filled with calcite, hematite, and pyrite. The groundmass is either bleached, hematized, sericitized, or epidotized. Where the groundmass is least altered, a mosaic of quartz+(?)feldspar+sericite is still visible. Minor carbonate alteration is common. Cubic pyrite (3–4%, 1–3 mm) is common, may contain silicate inclusions, and is typically rimmed by hematite and magnetite. Platy to equant hematite grains (1–2%) may also be present.

### Burlington granodiorite and Cape Brulé granite porphyry

The Burlington granodiorite and Cape Brulé granite porphyry were originally considered to be Ordovician (Mattinson, 1975; Dallmeyer and Hibbard, 1984), but recent U/Pb ages of  $432 \pm 2$  Ma and  $440 \pm 2$  Ma on the Burlington granodiorite, and of  $430+5/-3$  Ma for the Cape Brulé granite porphyry (Cawood and Dunning, 1993; G.R. Dunning, pers. comm., 1996), indicate that they are Silurian, coeval with Cape St. John Group lavas. These granitoid bodies are affected by intense hydrothermal alteration. Epidote is a very common vein and groundmass phase, feldspar minerals are bleached or epidotized, and biotite is chloritized.

The Burlington granodiorite is grey to brown, medium- to coarse-grained (3–6 mm), and quite homogeneous, except near its contacts with the ophiolite, where numerous partly resorbed enclaves with reaction rims are present. The few examples of granodiorite we examined are composed of

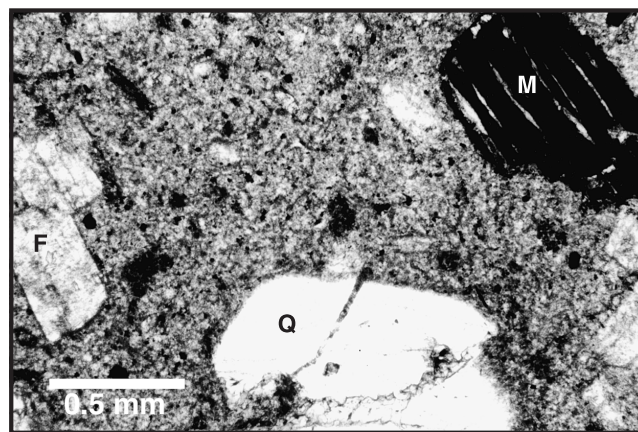


**Figure 23.** Plane light photomicrograph of a Silurian quartz-feldspar-mica-porphyrific dyke (sample BC-95-1009) from Tilt Cove. Note the euhedral quartz with rounded corners (Q), euhedral feldspar (F, turbid), and chloritized and/or hematized mica (M, dark).

about 30% acicular hornblende prisms, about 40% epidotized plagioclase±(?) alkali feldspar, and about 20% interstitial quartz.

A ring dyke that cuts the main body of the Burlington granodiorite is composed of medium-grained (3–4 mm), grey, weakly porphyritic granodiorite that contains rare feldspar phenocrysts (1 cm). The matrix has euhedral hornblende (15%) and unoriented biotite plates (5%). Feldspar (~60%) is mostly white, subhedral to euhedral, and may be zoned. Quartz is interstitial (20%).

Typical Cape Brulé granitoid rocks from the Nippers Harbour road have white, green, or red fractured euhedral plagioclase and alkali feldspar crystals (~10–20%, 5mm to 1 cm). Translucent quartz (15–20%, 2–5 mm) is euhedral to rounded, and may also be fractured. Minor (1%) chloritized mafic phenocrysts are present. Phenocrysts are set in a finer grained (1–2 mm), locally cataclastic-textured matrix. The rock may also contain a few (<1%) centimetre-scale enclaves or autoliths composed of beige aphanitic material with millimetre-sized quartz phenocrysts.

## DEFORMATION HISTORY

### *Preobduction structures*

Northwest- to southwest-trending faults with steep paleodips cut the cumulate rocks, the sheeted dykes, and overlying lavas and sedimentary rocks of the ophiolitic crust. Around Betts Cove (Fig. 4, 7), the offset of lithostratigraphic units implies that individual faults have throws up to 1 km, with original normal motions. These faults dissect the stratigraphy into horst-and-graben structures. Rare, higher grade shear zones with shallow paleodips found within the sheeted dykes may represent coeval ductile décollements (cf. Reston et al., 1996). Many of these faults, and related breccia-filled fissures in the adjoining lavas, have axial mafic dykes, or are impregnated by magmas, and so are clearly of intraoceanic origin, coeval with seafloor spreading.

Several of these normal faults rooted in the Betts Head Formation extend upsection into the overlying Mount Misery and Scrape Point formation lavas and metasedimentary rocks (Fig. 7). Measured throws decrease upsection, implying that the faults are syndepositional, and that significant, though decreasing, amounts of extension continued throughout deposition of the Snooks Arm Group. The lower part of some fault blocks record significant tilting and erosional planing-off prior to deposition of overlying sedimentary rocks, suggesting that the normal faults had listric geometries.

The abundance of plutonic clasts in some of the breccia units at Tilt Cove and Long Pond imply derivation from a heterogeneous source that included unroofed plutonic or mantle basement. The heterolithic nature of the breccia is consistent with an origin as oceanic fault-talus or slump deposits developed during seafloor spreading. Because some of the breccia is impregnated by magmas with the same composition as the clasts, we infer that the faults were synmagmatic. The occurrence of Betts Head Formation breccia fragments in Snooks

Arm Group talus breccia implies that renewed, synmagmatic extensional faulting occurred during eruption of Mount Misery and Scrape Point formation basalt units.

### *Obduction-related structures*

There is no direct age data on obduction-related structures in the Betts Cove complex, but comparison with other Notre Dame Subzone ophiolite massifs suggests that the Betts Cove obduction-related structures formed after 480–469 Ma (Dallmeyer and Williams, 1975; Dallmeyer, 1977), consistent with the timing inferred for the Taconian Orogeny in the Newfoundland Appalachians (e.g. Stevens, 1970; Williams, 1979; Hibbard, 1983).

The most important obduction-related structure at Betts Cove is a northwest-verging thrust fault (Fig. 2, 4). In the north (Fig. 5, 7), this fault separates the Betts Head and Mount Misery lavas from the talc-serpentinite schist unit. Near Betts Cove (Fig. 4), this fault splays upsection, and juxtaposes Mount Misery lavas against cumulate rocks and sheeted dykes. This thrust fault is unconformably overlain by Cape St. John Group sedimentary rocks and lavas (Fig. 5), providing a Silurian (ca. 430 Ma) upper age limit. Shear-sense indicators indicate northwestward movement of the hanging wall (Tremblay et al., 1997).

Some of the normal faults related to seafloor spreading may contain ultramafic slivers and kinematic indicators (C/S structures) with steeply dipping fibres indicating vertical reverse motions. These fabrics are inconsistent with the sense of movement inferred from lithostratigraphic offsets, and so we infer that the intensely chloritized spreading-related faults were reactivated during obduction. Faults that were not originally chloritized were not reactivated to the same extent.

### *Silurian structures*

Following structural docking, the Betts Cove ophiolitic complex was affected by northwest- and northeast-dipping normal faults. In the Long Pond area (Fig. 5), normal-sense shearing is associated with a brittle-ductile deformation zone separating serpentinite–talc–carbonate schist and a quartz+two feldspar+biotite-porphyratic intrusion emplaced into Cape St. John volcanic rocks. The deformation zone is marked by a mylonitic fabric that dips (~60°) north-northwest. Shear-sense indicators (Tremblay et al., 1997) are consistent with a normal sense of movement, with the upper plate descending towards the north-northwest.

In the Tilt Cove–Beaver Cove Pond area (Fig. 6), normal faulting relationships are obscured by later folding and thrusting. Normal-sense faults are found near the sheared contact between ophiolitic and Cape St. John rocks. Quartz+two feldspar+biotite-porphyratic intrusions are commonly associated with the faults. Field relations show that the normal-sense deformation zone crosscuts the basal unconformity of the Cape St. John Group (Tremblay et al., 1997). This provides a maximum age for this event — Silurian or younger. Immediately to the east of Beaver Cove Pond (Fig. 6), the fabric in the normal fault cutting Cape St. John Group rocks has been

refolded and defines a northeast-plunging anticline with an axial-planar crenulation cleavage coplanar to the regional foliation. This demonstrates that the normal faulting predates regional compression.

The common association between normal faults and quartz+two feldspar+biotite-porphyratic intrusions suggests a genetic link. We infer that the porphyritic intrusions ascended in active normal faults, since this represents a favourable pathway. If the porphyritic intrusions and the Cape St. John and Cape Brulé–Burlington suite are cogenetic, this implies that extensional faulting occurred in the Early Silurian (i.e. ca. 435–425 Ma).

In the Betts Cove area (Fig. 2, 4), the fault that marks the base of the ophiolite is assigned to the normal fault system described above (Tremblay et al., 1997). This explains the presence of upper Snooks Arm Group rocks west of the cumulate sequence, i.e. these are downthrown blocks in the hanging wall of a normal fault.

Regional studies of post-Ordovician volcanism and plutonism in Newfoundland indicate that sedimentary, volcanic, and plutonic patterns were fault controlled (Hibbard, 1983; Strong and Coyle, 1987). Neale (E.R.W. Neale, unpub. manuscript, 1962) interpreted the Cape Brulé granite porphyry as a centre of post-Ordovician volcanism and a site of major cauldron subsidence. The country rocks surrounding such cauldrons are commonly injected by ring dykes, are subjected to intense faulting and hydrothermal alteration, and represent favourable environments for epithermal ore deposition.

The Cape Brulé or Dunamagon granitoid rocks are of the same age as the Burlington granodiorite, and it seems reasonable to infer that the quartz+two feldspar+biotite-porphyratic rocks found within the Betts Cove ophiolite might represent rapidly cooled offshoots from this composite granitoid batholith. Pre-Silurian ophiolitic rocks (e.g. the Pacquet Harbour Group) occur as irregularly shaped masses all along the boundaries of this granitoid batholith, as do the Silurian Cape St. John lavas and sedimentary rocks, and their correlatives, the Micmac Lake and Flat Water Pond groups (Fig. 1). We suggest that these are roof pendants of the Silurian cauldron. The similarity of ages and petrographic signatures suggest that the Cape St. John rhyolitic volcanic rocks are the volcanic ejecta from this granitoid batholith. Coyle (1990) proposed a similar eruptive context for the contemporaneous Springdale Group, inferring a link with the underlying anorogenic Topsails batholith.

Silurian timing for the magmatism we associate with extensional deformation in the Betts Cove area overlaps the range of  $^{40}\text{Ar}/^{39}\text{Ar}$  metamorphic ages (429–421 Ma; hornblende and mica ages respectively, Dallmeyer (1977)) and U/Pb ages for syn- to postkinematic felsic intrusions (427–423 Ma; monazite, zircon, and titanite, Cawood and Dunning (1993)) in the Fleur de Lys belt west of the Baie Verte road fault. Cawood et al. (1994, 1995) argued that these record peak metamorphism and synorogenic plutonism associated with continental collision and crustal thickening during the Salinic Orogeny. Instead, we favour a model

involving a Silurian period of postorogenic collapse and crustal extension (Jamieson et al., 1993; Hibbard et al., 1995; Tremblay et al., 1997).

### ***Compressional structures and regional folds and thrusts***

The most obvious deformation recorded in the Betts Cove ophiolite and the Snooks Arm Group is a large-scale synclinal structure (Fig. 2) with a locally prominent axial-planar slaty cleavage. The fold plunges slightly to moderately toward the northeast. The intensity of deformation increases toward the hinge zone, and near the contact with Silurian rocks to the north. In the Tilt Cove–Beaver Cove Pond area, these folds are commonly associated with north-east-dipping high-angle reverse faults, commonly localized by the presence of weak lithologies, such as serpentinite, sedimentary rocks embedded within massive lavas, or pre-existing faults.

The northwestern limb of the regional syncline is truncated by a major southeast-verging high-angle reverse fault which is best exposed in the Red Cliff Pond area (Fig. 5). This fault extends up to 10 km along the contact between the Betts Cove complex and Silurian rocks (Fig. 2), and can be traced along strike for another 20 km. We infer that it is a fault related to the southeast-verging compressive deformation responsible for regional folding, and Tremblay et al. (1997) proposed it be called the Red Cliff Pond shear zone. It is about 200 m thick and is marked by a penetrative north-east-trending mylonitic foliation that dips about  $70^\circ$  toward the northwest, and is associated with downdip stretching lineations. Shear-sense indicators imply reverse movement (Tremblay et al., 1997).

Regional-scale folds and faults in the Baie Verte belt are younger than the Silurian–Devonian rocks affected by these structures, and older than flat-lying, undeformed Carboniferous rocks that unconformably overly Silurian–Devonian granitoid rocks to the south (Dean and Strong, 1975; Hibbard, 1983). This suggests that the deformation recorded by the Silurian–Devonian rocks is related to the Acadian, rather than the Alleghanian Orogeny.

## **MINERAL CHEMISTRY, GEOCHEMISTRY, AND PETROGENESIS**

### ***Mineral chemistry***

Electron microprobe data was generated at McGill University with a JEOL superprobe. Methods and accuracy are described in Bédard and Hébert (1996), and the data is presented in Tables 1–3. Additional data shown on the figures was compiled from Coish (1977a).

Analysis of chromite from cumulate rocks occupy a limited compositional range (Fig. 24, Table 1), with high Cr# (100·Cr/Cr+Al) (70–85). Phenocrysts in dykes have similar or slightly higher Cr#, typical of those found in boninite (e.g. Crawford et al., 1989), but with a wider range in Fe2#

**Table 1.** Spinel analyses from Betts Cove rocks.

	Talc- magnesite- carbonate schist	Websterite	Ortho- pyroxenite	Ortho- pyroxenite	Dunite	Dunite	Boninitic dyke		
	94-72	94-383	94-388	94-390	94-741	94-749	95-534		
SiO <sub>2</sub>	0.07	0.02	0.04	0.03	<dl	0.01	0.06		
Al <sub>2</sub> O <sub>3</sub>	18.71	10.86	12.74	11.61	9.53	9.30	8.65		
Cr <sub>2</sub> O <sub>3</sub>	49.28	52.82	52.00	52.57	54.96	55.97	58.84		
TiO <sub>2</sub>	0.03	0.06	0.07	0.04	0.10	0.13	0.02		
V <sub>2</sub> O <sub>3</sub>	0.27	0.26	0.26	0.28	0.24	0.25	0.18		
Fe <sub>2</sub> O <sub>3</sub>	3.91	6.92	7.04	6.89	6.58	4.92	5.98		
(FeO*)	17.33	25.26	22.49	22.86	25.11	23.19	16.09		
FeO	13.82	19.04	16.17	16.67	19.19	18.78	10.71		
MnO	0.30	0.40	0.34	0.38	0.42	0.42	0.32		
MgO	13.47	9.18	11.36	10.73	9.14	9.13	14.27		
NiO	0.07	0.08	0.09	0.10	0.05	0.08	0.08		
CaO	<dl	0.02	0.02	0.00	0.00	0.00	0.01		
Total (FeO*)	99.53	98.95	99.40	98.59	99.55	98.49	98.49		
Ti	0.005	0.012	0.013	0.008	0.020	0.026	0.004		
Si	0.019	0.006	0.010	0.007	<dl	0.003	0.015		
Al	5.501	3.409	3.896	3.609	2.996	2.957	2.659		
Cr	9.718	11.129	10.659	10.956	11.590	11.941	12.136		
V	0.054	0.055	0.054	0.059	0.051	0.054	0.037		
Fe <sup>3+</sup>	0.735	1.388	1.375	1.368	1.323	0.999	1.175		
sum	16.032	16.000	16.006	16.006	15.981	15.981	16.025		
Fe <sup>2+</sup>	2.882	4.247	3.503	3.672	4.278	4.234	2.336		
Ni	0.015	0.017	0.020	0.021	0.011	0.017	0.016		
Mg	5.008	3.639	4.392	4.215	3.634	3.671	5.549		
Mn	0.063	0.090	0.075	0.085	0.095	0.096	0.071		
Ca	<dl	0.007	0.005	0.001	0.001	0.001	0.003		
sum	7.968	8.000	7.994	7.994	8.019	8.019	7.975		
Cr#	63.853	76.552	73.234	75.223	79.458	80.153	82.025		
Fe2#	36.527	53.853	44.370	46.562	54.070	53.565	29.621		
Fe3#	4.605	8.716	8.631	8.585	8.317	6.284	7.356		
<b>Lherzolite</b>									
	95-667	95-668	95-670	95-671	95-672	95-674	95-675	95-676	95-681
SiO <sub>2</sub>	0.06	0.03	0.03	0.04	0.02	0.02	0.04	0.03	0.03
Al <sub>2</sub> O <sub>3</sub>	8.75	12.30	10.17	11.45	13.08	11.72	12.03	11.89	13.10
Cr <sub>2</sub> O <sub>3</sub>	54.83	51.50	53.92	52.69	50.35	52.15	52.14	51.58	50.49
TiO <sub>2</sub>	0.05	0.08	0.08	0.09	0.11	0.16	0.10	0.10	0.09
V <sub>2</sub> O <sub>3</sub>	0.23	0.30	0.25	0.26	0.28	0.28	0.27	0.27	0.28
Fe <sub>2</sub> O <sub>3</sub>	7.11	7.66	7.01	7.00	7.25	7.30	7.31	7.25	7.57
(FeO*)	24.57	22.86	22.17	22.20	24.09	24.14	20.81	24.89	24.12
FeO	18.17	15.97	15.86	15.91	17.56	17.58	14.24	18.37	17.32
MnO	0.37	0.34	0.34	0.37	0.36	0.37	0.34	0.40	0.35
MgO	9.38	11.34	11.06	11.17	10.42	10.38	12.29	9.76	10.63
NiO	0.06	0.13	0.09	0.11	0.06	0.11	0.13	0.10	0.11
CaO	<dl	0.01	0.01	0.02	0.01	0.01	0.01	0.00	0.01
Total (FeO*)	98.29	98.87	98.10	98.39	98.77	99.33	98.15	99.03	99.19
Ti	0.010	0.016	0.017	0.018	0.021	0.031	0.021	0.021	0.017
Si	0.016	0.008	0.007	0.009	0.006	0.005	0.010	0.007	0.007
Al	2.786	3.784	3.186	3.556	4.042	3.624	3.705	3.701	4.024
Cr	11.712	10.624	11.330	10.973	10.431	10.816	10.768	10.765	10.403
V	0.049	0.062	0.053	0.056	0.060	0.059	0.057	0.058	0.058
Fe <sup>3+</sup>	1.448	1.507	1.405	1.389	1.432	1.443	1.439	1.442	1.487
sum	16.022	16.000	15.997	16.001	15.991	15.978	16.000	15.993	15.996
Fe <sup>2+</sup>	4.104	3.483	3.523	3.503	3.846	3.854	3.108	4.053	3.771
Ni	0.012	0.026	0.020	0.024	0.012	0.024	0.027	0.022	0.022
Mg	3.776	4.412	4.381	4.385	4.067	4.059	4.786	3.841	4.131
Mn	0.086	0.074	0.077	0.082	0.080	0.083	0.076	0.090	0.077
Ca	<dl	0.004	0.002	0.005	0.004	0.002	0.003	0.001	0.003
sum	7.978	8.000	8.003	7.999	8.009	8.022	8.000	8.007	8.004
Cr#	80.783	73.737	78.053	75.522	72.073	74.903	74.401	74.415	72.108
Fe2#	52.076	44.120	44.574	44.407	48.600	48.708	39.371	51.346	47.725
Fe3#	9.079	9.469	8.823	8.724	9.005	9.088	9.044	9.064	9.345

Note: <dl = less than detection limit

**Table 2.** Clinopyroxene analyses from Betts Cove rocks.

	Scrape Point lavas									
	MMDYK?	Groundmass		Groundmass		Phenocryst	Groundmass		Phenocryst	Groundmass
	95-522	95-301	95-702	95-715	95-716	95-726	95-1077			
SiO <sub>2</sub>	52.67	46.53	48.00	50.55	51.40	51.28	50.24	49.21		
Al <sub>2</sub> O <sub>3</sub>	1.47	4.82	5.22	3.01	3.09	3.01	3.05	4.30		
Cr <sub>2</sub> O <sub>3</sub>	1.33	3.07	2.62	2.06	1.37	1.82	3.86	3.38		
FeO	2.54	7.09	6.61	5.24	2.53	5.11	5.59	5.45		
FeO*	4.81	11.61	10.26	8.10	4.92	7.53	9.88	9.21		
TiO <sub>2</sub>	0.03	2.15	1.66	0.95	0.46	0.72	1.09	1.48		
Cr <sub>2</sub> O <sub>3</sub>	0.72	0.11	0.09	0.18	0.69	0.03	0.06	0.15		
MgO	19.08	12.17	14.01	16.00	16.91	16.52	15.34	15.31		
MnO	0.15	0.24	0.29	0.20	0.13	0.20	0.28	0.20		
CaO	20.32	20.42	19.51	20.14	21.65	20.37	20.49	20.48		
Na <sub>2</sub> O	0.05	0.50	0.43	0.32	0.28	0.23	0.43	0.41		
K <sub>2</sub> O	0.02	0.01	0.01	0.02	0.02	0.02	0.02	<dl		
Total (FeO*)	99.33	98.58	99.49	99.47	99.54	99.90	100.46	100.37		
Fe# (wt %)	20.14	48.83	42.13	33.57	22.53	31.33	39.20	37.56		
Si	1.925	1.775	1.796	1.873	1.884	1.886	1.845	1.807		
Al (total)	0.064	0.217	0.230	0.132	0.134	0.131	0.132	0.186		
Al (iv)	0.075	0.225	0.204	0.127	0.116	0.114	0.132	0.186		
Al (vi)	-	-	0.026	0.004	0.018	0.016	-	-		
Fe <sup>+3</sup>	0.069	0.144	0.114	0.088	0.073	0.074	0.132	0.115		
Fe <sup>+2</sup>	0.078	0.226	0.207	0.162	0.077	0.157	0.172	0.167		
Ti	0.001	0.062	0.047	0.027	0.013	0.020	0.030	0.041		
Cr	0.021	0.003	0.003	0.005	0.020	0.001	0.002	0.004		
Mg	1.039	0.692	0.781	0.884	0.924	0.905	0.839	0.838		
Mn	0.005	0.008	0.009	0.006	0.004	0.006	0.009	0.006		
Ca	0.796	0.835	0.782	0.799	0.850	0.803	0.807	0.806		
Na	0.003	0.037	0.031	0.023	0.020	0.016	0.031	0.029		
K	0.001	0.001	0.001	0.001	0.001	0.001	0.001	<dl		
	<b>Bobby Cove Fm</b>					<b>Round Harbour lava</b>		<b>Venam's Bight Fm</b>		
	<b>Andesite clast</b>	<b>Mafic tuff</b>	<b>Hematized lava</b>	<b>Dacite tuff</b>	<b>Andesite clast</b>	<b>Phenocryst</b>	<b>Groundmass</b>	<b>Phenocryst lava</b>		
	<b>95-307</b>	<b>94-389</b>	<b>95-397</b>	<b>95-442</b>	<b>95-493</b>	<b>94-83</b>		<b>94-803</b>		
SiO <sub>2</sub>	51.39	51.27	51.93	50.28	52.14	50.87	50.29	50.40		
Al <sub>2</sub> O <sub>3</sub>	3.36	3.01	2.41	2.99	2.53	2.70	2.70	3.43		
Fe <sub>2</sub> O <sub>3</sub>	1.08	1.13	0.94	1.68	1.51	2.52	3.18	1.56		
FeO	1.57	5.20	3.58	2.46	3.53	5.16	7.30	5.56		
FeO*	4.11	6.46	4.62	6.35	5.73	7.96	10.84	7.30		
TiO <sub>2</sub>	0.31	0.44	0.25	0.38	0.35	0.64	0.80	0.68		
Cr <sub>2</sub> O <sub>3</sub>	0.48	0.31	0.38	0.30	0.25	0.29	0.15	0.33		
MgO	16.64	16.72	17.92	15.93	16.42	17.11	15.89	16.61		
MnO	0.10	0.14	0.11	0.17	0.14	0.21	0.34	0.16		
CaO	22.95	22.19	22.51	22.16	22.44	20.23	19.01	20.93		
Na <sub>2</sub> O	0.21	0.25	0.17	0.22	0.20	0.32	0.35	0.32		
K <sub>2</sub> O	0.01	0.02	0.02	0.01	0.01	0.02	0.02	0.02		
Total (FeO*)	99.55	100.68	100.22	98.79	100.22	100.04	100.03	100.01		
Fe# (wt %)	19.81	27.880	20.510	28.34	25.67	31.60	39.98	30.51		
Si	1.881	1.862	1.882	1.867	1.906	1.860	1.857	1.845		
Al (total)	0.145	0.129	0.103	0.131	0.109	0.116	0.118	0.148		
Al (iv)	0.119	0.129	0.103	0.133	0.094	0.116	0.118	0.148		
Al (vi)	0.026	-	-	-	0.015	-	-	-		
Fe <sup>+3</sup>	0.078	0.038	0.032	0.121	0.067	0.086	0.110	0.053		
Fe <sup>+2</sup>	0.048	0.158	0.109	0.076	0.108	0.158	0.226	0.170		
Ti	0.008	0.012	0.007	0.011	0.010	0.017	0.022	0.019		
Cr	0.014	0.009	0.011	0.009	0.007	0.008	0.004	0.010		
Mg	0.908	0.905	0.968	0.882	0.894	0.933	0.874	0.906		
Mn	0.003	0.004	0.004	0.005	0.004	0.006	0.011	0.005		
Ca	0.900	0.864	0.874	0.882	0.879	0.792	0.752	0.821		
Na	0.015	0.017	0.012	0.016	0.014	0.022	0.025	0.023		
K	0.001	0.001	0.001	0.001	0.001	0.001	0.001	0.001		

MMDYK? = dyke of probable Fly Pond affinity from within the Betts Head Formation lavas  
 - = no data. <dl = below detection limit

Table 2. (cont.)

	Oikocrysts in peridotite cumulate									
	95-667	95-668	95-670	95-671	95-672	95-674	95-675	95-677	95-681	
SiO <sub>2</sub>	53.03	53.23	53.10	52.85	53.05	53.41	52.84	52.20	52.95	
Al <sub>2</sub> O <sub>3</sub>	1.84	1.60	1.60	1.89	1.82	1.52	1.62	1.84	1.57	
Fe <sub>2</sub> O <sub>3</sub>	1.37	1.02	0.99	1.09	1.07	1.01	1.02	0.99	1.11	
FeO	3.27	2.05	2.31	2.31	2.22	2.25	1.96	1.40	1.85	
FeO*	5.25	3.72	3.75	4.02	3.93	3.77	3.68	3.82	4.02	
TiO <sub>2</sub>	0.03	0.02	0.01	0.02	0.02	0.02	0.02	0.03	0.03	
Cr <sub>2</sub> O <sub>3</sub>	0.33	0.79	0.80	0.77	0.84	0.82	0.84	0.88	0.62	
MgO	18.37	19.57	19.28	19.09	19.24	19.67	19.00	19.01	19.29	
MnO	0.17	0.14	0.11	0.13	0.12	0.12	0.11	0.10	0.14	
CaO	21.02	20.49	20.58	20.58	20.66	20.39	21.05	20.86	20.72	
Na <sub>2</sub> O	0.07	0.06	0.07	0.07	0.06	0.06	0.06	0.06	0.08	
K <sub>2</sub> O	0.01	0.02	0.02	0.02	0.02	0.02	0.01	0.02	0.02	
Total (FeO*)	100.12	99.65	99.31	99.43	99.77	99.79	99.22	98.83	99.44	
Fe# (wt %)	22.21	15.97	16.28	17.38	16.95	16.08	16.21	16.72	17.22	
Si	1.927	1.931	1.935	1.925	1.925	1.935	1.929	1.912	1.927	
Al (total)	0.079	0.069	0.069	0.081	0.078	0.065	0.070	0.080	0.067	
Al (iv)	0.073	0.069	0.065	0.075	0.075	0.065	0.071	0.088	0.073	
Al (vi)	0.006	—	0.003	0.006	0.003	—	—	—	—	
Fe <sup>+3</sup>	0.060	0.051	0.044	0.052	0.052	0.046	0.052	0.074	0.066	
Fe <sup>+2</sup>	0.099	0.062	0.070	0.070	0.067	0.068	0.060	0.043	0.056	
Ti	0.001	0.001	0.000	0.001	0.001	0.000	0.000	0.001	0.001	
Cr	0.010	0.023	0.023	0.022	0.024	0.024	0.024	0.026	0.018	
Mg	0.995	1.058	1.047	1.036	1.041	1.062	1.034	1.038	1.046	
Mn	0.005	0.004	0.003	0.004	0.004	0.004	0.003	0.003	0.004	
Ca	0.819	0.796	0.803	0.803	0.803	0.792	0.823	0.819	0.808	
Na	0.005	0.004	0.005	0.005	0.004	0.004	0.004	0.004	0.005	
K	0.001	0.001	0.001	0.001	0.001	0.001	0.001	0.001	0.001	
	Websterite phenocryst				Orthopyroxenite phenocryst	Websterite phenocryst		Websterite oikocryst		
	94-383	94-384	94-386	94-387	94-388	94-389	95-682	94-390		
SiO <sub>2</sub>	52.44	52.73	52.08	52.90	52.52	52.52	52.68	52.92		
Al <sub>2</sub> O <sub>3</sub>	1.95	1.88	2.19	1.69	1.90	1.95	1.71	1.54		
Fe <sub>2</sub> O <sub>3</sub>	0.61	0.56	1.47	1.27	1.34	1.35	1.15	1.02		
FeO	3.91	4.11	3.10	2.50	2.65	2.67	2.09	1.81		
FeO*	4.59	4.73	5.40	4.60	4.86	4.89	4.12	3.66		
TiO <sub>2</sub>	0.05	0.04	0.06	0.03	0.06	0.05	0.07	0.03		
Cr <sub>2</sub> O <sub>3</sub>	0.40	0.37	0.49	0.51	0.60	0.57	0.69	0.80		
MgO	19.19	19.14	17.80	18.80	18.09	18.31	18.86	19.45		
MnO	0.12	0.15	0.15	0.14	0.15	0.12	0.13	0.12		
CaO	21.26	21.28	21.03	20.84	21.37	21.05	20.90	20.50		
Na <sub>2</sub> O	0.07	0.08	0.08	0.08	0.08	0.08	0.08	0.08		
K <sub>2</sub> O	0.02	0.02	0.01	0.02	0.01	0.02	0.02	0.02		
Total	100.03	100.36	99.29	99.61	99.65	99.56	99.26	99.11		
Fe# (wt %)	19.30	19.811	23.24	19.64	21.19	21.04	17.93	15.84		
Si	1.897	1.903	1.912	1.927	1.918	1.918	1.924	1.930		
Al (total)	0.083	0.080	0.095	0.072	0.082	0.084	0.073	0.066		
Al (iv)	0.083	0.080	0.088	0.073	0.082	0.082	0.076	0.070		
Al (vi)	—	—	0.006	—	—	0.002	—	—		
Fe <sup>+3</sup>	0.021	0.019	0.071	0.064	0.067	0.068	0.062	0.056		
Fe <sup>+2</sup>	0.118	0.124	0.095	0.076	0.081	0.082	0.064	0.055		
Ti	0.001	0.001	0.002	0.001	0.002	0.001	0.002	0.001		
Cr	0.011	0.011	0.014	0.015	0.017	0.017	0.020	0.023		
Mg	1.035	1.029	0.974	1.021	0.985	0.997	1.027	1.057		
Mn	0.004	0.005	0.005	0.004	0.005	0.004	0.004	0.004		
Ca	0.824	0.823	0.827	0.813	0.836	0.824	0.818	0.801		
Na	0.005	0.006	0.006	0.006	0.006	0.006	0.006	0.006		
K	0.001	0.001	0.001	0.001	0.001	0.001	0.001	0.001		

— = no data



Table 2. (cont.)

	Late intrusive series		(?) Layered cumulate series			
	Gabbro oikocryst	LAYGABB phenocryst	Sieved gabbronorite vein	Trondhjemite vein phenocrysts		Websterite
	95-537	94-396	95-619V	Dark	Light	
				95-684V		95-619H
SiO <sub>2</sub>	52.30	52.99	51.91	52.60	51.01	51.87
Al <sub>2</sub> O <sub>3</sub>	1.86	1.66	1.49	0.53	1.69	1.49
Fe <sub>2</sub> O <sub>3</sub>	1.50	1.00	1.87	2.41	2.75	1.89
FeO	3.24	4.42	4.51	6.22	9.26	4.29
FeO*	5.55	5.53	7.18	9.58	12.64	7.10
TiO <sub>2</sub>	0.18	0.04	0.18	0.04	0.53	0.17
Cr <sub>2</sub> O <sub>3</sub>	0.16	0.22	0.32	0.01	<dl	0.31
MgO	17.65	19.13	16.48	13.16	10.87	16.46
MnO	0.16	0.15	0.20	0.11	0.13	0.18
CaO	21.00	21.00	21.47	23.62	22.61	21.62
Na <sub>2</sub> O	0.19	0.05	0.12	0.62	0.80	0.13
K <sub>2</sub> O	0.02	0.02	0.02	0.02	0.01	0.02
Total	99.07	100.68	99.37	100.27	100.31	99.35
Fe# (wt %)	23.93	22.439	30.26	42.09	53.77	30.06
Si	1.924	1.909	1.921	1.958	1.923	1.920
Al (total)	0.081	0.070	0.065	0.023	0.075	0.065
Al (iv)	0.076	0.070	0.079	0.042	0.077	0.080
Al (vi)	0.005	—	—	—	0.002	—
Fe <sup>+3</sup>	0.071	0.034	0.083	0.104	0.107	0.087
Fe <sup>+2</sup>	0.100	0.133	0.140	0.194	0.292	0.133
Ti	0.005	0.001	0.005	0.001	0.015	0.005
Cr	0.005	0.006	0.009	0.001	<dl	0.009
Mg	0.968	1.027	0.909	0.730	0.611	0.908
Mn	0.005	0.004	0.006	0.003	0.004	0.006
Ca	0.828	0.811	0.852	0.942	0.914	0.857
Na	0.013	0.004	0.009	0.044	0.059	0.010
K	0.001	0.001	0.001	0.001	0.001	0.001

LAYGABB = gabbronorite interlayered with pyroxenite  
 <dl = below detection limit

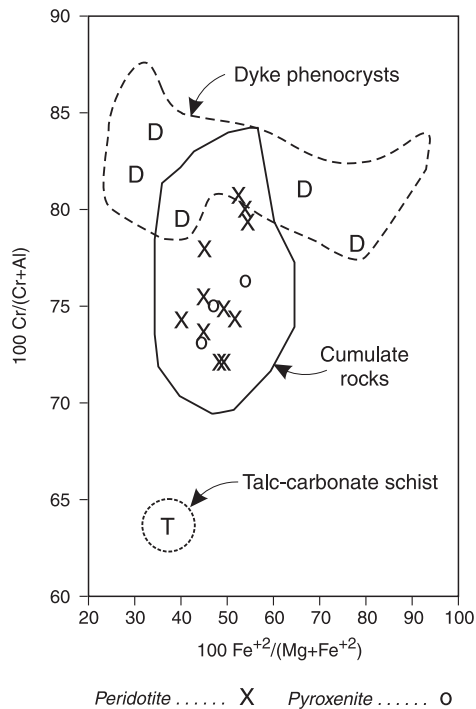


Figure 24.

*Cr/(Cr+Al) versus  $Fe^{+2}/(Mg+Fe^{+2})$  in Cr-spinel phenocrysts from Betts Cove cumulate rocks and dykes. Note the wider range of  $Fe^{+2}/(Mg+Fe^{+2})$  of Cr-spinel phenocrysts in dykes versus cumulate rocks, reflecting a diversity of quenching temperatures. Note also how Cr-spinel phenocrysts in the talc-carbonate schist differ considerably from those of ultramafic cumulate rocks, suggesting that the former are not reworked equivalents of the latter.*

**Table 3.** Amphibole analyses from Betts Cove rocks.

	Betts Head sill		Bobby Cove felsic/intermediate pyroclastic rocks			
	95-526		94-389	95-132	95-307	95-440
	Xenocryst core	Phenocryst rim	Mafic tuff	Dacitic tuff	Andesitic clast	Dacitic clast
SiO <sub>2</sub>	42.07	43.27	39.05	45.01	41.53	41.47
Al <sub>2</sub> O <sub>3</sub>	11.69	10.62	15.52	11.32	14.34	12.43
TiO <sub>2</sub>	2.27	2.42	1.91	1.12	1.15	1.66
Cr <sub>2</sub> O <sub>3</sub>	<dl	0.02	0.01	0.06	0.05	0.02
Fe <sub>2</sub> O <sub>3</sub>	7.31	8.83	9.23	11.68	9.07	11.96
FeO	5.33	2.39	5.95	0.79	0.08	8.39
FeO*	11.90	10.33	14.25	11.29	8.23	19.14
MnO	0.18	0.13	0.18	0.22	0.11	0.38
MgO	14.44	16.34	12.24	15.23	16.21	10.00
CaO	11.68	11.51	12.05	10.79	12.14	10.52
Na <sub>2</sub> O	2.10	2.14	2.16	1.71	2.13	2.14
K <sub>2</sub> O	0.98	1.09	0.67	0.45	0.38	0.42
Total	98.05	98.77	98.96	98.36	97.19	99.38
Si	6.134	6.200	5.697	6.390	5.967	6.084
Al (total)	2.012	1.795	2.670	1.894	2.429	2.149
Al (iv)	1.853	1.800	2.303	1.610	2.033	1.916
Al (vi)	0.159	–	0.368	0.285	0.396	0.233
Fe <sup>+3</sup>	0.795	0.952	1.013	1.247	0.979	1.319
Fe <sup>+2</sup>	0.659	0.286	0.726	0.094	0.010	1.029
Ti	0.249	0.261	0.210	0.119	0.124	0.183
Cr	<dl	0.002	0.001	0.007	0.005	0.002
Mg	3.129	3.489	2.662	3.222	3.471	2.186
Mn	0.022	0.015	0.022	0.027	0.013	0.047
Ca	1.826	1.768	1.883	1.641	1.869	1.654
Na	0.593	0.593	0.610	0.469	0.595	0.610
Nam4	0.161	0.227	0.117	0.359	0.131	0.346
NaA	0.432	0.366	0.494	0.111	0.464	0.263
K	0.183	0.200	0.125	0.081	0.070	0.078

<dl = below detection limit  
– = no data

the Snooks Arm road immediately east of Red Cliff Pond contains chromite with a very different signature, suggesting it may not represent a reworked cumulate rock.

Analysis of calcic pyroxene crystals show progressive Fe-enrichment from peridotite to gabbro and trondhjemite (Fig. 25). All are Ti poor (Table 2), consistent with a boninitic affinity (*see* Beccaluva et al., 1989). The composition of clinopyroxene crystals from the sheeted dykes show considerable scatter in Wo content, as do groundmass pyroxene in the Snooks Arm Group lavas. This probably reflects lack of full equilibration in rapidly cooled grains (Hall et al., 1985). Phenocrysts in Snooks Arm Group tholeiitic lavas and sills occupy a limited compositional range. Phenocrysts in Bobby Cove andesite and basalt have higher Wo contents.

### Geochemistry and petrogenesis

New geochemical data were generated at the Centre géoscientifique de Québec (CGQ) laboratories. Altered margins of samples and prominent veins were removed with a

saw. Sawmarks were removed with sandpaper. Samples were crushed in a steel jaw crusher, and then reduced to powder in an agate shatterbox. Major elements and Cr, Ni, Cu, Zn, Sr, and Ba were analyzed by conventional X-ray fluorescence or ICP-AES methods for samples collected in 1994, and by ICP-AES for samples collected in 1995, 1996, and 1997. Other trace elements were analyzed either by instrumental neutron activation or by ICP-MS on a VG Turbo Plasma Quad<sup>2+</sup> ICP-MS, using a method similar to that described in Varfalvy et al. (1997). Analytical precision for ICP-MS analysis of tholeiitic lavas is better than 1% for La, Ce, Pr, Nd, Eu, Tb, Lu, and Ba; 2% for Sm, Gd, Dy, Ho, Er, Tm, Yb, Th, Rb, and Sr; 4% for Zr, Cs, Y, and U; and about 10% for Nb and Pb. Precision is lower for the extremely depleted boninitic rocks, in which elemental abundances approach detection limits. Laflèche et al. (1998, his Appendix 1) have published analyses of international rock standards obtained in the CGQ laboratories. The 353 new analyses are supplemented by previously published data from Upadhyay (1973), DeGrace et al. (1976), Jenner (1977), Coish (1977a), Coish et al. (1982), Hurley (1982), Saunders (1985), Al (1990), and Swinden et al. (1997)

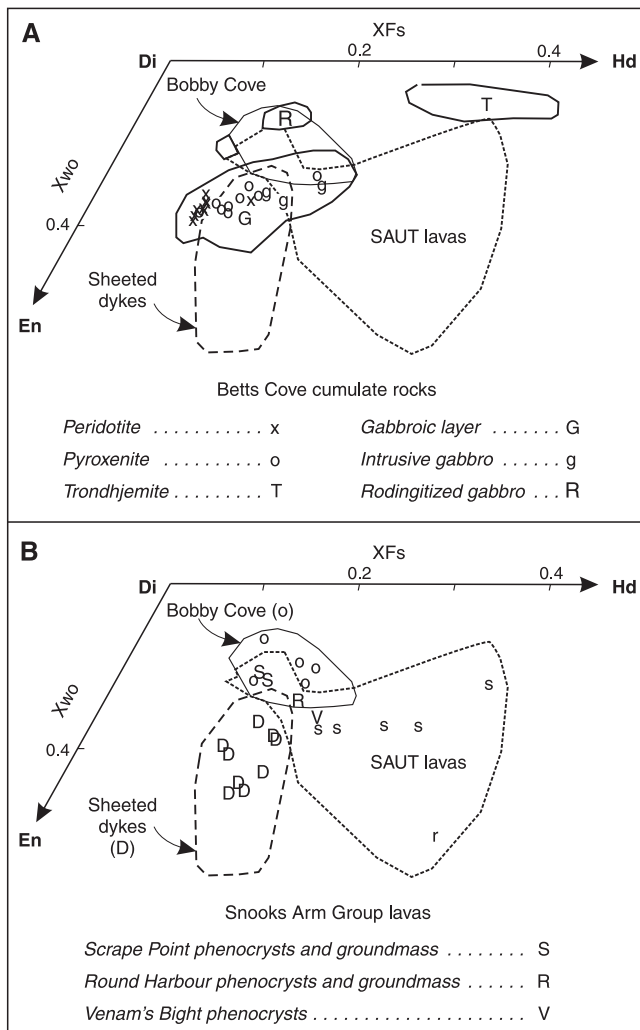


**Figure 25.** Clinopyroxene analyses from Betts Cove rocks represented in the ternary enstatite-wollastonite-ferrosilite diagram. Di = diopside, Hd = hedenbergite, En = enstatite. Enveloping fields include all spot analyses. The symbols represent the average analysis for a given rock. Data from this study and Coish (1977a). **A**) Cumulate rocks, **B**) lavas and dykes. Note how phenocrysts in lavas have lower Fe-contents than groundmass prisms, and the higher wollastonite content of pyroxene from rocks of the Bobby Cove Formation. SAUT = Snooks Arm upper tholeiitic series rocks.

which were compiled to yield the 'average' analyses. Most of the older trace element data was not included, however. All sample locations, together with the complete structural and analytic database, and a digital version of the map, are available in Bédard et al. (in press). Averages for different lithostratigraphic units are in Tables 4 and 5.

### Impact of hydrothermal metamorphism

Samples affected by obvious hydrothermal alteration related to ore deposition (i.e. marked S- and Fe-enrichment), and extreme enrichment or depletion in Na<sub>2</sub>O, K<sub>2</sub>O, or CaO, were

excluded from the data set used for petrogenetic interpretation and from the computed averages. Coish (1977b), Coish and Church (1979), and Coish et al. (1982) concluded that Ti, P, Ni, Cr, Zr, Y, the rare-earth elements (REEs), Al<sub>2</sub>O<sub>3</sub>, and FeO\*/MgO in the Betts Cove rocks largely reflect magmatic abundances. The concentrations of elements such as CaO and Na<sub>2</sub>O are commonly perturbed, however. Consequently it is not possible to classify the Betts Head magmas in a reliable way using the Crawford et al. (1989) scheme, which requires accurate values for CaO, SiO<sub>2</sub>, and alkali elements. Instead, the Betts Cove lavas and dykes have been subdivided using relatively immobile trace elements, upon which the petrogenetic interpretations outlined below also principally depend.

The elements Rb, Cs, and K display random positive or negative anomalies on MORB-normalized trace-element variation diagrams (not shown) that are attributable to hydrothermal remobilization. Nevertheless, averaged values of these elements (excluding data from obvious metasomatic zones) do not show large anomalies on such diagrams in comparison to nearby, more immobile elements (Th, La), suggesting that Rb, Cs, and K were internally redistributed within map units, but were not systematically leached or enriched from the ophiolitic complex (Bédard, 1999). Comparison of U versus Th distributions in Betts Head lavas and dykes (Bédard, 1999) suggests that only a few strongly perturbed rocks have been enriched in U. On normalized trace-element diagrams, Betts Head lavas and dykes always show positive anomalies for Ba, U, Sr, and Pb, which bring their profiles into correspondence with those of recent fresh boninite (see below, Fig. 27A). One could speculate that these Betts Cove lavas had immobile elements identical to those of recent boninite, but had some unknown, different distribution of Ba, U, Sr, Pb, and Si, and that it is the action of pervasive hydrothermal metasomatism that somehow replicated boninitic signatures for these elements. But considering all the other evidence pointing towards a boninitic affinity for the Betts Head lavas, a hydrothermal origin for the resemblance to boninite for Ba, U, Sr, Pb, and Si seems providential, and so we conclude that these elements typically retain abundance levels similar to those in the original magmas. This is not to say that hydrothermal alteration had no impact at all on these elements. For example, Ba, Sr, and Pb (not shown) show rather poor correlations when plotted against Th. We conclude that hydrothermal alteration is responsible for the large degree of dispersion of these elements in geochemical variation diagrams, but that the high abundances of Ba, U, Sr, Pb, and Si seen in most of these rocks are not in themselves of hydrothermal origin.

### Betts Head Formation and the sheeted dyke complex

Analyses of Betts Cove dyke complex rocks are indistinguishable from those of Betts Head Formation lavas (Fig. 26), implying that the sheeted dykes and lavas belong to a single comagmatic suite. The strongly porphyritic boninite (perknite) has very high Cr, Ni, and MgO contents indicative of phenocryst accumulation (Coish and Church, 1979).

**Table 4a.** Average Betts Head, Mount Misery, and Nippers Harbour lavas.

	Low-Ti boninite lavas and dykes			Intermediate-Ti boninite lavas and dykes			Mount Misery lavas and dykes			Nippers Harbour massif
	Average	FeO/MgO		Average	FeO/MgO		Average	FeO/MgO		
		>0.80	<0.61		>0.80	<0.74		>1.69	<1.14	
	Average	Average evolved	Average primitive	Average	Average evolved	Average primitive	Average	Average evolved	Average primitive	f/g
SiO <sub>2</sub>	55.03	56.58	53.38	53.81	54.95	52.64	52.57	53.52	52.32	55.80
TiO <sub>2</sub>	0.14	0.17	0.12	0.47	0.50	0.46	1.06	1.38	0.82	0.29
Al <sub>2</sub> O <sub>3</sub>	12.78	14.80	11.05	15.86	16.23	15.43	16.63	16.86	16.65	15.80
FeO*	8.39	8.38	8.54	8.13	8.61	7.98	10.61	12.68	9.34	9.53
MnO	0.17	0.16	0.17	0.20	0.26	0.15	0.21	0.25	0.20	0.17
MgO	12.91	8.65	16.78	10.48	8.91	12.25	7.70	5.60	9.25	6.88
CaO	7.53	7.22	8.05	6.72	5.96	7.12	6.22	4.53	6.74	7.64
Na <sub>2</sub> O	2.85	3.93	1.66	4.05	4.64	3.36	3.96	4.46	3.44	3.39
K <sub>2</sub> O	0.27	0.25	0.27	0.48	0.35	0.74	1.18	1.13	1.45	0.46
P <sub>2</sub> O <sub>5</sub>	0.02	0.03	0.02	0.04	0.04	0.04	0.09	0.12	0.09	0.04
LOI	4.20	3.42	4.89	4.29	4.71	4.11	5.65	4.67	6.13	2.17
FeO*#	40.7	49.6	34.2	44.1	49.1	39.8	58.1	69.6	50.3	58.5
FeO/MgO	0.71	1.00	0.52	0.81	0.99	0.66	1.49	2.38	1.02	1.45
S	371	348	469	778	778	–	921	–	921	–
Cr	625	189	1028	352	326	380	227	73	371	109
Ni	227	83	387	151	121	171	106	56	160	64
V	251	280	236	245	252	239	293	373	248	330
Cu	61	55	50	79	89	69	47	26	66	26
Zn	68	76	64	154	340	55	112	128	145	58
Sc	38	42	34	36	39	33	38	41	36	–
Co	48	41	51	69	66	70	45	54	44	51
Rb	3.1	1.1	1.1	1.0	0.9	1.0	21.2	33.7	22.5	18.2
Ba	24	15	22	58	49	46	97	127	76	–
Sr	88	111	69	129	132	122	110	97	93	143
Nb	0.47	0.45	0.30	0.47	0.47	0.46	1.11	1.08	0.71	–
Ta	0.05	0.03	0.03	0.05	0.04	0.05	0.12	0.12	0.13	–
Zr	14	16	14	24	24	25	52	62	40	42
Y	6.7	9.4	2.9	12	12	12	20	24	17	12
Hf	0.33	0.36	0.27	0.59	0.66	0.52	1.47	2.24	0.90	–
La	0.714	0.757	0.738	1.027	1.127	0.954	1.948	2.263	1.581	–
Ce	1.692	1.880	1.649	3.241	3.292	3.081	6.116	7.229	4.847	–
Nd	0.922	1.111	0.779	2.718	2.564	2.960	5.740	7.178	4.026	–
Sm	0.296	0.355	0.235	0.946	0.902	1.049	2.047	2.453	1.576	–
Eu	0.111	0.121	0.102	0.382	0.370	0.449	0.785	0.949	0.603	–
Gd	0.415	0.543	0.282	1.511	1.320	1.698	2.628	3.059	2.177	–
Tb	0.091	0.113	0.064	0.274	0.248	0.297	0.527	0.648	0.416	–
Dy	0.691	0.877	0.472	2.140	1.837	2.477	3.331	3.841	2.802	–
Ho	0.164	0.205	0.115	0.415	0.428	0.383	0.684	0.760	0.595	–
Er	0.564	0.708	0.421	1.585	1.378	1.876	2.074	2.317	1.857	–
Tm	0.112	0.112	0.072	0.172	0.172	0.173	0.308	0.349	0.277	–
Yb	0.699	0.837	0.549	1.250	1.253	1.166	2.156	2.607	1.751	–
Lu	0.120	0.150	0.100	0.179	0.179	0.161	0.304	0.344	0.255	–
Pb	2.2	2.6	1.5	5.8	6.0	4.7	5.2	5.5	6.8	–
Th	0.140	0.144	0.153	0.152	0.160	0.133	0.195	0.159	0.183	–
U	0.092	0.079	0.087	0.250	0.255	0.242	0.286	0.568	0.092	–
Cs	0.082	0.059	0.087	0.268	0.220	0.259	0.718	1.224	0.483	–
As	39.0	–	66.0	2.0	2.0	–	3.0	–	3.5	–
Ag	–	–	–	–	–	–	5.4	–	5.7	–
Au	13.2	–	5.0	8.4	9.3	4.9	1.7	–	1.3	–

<dl = below detection limits  
– = no data available. All trace elements in ppm.

**Table 4b.** Average Snooks Arm Group upper tholeiitic and sedimentary rocks.

	Scrape Point lavas					Diabase/ gabbro sills	Venam's Bight lavas	Round Harbour lavas	Balsam Bud Cove	
	Average	Average aphyric	Average porphyritic	FeO/MgO					Lav	Sandstone matrix
				>1.70	<1.50					
				Average evolved	Average primitive					
SiO <sub>2</sub>	50.68	51	49.64	51.99	50.78	49.21	49.49	49.37	49.95	48.44
TiO <sub>2</sub>	1.94	2.1	1.42	2.51	1.91	2.29	1.95	1.79	1.46	1.30
Al <sub>2</sub> O <sub>3</sub>	15.87	15.05	18.52	14.16	15.56	16.03	15.69	16.32	19.16	19.92
FeO*	10.71	11.28	8.88	12.71	10.30	12.08	11.83	11.41	10.67	10.55
MnO	0.20	0.22	0.16	0.25	0.25	0.21	0.21	0.22	0.21	0.25
MgO	6.60	6.56	6.71	5.53	7.33	6.68	6.46	6.30	4.96	5.77
CaO	9.82	9.52	10.81	8.20	9.78	8.64	9.97	10.81	8.56	7.68
Na <sub>2</sub> O	3.61	3.89	2.69	4.38	3.62	4.00	3.71	3.21	2.21	2.94
K <sub>2</sub> O	0.44	0.25	1.07	0.19	0.32	0.35	0.47	0.40	2.58	2.90
P <sub>2</sub> O <sub>5</sub>	0.15	0.16	0.12	0.19	0.16	0.22	0.22	0.19	0.24	0.25
LOI	4.02	3.18	6.53	3.83	3.00	4.42	3.04	2.41	3.37	3.51
FeO*#	61.8	63.2	57.1	69.7	58.5	64.1	64.7	64.5	68.1	64.7
FeO/MgO	1.69	1.78	1.40	2.35	1.38	1.94	1.86	1.85	2.14	1.84
Cr	217	190	289	95	220	177	145	160	70	96
Ni	72	64	107	42	69	49	58	76	16	36
V	321	340	247	346	334	428	412	433	482	327
Cu	56	55	59	33	67	51	77	102	96	27
Zn	79	82	65	80	81	75	97	93	101	96
Sc	40	41	38	38	41	37	40	39	39	–
Co	62	61	62	47	60	65	76	105	55	53
Rb	8.0	4.3	20.0	3.0	5.7	6.4	14	18	44	42
Ba	73	47	138	58	26	55	161	161	689	378
Sr	196	179	251	166	159	231	207	287	369	424
Nb	4.50	4.84	3.52	5.96	4.21	5.84	6.80	6.33	13.0	29.0
Ta	0.39	0.43	0.20	0.55	0.35	0.96	0.56	0.50	0.38	–
Zr	112	123	78	125	120	132	133	124	115	101
Y	31	35	22	37	33	31	34	30	29	19
Hf	2.58	2.78	1.83	2.95	2.42	2.91	3.22	3.07	3.26	–
La	5.47	5.86	3.62	6.66	5.49	6.81	10.41	11.55	13.91	–
Ce	17.28	18.50	11.51	20.81	17.36	22.36	27.81	28.81	34.20	–
Nd	13.64	14.56	9.27	15.93	13.66	15.44	18.59	19.32	21.33	–
Sm	4.28	4.55	2.98	5.01	4.17	4.31	5.44	5.27	5.24	–
Eu	1.53	1.62	1.12	1.71	1.54	1.55	2.04	2.03	1.73	–
Gd	5.03	5.40	3.55	5.57	5.28	4.49	7.02	6.36	–	–
Tb	0.85	0.91	0.62	0.95	0.78	0.84	0.89	–	0.95	–
Dy	5.87	6.32	4.05	6.38	6.29	4.95	7.33	6.42	–	–
Ho	1.00	1.06	0.77	1.22	0.85	0.85	0.90	0.73	0.79	–
Er	3.24	3.44	2.35	3.71	3.11	2.65	4.01	3.10	–	–
Tm	0.43	0.46	0.33	0.49	0.37	0.38	0.49	0.32	0.42	–
Yb	2.84	3.02	2.08	3.09	2.66	2.57	3.01	2.91	3.06	–
Lu	0.41	0.43	0.29	0.44	0.38	0.38	0.46	0.43	0.45	–
Pb	3.3	3.4	2.7	2.1	5.4	7.0	9.0	13.0	13.7	9.5
Th	0.33	0.35	0.22	0.43	0.28	0.85	1.10	0.88	2.61	–
U	0.17	0.19	0.10	0.21	0.20	0.54	0.80	0.53	1.16	–
Cs	0.63	0.38	1.68	0.44	0.32	0.59	0.55	1.11	1.11	–
As	17.2	17.3	16.4	–	15.3	–	–	35.7	16.2	–
Ag	4.6	–	4.6	–	–	–	–	–	–	–

<dl = below detection limits  
– = no data available. All trace elements in ppm.

**Table 4c.** Average Snooks Arm Group dacite, rhyolite, and sedimentary rocks.

	DACITE				RHYOLITE			Scrape Point Fm		
	Balsam Bud Cove Fm	Bobby Cove Fm	Snooks Arm Gp	Round Harbour road dykes	Balsam Bud Cove Fm	Bobby Cove Fm	Snooks Arm Gp	Shale	Magnetite-rich sandstone	Magnetite-rich siltstone
SiO <sub>2</sub>	65.36	61.87	63.03	64.95	76.31	76.08	76.15	75.83	46.43	60.67
TiO <sub>2</sub>	0.78	0.65	0.70	0.29	0.33	0.18	0.23	0.25	0.43	0.50
Al <sub>2</sub> O <sub>3</sub>	14.74	17.15	16.35	18.18	12.38	13.49	13.16	6.39	8.98	11.04
FeO*	7.77	5.75	6.42	4.49	3.19	1.60	2.08	10.84	35.36	19.20
MnO	0.19	0.10	0.13	0.15	0.06	0.06	0.06	0.65	1.21	0.31
MgO	2.47	3.09	2.88	1.38	0.95	0.59	0.70	3.43	3.56	1.70
CaO	2.34	5.43	4.40	4.52	2.31	2.62	2.53	1.58	0.78	1.93
Na <sub>2</sub> O	5.29	4.02	4.44	4.74	3.32	2.48	2.73	1.00	1.55	3.71
K <sub>2</sub> O	0.93	1.79	1.50	1.16	1.12	2.86	2.34	0.02	1.47	0.77
P <sub>2</sub> O <sub>5</sub>	0.14	0.16	0.16	0.13	0.02	0.07	0.05	0.04	0.25	0.17
LOI	3.16	2.43	2.67	1.64	1.95	1.50	1.64	2.71	2.71	2.15
FeO*#	75.6	65.0	68.5	76.3	77.4	72.3	73.8	76.0	90.9	91.9
FeO/MgO	3.11	1.98	2.36	3.23	3.48	2.81	3.01	3.16	10.0	11.3
Cr	39	110	86	82	47	45	45	138	193	118
Ni	15	55	41	–	8	8	8	20	83	64
V	–	89	89	23	21	23	22	41	278	26
Cu	60	14	30	5	11	7	8	20	98	4
Zn	101	72	82	69	80	36	49	25	209	23
Sc	28	9.9	15.8	7.2	8.5	7.5	7.8	–	–	–
Co	44	16	25	16	11	–	11	39	229	81
Rb	27	41	36	30	32	70	59	3.0	35	31
Ba	314	219	250	208	218	223	222	–	622	–
Sr	120	285	230	289	226	173	189	83	35	23
Nb	4.00	10.4	8.24	<3	10.0	15.9	14.1	3.50	6.5	7.00
Ta	–	0.50	0.50	<.3	–	1.78	1.78	–	–	–
Zr	164	149	154	77	219	82	123	50	65	89
Y	42	25	31	17	39	27	31	27	30	28
Hf	2.53	3.30	3.05	1.75	–	3.02	3.02	48.0	–	–
La	15.97	18.37	17.57	4.73	–	9.07	9.07	–	–	–
Ce	36.37	41.35	39.69	10.52	–	28.84	28.84	–	–	–
Nd	18.3	18.4	18.4	7.42	–	10.7	10.7	–	–	–
Sm	4.71	3.95	4.20	1.71	–	3.44	3.44	–	–	–
Eu	1.52	1.13	1.26	0.61	–	0.62	0.62	–	–	–
Gd	6.29	2.83	3.98	–	–	3.67	3.67	–	–	–
Tb	–	0.43	0.43	0.32	–	0.67	0.67	–	–	–
Dy	6.91	2.04	3.66	–	–	4.33	4.33	–	–	–
Ho	0.59	0.32	0.41	<.5	–	0.83	0.83	–	–	–
Er	4.64	0.98	2.20	–	–	3.08	3.08	–	–	–
Tm	0.42	0.13	0.22	<.2	–	0.38	0.38	–	–	–
Yb	3.43	0.87	1.73	1.45	–	3.03	3.03	–	–	–
Lu	0.50	0.14	0.26	0.25	–	0.46	0.46	–	–	–
Pb	16.0	8.20	10.8	10.0	–	11.6	11.6	13.5	45.5	10.0
Th	2.76	5.15	4.35	0.73	–	6.35	6.35	–	–	–
U	1.70	2.36	2.14	<.5	–	3.29	3.29	–	–	–
Cs	–	1.53	1.53	0.65	–	1.10	1.10	–	–	–
As	7.5	–	7.5	4.6	–	1.3	1.3	–	–	–
Ag	–	–	–	<5	–	<5	<5	–	–	–
Au	0.02	–	0.02	<.005	–	<.005	<.005	–	–	–

<dl = below detection limits  
– = no data available. All trace elements in ppm.

**Table 4d.** Average Snooks Arm Group lavas and tuffs, and Silurian granitoid rocks.

	Bobby Cove Fm lavas			Scrape Point Fm mafic tuffs	Cape St. John Gp lavas			Cape Brulé granite	Burlington granodiorite rocks	QFP* dykes
	High-Ti	Low-Ti	Mafic tuffs		Basalt	Andesite	Felsic			
SiO <sub>2</sub>	50.95	52.59	53.54	55.74	47.95	56.68	69.44	73.41	65.66	68.48
TiO <sub>2</sub>	1.30	0.87	0.95	0.94	2.01	2.52	0.82	0.27	0.56	0.47
Al <sub>2</sub> O <sub>3</sub>	17.38	16.12	16.53	17.95	18.19	14.68	14.38	12.68	16.63	15.80
FeO*	11.34	9.10	8.72	8.29	11.27	11.24	4.55	2.39	3.41	3.27
MnO	0.21	0.17	0.18	0.20	0.19	0.22	0.09	0.06	0.06	0.06
MgO	5.59	7.48	7.02	6.23	8.48	2.74	1.31	0.52	2.17	2.07
CaO	8.76	9.09	7.03	4.10	7.48	5.30	2.14	1.09	4.28	3.26
Na <sub>2</sub> O	4.01	3.59	4.42	5.11	3.29	4.72	3.63	3.27	4.89	2.77
K <sub>2</sub> O	0.26	0.92	1.55	1.34	0.90	1.27	3.42	6.25	2.14	2.53
P <sub>2</sub> O <sub>5</sub>	0.20	0.08	0.07	0.10	0.24	0.84	0.21	0.06	0.19	0.17
LOI	3.44	3.87	3.94	4.52	7.25	4.05	2.47	1.32	1.51	2.96
FeO*#	67.3	55.3	57.9	57.2	57.9	81.0	77.9	83.2	61.2	61.2
FeO/MgO	2.19	1.27	1.57	1.34	1.50	4.77	3.76	5.19	1.58	1.61
S	–	–	–	–	–	–	–	–	–	–
Cr	99	166	204	288	168	28	41	22	41	43
Ni	21	69	63	106	114	8	11	8	34	27
V	327	288	264	216	355	159	41	18	60	49
Cu	75	76	63	31	36	10	3	3	16	18
Zn	116	66	74	64	93	131	94	68	48	40
Ga	–	–	–	–	19	23	19	–	–	–
Sc	35	40	33	38	32	27	–	–	–	2
Co	40	30	34	33	66	43	17	7	9	1
Rb	5.7	15	29	20	21	42	93	101	47	62
Ba	37	94	135	465	94	656	810	1257	557	520
Sr	169	176	145	265	202	196	–	97	669	189
Nb	2.10	2.98	3.25	4.86	4.00	16.3	20.3	12.5	2.00	5.45
Ta	0.18	0.10	1.50	0.32	0.08	1.05	–	–	–	0.18
Zr	66	56	66	79	132	330	411	313	107	105
Y	27	19	16	20	29	56	47	50	7	17
Hf	1.65	1.31	1.45	2.07	3.12	7.96	–	–	–	0.67
La	4.20	4.27	6.11	9.22	8.83	23.44	–	–	–	5.33
Ce	11.46	10.36	16.08	22.25	22.18	61.47	–	–	–	16.91
Nd	8.17	7.41	11.04	11.67	15.28	38.04	–	–	–	13.47
Sm	2.69	2.46	2.56	3.04	4.15	9.64	–	–	–	1.17
Eu	1.005	0.893	0.952	1.03	1.54	2.92	–	–	–	0.221
Gd	3.68	2.59	3.07	3.28	–	10.72	–	–	–	1.59
Tb	0.614	0.499	0.488	0.554	0.827	1.642	–	–	–	0.272
Dy	4.52	3.20	3.37	3.36	–	11.96	–	–	–	1.48
Ho	0.963	0.640	0.642	0.685	0.742	1.846	–	–	–	0.271
Er	2.93	2.02	1.94	2.10	–	7.49	–	–	–	0.125
Tm	0.414	0.289	0.266	0.271	0.356	0.789	–	–	–	0.940
Yb	2.39	1.97	1.54	1.71	2.88	5.50	–	–	–	0.852
Lu	0.369	0.284	0.219	0.265	0.421	0.813	–	–	–	0.142
Pb	14.0	6.0	7.3	5.8	9.0	4.7	19.0	21.5	<5	6.5
Th	0.663	0.912	1.19	2.25	1.02	3.36	–	–	–	6.07
U	0.313	0.458	0.560	1.01	0.446	1.26	–	–	–	2.67
Cs	0.079	0.600	1.10	0.375	0.986	1.10	–	–	–	1.24
As	5.0	6.6	<1	–	–	–	–	–	–	–
Ag	<5	<5	<5	–	–	–	–	–	–	–
Au	<.005	<.005	<.005	–	–	–	–	–	–	–

\*QFP dykes = quartz-feldspar porphyry dykes from within the Betts Cove massif. <dl = below detection limits  
 – = no data available. All trace elements in ppm.

**Table 5a.** Average geochemical data for Betts Cove cumulate rocks. Sources of data given in text.

	Talc-magnesite carbonate schist	Quartz-hematite carbonate schist	Serpentine-magnesite schist	Peridotite cumulate	Orthopyroxene layers	Websterite layers	Clinopyroxene-websterite layers	Clinopyroxene dykes
SiO <sub>2</sub>	50.14	45.07	46.05	49.58	54.95	53.28	53.54	51.33
TiO <sub>2</sub>	0.05	<dl	<dl	0.04	0.05	0.06	0.07	0.07
Al <sub>2</sub> O <sub>3</sub>	0.79	1.47	0.46	2.07	3.42	6.30	3.71	6.61
FeO*	8.09	8.62	7.25	9.33	8.01	8.23	6.68	7.20
MnO	0.08	0.34	0.07	0.15	0.15	0.15	0.16	0.16
MgO	38.92	26.02	45.87	36.33	29.15	22.76	21.23	21.37
CaO	1.91	18.42	0.25	2.76	4.06	8.79	14.40	12.64
Na <sub>2</sub> O	0.02	0.01	0.01	0.08	0.18	0.37	0.18	0.38
K <sub>2</sub> O	<dl	0.04	<dl	0.01	0.01	0.04	0.01	0.26
P <sub>2</sub> O <sub>5</sub>	0.02	0.01	0.04	0.02	0.02	0.02	0.02	0.02
LOI	17.3	27.5	14.2	9.99	6.61	5.41	3.35	4.25
FeO*#	17.4	31.0	13.7	20.5	21.7	26.6	24.0	25.2
FeO/MgO	0.21	0.33	0.16	0.26	0.28	0.36	0.32	0.34
S	--	--	--	0.22	--	--	--	--
Cr	2129	2383	2144	2738	2724	1596	2037	1471
Ni	1801	1187	2061	1324	600	843	416	307
V	44	43	30	87	145	152	234	251
Cu	95	6	--	14	5	19	19	4
Zn	37	52	14	45	53	53	48	43
Ga	3	--	--	3.9	4.2	6.2	5.0	4.5
Sc	6.3	8.7	6.9	16.5	--	37.0	--	--
Co	77.4	68.6	104	94.7	63.2	69.8	46.7	53.0
Rb	0.18	24.5	--	0.73	1.1	0.28	0.28	0.31
Ba	6.43	17.7	--	2.9	2.4	6.9	2.0	1.6
Sr	43.7	227	13.0	5.5	6.8	12.7	6.7	4.5
Nb	--	--	--	0.16	0.21	0.16	2.71	0.15
Ta	--	--	--	0.01	0.01	0.02	0.01	0.01
Zr	7.7	6.3	3.0	2.8	2.7	3.9	3.3	3.2
Y	--	2.0	--	0.7	1.1	1.5	1.9	1.9
Hf	--	--	--	0.06	0.07	0.12	0.11	0.10
La	0.114	0.173	--	0.144	0.301	0.394	0.359	0.287
Ce	0.193	0.261	--	0.249	0.359	0.647	0.548	0.470
Pr	0.024	0.041	--	0.033	0.058	0.097	0.100	0.095
Nd	0.086	0.185	--	0.116	0.138	0.331	0.272	0.254
Sm	0.018	0.057	--	0.038	0.058	0.095	0.106	0.098
Eu	0.021	0.029	--	0.017	0.020	0.027	0.035	0.024
Gd	0.020	0.087	--	0.057	0.079	0.129	0.154	0.129
Tb	0.004	0.016	--	0.012	0.018	0.028	0.036	0.031
Dy	0.029	0.102	--	0.105	0.155	0.233	0.305	0.275
Ho	0.007	0.019	--	0.028	0.042	0.063	0.081	0.074
Er	0.026	0.054	--	0.064	0.156	0.176	0.289	0.271
Tm	0.004	0.007	--	0.047	0.029	0.083	0.051	0.049
Yb	0.033	0.039	--	0.121	0.215	0.280	0.360	0.345
Lu	0.006	0.006	--	0.022	0.041	0.051	0.066	0.064
Pb	--	--	--	1.30	0.32	0.29	0.63	0.08
Th	0.10	0.07	--	0.040	0.047	0.072	0.059	0.054
U	0.167	1.0	--	0.065	0.013	0.029	0.026	0.019
Cs	--	--	--	0.438	0.595	0.097	0.146	0.225

<dl = below detection limit  
-- = no data available

The lavas of the Betts Head Formation were subdivided by Coish and Church (1979) and Coish (1989) into 'low-Ti' and 'intermediate-Ti' suites; this first-order subdivision is adopted here. Rocks of the low-Ti suite correspond to the olivine+orthopyroxene+chromite±clinopyroxene pyritic dykes and lavas, whereas rocks of the intermediate-Ti suite correspond to the clinopyroxene+plagioclase pyritic dykes and lavas. In practice, many previously published analyses were assigned to these suites on the basis of their TiO<sub>2</sub> versus FeO\*/MgO (Fig. 26C) and La/Nd versus La (Fig. 26D) distributions.

Overall, the Betts Cove low-Ti lavas and dykes define trends of decreasing Cr and Ni (not shown, Bédard, 1999) with increasing FeO\*/MgO, and a steep, diffuse trend of SiO<sub>2</sub> enrichment (Fig. 26A). Rocks of the low-Ti suite have low contents of most incompatible elements (Fig. 26B, 27A). Their normalized trace-element profiles show relative enrichment in LILE (large-ion lithophile elements) and LREE (light rare-earth elements), in comparison to the middle REEs, which gives them 'U' shapes (Fig. 27A). Enrichment in LREEs is variable, as reflected in the wide range of La/Nd ratios (Fig. 26D). Negative Nb anomalies and positive Sr and Zr anomalies are common (Fig. 27A), as are positive Pb anomalies (not shown).



**Table 5b.** Gabbroic rocks.

	Layered gabbro-norite	Intrusive gabbro	Trondhjemite	Baie Verte gabbro	Nippers Harbour gabbro
SiO <sub>2</sub>	52.44	52.45	69.79	47.44	56.37
TiO <sub>2</sub>	0.08	0.53	0.23	0.12	0.20
Al <sub>2</sub> O <sub>3</sub>	17.57	15.12	14.66	13.17	15.82
FeO*	5.49	7.72	2.92	4.69	8.94
MnO	0.11	0.15	0.05	0.11	0.16
MgO	10.94	10.39	3.22	16.23	6.85
CaO	9.37	10.33	4.00	17.96	7.54
Na <sub>2</sub> O	2.28	2.59	4.95	0.27	3.35
K <sub>2</sub> O	1.70	0.74	0.16	<dl	0.73
P <sub>2</sub> O <sub>5</sub>	0.02	0.05	0.04	0.01	0.04
LOI	4.15	4.73	1.72	6.17	1.91
FeO*#	33.48	43.11	43.16	22.43	56.97
FeO/MgO	0.52	0.83	1.08	0.29	1.34
Cr	307	427	46	1206	171
Ni	155	151	34	230	72
V	204	230	159	130	341
Cu	6	48	8	5	29
Zn	37	51	20	19	57
Ga	10.8	12.6	12.0	5.0	14.5
Sc	–	40.4	19.5	–	–
Co	34.2	43.2	–	23.0	50.5
Rb	20.8	12.5	2.1	7.0	18.7
Ba	144	67	53	–	–
Sr	178	173	122	91	121
Nb	0.50	1.02	1.46	–	–
Ta	0.04	0.11	0.10	–	–
Zr	5.6	28.4	45.0	24.0	35.5
Y	2.2	10.8	17.4	9.0	10.5
Hf	0.15	0.80	0.83	–	–
La	0.639	1.52	3.49	–	–
Ce	1.023	4.28	7.42	–	–
Pr	0.159	0.703	0.619	–	–
Nd	0.462	3.32	2.71	–	–
Sm	0.147	1.19	0.698	–	–
Eu	0.047	0.467	0.123	–	–
Gd	0.211	1.43	1.35	–	–
Tb	0.037	0.267	0.288	–	–
Dy	0.317	1.85	2.40	–	–
Ho	0.084	0.392	0.560	–	–
Er	0.311	0.239	0.320	–	–
Tm	0.055	1.16	1.84	–	–
Yb	0.400	1.19	1.77	–	–
Lu	0.073	0.181	0.275	–	–
Pb	0.184	0.603	0.189	–	–
Th	0.119	0.215	0.656	–	–
U	0.071	0.091	0.197	–	–
Cs	0.494	0.500	0.049	–	–
<dl = below detection limits – = no data available. All trace elements in ppm.					

Most low-Ti suite rocks are geochemically indistinguishable from Bonin Island low-Ca boninite (Fig. 26, 27). They also have similar mineralogical characteristics, such as low-Ti pyroxene (Table 2), high-Cr/(Cr+Al) chromite (Fig. 24, Table 1), and abundant orthopyroxene. The mineralogical and geochemical data support the inference that rocks of the low-Ti suite are true boninite, in accord with the conclusions of Upadhyay (1980), Coish et al. (1982), Coish (1989), and Swinden et al. (1989). The strong resemblance to Bonin Island lavas suggests they should be classified as type 3 low-Ca boninite (Crawford et al., 1989).

Intermediate-Ti suite lavas and dykes (plagioclase+clinopyroxene-phyric) have flatter normalized trace-element profiles than do the low-Ti boninite, with overall higher contents of moderately incompatible elements, similar LILE contents, negative Nb anomalies, and positive Pb and Sr anomalies (Fig. 26, 27B). Whether the intermediate-Ti suite rocks are best classified as arc tholeiite or boninite is uncertain (cf. Coish, 1989). Swinden et al. (1997) refer to them as arc tholeiite. The presence of feldspar phenocrysts does suggest an affinity to tholeiite, and they are transitional towards Mount Misery tholeiite in many respects (Fig. 26, 27).

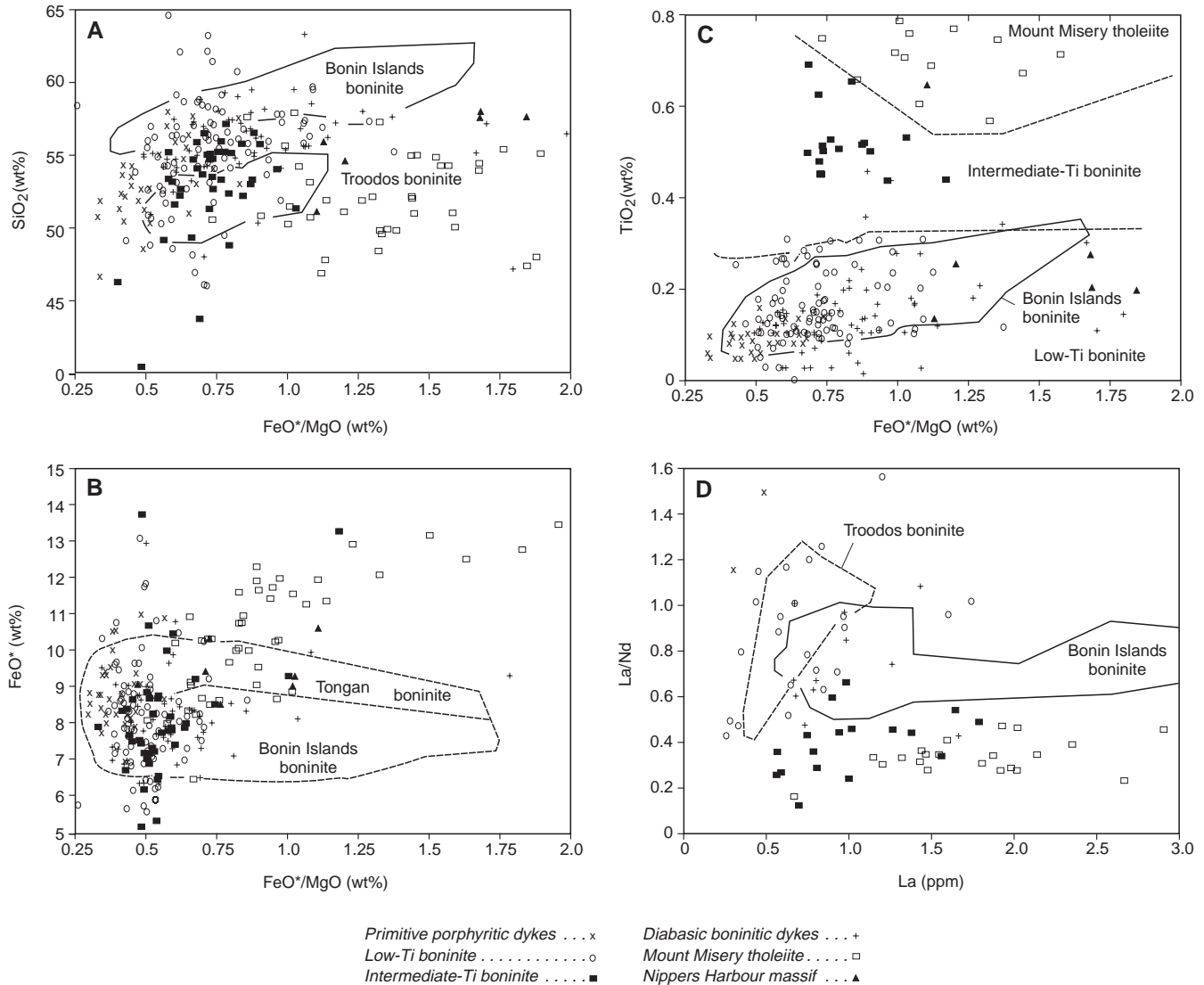


**Figure 26.** A) SiO<sub>2</sub> versus FeO\*/MgO, B) FeO\* versus FeO\*/MgO, C) TiO<sub>2</sub> versus FeO\*/MgO, and D) La/Nd versus La (ppm). Data from Betts Head Formation lavas, Betts Cove sheeted dykes, Nippers Harbour massif dykes and lavas, and Mount Misery Formation lavas (SALT). Most Nippers Harbour rocks resemble Betts Head boninite, but one of them more closely resembles the Mount Misery tholeiite (SALT). Fields for the Bonin Islands, Tongan, and Troodos boninite suites were defined with data from Jenner (1981), Hickey and Frey (1982), Crawford et al. (1989), Falloon et al. (1989), Falloon and Crawford (1991), Sobolev and Danyushevsky (1994), and Taylor et al. (1994). In Figure 26C, the dashed lines represent the discriminants used when classifying older data. (Modified from Fig. 5 in Bédard (1999).)

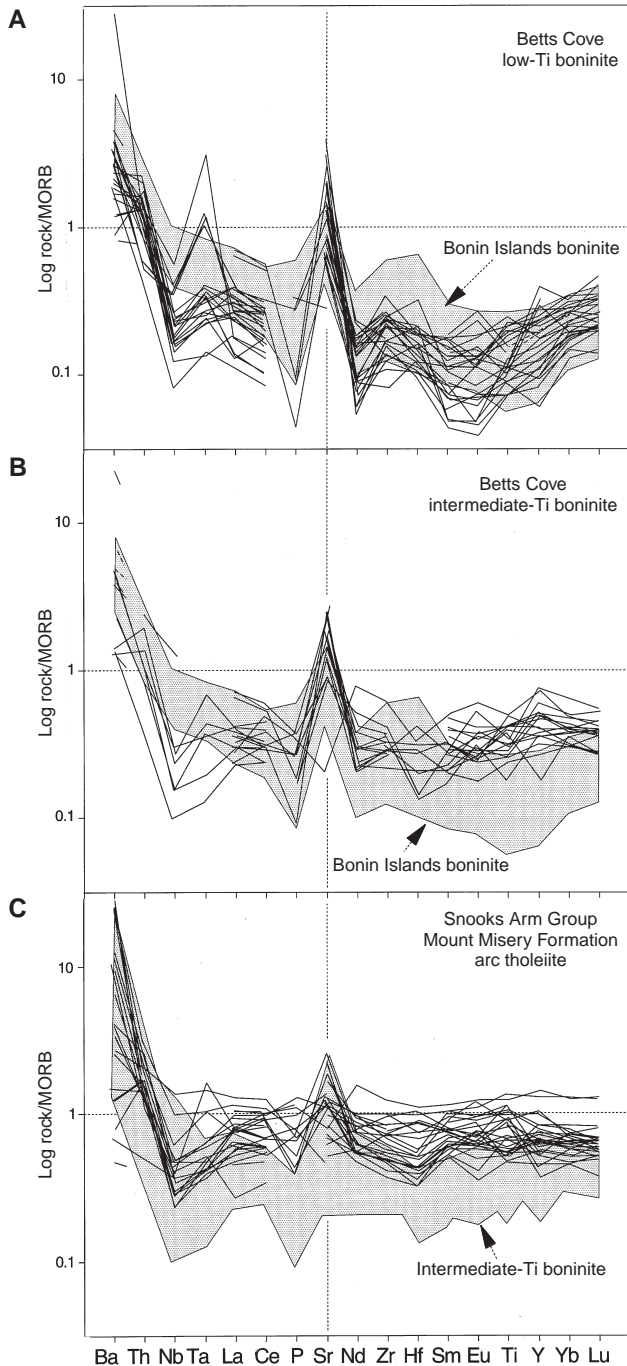


**Figure 27.** Extended trace element plots normalized to N-MORB. Normalizing factors for all similar plots are mostly from Sun and McDonough (1989) and are Ba=6.3, Th=0.12, Nb=2.33, Ta=0.132, La=2.5, Ce=7.5, P=510, Sr=90, Nd=7.3, Zr=74, Hf=2.05, Sm=2.63, Eu=1.02, Ti=7600, Y=28, Yb=3.05, Lu=0.455. **A)** Low-Ti boninite lavas (Betts Head Formation) and dykes from Betts Cove compared to Bonin Islands boninite lavas. **B)** Intermediate-Ti boninite lavas (Betts Head formation) and dykes from Betts Cove, compared to Bonin Islands boninite lavas. **C)** Mount Misery Formation tholeiitic lavas compared to field of data from intermediate-Ti boninite.

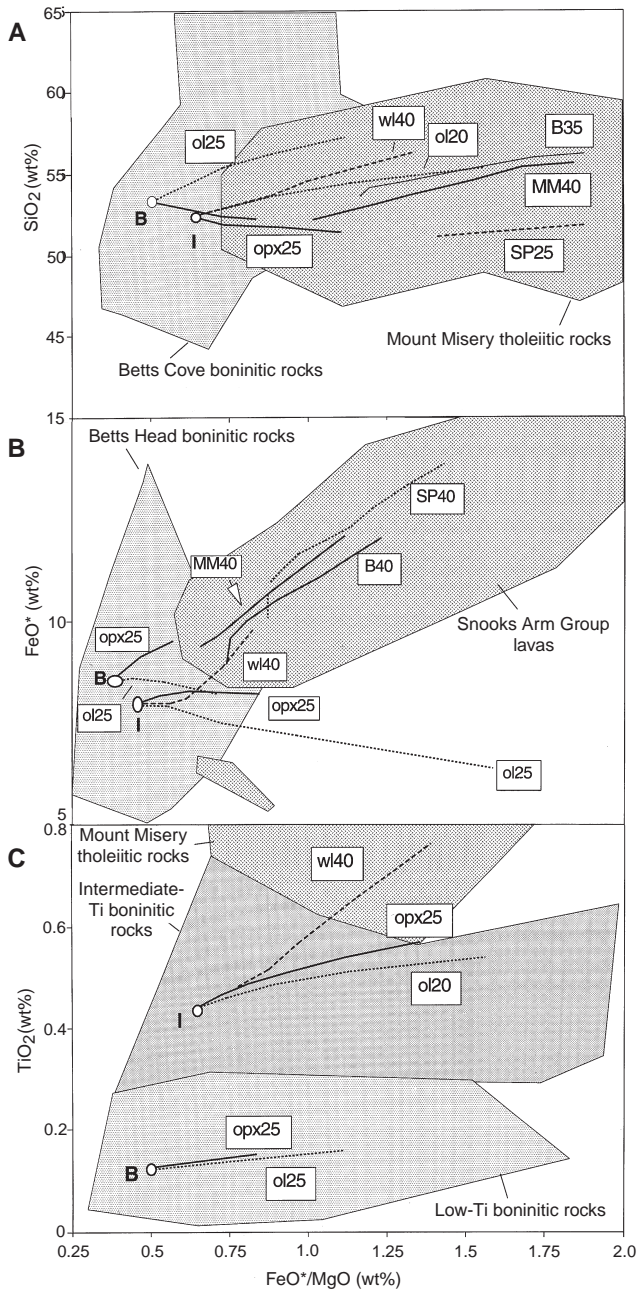
Although the tholeiitic rocks of the Mount Misery Formation have normalized incompatible-element profiles subparallel to those of intermediate-Ti boninite (Fig. 27C), the Mount Misery lavas have consistently higher  $\text{FeO}^*/\text{MgO}$ , as well as higher contents of moderately incompatible elements (Ti, REEs) than do the Betts Head lavas and sheeted dykes (Fig. 26, 27). In addition, the intermediate-Ti suite rocks are interbedded with low-Ti boninite (Fig. 4), and they fall within the compositional range of boninite on most variation diagrams (e.g. Fig. 26, 27B). In this Bulletin they will be referred to as boninite.

Fractionation of plausible mineral assemblages (olivine, orthopyroxene, and chromite) cannot explain the compositional range seen among the low- and intermediate-Ti Betts Head magmas with respect to major and incompatible elements (Fig. 28, 29, 30; Bédard et al., 1998; Bédard, 1999). Fractionation of Betts Head low-Ti series melts cannot generate residues similar either to the intermediate-Ti series, or to Mount Misery Formation lavas. Nor can fractional crystallization of intermediate-Ti Betts Head magmas generate residues similar to the Mount Misery tholeiite (Fig. 28, 29, 30).

The tremendous range of incompatible element ratios and contents (e.g. Fig. 26B, 26D, 29, 30) implies that the compositional range of Betts Head low-Ti boninite cannot result from fusion of a unique source (Fig. 29). Instead, Bédard (1999) proposed that small amounts (<1%) of a fertile 'SZ' (subduction zone) component were added to a variably depleted wedge peridotite ('L' on Fig. 30). The 'SZ' component was identified as a mixture of hydrous fluids derived from subducted, altered, oceanic crust; trondhjemitic partial melts of the subducted oceanic crust; and partial melts of subducted sedimentary rocks (Bédard, 1999). Intermediate-Ti boninite and Mount Misery tholeiite originate from a less-depleted mantle wedge, and seem to incorporate a much larger proportion of the hydrous subduction zone components in their make-up, as reflected in their higher Ba/La ratios (Fig. 30; Bédard, 1999).

#### Layered cumulate rocks, trondhjemite, and the late intrusive suite

The chemistry of Betts Cove cumulate rocks (Table 5) reflect the cumulus mode, with high abundances of MgO and NiO in peridotite and pyroxenite reflecting abundant cumulus olivine and orthopyroxene; high CaO in websterite and gabbro reflecting the abundance of cumulus clinopyroxene; and high Sr, Eu, and  $\text{Al}_2\text{O}_3$  in gabbro reflecting the abundance of cumulus feldspar. The trace-element contents of liquids in equilibrium with these rocks were calculated using the equilibrium distribution method of Bédard (1994), with the revised partition coefficient data set of Bédard (1999). These calculations require modal data and an estimate of the trapped melt fraction (TMF). Due to the effects of hydrothermal metamorphism, rigorous quantification of the mode was not possible. We used visual estimates from the outcrop, buttressed by examination of cut slabs, thin sections, and norm calculations. In most models, we varied the modes by 10–15% to encompass the limits of possible variations. Fluctuations of this order produced negligible changes in the



calculated melt profiles. Variations in trapped melt fraction produce more significant variations, with low assumed trapped melt fraction (<10%) yielding model liquids that did not fit any plausible target lava. By trial and error, we found that trapped melt fraction around 20% for ultramafic cumulate rocks gave good fits to Betts Head Formation low-Ti boninite (Fig. 31A), and so we used this value for most calculations. Ultramafic cumulate rocks at Betts Cove generally contain high proportions of poikilitic clinopyroxene (20–30%), consistent with the high inferred trapped melt fraction.

**Figure 28.** A)  $\text{SiO}_2$  versus  $\text{FeO}^*/\text{MgO}$  (modified from Fig. 8a, Bédard, 1999) B)  $\text{FeO}^*$  versus  $\text{FeO}^*/\text{MgO}$ , and C)  $\text{TiO}_2$  versus  $\text{FeO}^*/\text{MgO}$ , comparing results of fractionation models to fields of data from Figure 26. ‘B’ and ‘I’ are, respectively, primitive end-member magmas of the low- and intermediate-Ti series boninite of the Betts Head Formation (Table 4). Symbols ‘opx25’ and ‘ol25’ refer to fractionation of 25% orthopyroxene and olivine, respectively (see Bédard (1999) for method). Symbol ‘wl40’ refers to results of 40% fractionation of the intermediate-Ti boninite parent (I) using the program of Weaver and Langmuir (1980), run at 2 kbar, with the CaO and  $\text{Na}_2\text{O}$  contents of the parent magma adjusted to 10 wt % and 2 wt % (respectively) to correct for the effects of hydrothermal alteration. The curves marked ‘MM’, ‘SP’, and ‘B’ record results of fractionation of the primitive Mount Misery, Scrape Point, and low-Ti Bobby Cove formation lavas, respectively, using the Weaver and Langmuir (1980) program at 2 kbar. The adjacent number reflects the per cent fractionation. The CaO and  $\text{Na}_2\text{O}$  contents of the Mount Misery parent were adjusted to 10 wt % and 2 wt % (respectively), to correct for the effects of hydrothermal alteration (modified from Fig. 8b, Bédard, 1999)

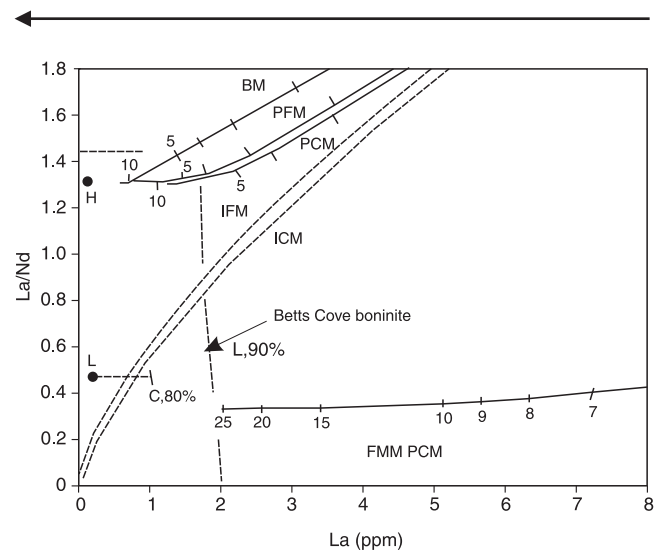


**Figure 29.**  $\text{La}/\text{Nd}$  versus  $\text{La}$  (ppm) showing fractionation and melting vectors compared to field of data of Betts Cove boninitic rocks. Numbers next to the tics represent per cent melting or fractionation. Curve labelled ‘C,80%’ tracks 80% fractional crystallization of olivine+spinel (99:1) from a low-Ti boninite parent with a low  $\text{La}/\text{Nd}$  ratio, labelled ‘L’. Curve ‘FMM PCM’ tracks the evolution of pooled critical melts (1/3 melt retention assumed) extracted from a fertile MORB mantle (FMM) source. Curves labelled ‘BM’, ‘PFM’, and ‘PCM’ track the evolution of batch (equilibrium), fractional and critical melts (respectively) of the high- $\text{La}/\text{Nd}$  low-Ti boninite source mantle ‘H’ calculated by Bédard, (1999). Curves ‘IFM’ and ‘ICM’ are, respectively, instantaneous fractional and critical melts of this same high- $\text{La}/\text{Nd}$  boninitic source mantle. See Bédard (1999) for methods of calculation, and compositions of FMM and the high  $\text{La}/\text{Nd}$  source (modified from Fig. 8c, Bédard, 1999)

Lherzolitic, dunitic, and harzburgitic rocks all yield similar, depleted, U-shaped calculated liquid profiles (Fig. 31A). These calculated liquids overlap with the compositions of primitive low-Ti Betts Head boninite, which is consistent with a comagmatic relationship.

Pyroxenite and gabbroic rocks from the layered cumulate rocks and late intrusive suite yielded a diverse array of model liquids. Three gabbroic intrusions of the late intrusive suite from the sheeted dykes south of the Betts Cove mine, and two discordant trondhjemitic veins from within the layered cumulate rocks, yielded model profiles that are subparallel to those from the low-Ti Betts Head boninite for 20% assumed trapped melt fraction (Fig. 31A). These rocks are plausibly interpreted as residues from the fractionation of the low-Ti boninite.

The conformable, cumulate gabbroic beds are compositionally distinct (lower Ti, Table 5) from the Fe-Ti-oxide-bearing gabbro of the late intrusive suite (c.f. Church and Riccio, 1974; Church, 1977, 1979; Upadhyay, 1979). Most of the late intrusive suite gabbro yielded model

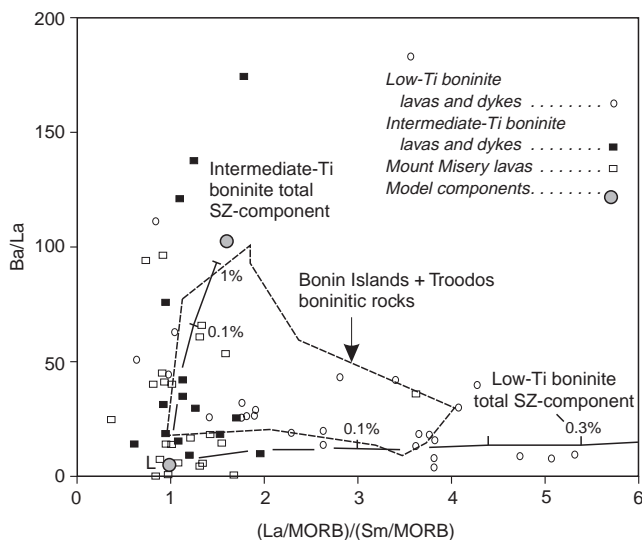


**Figure 30.** Ba/La versus La/Sm (normalized to N-MORB) ratio plot constructed by adding the low-Ti and intermediate-Ti total subduction-zone (SZ) components calculated by Bédard (1999) to the depleted mantle wedge component 'L'. The percentages near the tics refer to the percentage of SZ component added to L. Fields for Tertiary and ophiolitic boninite delimited from Jenner (1981), Hickey and Frey (1982), Crawford et al. (1989), Falloon et al. (1989), Falloon and Crawford (1991), Sobolev and Danyushevsky (1994), and Taylor et al. (1994). Increases in the Ba/La ratio is thought to be primarily the result of adding hydrous SZ component, whereas increasing La/Sm better reflect addition either of partial melts from the subducted crust or subducted sediment. Note that the Betts Head intermediate-Ti boninite and Mount Misery tholeiite seem to contain a higher proportion of SZ-hydrous material.

liquid profiles at 20% trapped melt fraction that are nearly identical to those of the intermediate-Ti boninite (Fig. 31B). Hence, we infer that these gabbro bodies are plutonic equivalents, and possibly feeders, to the intermediate-Ti boninite lavas.

### Snooks Arm Group magmas

Magmatic rocks in the Snooks Arm Group belong to three suites. The first is the Snooks Arm lower tholeiitic series (SALT), comprised of basaltic lavas from the Mount Misery

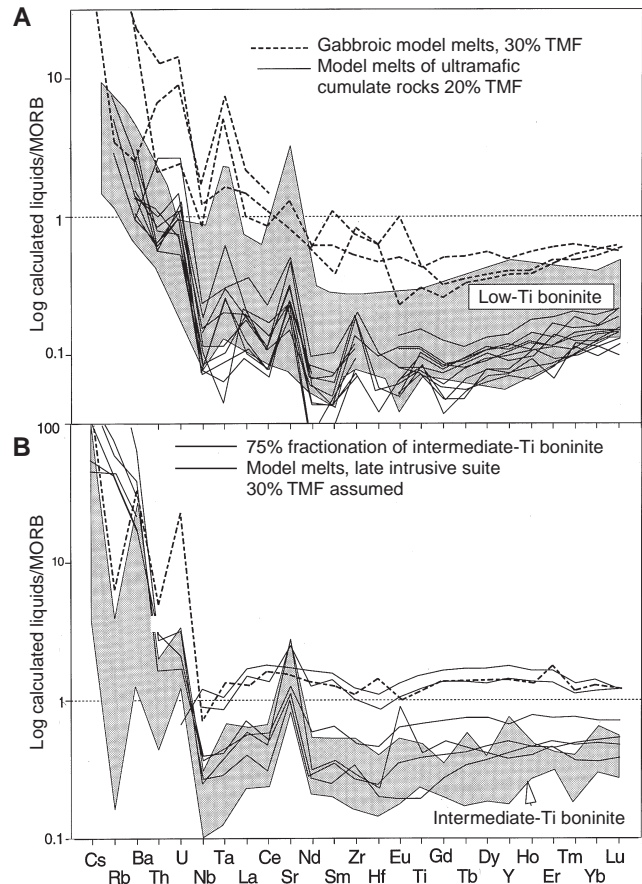


**Figure 31.** Extended trace element profiles for melts coexisting with Betts Cove cumulate rocks calculated using the method of Bédard (1994), and normalized to N-MORB. All models assume 20–30% trapped melt fraction (TMF). **A)** Model liquids calculated from Betts Cove lherzolite cumulate rocks, from three gabbroic bodies of the late intrusive suite, and from two trondhjemitic layers or dykes located within the layered cumulate sequence. Note the close resemblance between lherzolitic model melts and low-Ti boninite lavas from Betts Cove. **B)** Model liquids calculated from gabbroic bodies of the late intrusive suite. Note the close resemblance with intermediate-Ti boninite suite from Betts Cove. The fractionation model extracted spinel:olivine:orthopyroxene:clinopyroxene:plagioclase (1:9:20:30:40) from the average primitive intermediate-Ti composition.

Formation, and some of the more Ti-rich Bobby Cove Formation lavas. The second is the Snooks Arm upper tholeiitic series (SAUT), and comprises basaltic lavas from the Scrape Point, Venam's Bight, and Round Harbour formations, mafic lava clasts in Balsam Bud Cove Formation debrite units, and ferrogabbroic sills occurring throughout the Snooks Arm Group. The third is the Snooks Arm calc-alkaline (SACA) series, comprising Fe-Ti-poor basaltic to rhyolitic lavas and tuffs of the Bobby Cove, Scrape Point, and Balsam Bud Cove formations, felsic clasts in the Balsam Bud Cove Formation debrite units, and felsic dykes from the Round Harbour Formation. We will discuss each of these series in turn.

*Snooks Arm Group lower tholeiitic series (SALT)*

Compared to the boninitic rocks, Mount Misery Formation basaltic lavas have systematically lower  $\text{SiO}_2$ , Cr, and Ni, have higher  $\text{FeO}^*/\text{MgO}$  ratios (Fig. 26, Table 4), higher contents of high field-strength cations, flatter normalized trace-element profiles, with negative Nb anomalies, and large-ion-lithophile element (LILE) enrichment (Fig. 27). Snooks Arm Group lower tholeiitic lavas exhibit a weak iron-enrichment trend and show little or no  $\text{TiO}_2$  or  $\text{SiO}_2$  enrichment (Fig. 26). These trends are in accord with low-pressure fractionation models (Fig. 28, 29, 30). Snooks Arm Group lower tholeiitic magmas straddle the tholeiitic-calc-alkaline boundary on many discriminant diagrams

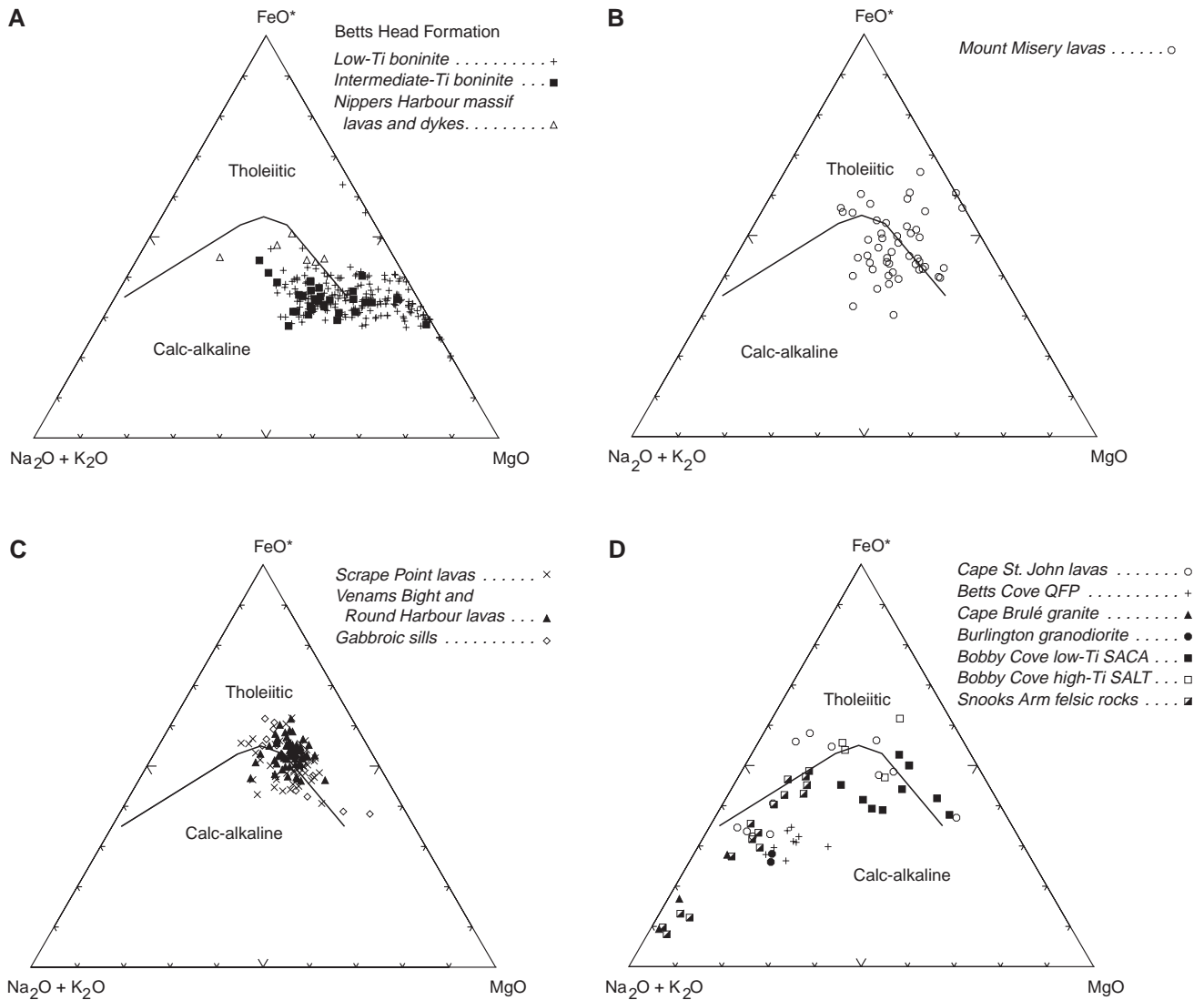


**Figure 32.** A–D)  $\text{Na}_2\text{O}+\text{K}_2\text{O}-\text{FeO}^*-\text{MgO}$  (AFM) diagrams (Irvine and Baragar, 1971). Strongly porphyritic Snooks Arm Group upper tholeiitic lavas are not plotted. QFP = quartz-feldspar porphyry; SACA=Snooks Arm Group calc-alkaline series; SALT=Snooks Arm Group lower tholeiitic series

(e.g. Fig. 32). On most paleotectonic discriminant diagrams these magmas plot either as low-K or arc tholeiite, or straddle the ocean-floor–arc basalt fields (Fig. 32–38). We concur with the proposals of Jenner and Fryer (1980) and Coish (1989), who interpreted them as a sequence of arc tholeiite, but do not agree with Swinden et al. (1997), who call them mid-ocean ridge basalt. These lavas show a pattern of steep Ba/La enrichment for only moderate La/Sm enrichment (Fig. 30), suggesting that a subduction zone component dominated by hydrous fluids was involved in their genesis.

#### Snooks Arm Group upper tholeiitic series (SAUT)

The phenocryst-poor upper tholeiitic series magmas exhibit almost the same tholeiitic FeO\* and SiO<sub>2</sub> versus FeO\*/MgO trend as the lower tholeiitic series (Fig. 39), but this is coupled to progressive enrichment in TiO<sub>2</sub> — a pattern consistent

with low-pressure fractional crystallization of these magmas. Phenocryst-poor Scrape Point Formation basaltic flows are the most primitive in this series, with the lowest FeO\*/MgO and TiO<sub>2</sub> contents (Table 4). Venam's Bight and Round Harbour lavas are almost indistinguishable from one another. The compositional range of phenocryst-poor Venam's Bight and Round Harbour basalt overlaps with the more evolved Scrape Point lavas (see Fig. 41). Normalized incompatible trace-element profiles of Venam's Bight and Round Harbour basalt are slightly more enriched than those of Scrape Point basalt (see Fig. 41), though essentially parallel.

In comparison to the phenocryst-poor facies, strongly feldspar-porphyrific upper tholeiitic lavas have systematically lower contents of FeO\*, TiO<sub>2</sub>, Na<sub>2</sub>O, MgO, P<sub>2</sub>O<sub>5</sub>, SiO<sub>2</sub>, and most incompatible elements (La, Zr, Y, etc.), with higher Al<sub>2</sub>O<sub>3</sub> and CaO (see Table 4). This pattern is compatible with the passive accumulation or entrainment of plagioclase phenocrysts.

The diabasic to gabbroic sills that occur throughout the Snooks Arm Group are chemically almost indistinguishable from upper tholeiitic lavas (Fig. 32, 41), and are interpreted to be subvolcanic feeders. Most basaltic clasts and olistoliths in the Balsam Bud Cove Formation debris units are very similar to Venam's Bight lavas (e.g. Fig. 40, 41C, Table 4), suggesting that these clasts were principally derived from erosion and/or mass wasting of lava flows (and some ferrogabbroic intrusions) cogenetic with the Venam's Bight lavas. The coarse nature of the Balsam Bud Cove epiclastic deposits suggests a very proximal source (Kessler and Bédard, 1998, 2000). Bulk analyses of volcanogenic sandstone from the Balsam Bud Cove Formation are similar to the chemical signatures of individual basaltic clasts (Fig. 40, 42D), suggesting that they are probably derived from erosion of this lava field. However, one large (2 m x 10 m) spherulitic basalt clast had a chemical composition similar to intermediate-Ti lavas of the Betts Head Formation, indicating that locally, boninitic basement was also being eroded.

Extended-REE profiles of all upper tholeiitic lavas are very similar (Fig. 41), and all of these magmas are inferred to represent a common differentiation series. Though most compositional variations can be attributed to low-pressure fractional crystallization (Fig. 39, 40), some of the range in trace-element ratios probably record variations in the degree of melting or/and source composition.

Phenocryst-poor Snooks Arm Group upper tholeiitic series magmas plot in the tholeiitic field on major element discriminant diagrams (Fig. 32, 39, 40). Lavas of the upper tholeiitic series contain higher abundances of incompatible elements than Snooks Arm Group lower tholeiitic series lavas, overall, with steeper extended-REE profiles (Fig. 41). This is inconsistent with an origin by fractional crystallization from lower tholeiitic series parents. Upper tholeiitic series magmas have no Ta anomaly, and only a weak negative Nb anomaly, and show less relative large-ion-lithophile element enrichment (Ba and Th) than lower tholeiitic series or boninitic lavas (Fig. 41). On tectonic discriminant diagrams, upper tholeiitic series magmas plot as mid-ocean ridge basalt (Fig. 37), or ocean-floor tholeiite (Fig. 33, 35, 38), extending

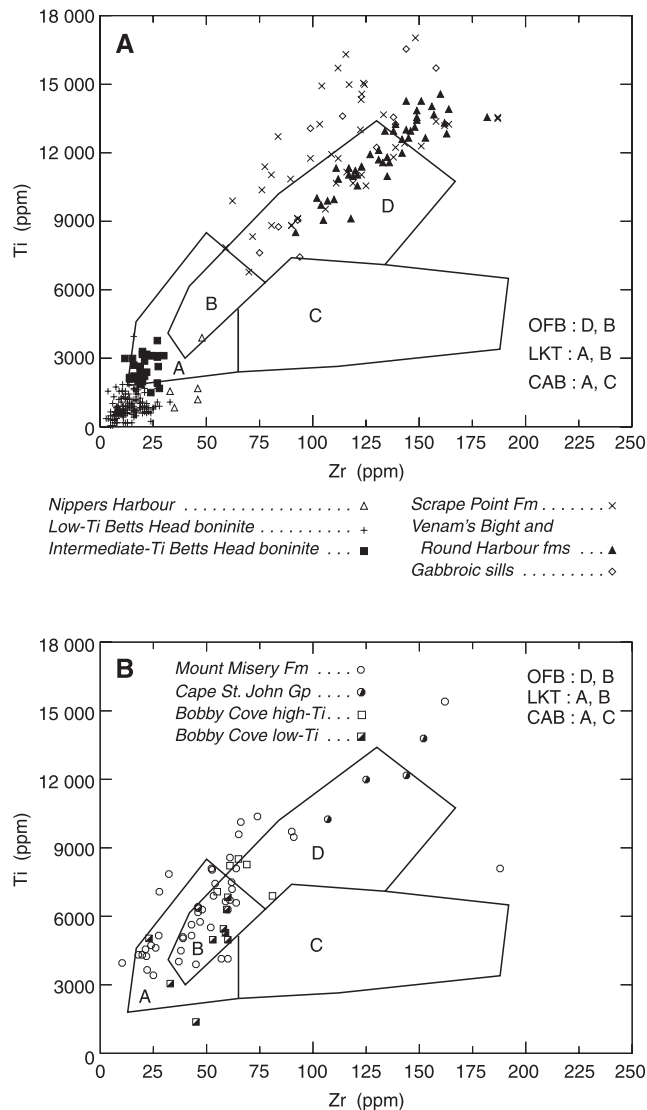


**Figure 33. A, B** Ti versus Zr tectonic discriminant plot from Pearce and Cann (1973). OFB=ocean floor basalt, LKT=low-K tholeiite, CAB=calc-alkaline basalt

partly into the within-plate basalt field (Fig. 34, 36). They are best interpreted as mature back-arc tholeiite, derived from essentially undepleted MORB-like mantle sources with only a weak arc signature. A similar conclusion was reached by Jenner and Fryer (1980).

*Snooks Arm Group calc-alkaline series (SACA)*

The common juvenile porphyritic pyroclasts and the low-Ti lavas in the Bobby Cove Formation have a basaltic to andesitic bulk chemistry (Table 4). Together with dacitic to rhyolitic clasts and tuffs, these rocks follow a normal calc-alkaline evolutionary trend, with FeO-TiO<sub>2</sub> depletion and SiO<sub>2</sub> enrichment (Fig. 32, 40). Snooks Arm Group calc-alkaline series basalt and andesite have prominent

negative Nb and Ta anomalies (Fig. 42), and generally straddle the ocean floor–island-arc, low-K or calc-alkaline basalt fields on paleotectonic classification diagrams (Fig. 33–38). Most Bobby Cove mafic to intermediate tuffs, Scrape Point Formation tuffs, and tuffaceous turbidite from the Upper Member of the Bobby Cove Formation, have compositions very similar to those of low-Ti Bobby Cove juvenile lavas and clasts (Fig. 40, 42), suggesting a common Snooks Arm Group calc-alkaline series-like source for all of them. This suggests that Scrape Point Formation tuffs represent an early distal eruptive event from the same magma reservoir that produced the paroxysmal Bobby Cove tuffaceous conglomerate flow units; whereas Balsam Bud Cove rhyolite would represent a recrudescence of activity.

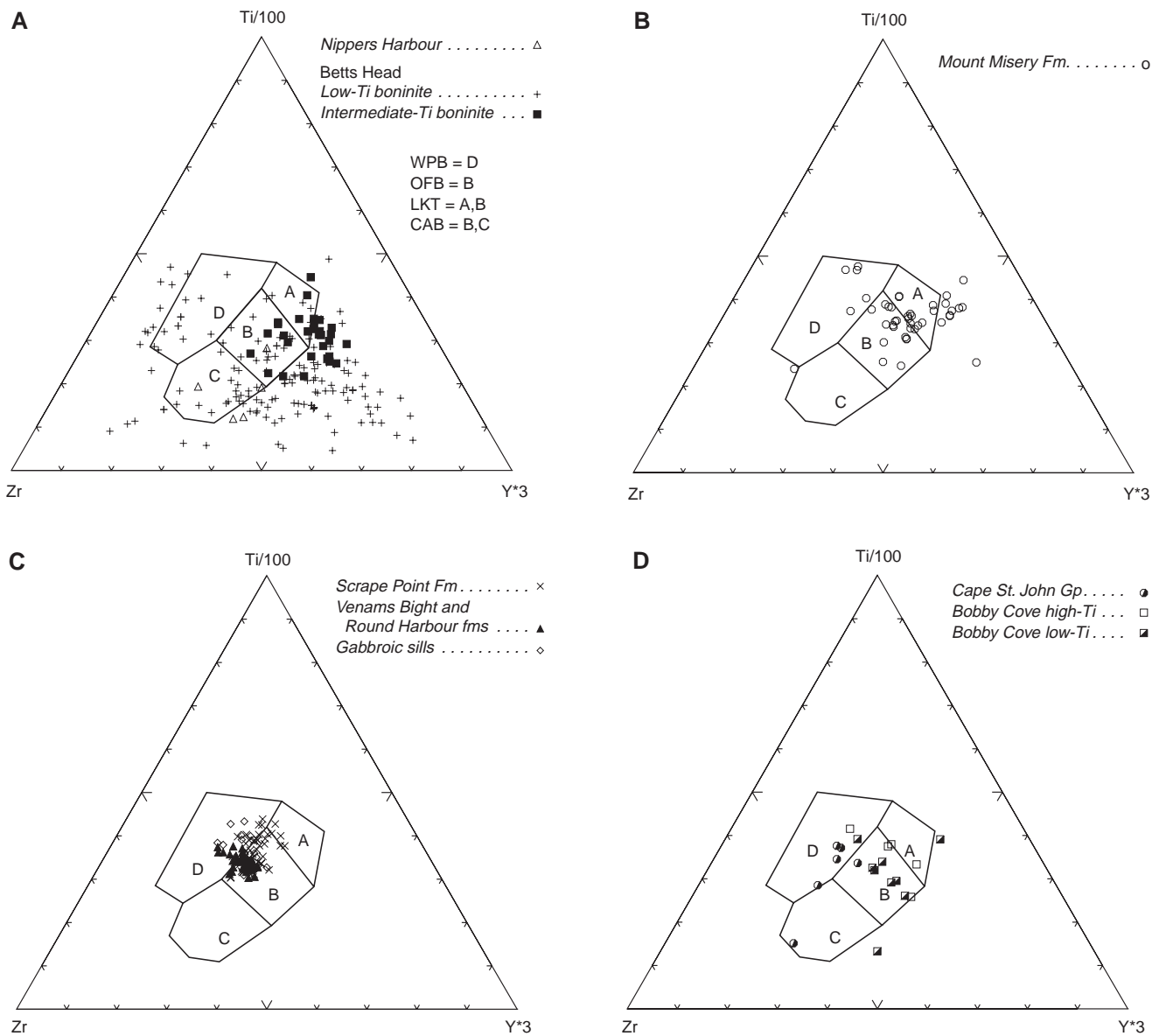


**Figure 34.** A)–D) Ti/100-Zr-Y\*3 tectonic discriminant plot from Pearce and Cann (1973). WPB=within-plate basalt, OFB=ocean floor basalt, LKT=low-K tholeiite, CAB=calc-alkaline basalt



Most felsic Snooks Arm Group lavas, tuffs, dykes, and pyroclastic rocks define a scattered calc-alkaline-like trend on variation diagrams (Fig. 32, 40). On granitoid paleotectonic classification diagrams (Fig. 43) the felsic rocks plot mostly as arc or orogenic lavas, with a few extending to the within-plate field.

On extended REE plots, the Bobby Cove (SACA) basalt and andesite have higher LREE contents, and lower HREE contents than do lower tholeiitic or upper tholeiitic series lavas and so cannot represent closed-system differentiates of either (Fig. 41). Anhydrous differentiation of Mount Misery or low-Ti Bobby Cove basalt (Fig. 39, 40) does not yield residues similar to the Bobby Cove andesite and dacite. Attempts to model differentiation of the Snooks Arm Group calc-alkaline series using least-squares methods were unsuccessful, perhaps because elements such as CaO and Na<sub>2</sub>O have been seriously perturbed by hydrothermal alteration. At this time we note only that the abundance of amphibole and magnetite phenocrysts in Snooks Arm Group calc-alkaline series andesite implies that extraction of these phases was probably involved in depleting the magma of Fe and Ti.

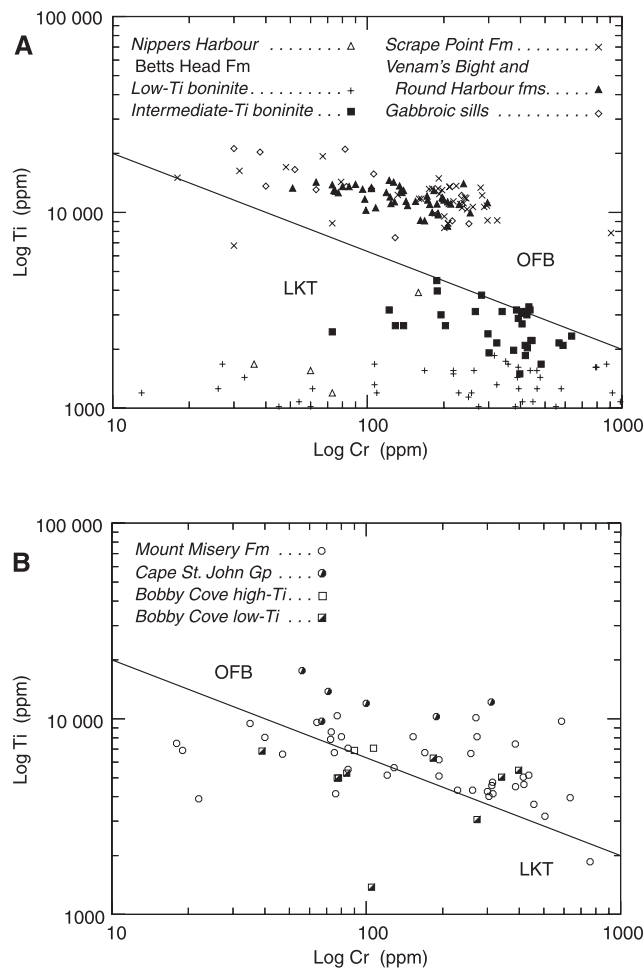


**Figure 35. A, B)** Log Ti versus log Cr tectonic discriminant plot from Pearce (1975). OFB = ocean floor basalt; LKT = low-K tholeiite

The rhyolitic rocks exhibit considerable scatter on all diagrams, with wide ranges of SiO<sub>2</sub>, TiO<sub>2</sub>, and FeO\* (Fig. 39, 40). Low-Fe-Ti rhyolite could represent the end products of differentiation of the Snooks Arm Group calc-alkaline series, whereas high-Fe-Ti rhyolite could have lower tholeiite-like salt parents. Snooks Arm Group calc-alkaline series dacite and rhyolite have spiky extended trace-element plots (Fig. 41) with prominent negative Ti, Sr, and Eu anomalies attributable to feldspar and Fe-Ti-oxide fractionation, whereas large-ion-lithophile element enrichment and prominent negative Nb-Ta anomalies are probably signatures inherited from their parental, arc-related magmas.

A pair of dykes that cut basaltic lavas of the Round Harbour Formation have geochemical signatures very similar to the Snooks Arm Group calc-alkaline series (Fig. 41D), suggesting that calc-alkaline magmas continued to be available after eruption of Round Harbour basalt. Alternation of

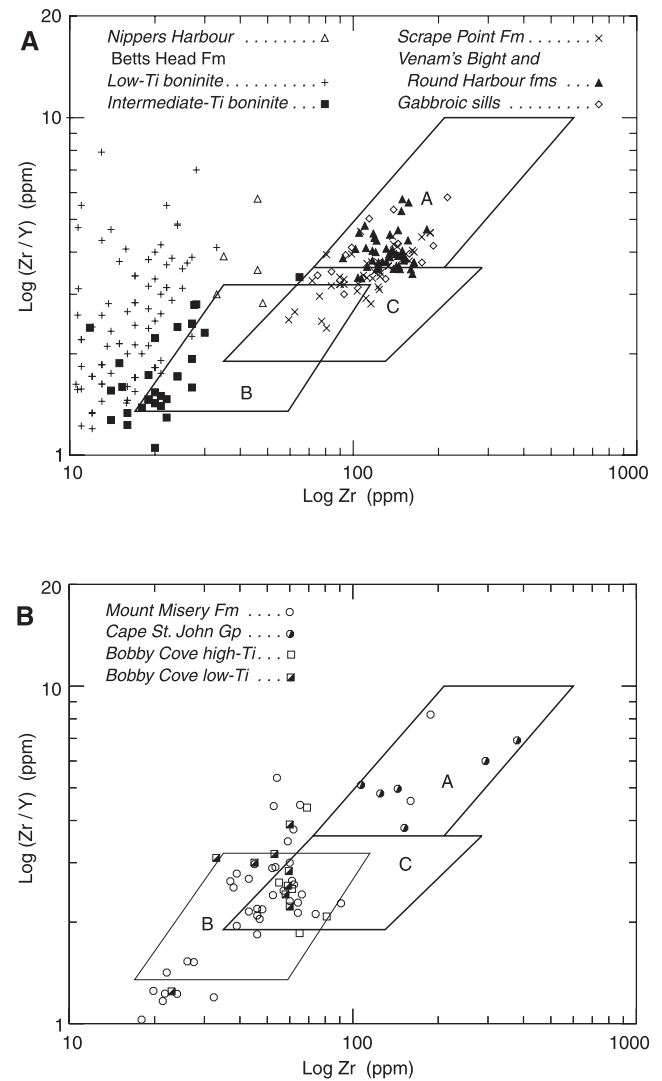


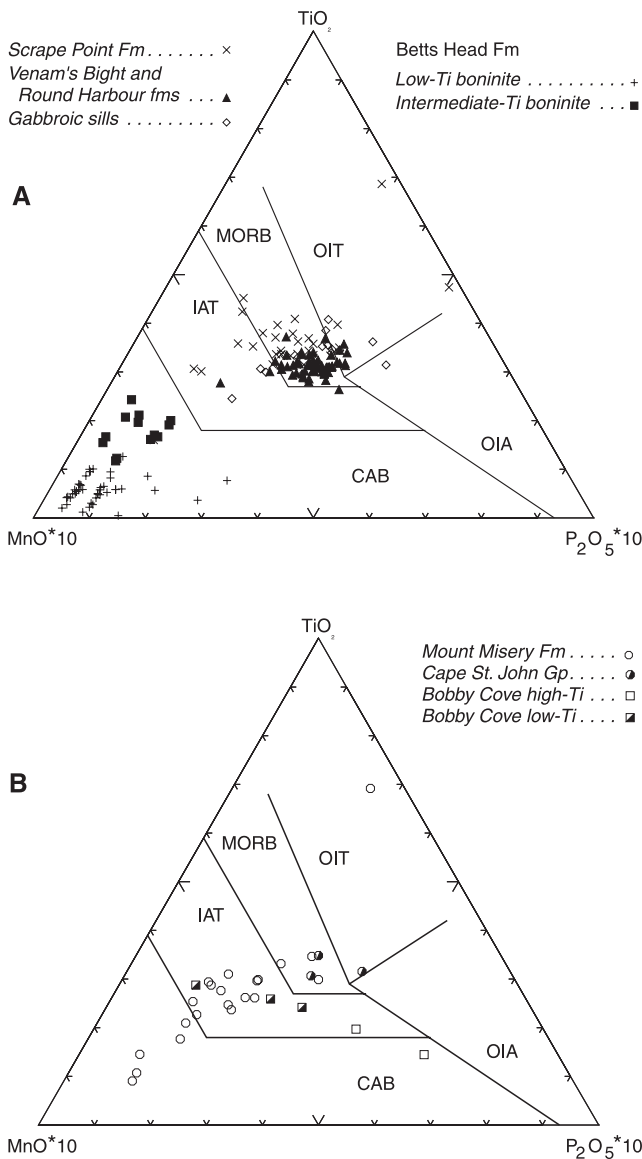
**Figure 36. A, B)** Log (Zr/Y) versus log Zr tectonic discriminant plot from Pearce and Norry (1979). Zones on figures: A = within-plate basalt; B = island-arc basalt; C = mid-ocean ridge basalt

Snooks Arm Group upper tholeiitic and calc-alkaline series magmas throughout deposition of the Snooks Arm Group implies that both sources were available. The proximal nature of the lavas and tuffs of both series implies that these sources were situated almost immediately beneath the ophiolite.

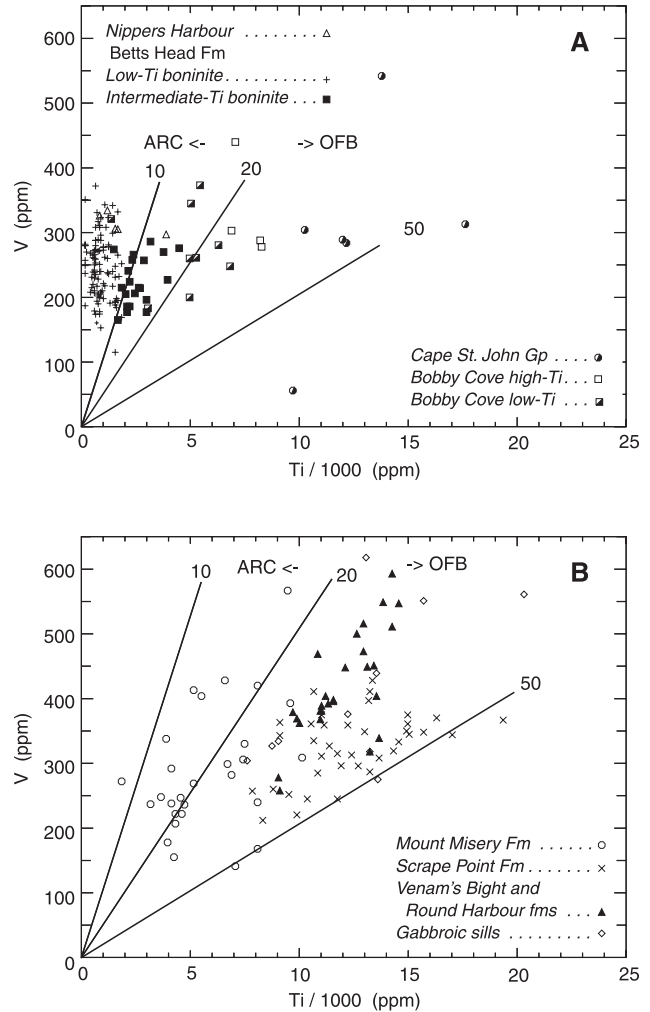
### Nippers Harbour ophiolitic massif

Sheeted dykes and intragabbroic dykes from the Nippers Harbour ophiolitic massif are high-MgO andesite, or siliceous basalt, with low incompatible element contents (Table 4). On geochemical variation diagrams, most of them could represent differentiation products of boninite similar to the Betts

Head lavas, with one rock more closely resembling the Mount Misery tholeiite (Fig. 26, 32–38). This suggests that the Nippers Harbour and Betts Cove ophiolite are correlative.



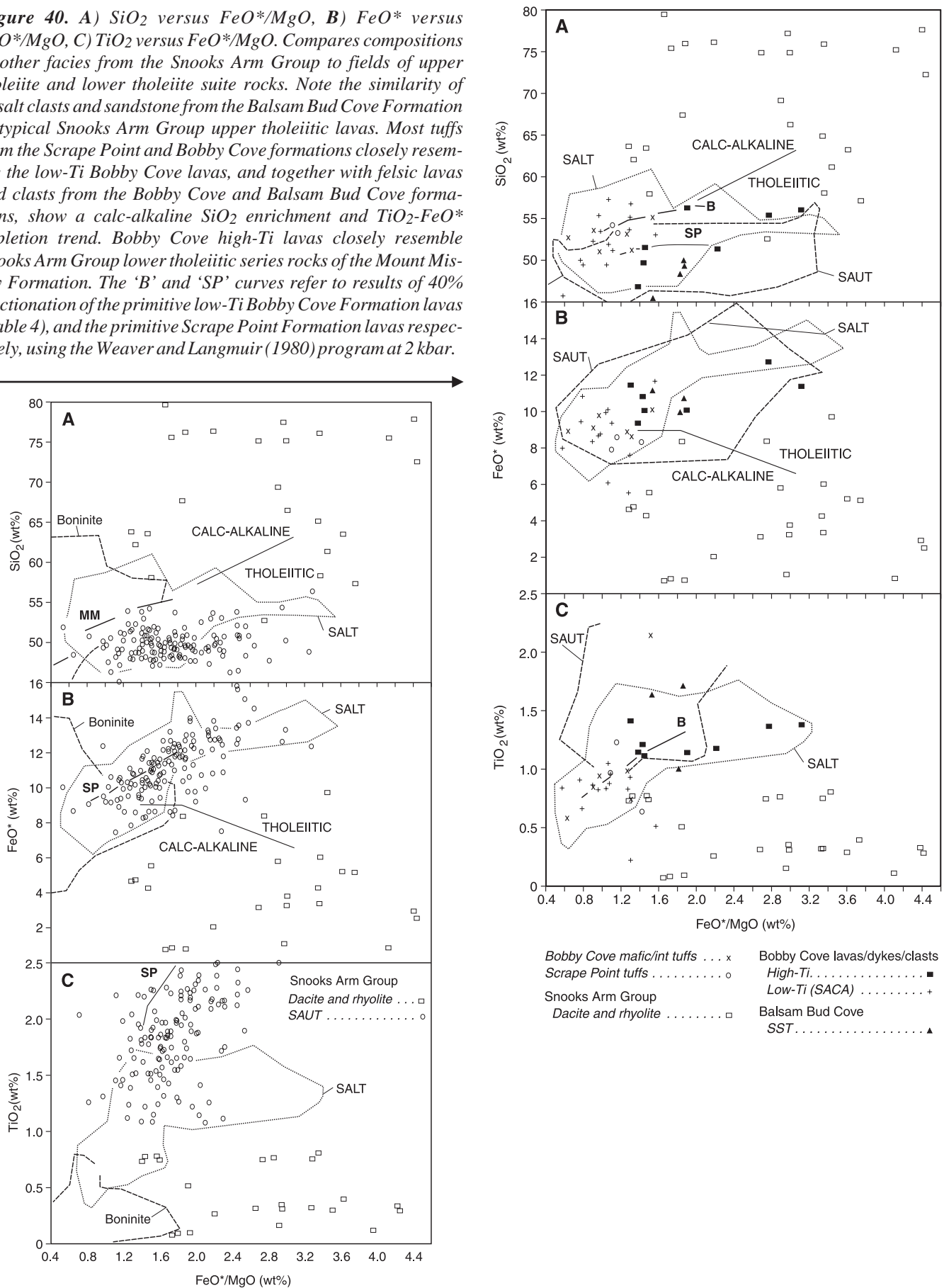
**Figure 37. A)–B)** MnO\*10-TiO<sub>2</sub>-P<sub>2</sub>O<sub>5</sub>\*10 tectonic discriminant plot from Mullen (1983). CAB = calc-alkaline basalt, IAT = island-arc tholeiite, MORB = mid-ocean ridge basalt, OIA = ocean-island andesite, OIT = ocean-island tholeiite.



**Figure 38. A), B)** V versus Ti tectonic discriminant plot from Shervais (1982). ARC = arc-related basalt, OFB = ocean-floor basalt.

**Figure 39. A)** SiO<sub>2</sub> versus FeO\*/MgO, **B)** FeO\* versus FeO\*/MgO, **C)** TiO<sub>2</sub> versus FeO\*/MgO. Snooks Arm Group upper tholeiitic (SAUT) lavas from the Venam's Bight, Round Harbour, and Scrape Point formations, and diabasic sills; compared to field of Betts Head boninite and Mount Misery Formation arc tholeiite (SALT). Tholeiitic and/or calc-alkaline discriminant plot from Miyashiro (1973). The curves marked 'MM' and 'SP' refer to results of 40% fractionation of the primitive Mount Misery and Scrape Point formation lavas (Table 4), respectively, using the Weaver and Langmuir (1980) program at 2kbar. In Figure 39B the 'SP' and 'MM' curves overlap.

**Figure 40.** A)  $\text{SiO}_2$  versus  $\text{FeO}^*/\text{MgO}$ , B)  $\text{FeO}^*$  versus  $\text{FeO}^*/\text{MgO}$ , C)  $\text{TiO}_2$  versus  $\text{FeO}^*/\text{MgO}$ . Compares compositions of other facies from the Snooks Arm Group to fields of upper tholeiite and lower tholeiite suite rocks. Note the similarity of basalt clasts and sandstone from the Balsam Bud Cove Formation to typical Snooks Arm Group upper tholeiitic lavas. Most tuffs from the Scrape Point and Bobby Cove formations closely resemble the low-Ti Bobby Cove lavas, and together with felsic lavas and clasts from the Bobby Cove and Balsam Bud Cove formations, show a calc-alkaline  $\text{SiO}_2$  enrichment and  $\text{TiO}_2$ - $\text{FeO}^*$  depletion trend. Bobby Cove high-Ti lavas closely resemble Snooks Arm Group lower tholeiitic series rocks of the Mount Misery Formation. The 'B' and 'SP' curves refer to results of 40% fractionation of the primitive low-Ti Bobby Cove Formation lavas (Table 4), and the primitive Scrape Point Formation lavas respectively, using the Weaver and Langmuir (1980) program at 2 kbar.



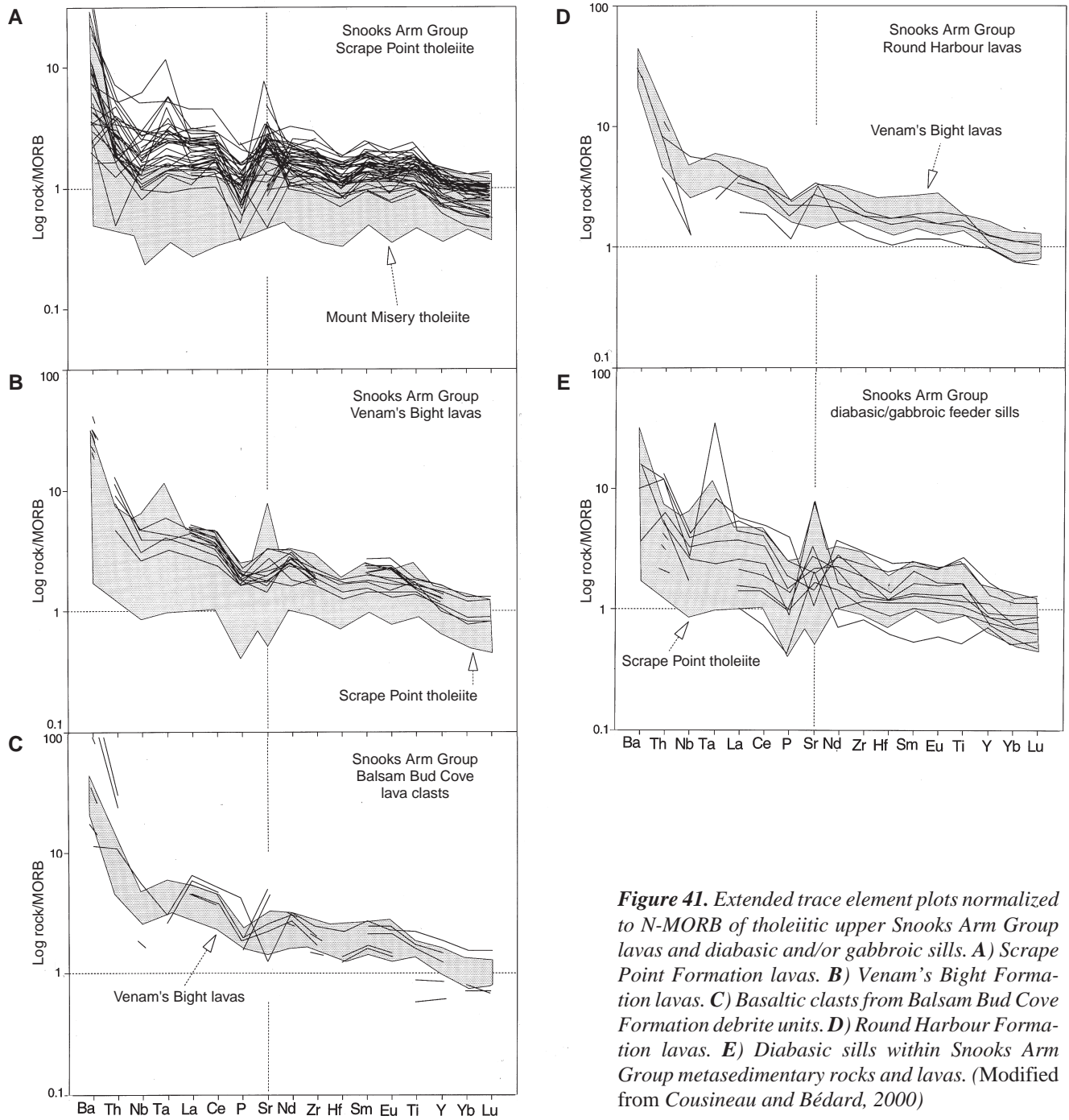


**Figure 41.** Extended trace element plots normalized to N-MORB of tholeiitic upper Snooks Arm Group lavas and diabasic and/or gabbroic sills. **A)** Scrape Point Formation lavas. **B)** Venam's Bight Formation lavas. **C)** Basaltic clasts from Balsam Bud Cove Formation debrite units. **D)** Round Harbour Formation lavas. **E)** Diabasic sills within Snooks Arm Group metasedimentary rocks and lavas. (Modified from Cousineau and Bédard, 2000)

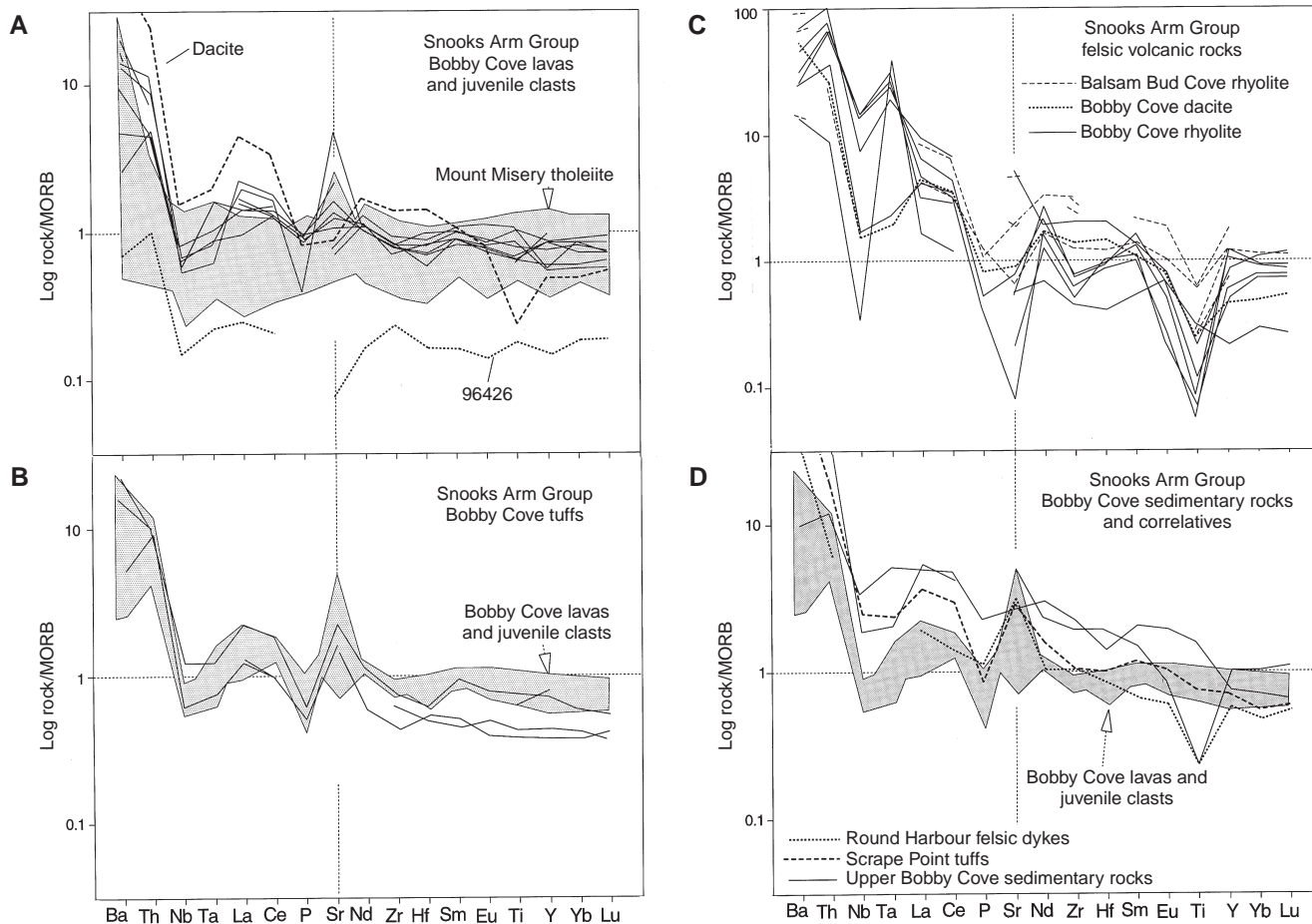


**Figure 42.** Extended trace element plots normalized to N-MORB of Snooks Arm Group calc-alkaline series lavas, juvenile clasts, and tuffs. **A)** Basaltic and andesitic lavas and juvenile clasts from Bobby Cove Formation, with one dacite clast from a pyroclastic flow. **B)** Intermediate and mafic tuffs from the Bobby Cove Formation. **C)** Felsic tuffs and lavas from the Balsam Bud Cove and Bobby Cove formations. **D)** Tuffaceous sedimentary rocks from the Upper (turbiditic) Member of the Bobby Cove Formation and the Scrape Point Formation Sedimentary Member. Also shown is the average of two felsic dykes cutting basaltic rocks of the Round Harbour Formation.

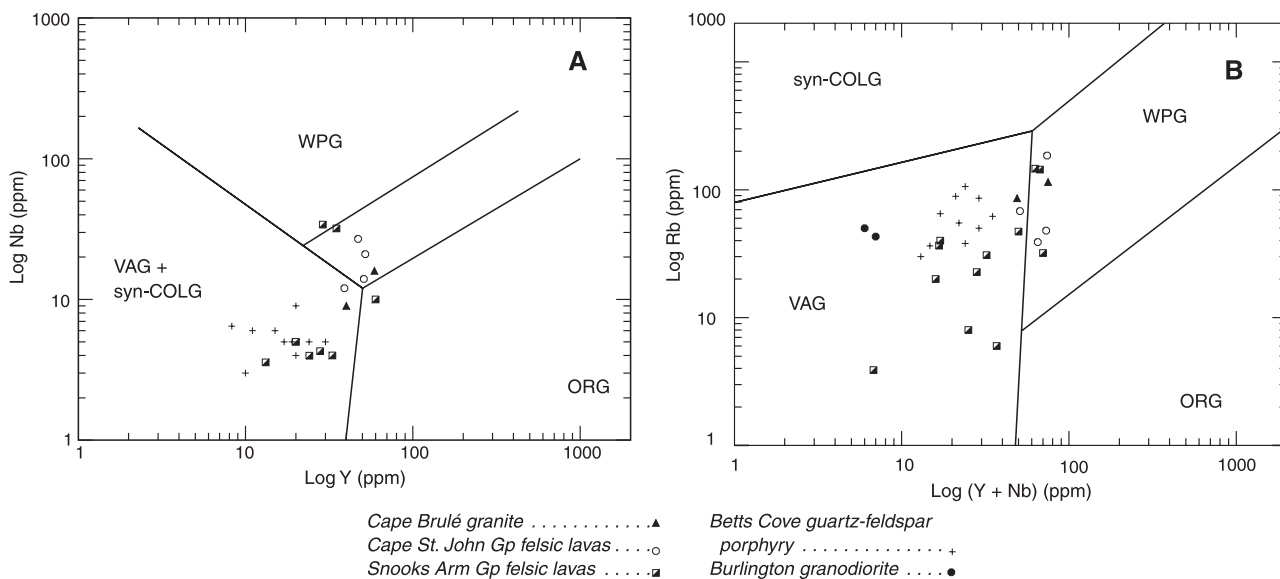


**Figure 43.** **A)** Log Nb versus log Y, and **B)** Log Rb versus log (Y+Nb) tectonic discriminants of Pearce et al. (1984) for felsic and granitoid rocks from Betts Cove and environs. ORG = ocean-ridge granite, syn-COLG = syn-collision granite, VAG = volcanic-arc granite, WPG = within-plate granite.

## Cape St. John Group

Our sample set for Silurian rocks is restricted, which limits interpretation. The Cape St. John basalt is iron-rich tholeiite, very similar in many respects to typical Snooks Arm Group upper tholeiitic lavas (Table 4). Extended-REE plots exhibit clear negative Nb-Ta anomalies and large-ion-lithophile element enrichment, yet high field-strength cation abundances (e.g.  $\text{TiO}_2$ , Zr) are high (Fig. 44, 45). Paleotectonic discriminants classify them as ocean-floor or within-plate basalt (Fig. 32–38). Crustal contamination of tholeiitic basalt is an effective mechanism for producing negative Nb-Ta anomalies and concomitant LILE-enrichment, and so Cape St. John lavas could represent contaminated continental basalt (cf. Thompson et al., 1984; Bédard, 1986; Hooper and Hawkesworth, 1993; Bédard and Wilson, 1997). The high Zr

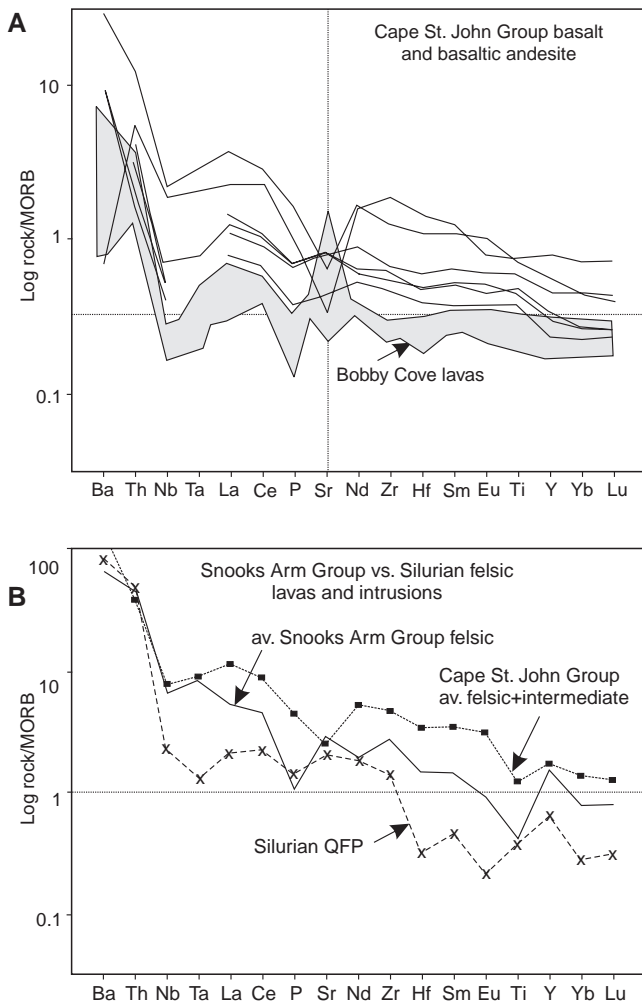


**Figure 44.** Extended trace element plots normalized to N-MORB of Silurian lavas and plutons; **A**) mafic Cape St. John Group lavas, and mafic dykes thought to be cogenetic with them; **B**) felsic Cape St. John Group lavas and tuffs, compared to the average Silurian quartz-feldspar porphyry (QFP), and the average Snooks Arm Group felsic volcanic rock.

contents of evolved Cape St. John lavas (Fig. 45C) is also consistent with crustal contamination. Alternatively, the negative Nb-Ta anomalies and LILE-enrichment of Cape St. John basalt could signify that it is derived from a mantle that was previously metasomatized by subduction-zone

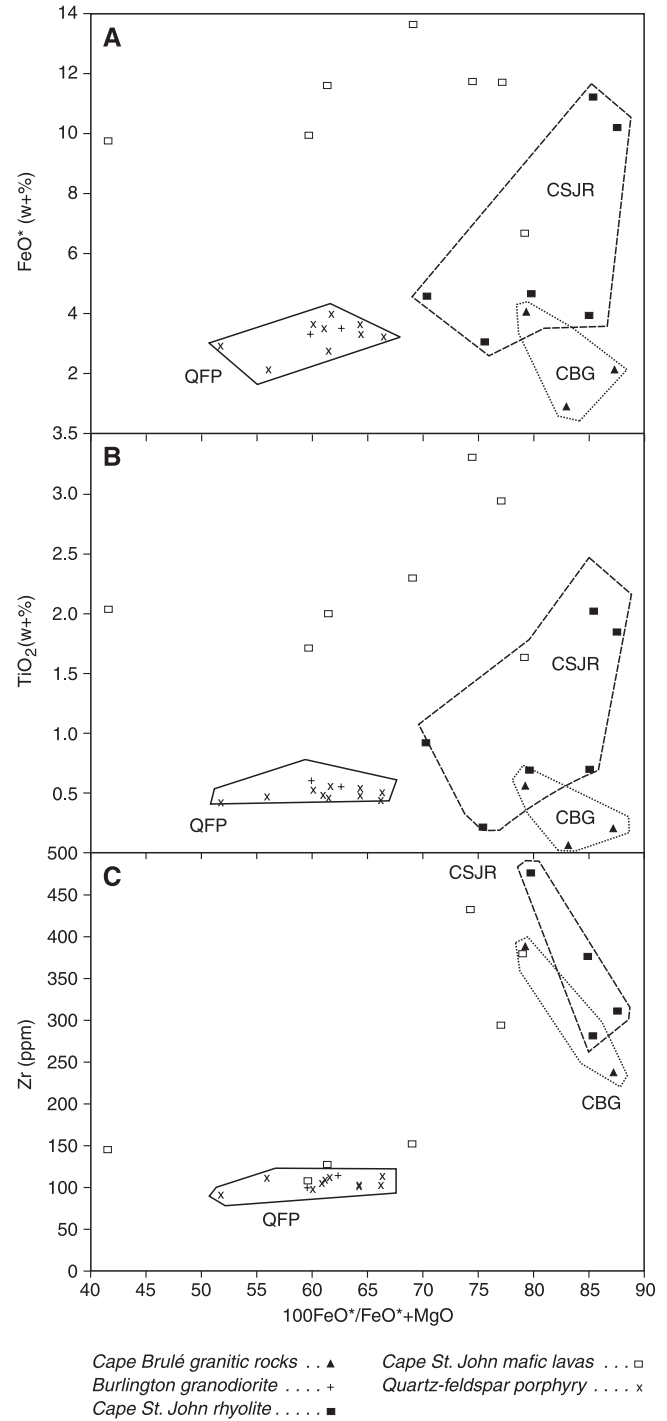


**Figure 45.** **A**)  $\text{FeO}^*$  versus  $100\text{FeO}^*/(\text{MgO}+\text{FeO}^*)$ , **B**)  $\text{TiO}_2$  versus  $100\text{FeO}^*/(\text{MgO}+\text{FeO}^*)$ , **C**) Zr versus  $100\text{FeO}^*/(\text{MgO}+\text{FeO}^*)$ . Silurian igneous rocks. CSJR = Cape St. John rhyolite, CBG = Cape Brulé granite, QFP = quartz-feldspar porphyritic dykes from within the ophiolitic massif.

magmatism, or that it is indeed arc related. We do not favour the last interpretation because of the high  $\text{TiO}_2$  contents and consistent paleotectonic classifications. Our database is not adequate to discriminate between mantle source contamination and intracrustal contamination scenarios.

Cape St. John Group rhyolite appears to form two groups — one enriched in  $\text{FeO-TiO}_2$ , the other depleted in these elements (Fig. 45). The depleted group closely resemble typical Cape Brulé granite, and may represent eruptive equivalents. The Fe-Ti-enriched group fall along the extension of the trend defined by Cape St. John basalt and andesite, and may represent the fractionation residua of these magmas. On paleotectonic discriminant plots (Fig. 43), the Cape St. John rhyolite is classified as within plate or anorogenic.

### Silurian granitoid rocks

The Burlington granodiorite underlies a large proportion of the Baie Verte Peninsula. A representative sample (BGD) was taken in the centre of this body, and another from a ring dyke (CBGR in Hibbard (1983)) that outcrops along the road to Nippers Harbour. The two samples are almost indistinguishable (Fig. 45). The quartz-feldspar porphyry (QFP) intrusions that cut the Betts Cove ophiolite show a restricted compositional range, and closely resemble typical Burlington granodiorite (Fig. 43–45, Table 4). Considered together, these rocks define a trend of increasing  $\text{FeO}^*/\text{MgO}$ , Zr, and Y, with little variation in  $\text{FeO}^*$ ,  $\text{SiO}_2$ , or  $\text{TiO}_2$ , and steadily decreasing  $\text{P}_2\text{O}_5$  and MgO. They plot as calc-alkaline on major element discriminant diagrams (Fig. 32). Paleotectonic classifications also imply that these rocks have arc affinities (Fig. 43).

Available Cape Brulé granite analyses suggest a link with the Cape St. John rhyolite (Fig. 45). Paleotectonic discriminants suggest they are transitional between within-plate anorogenic, volcanic-arc, and orogenic environments (Fig. 43). We do not have enough data to evaluate genetic relationships among these suites.

## TECTONIC MODELS

### *Seafloor spreading in a marginal fore-arc, and the transition to a mixed arc-back-arc volcanic association*

The consensus view is that modern boninite forms as low-pressure, second-stage melts of hot, depleted harzburgite mantle, and that such depleted sources can only melt in response to an influx of hydrous fluids and/or melts enriched in LILE (principally Ba, Rb, Th,  $\text{K}_2\text{O}$ , La, U) emanating from a subducting lithospheric slab (Cameron et al., 1979; Coish et al., 1982; Hickey and Frey, 1982; Kostopoulos and Murton, 1992; Sobolev and Danyushevsky, 1994; Bédard, 1999).

At Betts Cove, the field, geochemical, and petrographic data imply that all of the dykes in the sheeted dyke complex, the cumulate rocks, and most of the Betts Head Formation pillow lavas, are comagmatic with boninitic affinities. Consequently, we infer that the Betts Cove oceanic crust formed by fore-arc seafloor spreading, since recent boninite appears to

be restricted to fore-arc environments (Bédard et al., 1998). The extreme depletion inferred (19–21% prior melting; Bédard (1999)) for the source mantle of the Betts Cove low-Ti boninite suggests that this mantle may have been affected by an older arc magmatic event.

Linear arc volcanic chains are interpreted to be a response to focused effluxes of fertile ‘arc’ components from the subducting slab into the mantle wedge (Fig. 46A; Gill, 1981; Hawkins et al., 1984; Tatsumi, 1989; Arculus, 1994; Brenan et al., 1995; Keppler, 1996). Current Appalachian tectonic models call for southeastward subduction (present co-ordinates) of the Laurentian continental margin beneath oceanic terranes in the Ordovician (Williams, 1979; Stanley and Ratcliffe, 1985; Pinet and Tremblay, 1995). Attempted subduction of the continental margin on promontories beneath the Taconic arcs would have slowed convergence, allowing trench rollback and extension of the overriding plate within re-entrants (*see* Coish, 1989; Harris, 1992; Cawood and Suhr, 1992). Changes in the geometry of subduction (e.g. trench rollback) would disrupt the focused volatile-rich efflux from the slab, and distribute it over a larger volume of the depleted mantle wedge (Bédard et al., 1998). If the overriding plate experiences significant extension, then the mantle beneath must well up to fill the space (Fig. 46B), which creates the potential for decompression melting of the upwelling wedge mantle (Pearce and Peate, 1995). If slab rollback and extension of the overriding plate occur synchronously, then the combination of high ambient volatile contents (dispersed volatile efflux), decompression-melting at low ambient pressures, and a depleted wedge source, would all favour production of voluminous boninitic magmas. This provides the opportunity for magma-dominated extension (seafloor spreading) with boninitic rather than tholeiitic parental magmas. The huge volumes of boninitic melt at Betts Cove appears to require the action of decompression melting, since the small proportion of calculated subduction zone component added to the wedge would only generate a small amount of flux melt (*cf.* Pearce and Peate, 1995).

At Betts Cove, there is a systematic upward progression from extremely trace-element depleted low-Ti boninite (Betts Head Formation), to less-depleted intermediate-Ti boninite, to still less-depleted arc tholeiite (SALT, Mount Misery Formation), and eventually to undepleted tholeiite (SAUT, upper Snooks Arm Group). The last are interstratified with calc-alkaline lavas and pyroclastic rocks. This systematic stratigraphic relationship is inconsistent with a model where the chemical signatures of the different lava types reflect the heterogeneous distribution of fertile components in the wedge, since the most fertile mantle domains should melt first, not the most refractory ones. One must therefore posit a spatial compositional zonation in the mantle beneath the Betts Cove ophiolite in the Ordovician. Since the magmas derived from the more fertile mantle (SAUT) domains post-date the onset of boninitic seafloor spreading, it seems reasonable to infer that the fertile mantle from which the upper tholeiitic magmas were derived were located at greater depth, and that they were entrained into the extending supra-subduction zone wedge to fill the space created by slab rollback and seafloor spreading (Fig. 46C).

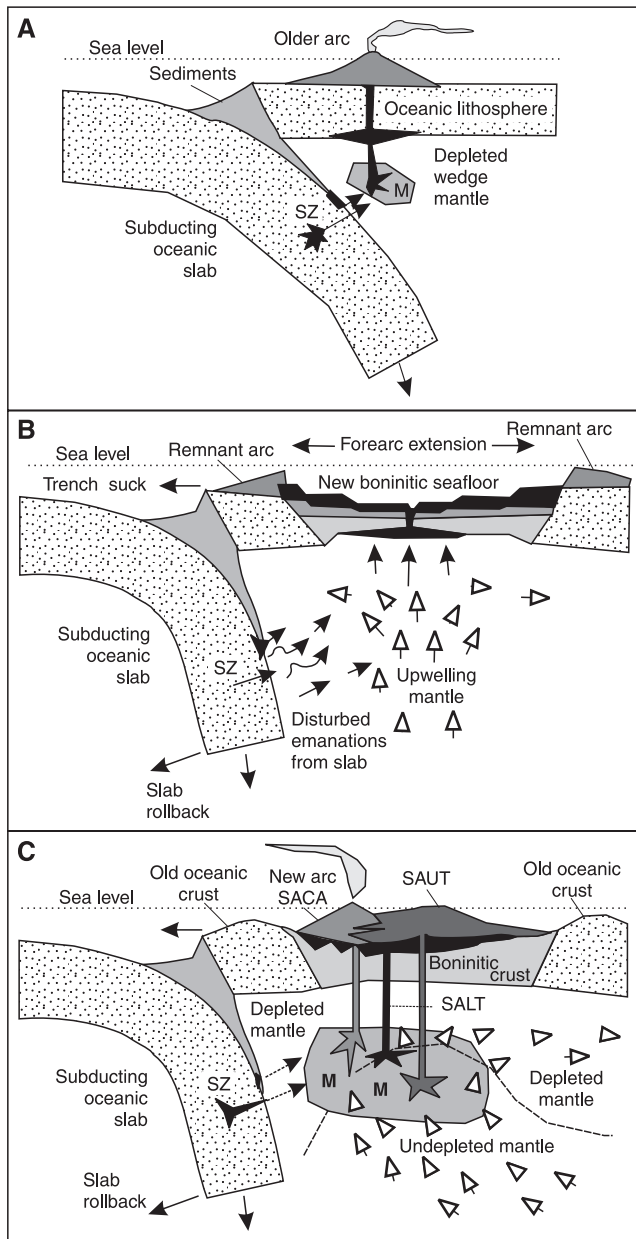


**Figure 46.** Schematic cross-section illustrating the evolution of the Betts Cove ophiolite and its cover rocks. **A)** A stable arc system (pre-Betts Cove) depleted the mantle of basaltic components. The melting zone 'M' is localized by a focused flux of fertile components derived from the downgoing slab labelled 'SZ'. These include hydrous fluids originating in the altered oceanic crust, trondhjemitic partial melts of hydrated oceanic crust, and partial melts of subducted sediments. **B)** Slab rollback causes extension of the overriding plate and disrupts the volatile efflux throughout the depleted wedge. The old arc splits, and new boninitic seafloor is generated. As the hydrated mantle upwells to fill space caused by extension, it melts at shallow levels, yielding low-Ti boninite. **C)** Ongoing slab-fluxed melting at shallow levels yields the Snooks Arm Group calc-alkaline magmas. Decompression melting of undepleted mantle sucked into the wedge to fill space created by slab rollback and seafloor spreading yields the Snooks Arm Group upper tholeiitic series. The intermediate-Ti boninite and Mount Misery tholeiite represent a source with intermediate fertility, and moderate fluxing by subduction-related fluid components.

### Silurian extensional and 'Acadian' compressional events

Cawood et al. (1995) concluded that the Salinic event must be related to continental collision, because the syn- to postkinematic Early Silurian plutonism of the Humber Zone has an overall calc-alkaline evolution trend. However, felsic melts produced during extensional orogenic collapse may have a wide variety of geochemical signatures. Anatexis of older, continentally derived detritus, or coupled intracrustal assimilation-fractionation processes, could generate a calc-alkaline-like trend (Bédard, 1986; Harris et al., 1990; Inger, 1994; Innocent et al., 1994). Geochemical data from the mafic lavas of the Cape St. John Group (Fig. 32–38) suggest that they are anorogenic, with indications that crustal contamination was involved.

The alternation of tholeiitic and calc-alkaline lavas and tuffs throughout deposition of the Snooks Arm Group implies that both the depleted arc-dominated and the undepleted mantle sources were simultaneously present beneath Betts Cove. The abundance of thick, proximal juvenile calc-alkaline tuffs in the lower Bobby Cove Formation suggests that a new arc began to form after stabilization of the new subduction geometry. Thus, calc-alkaline magmas would represent shallow melting of depleted wedge sources in response to volatile effluxes from ongoing subduction, whereas upper tholeiitic magmas would represent decompression melting at greater depths of rather undepleted mantle entrained into the wedge by slab rollback (Fig. 46C).

As a possible alternative to the petrogenetic interpretation of Cawood et al. (1995), Early Silurian granitoid intrusions crosscutting the Fleur de Lys belt (Wild Cove igneous suite and correlatives) have been attributed to crustal melting induced either by internal heating and subsequent isothermal decompression of a tectonically thickened crust (Jamieson and O'Beirne-Ryan, 1991), or as a response to enhanced basal heat flow through the lithosphere-asthenosphere boundary caused by magmatic underplating (Inger, 1994). We broadly agree with these latter interpretations (Jamieson and O'Beirne-Ryan, 1991; Inger, 1994), and suggest that, the 'calc-alkaline' chemical signatures of the Burlington and Cape Brulé suites could reflect extensive reactivation of older arc-related basement rocks. A more comprehensive study of these rocks appears necessary to distinguish between the two hypotheses, however.



## MINERAL DEPOSITS

The Betts Cove ophiolite has a long history of mineral production. The most important mineral occurrences are the Cyprus-type, ophiolite-hosted, volcanogenic copper deposits located at Tilt Cove and Betts Cove. Hibbard (1983) compiled and summarized the geology of the Tilt Cove deposit. More recent work based at the Memorial University of Newfoundland (Squires, 1981; Strong, 1984; Saunders, 1985; Hudson, 1988; Strong and Saunders, 1988) and elsewhere (Hurley, 1982) focused mainly on the Tilt Cove and Betts Cove mine areas. The mineral occurrences of the Betts Cove ophiolite have been reviewed for several field trip guides (Saunders, 1990; Saunders and Strong, 1988).

Exploration for gold in the Burlington peninsula began in the early 1980s and continued intensively for about ten years. The Nugget Pond gold deposit was found by the Bitec Corporation in 1988–1989 and it was put into production in 1997 by Richmond Mines Inc. Nugget Pond is a hybrid replacement deposit probably related to postophiolite granitoid intrusions. Minor gold occurrences are relatively abundant elsewhere in the lowermost sedimentary package of the Scrape Point Formation, known colloquially as the Nugget Pond horizon; in altered ultramafic rocks of the ophiolite; and in rocks of the Cape St. John Group near the structural contact between the two units.

### *Copper and copper-gold occurrences*

#### **Tilt Cove mine**

Copper mineralization was first recognized in the Betts Cove ophiolite at Tilt Cove in 1857. Exploitation began in 1864 and continued through two periods of operation until final closure in 1967 (Hibbard, 1983). In total, about 8.2 million tons (7.4 million tonnes) were mined at Tilt Cove. The greatest production was from 1957 to 1967, when approximately 7.4 million tons (6.7 million tonnes) of ore grading 1.24% Cu and containing 42 500 ounces (1 204 853.75 g) of gold were extracted (Strong, 1984).

The sulphide deposits at Tilt Cove occur within a 400 m thick zone of massive and pillowed basalt and basalt breccia located approximately at the contact (Fig. 6) between boninitic and tholeiitic rocks of the Betts Head and Mount Misery formations, respectively. These lavas are in structural contact with the underlying ultramafic unit (Tremblay et al., 1997), which is mainly composed of serpentinite and talc-carbonate schist. The sheeted dyke unit is not well developed at Tilt Cove, although the lowermost exposed Betts Head lavas contain 30–50% basalt dykes. The ore-bearing lavas and breccia units are overlain by a thick sedimentary sequence belonging to the Sedimentary Member of the Scrape Point Formation. These contain basal, locally magnetite-bearing red argillite and chert, succeeded by grey chert and greywacke that is extensively intruded by fine-grained ferrogabbro sills. The sedimentary and volcanic units are cut by numerous, large, Silurian dacitic (quartz-feldspar porphyry) sheets.

Mineral production at Tilt Cove came from several zones distributed east and west of the village site (Fig. 6). The West zone deposit consisted mainly of disseminated and stringer chalcopyrite+pyrite mineralization in a steeply dipping pipe-like body (Squires, 1981). The ore zone was contained in massive and pillowed mafic lavas and breccia. The ore directly overlays boninitic lavas and breccia, which form the ridge immediately north of the pit. A small lens of massive sulphide (the Cove zone) just south of the west zone at depth is truncated by the Valley Fault.

The Valley Fault separates the East and West zones. It is 50–75 m wide and consists of serpentinite and talc-carbonate schist as well as chloritized Silurian quartz-feldspar porphyry dykes, which are spatially associated with West zone mineralization. Movement on the Valley Fault has been interpreted as normal, east side down (Squires, 1981; Tremblay et al., 1997).

The East zone is constituted of several smaller orebodies. These include the low-grade stockwork “A” zone, the adjacent, massive Cliff zone (“Bogden’s lode”) and farther east, the Main zone which itself is composed of a number of medium to smaller massive sulphide lenses (Hibbard, 1983; Fig. 6, 47). Surface basalt exposure in the Main zone mine is entirely composed of mafic lava breccia. However, sections of the workings by Donoghue et al. (1959, Fig. 47) indicate that the breccia in the Main zone area gives way to massive ‘andesite’ at a shallow depth. The east end of the Main zone is terminated by a normal fault (East Limit Fault) which puts the host Betts Head–Mount Misery formation lavas in contact with the overlying sedimentary rocks of the Scrape Point Formation. The East Limit fault zone is occupied by sheared Silurian quartz-feldspar porphyry intrusion. Both the East Limit and Valley faults are interpreted to be Silurian (Tremblay et al., 1997). East of the main ore zone, the only known mineralization (Fig. 6) consists of blocks of sulphide in talc carbonate (Scrape showing) and a small occurrence of sulphide minerals related to iron-formation (Beaver Cove Pond showing).

The chemistry of the Tilt Cove deposits is rather simple. Copper is the main element present (Table 6). Both lead and zinc abundances are very low. Gold production has been reported but gold contents of the samples analyzed is overall very low, with occasional values in the 1–2 ppm range. Nickel and cobalt values are also low, and the recent analyses do not reflect the small amount of nickel ore that was produced from the West zone in the period between 1869 and 1876. The nickel mineralization was probably a secondary product, as it was associated with the contact between talc-carbonate schist (altered peridotite) and basaltic and/or boninitic rocks in the West mine. Mineralization consisted of sulphide and arsenide minerals of nickel, principally niccolite, maucherite, chloanthite, gersdorffite, arsenopyrite, and millerite (Papezik, 1964). Elevated As values occur in all analyzed samples (Table 6). Additional data and illustrations can be found in Santaguida and Hannington (1996).

Alteration associated with the deposits is dominantly chloritic, with ancillary carbonate and some stilpnomelane. Intense alteration is restricted to a relatively narrow zone

around the sulphide deposits (Fig. 47). On the east side of the Main zone, alteration associated with the East Limit fault has produced the assemblage specularite-chlorite-sulphide. Specularite is also common in the vicinity of the Valley Fault, and is associated with sulphide mineralization in Cape St. John Group rocks immediately to the north.

Without access to underground geology and with little mineralization available on surface, it is difficult to model the Tilt Cove deposit. Squires (1981) interpreted the various lenses as part of a single ophiolite-type copper-depositing system. The West and "A" zones were considered the deepest and intermediate portions of the feeder zone respectively, and the Main zone massive sulphide minerals were interpreted to be the overlying massive pods, separated from the "A" zone by a system of flat faults which were reported from sites in the underground workings.

The new mapping and stratigraphy confirms the general interpretations of Strong and Saunders (1988) that the Tilt Cove deposits can be classified as ophiolite-type copper deposits (Galley and Koski, 1999). Our work suggests that the ore is subconcordant (Fig. 5), located approximately at the boundary between the Betts Head and Mount Misery formations. The common breccia zones that provided the necessary porosity for sulphide deposition are principally talus breccia, associated with the movement of synoceanic normal faults. Subvolcanic gabbroic intrusions provided the localized high-level heat sources needed to drive hydrothermal cells

from which the ore was deposited. Repeated movement at the time the Mount Misery and Scrape Point formations were being deposited rejuvenated the normal faults and provided the opportunity for renewed hydrothermal activity that may have redistributed the sulphide ore to some extent. Silurian faulting dissected the different orebodies. It is still not clear to what extent Silurian magmatism and associated hydrothermal activity may have affected the textures and composition of the ore.

### Betts Cove mine

The Betts Cove deposit was found in 1864 and 130 682 tons (118 530 t) of hand-cobbed ore grading up to 10% Cu was shipped before the mine was closed by collapse of the hanging wall volcanic rocks into the workings in 1886. The Betts Cove deposit is the most polymetallic occurrence in the area; containing abundant zinc, minor lead, and high levels of gold (Table 6). The Au is present as free gold with up to 20% contained Ag. The amount of gold present seems to vary more or less directly with the zinc grade of the ore (Table 6) (Hurley and Crocket, 1985). Traces of galena, PbTe, and AgTe are also present.

The Betts Cove mine and the associated Joey's Pond occurrence (occurrences 2 and 3, Fig. 4, 48) outcrop in the complex transition zone between the sheeted dyke unit and the Betts Head Formation lavas. At the mine, concentrations

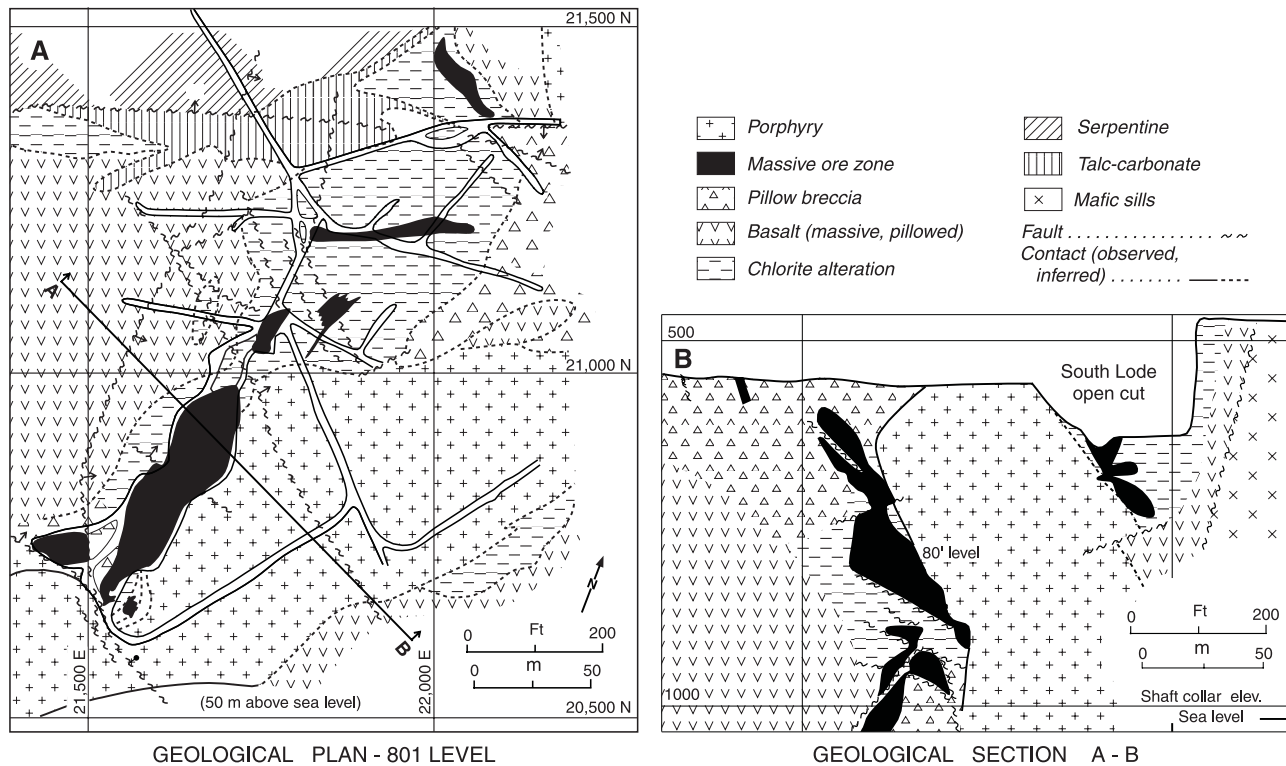


**Table 6.** Selected element and trace element analyses of mineral occurrences from the Betts Cove ophiolite.

Sample	Area	Lithology	Au (ppb)	Au-A (g/t)	As (ppm)	Cu (ppm)	Zn (ppm)	Pb (ppm)	Ag (ppm)	Co (ppm)	Ni (ppm)
<b>NUGGET POND HORIZON (NPH)</b>											
<b>West Pond - east end</b>											
TC063	NPH-West Pond	Argillite, pyritic	8		57	201	129	23	1.5	21	48
TC064	NPH-West Pond	Argillite, pyritic	12		149	578	90	137	1.6	61	123
TC068	NPH-West Pond	Argillite, pyritic	2		54	83	77	15	<0.2	9	65
TC070	NPH-West Pond	Argillite, pyritic	2		63	68	77	7	<0.2	9	82
TC071	NPH-West Pond	Argillite, pyritic	4		43	60	31	<2	<0.2	5	32
TC072	NPH-West Pond	Argillite, pyritic	1		165	50	80	<2	<0.2	24	76
TC072A	NPH-West Pond	Argillite, pyritic	<1		37	38	58	47	0.6	5	5
TC1020	NPH-West Pond	Argillite, pyritic	<1		52	99	70	86	0.6	14	73
<b>East Pond area</b>											
TC097	NPH-East Pond-west side	Argillite, pyrite	3		19	14	66	<2	0.6	12	12
TC1039	NPH-East Pond	Argillite, pyrite cubic	1		<3	43	113	4	0.5	45	65
TC1040	NPH-East Pond	Argillite, pyrite	6		<3	3	51	<2	0.4	15	24
TC1038	NPH-East Pond	Argillite, pyrite cubic	<1		<3	15	78	<2	0.4	17	29
TC1035	NPH-East Pond	Argillite, xenolith in quartz vein	5		<3	8	4	<2	<0.2	4	9
TC1036	NPH-East Pond	Argillite, xenolith in quartz vein	4		<3	52	146	2	0.6	26	26
TC082	NPH-East Pond Peninsula	Argillite, pyrite	1		38	181	122	<2	0.8	9	51
<b>Red Cliff Pond area</b>											
TC1043	NPH-Red Cliffe Pond	Argillite, pyritic	<1		<3	49	43	9	0.4	18	25
TC1063	NPH-low water area	Argillite, pyritic	22		<3	57	72	3	0.9	24	165
TC1064	NPH-low water area	Argillite, pyritic	18		<3	43	65	2	0.9	14	113
TC1065	NPH-low water area	Argillite, pyritic	51		14	58	24	21	0.9	10	67
TC1044	NPH-Red Cliff Pond island	Argillite, pyritic	73		53	90	99	22	1.0	19	43
<b>Tilt Cove area</b>											
TC901B	NPH-Tilt coast	Red chert/argillite	<1		17	22	17	3	0.5	18	83
<b>Long Pond East gold occurrence</b>											
TC109	NPH-Iron Island	Iron-formation	51		8	255	13	21	1.0	16	396
TC004	NPH-Long Pond East	Talc-carbonate-magnetite-pyrite schist	2190		76	48	53	25	0.2	94	1680
TC006	NPH-Long Pond East	Argillite; green, pyritic	355		282	537	348	157	0.5	122	818
TC007	NPH-Long Pond East	Argillite; green, pyritic	489		283	405	350	182	1.2	128	890
TC008	NPH-Long Pond East	Argillite; green, pyritic	124		116	598	326	74	0.3	98	592
TC009	NPH-Long Pond East	Argillite; red, pyritic	14		28	343	220	12	<0.2	49	698
TC130	NPH-Long Pond East		1		19	107	104	13	1.5	29	55
<b>Castle Rock gold occurrence</b>											
TC013	NPH-Castle Rock Au	Argillite, chlorite-magnetite-pyrite	139		182	179	213	76	1.3	149	205
TC014	NPH-Castle Rock Au	Argillite, chlorite-magnetite-pyrite	41		111	108	296	10	<0.2	27	111
TC015A	NPH-Castle Rock Au	Iron-formation	5		6	101	43	28	0.6	67	143
TC015B	NPH-Castle Rock Au	Iron-formation	25		11	159	41	36	0.4	75	141
TC016	NPH-Castle Rock Au	Carbonate unit, oxide	43		45	480	245	40	<0.2	142	2740
TC017	NPH-Castle Rock Au	Carbonate unit	24		35	67	100	29	<0.2	67	1180
TC018	NPH-Castle Rock Au	Argillite, pyritic		15	9	92	54	66	3.5	134	347
TC019	NPH-Castle Rock Au	Argillite, pyritic		41	3	280	103	44	5.3	116	324
TC164	NPH-Castle Rock Au	Carbonate unit	<1		6	<0.5	41	7	0.9	37	933
<b>OPHIOLITE-HOSTED BASE-METAL-GOLD OCCURRENCES</b>											
<b>Burton's Pond copper-gold occurrence</b>											
TC1350	Burton's Pond	Silicified basalt-disseminated sulphide	1420		4	>max	672	13	33	92	210
TC1351	Burton's Pond	Silicified basalt-stringer sulphide	237		27	8570	197	8	8.0	127	269
TC1352	Burton's Pond	Submassive sulphide minerals	1220		108	>max	615	16	33	252	501
TC1353	Burton's Pond	Submassive sulphide minerals		143	<3	>max	362	17	20	253	651
TC1356	Burton's Pond	Silicified basalt-disseminated sulphide	1200		<3	21 800	493	9	31	111	226
<b>Betts Cove copper-zinc-gold occurrence</b>											
TC1311	Betts Cove mine	Submassive chalcocopyrite	3090		<3	>max	1460	591	14	258	26
TC1312	Betts Cove mine	Chlorite schist pyrite	4670		80	7380	464	126	14	331	7
TC186	Betts Cove mine	Basalt, chloritic, pyrite/chalcocopyrite	555		<3	9090	116	<2	0.9	44	49
TC187	Betts Cove mine	Basalt, chloritic, pyrite/chalcocopyrite	67		<3	18 500	140	<2	2.0	45	56
TC191	Betts Cove mine	Basalt, chlorite schist	507		16	2040	1370	9	<0.2	19	<1
TC192	Betts Cove mine	Basalt, chloritic, pyrite/chalcocopyrite	103		<3	1900	91	<2	0.3	76	48
TC199	Betts Cove mine	Basalt	1		<3	330	111	<2	<0.2	31	50
TC200	Betts Cove mine	Basalt	16		<3	866	211	<2	0.6	39	39
TC202	Betts Cove mine	Basalt, chloritic	9280		188	5840	6050	143	12	31	11
TC203	Betts Cove mine	Pyrite, massive	2320		107	61 700	1100	39	12	201	33
TC204	Betts Cove mine	Pyrite, massive	1200		148	7660	287	60	4.0	155	78
TC205	Betts Cove mine	Pyrite, massive	7560		180	31 300	43 000	173	31	319	21
TC206	Betts Cove mine	Pyrite, massive		13	612	840	158 000	485	22	3	14
TC207	Betts Cove mine	Pyrite, massive		16	472	3230	84 100	490	45	49	51

Table 6. (cont.)

Sample	Area	Lithology	Au (ppb)	Au-A (g/t)	As (ppm)	Cu (ppm)	Zn (ppm)	Pb (ppm)	Ag (ppm)	Co (ppm)	Ni (ppm)
<b>Mount Misery copper occurrence</b>											
TC167	Mount Misery	Basalt, pyrite/chalcopyrite	23		<3	2180	219	12	0.5	115	48
TC170	Mount Misery	Pyrite, massive	548		82	12 300	36	29	1.5	647	21
TC171	Mount Misery	Pyrite, massive	636		129	5310	681	38	1.1	710	41
TC172	Mount Misery	Pyrite, massive	2090		92	6840	67	23	5.4	278	55
TC173	Mount Misery	Basalt, silicified, chalcopyrite	70		<3	57 100	394	2	2.1	47	9
TC174	Mount Misery	Basalt, chloritic/pyrrhotite	3		<3	17	109	<2	<0.2	43	63
TC175	Mount Misery	Basalt, silicified	136		3	43 900	387	3	1.9	95	20
TC178	Mount Misery	Basalt, quartz/pyrite stockwork	51		<3	4750	663	10	0.9	524	73
TC179	Mount Misery	Basalt, silicified/pyrite	26		<3	469	40	124	<0.2	61	15
TC182	Mount Misery	Basalt breccia, quartz/sulphide	120		55	654	87	8	0.7	1340	56
TC183	Mount Misery	Pyrite/chalcopyrite/pyrrhotite-massive	128		13	28 500	277	20	4.2	1550	170
<b>Nudulama copper-gold occurrence</b>											
TC041	Nudulama adit	Pyrite, siliceous	231		301	367	69	14	0.2	367	23
TC042	Nudulama adit	Basalt, pyrite stringers	671		641	16 100	193	76	5.3	2430	84
TC043	Nudulama adit	Vein	540		414	41 100	675	7	6.9	112	26
TC047	Nudulama shaft	Basalt, pyrite stringers		24	10 200	64 500	667	22	18	6180	445
TC048	Nudulama shaft	Basalt, pyrite stringers	249		300	27 900	746	9	5.8	594	106
TC049	Nudulama shaft	Basalt, pyrite stringers	3970		436	24 600	627	30	6.0	728	81
<b>Tilt Cove copper deposit</b>											
TC533	Tilt Cove	Serpentine-carbonate-magnetite	<1		196	24	41	<2	0.5	102	1230
TC535	Tilt Cove	Basalt, silicified	24		24	274	1730	<2	<0.2	29	82
TC540	Tilt Cove	Basalt, sulphide	57		47	290	455	<2	0.4	50	83
TC541	Tilt Cove	Basalt, sulphide	87		20	202	231	<2	0.6	33	35
TC542	Tilt Cove	Basalt, sulphide	135		246	2110	119	4	1.0	147	21
TC549	Tilt Cove	Basalt breccia	30		16	164	1300	<2	1.0	20	16
TC564	Tilt Cove	Basalt breccia, pyrite	44		668	9390	141	6	3.4	851	361
TC566	Tilt Cove	Basalt, pyrite, magnetite	2		<3	2930	330	<2	1.3	90	143
TC567	Tilt Cove	Basalt, magnetite	5		<3	1180	295	<2	0.8	41	22
TC570	Tilt Cove	Chalcopyrite-pyrite	494		60	137 000	503	49	12	530	76
TC577A	Tilt Cove	Carbonate altered basalt	<1		<3	2390	44	<2	0.4	97	1060
TC577B	Tilt Cove	Carbonate altered basalt	<1		12	255	46	2	<0.2	91	1370
TC578	Tilt Cove	Carbonate vein	8		357	56	38	9	0.3	58	886
TC595	Tilt Cove	Magnetite, massive, pyrite/chalcopyrite	38		<3	15 100	<0.5	18	1.4	225	63
TC596	Tilt Cove	Magnetite, massive, pyrite/chalcopyrite	56		195	10 100	<0.5	15	1.4	357	117
TC597	Tilt Cove	Basalt, chlorite, sulphide minerals	11		43	5440	18	<2	0.6	321	94
TC599	Tilt Cove	Basalt, chlorite, sulphide minerals	90		354	16 300	55	<2	1.5	460	27
TC600	Tilt Cove	Basalt, chlorite, sulphide minerals	55		325	13 700	48	<2	0.7	566	48
TC601	Tilt Cove	Basalt, chlorite, sulphide minerals	37		313	5660	176	5	0.5	420	58
TC604	Tilt Cove	Basalt, chlorite, sulphide minerals	7		<3	359	177	<2	0.2	30	34
TC624A	Tilt Cove	Chert, red	3		<3	62	46	<2	<0.2	29	35
TC638	Tilt Cove	Basalt	<1		<3	56	104	<2	<0.2	40	8
TC644	Tilt Cove	Quartz-feldspar porphyry	2		<3	23	46	8	<0.2	8	21
TC647	Tilt Cove	Specular hematite-chlorite	30		442	113	13	17	0.8	513	699
TC648	Tilt Cove	Specular hematite-chlorite	357		72	2410	351	44	1.1	594	311
TC649	Tilt Cove	Specular hematite-pyrite	1030		270	18 400	165	50	2.2	1300	457
TC650	Tilt Cove	Specular hematite-pyrite	786		210	16 600	228	48	1.5	1180	470
TC652	Tilt Cove	Specular hematite	143		194	327	15	13	0.9	556	439
TC669	Tilt Cove	Siltstone	16		<3	123	91	<2	<0.2	29	22
TC671	Tilt Cove	Chert, red	10		<3	55	63	25	<0.2	19	17
TC672	Tilt Cove	Chert, grey	9		<3	85	96	<2	0.2	21	10
TC681	Tilt Cove	Cherty argillite; red, magnetite	<1		12	36	63	<2	0.6	20	42
TC683	Tilt Cove	Siltstone, magnetite	7		<3	57	82	<2	<0.2	25	20
TC684	Tilt Cove	Siltstone, magnetite	4		<3	6	69	<2	<0.2	33	37
TC685	Tilt Cove	Siltstone, magnetite	<1		<3	137	80	<2	<0.2	25	21
TC690	Tilt Cove	Sulphide, chlorite	391		215	8530	461	35	3.2	1990	109
TC693	Tilt Cove	Sulphide, chlorite	687		382	29 500	3280	15	4.3	1460	170
TC694	Tilt Cove	Sulphide, chlorite	119		507	427	1870	203	10	240	8
TC695	Tilt Cove	Sulphide, chlorite	890		207	8520	11 700	124	6.0	417	114
TC026	Tilt Cove West pit hilltop	Basalt	17		<3	1440	107	<2	0.9	88	70
TC027	Tilt Cove West pit hilltop	Basalt, pyrite/chalcopyrite	23		8	3460	68	4	0.9	182	72
TC031	Tilt Cove West pit hilltop	Basalt, pyrite stringers	72		<3	979	64	3	0.5	174	160
TC032	Tilt Cove West pit hilltop	Basalt, pyrite vesicles	15		<3	1130	63	<2	<0.2	107	108
TC033	Tilt Cove West pit hilltop	Basalt, pyrite vesicles	48		4	1060	58	5	0.3	298	103
TC034	Tilt Cove West pit hilltop	Basalt, pyrite stringers	201		18	788	24	8	<0.2	39	31
TC035	Tilt Cove West pit hilltop	Basalt, pyrite stringers	1480		75	8150	92	<2	1.0	150	30
TC036	Tilt Cove West pit hilltop	Basalt, pyrite stringers	55		45	815	79	<2	0.3	67	69
<b>MISCELLANEOUS OCCURRENCES</b>											
TC1047	Red Cliff FeCu	Massive magnetite-pyrite	936		56	2070	272	60	4.6	429	218
TC1034	Arrowhead pond chips	Oxidized sulphide in talc-carbonate		20.3	<3	8000	36	3	>max	67	1170
TC1049	George occurrence	Hematitic rhyolite+quartz vein	3		<3	11	9	4	0.3	3	10

of pyrite with low contents of copper and gold are found within chloritic shear zones that range from 1–3 m in thickness (Fig. 48). Two sets of mineralized shear zones are present; one striking about 315–345° appears to be the zone that was mined; and a second striking 050–060° offsets the northwest-trending veins. At Joey's Pond, 300 m north of the Betts Cove mine (Fig. 48), a shear zone with a similar orientation to the northwest-southeast shear zone at Betts Cove contains stringer pyrite-chalcopyrite mineralization and may be the strike extension of the ores mined at Betts Cove. To the south-east of the Betts Cove mine, the northeast-southwest shear can be traced for several hundred metres, both on the surface, and from data from drilling by Noveder, Inc. The shear zone is markedly discordant to the stratigraphy (Fig. 4). Several other minor occurrences are known in the area of the Betts Cove deposit including the Betts Head and Dolphin occurrences (4 and 5, Fig. 4).

The mineralized shear zones are interpreted to represent synoceanic normal faults. They are rich in chlorite, with associated highly strained quartz and locally abundant anthophyllite, tremolite, calcite, and stilpnomelane. The abundance of chlorite, and the zonation of the surrounding alteration halo, led Saunders (1985), Saunders and Strong (1986), and Swinden et al. (1989) to conclude that the ore was deposited from a major hydrothermal convection cell, and that hydrothermal flow was focused within the relatively porous fault zone. The new mapping confirms the synkinematic timing of the large gabbroic sheets found immediately adjacent the

orebody. It seems logical to infer that these gabbroic sheets provided the localized heat sources necessary to drive hydrothermal convection.

However, kinematic indicators along these chloritized faults are inconsistent with the sense of motion inferred from stratigraphic offsets, leading Tremblay et al. (1997) to propose that the highly chloritized faults were reactivated during obduction of the ophiolite.

The high-grade massive ore that was mined from the deposit is now seen only in dumps and is no longer visible in outcrop, being buried below the caved area. It consists of brecciated pyrite with chalcopyrite, sphalerite, and gold sulphide minerals. Lamination is common in the massive ore, which Upadhyay and Strong (1973) interpreted as a northwest-striking exhalative massive sulphide lens that was subsequently modified by southwest-northeast shear zones into which some of the earlier sulphide minerals have been remobilized. The common presence of fold closures and porphyroclasts in the banded ore lead us to favour a tectonic origin for the banding, as did Santaguida and Hannington (1996). It is not possible to completely exclude a primary origin for the sulphide banding, but we note that both in modern seafloor analogues of massive sulphide deposits (Herzig and Hannington, 1995), and in Australian massive sulphide mineralization (Large, 1992), the layered sulphide deposits form a relatively small part of a sulphide lens, most of which is composed of rather massive or brecciated ore.

#### Mount Misery and Foot Pond occurrences

The Mount Misery occurrence occupies a roughly north-east-trending shear zone that forms a strong airphoto lineament (Fig. 4). The lineament appears to represent a synoceanic décollement zone, now largely consumed by late intrusive gabbroic rocks.

The mineralized part of the Mount Misery occurrence extends eastward for about 500 m from the head of Betts Cove. The mineralization is found in a shear zone that forms the contact between the sheeted dyke unit and the overlying Betts Head lavas. The Mount Misery occurrence contains very variable but commonly low levels of disseminated pyrite and chalcopyrite. The best mineralization is on the height of land between Betts Cove and Foot Pond. Here, the sheared basaltic lavas host a zone up to 50 m wide of disseminated pyrite and chalcopyrite. Massive pyrite veins up to 10 cm thick are exposed in a pit at the west end of the occurrence. On the face of the cliff above Betts Cove, the zone is only 2 m thick and is composed of silicified and pyritized sheared basalt whereas at Betts Cove, dumps contain basalt breccia with a quartz matrix that carries minor chalcopyrite and pyrrhotite.

#### Nudulama occurrence

The Nudulama occurrence is on the Sugarloaf peninsula on the southwestern shore of Long Pond (Fig. 5). Sugarloaf, a bald knob that is clearly visible from all points on the pond, consists of a small area of pillowed mafic lava embedded in

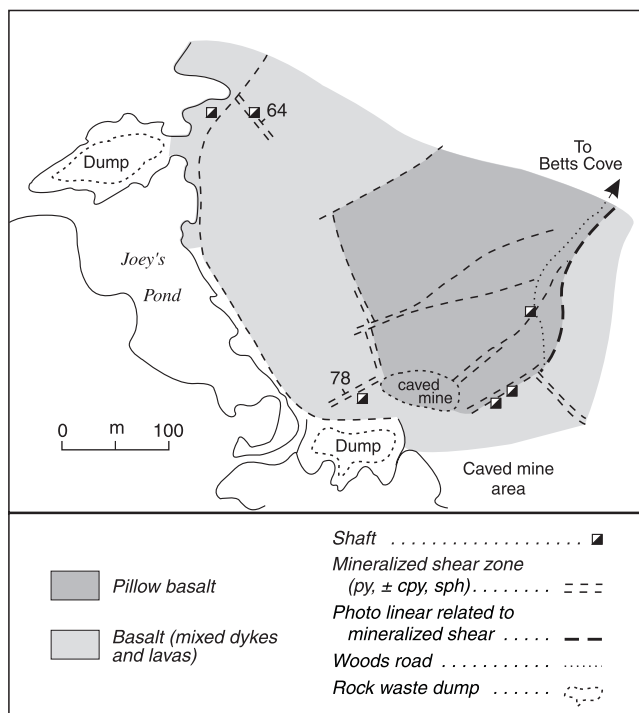


**Figure 48.** Distribution of mineralized shear zones and associated airphoto linear features, Betts Cove mine.

breccia which we interpret to represent a mixture of talus, fault, and hyaloclastite breccia. The mineral occurrence consists of two zones, the shaft zone and the adit zone.

At the shaft zone, on the point southeast of Sugarloaf, mineralization is only exposed at lowest water levels and consists of a few irregular, subvertical, chalcopryite stringers in a chloritic sheared zone. On the dump, however, some fragments of chloritic tectonic breccia are cemented mainly by chalcopryite and contain some gold. One sample analysis (Table 6) contains significant quantities of As, Ni, Co, and 24 g/t Au reflecting the presence of arsenopyrite, gersdorffite, and native Au.

The chlorite alteration that characterizes the shaft zone can be traced (at low water) along the edge of the peninsula to the adit zone. The adit zone is in the saddle immediately northwest of Sugarloaf, and is 'stratigraphically' higher than the shaft zone. The adit zone consists of low-grade and irregularly distributed disseminations of chalcopryite interstitial to breccia fragments.

### Burton's Pond occurrence

The Burton's Pond occurrence lies on the coast between Betts Cove and Nippers Harbour (Fig. 2) on a small rocky barrier that separates Burton's Pond from the Atlantic Ocean. The Burton's Pond occurrence extends north for about 100 m from the coast. Hudson (1988) studied it in detail.

The occurrence consists of siliceous shear zones and associated stockwork zones in boninitic rocks of the sheeted dyke unit and adjacent gabbro-norite. The best mineralization is developed in the boninitic rocks, which are strongly silicified along the sheared zone. Alteration is largely restricted to areas adjacent to shear zones and vein swarms. The silicified zone contains mainly quartz with carbonate and highly variable amounts of pyrrhotite, chalcopryite, and gold. Hudson (1988) characterized three alteration assemblages associated with the veins, chlorite+quartz ± albite, chlorite+sericite, and calcite+sericite. Anomalous traces of As, Co, and Ni (Table 6) are reflected in the presence of minor amounts of arsenopyrite, argentopentlandite, and cobaltite-gersdorffite solid solutions. Scanning electron microscope examination indicated a variety of micrometre-sized grains of several minerals and alloys, including sphalerite, stannite, native bismuth, BiFe(Cu), BiFe(Ag), PbFe(Se), electrum (Ag<sub>60</sub>Au<sub>40</sub>), and AgTe. The Burton's Pond occurrence is similar to the Nudulama occurrence on Long Pond in having elevated Ni, Co, and As. The amount of sulphide is highly variable, and ranges from submassive to weakly disseminated pyrrhotite ± chalcopryite in thin stockwork-like veinlets of similar composition.

### Gold deposits

#### Nugget Pond mine and Nugget Pond horizon

The Nugget Pond gold deposit (Fig. 7) is the only mine currently in production in the Betts Cove ophiolite. It was found by the Bitec Corporation in 1988–1989 and the deposit was put into production in 1997 by Richmond Mines Inc. with a reserve of 488 000 short tons (443 000 t) of ore grading 0.357 ounces of gold per ton (11.151 g/t) (Richmond Mines Inc. web site, March, 1998, www.richmond-mines.com). The gold deposit consists of manto-style disseminated pyrite-gold mineralization within the basal portion of the Sedimentary Member of the Scrape Point Formation, Snooks Arm Group, which is colloquially described as the Nugget Pond horizon.

#### Stratigraphic setting

The Nugget Pond horizon is a 40–60 m thick red-green turbidite and/or tuffaceous unit (Fig. 7, 49) that separates tilted and eroded basaltic pillow lavas of the underlying Mount Misery Formation from dominantly massive plagioclase-porphyritic lava flows, pillows, and subordinate subvolcanic sills of the volcanic member of the Scrape Point Formation.

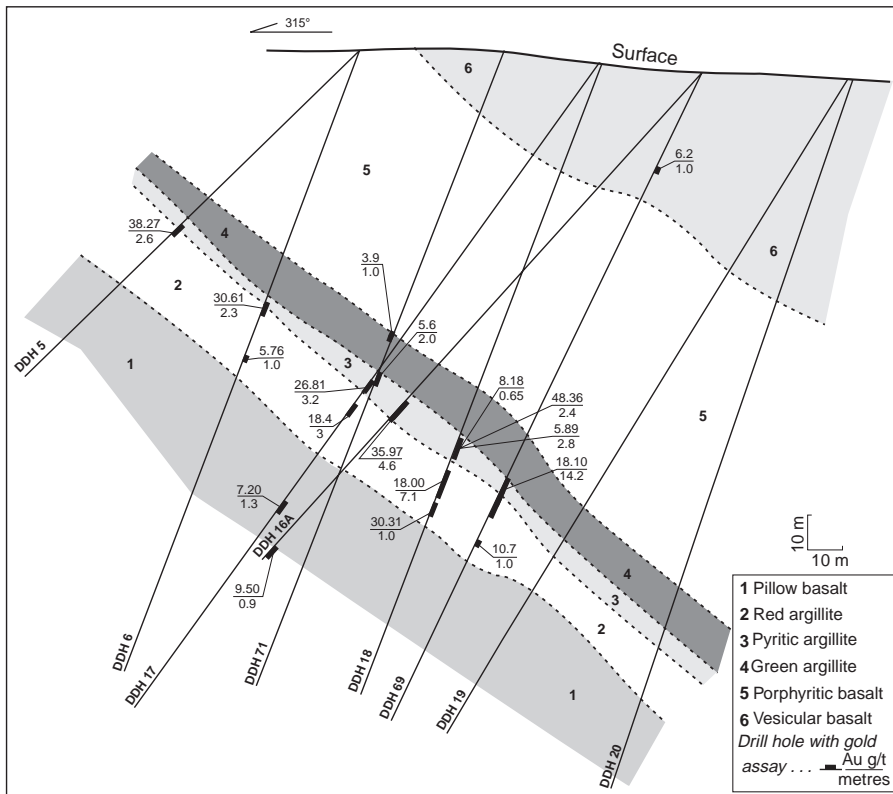


Figure 49. Geological drill and assay section, Nugget Pond gold mine.

Near the Nugget Pond mine, the Nugget Pond horizon is divisible into lower red and upper green clastic units. The red clastic unit is, in turn, divisible into a basal conglomerate, a lower magnetic unit, a middle brick red clastic unit, and an upper interlaminated brick red-green clastic unit transitional into the upper green clastic unit. The last commonly contains a basal, dark green sulphidic horizon that is overlain by a medium to light green finely laminated and graded turbiditic-tuffaceous sandstone and siltstone units.

### *Structural setting*

The Nugget Pond deposit lies in the basal sedimentary unit of the Scrape Point Formation at its intersection with a strong northeast-trending airphoto lineament which occurs in the footwall rocks but does not appear to extend very far into the hanging wall rocks. Tilting of bedding in the stratigraphically lower fault block, and the decrease in offset upwards, implies that this lineament is a syndepositional growth fault. The interpreted fault has recently been found in underground mine workings. Detailed structural geology has not been done in the deposit area, but a cursory examination at an early stage of the underground development indicates that the deposit is genetically related to an extensional array of hydrothermal quartz-albite-carbonate-pyrite veins within the metasedimentary rocks.

### *Hydrothermal pegmatite veins, mineralization, and alteration*

The mineralization and alteration at Nugget Pond are co-extensive with the network of quartz-albite-carbonate pyrite veins that cut the sedimentary rocks. The vein-pegmatite textures are variable and can be divided into two principle types of occurrence, veins with sharp to locally diffuse contacts (volumes of rock with irregular impregnation of pegmatitic material), and irregular patches of massive pegmatite.

The extensional vein array is composed of quartz+albite+carbonate  $\pm$  pyrite veins that strike parallel to the deposit with shallow to moderate dips to the south. They range from 1 m to about 5 m in dip dimension and vary in thickness from a few centimetres to 25 cm. The altered host rock commonly contains 25%, or even 50% of randomly disseminated, 1–10 cm clots of pegmatite that are compositionally similar to the veins. Where this material is abundant, it may coalesce into irregular pods of massive, carbonate-rich pegmatite, some of which are very auriferous. A single age determination on a single grain of xenotime from the pegmatite veins (R. Parrish and A. Sangster, unpub. data, 1995) gave a Devonian age of  $374 \pm 8$  Ma.

Metallic mineralization in the Nugget Pond gold deposit is dominantly pyrite with very subordinate chalcopyrite, galena, Ag-telluride, and native silver. The pyrite is commonly coarse grained and cubic with average grain size in the range from 0.5 cm to 2.0 cm; although cubic pyrite up to 10 cm has been observed. The pyrite may overgrow pre-existing pyrite within ores hosted by the lower green sedimentary unit and commonly overgrows magnetite in both the lower green unit and the red unit. The amount of magnetite in

pyritic rocks of the ore zones is less than is seen in unmineralized rocks indicating that much of the pyrite may have grown by sulphidation of magnetite. Pyrite is abundant in the quartz+albite+carbonate veins associated with the deposit. Pyrite also occurs in narrow quartz+albite+carbonate veins located stratigraphically below or above the deposit, in the lower basalt and overlying green turbidite and basaltic lavas respectively.

Free grains of native gold fill fractures in pyrite, coat pyrite grains, or occur as small irregular-shaped grains within stilpnomelane-rich altered rock. Some spherical gold inclusions are present within pyrite. The only spectacular gold-bearing samples have come from the coarse carbonate veins. Accessory minerals include ubiquitous but minor (<0.1%) chalcopyrite, and rare galena, occurring mainly as small inclusions in pyrite and as aggregates of coarser grains in the carbonate phase of the hydrothermal quartz+albite+carbonate veins. Silver is contained within native gold (5–15% Ag), as less than 5  $\mu$ m sized grains of an Ag-telluride that occurs as inclusions in pyrite, or as rare grains of native silver.

The primary alteration mineral at Nugget Pond is stilpnomelane (an Fe-rich brittle mica), which developed in preference to biotite because of the iron-rich character of the host rocks. The major alteration is in the sedimentary rocks and varies from weak where most sedimentary features are preserved to strong where the rock is composed almost exclusively of stilpnomelane and pyrite and all vestiges of sedimentary layering and colour have been destroyed. Initial indications of alteration on the fringes of the orebody consist of bleaching of the red and green argillite and the appearance of a 'spotted' texture due to the presence of rosettes of stilpnomelane. These are often restricted to particular sedimentary layers on the centimetre scale. With increasing alteration, the assemblage stilpnomelane, calcite, ilmenite, titanite, and pyrite $\pm$ rutile predominates. Biotite is present in minor amounts in the fringes of the alteration zone and is overgrown by stilpnomelane. In areas of most intense alteration, massive stilpnomelane is intimately associated with the hydrothermal pegmatite veins and itself forms veins which cut the sedimentary lithologies. In these areas the stilpnomelane is accompanied by albite  $\pm$  quartz.

In the footwall basalt, alteration is locally present but is generally much less extensive than in the sedimentary rocks. The principal alteration mineral is biotite, which overgrows the regional incipient chlorite alteration. In areas where increased alteration is present, the assemblage stilpnomelane, albite, calcite, quartz, and pyrite is observed with the stilpnomelane overgrowing the earlier biotite.

### **Long Pond East occurrence**

This occurrence is at the east end of Long Pond (Fig. 5) and is hosted by a wedge of green and red siltstone and sandstone units associated with banded hematite-magnetite iron-formation. On the shore of Long Pond, the clastic sedimentary rocks and iron-formation dip shallowly to the north under the adjacent gabbro, which is probably in fault contact. Low gold

values are associated with fine- to medium-grained irregular pyrite disseminations in the green siltstone (Table 6). Red siltstone is minor and occurs as irregularly shaped areas that are cut by reduction veins that carry pyrite. Exploration a number of years ago (P. Bradley, pers. comm., 1995) is reported to have encountered gold assays greater than one ounce per ton in small quartz veins. About 50 m to the east, beside the access road from Tilt Cove to Long Pond, similar auriferous green pyritic siltstone occurs in a small cliff face north of the road. Trenching and drilling has shown that the area immediately south of the occurrence is underlain by white talc-carbonate rock that is in part pyritic with gold contents of about 1 g/t (Table 6). Minor gold values are also present in hematite-magnetite iron-formation on a small island in the east end of Long Pond.

### **Castle Rock occurrence**

This occurrence is found on a north-facing slope south of a small pond about 500 m east of the Long Pond occurrence (Fig. 6); and is hosted by similar rocks. Numerous faults intersect in this locality. The gold (Table 6) is associated with 1 cm pyrite cubes in red siltstone that occur as fragments and screens within a complex talc+carbonate breccia. Associated fragments of pyritic green siltstone and hematite-magnetite iron-formation are not auriferous. The metasedimentary rocks and talc+carbonate breccia are in turn cut by quartz-feldspar porphyry dykes on three sides; and is probably in contact with basalt breccia on the fourth side.

### **Talc-carbonate schist-hosted occurrences from the base of the ophiolite**

The lower talc-carbonate-serpentinite schist unit of the Betts Cove ophiolite is in structural contact over much of its length with felsic tuffs of the Cape St. John Group (Fig. 2; Tremblay et al., 1997). The talc-carbonate rocks are intensely deformed and the felsic tuffs may or may not contain a strong foliation (Tremblay et al., 1997). Both the rocks of the Cape St. John Group and the talc-carbonate rocks host several types of small gold occurrences, many of which have been broadly grouped as listwaenite type (Beischer, 1988; Al, 1990; Lavigne, 1993).

### **Disseminated pyrite-quartz vein occurrences**

Several of the occurrences (Boneyard, Melange, Snooks Arm road; Fig. 5) consist of minor accumulations of pyrite in or on the borders of irregular extension quartz veins in rocks of the Cape St. John Group. The veins are generally perpendicular to the contact and in at least one case are associated with minor chloritic alteration. Gold values are low and generally restricted to samples representing a small volume of rock (Beischer, 1988). At the Boneyard occurrence a single heavy mineral concentrate in till gave a value of 79 700 ppb was obtained from talus but surface sampling and drilling gave only isolated values of a few hundred to a few thousand parts per billion (Beischer, 1988).

### **Hematite-quartz vein occurrences**

A second class of occurrence (Tom, George, George extension, and Long Pond West; Fig. 5) is similar to the pyritic occurrences described above except that minor irregular gold values are associated with quartz veins containing specular hematite (Beischer, 1988). Perhaps the most impressive is the Long Pond West occurrence, where a granular hematite-magnetite iron-formation hosts irregular 1–10 cm quartz veins that contain pockets of specular hematite that assay as much as 5000 ppb Au.

### **Carbonate-hosted occurrences**

Beischer (1988) describes the presence of anomalous gold associated with an area of massive carbonate replacement and quartz veining on the north side of Long Pond just west of the narrows at the west end of Long Pond (Fig. 5). The carbonate is very fine grained, mainly red mottled locally with green, veined by 1–5 cm quartz veins, and locally containing fuchsite. The gold anomalous samples (to 2800 ppb Au, Beischer, 1988) were collected beside the north boundary fault of the ophiolite. The remainder of the alteration is largely barren.

### **Talc-carbonate-hosted occurrences**

Numerous isolated occurrences of geochemically anomalous gold have been found throughout the talc-carbonate. Lavigne (1993) found erratic low-Au values in the tens to hundreds of parts per million in an area near Betts Big Pond (Fig. 7) where drilling had encountered values of several hundreds of parts per million (Beischer, 1988). Samples of talc-carbonate anomalous in gold are otherwise indistinguishable from the sterile rocks of the same type. At Arrowhead Pond (in the talc-carbonate schist, immediately west of the area at the edge of Fig. 5), the talc-carbonate schist is intruded by small quartz veins with associated chalcopyrite and gold (Table 6).

### **Origin of the gold mineralization**

All of the minor gold occurrences associated with the lower peridotite unit and the Nugget Pond horizon are associated with altered peridotite-derived talc-carbonate schist. Most of these occurrences are small and are local litho-geochemical anomalies associated with talc-carbonate or quartz veins in adjacent Cape St. John felsic pyroclastic rocks. Al (1990) and Lavigne (1993) have studied these rocks in detail and attribute the origin of the gold (Listwaenite model) to the alteration event that produced the talc-carbonate alteration of the peridotite.

The Nugget Pond horizon lies at least 1 km stratigraphically above the peridotite yet even at this stratigraphic level there is ample evidence that fluids involved in the alteration of the peridotite were involved. For example, talc-carbonate veins and vein breccia up to 25 m thick can be seen on the south shore at Long Pond and in the West mine area at Tilt Cove, where they cut Silurian quartz-feldspar porphyry dykes. Talc-carbonate rocks are also associated with the Castle Rock and Long Pond gold occurrences, and at Long Pond the



talc-rich rocks are mineralized. The association of gold with talc-carbonate suggests that these occurrences also formed from fluids involved in the alteration of peridotitic rocks.

There has as yet been no talc-carbonate recognized at the Nugget Pond deposit. Lavigne and others (J. Lavigne, S. Douma, and A.L. Sangster, unpub. report, 1994) studied the deposit in detail and attributed the mineralization to the presence of auriferous hydrothermal quartz-albite-K-feldspar-carbonate-pyrite veins intersecting the Nugget Pond horizon stratigraphy, and producing the disseminated auriferous pyrite body by a simple mechanism involving sulphidation of magnetite in the magnetite-rich strata of the sedimentary sequence. The fluids, however, are of granitic character and the granitic veins have been dated as Devonian. There are no known Devonian granitic intrusions cutting the Betts Cove ophiolite; however, there is evidence that there was active tectonism in the area during the Devonian (Tremblay et al., 1997) and it is probable that a major fluid flow event occurred at that time, altering the peridotite and providing materials for formation of the Nugget Pond deposit. Lavigne and others (J. Lavigne, S. Douma, and A.L. Sangster, unpub. report, 1994) pointed out the existence of a very strong northwest-striking photolinear intersection in the footwall rocks to the deposit. We concur with their interpretation of this linear as a synvolcanic fault. Lavigne and co-workers (J. Lavigne, S. Douma, and A.L. Sangster, unpub. report, 1994) proposed that this early fault was reactivated during the Devonian as the conduit for the mineralizing fluids.

## CONCLUSIONS

The Betts Cove ophiolite records the initiation of seafloor spreading in a fore-arc marginal basin, since all of the sheeted dyke complex, the lower lavas (the Betts Head Formation), and most cumulate rocks have boninitic affinities. Synmagmatic extensional faults dissect the stratigraphy into horst-and-graben structures, and localized hydrothermal flow leading to sulphide deposition. The Snooks Arm Group cover rocks are composed of the following three magma series: an arc tholeiite sequence (Mount Misery Formation), a series of evolved tholeiitic basalt (Scrape Point, Venam's Bight, and Round Harbour formations), and a calc-alkaline series (Scrape Point Formation tuffaceous sedimentary rocks, Bobby Cove and Balsam Bud Cove formations). The magnetite in basal ironstones of the Scrape Point Formation is not detrital, and records volcanogenic exhalations. The associated tuffaceous sandstone units also have calc-alkaline bulk chemistries, and are probably distal facies of the paroxysmal eruption event represented by the lower member of the Bobby Cove Formation. The volcanoclastic debrite and turbidite units of The Balsam Bud Cove Formation were derived from erosion of basaltic lavas similar to the underlying Venam's Bight Formation. During obduction onto North America, the ophiolite and its cover rocks were thrust above a talc-serpentinite unit. In the Silurian, granitoid batholiths (Burlington and Cape Brulé) formed the root zone of a caldera complex, with felsic pyroclastic rocks of the Cape St. John Group representing its effusive member. The Silurian Cape St. John Group deposited unconformably over the

ophiolite. Quartz-feldspar-porphry dykes intruded the ophiolite along a system of active north- and east-dipping normal faults, and probably fed the felsic pyroclastic rocks of the Cape St. John Group. Subsequently, the entire package was thrust towards the southeast and refolded in the Acadian Orogeny.

## REFERENCES

- Al, T.A.**  
1990: The character and setting of gold mineralization associated with the Betts Cove Ophiolite; M.Sc. thesis, Memorial University of Newfoundland, St. John's, Newfoundland, 151 p.
- Arculus, R.J.**  
1994: Aspects of magma genesis in arcs; *Lithos*, v. 33, p. 189–208.
- Beccaluva, L., Macciotta, G., Piccardo, G.B., and Zeda, O.**  
1989: Clinopyroxene compositions of ophiolite basalts as petrogenetic indicator; *Chemical Geology*, v. 77, p. 165–182.
- Bédard, J.H.**  
1986: Pre-Acadian magmatic suites of the southeastern Gaspé Peninsula; *Bulletin of the Geological Society of America*, v. 97, p. 1177–1191.  
1994: A procedure for calculating the equilibrium distribution of trace elements in the minerals of cumulate rocks, and the concentration of trace elements in the coexisting liquids; *Chemical Geology*, v. 118, p. 143–153.  
1999: Petrogenesis of boninites from the Betts Cove ophiolite, Newfoundland, Canada: identification of subducted source components; *Journal of Petrology*, Oxford University Press, v. 40, no. 12, p. 1853–1889.
- Bédard, J.H. and Hébert, R.**  
1996: The lower crust of the Bay of Islands ophiolite, Canada: petrology, mineralogy, and the importance of syntaxis in magmatic differentiation in ophiolites and at ocean ridges; *Journal of Geophysical Research*, v. 101, p. 25 105–25 124.
- Bédard, J.H. and Wilson, C.**  
1997: Fractionation and contamination of Maquereau Group lavas, southern Gaspé, Québec Appalachians; in *The Nature of Magmatism in the Appalachian Orogen*, (ed.) A.K. Sinha, J.B. Whalen, and J.P. Hogan; Geological Society of America, Memoir 191, p. 87–106.
- Bédard, J.H., Lauzière, K., Boisvert, É., Deblonde, C., Sangster, A., Tremblay, A., and Dec, T.**  
in press: Betts Cove geological dataset for GIS applications; Geological Survey of Canada, Open File D3623.
- Bédard, J.H., Lauzière, K., Boisvert, É., Sangster, A., Tellier, M., Tremblay, A., and Dec, T.**  
1999: Geological map of the Betts Cove ophiolitic massif and its cover rocks; Geological Survey of Canada, Map 1969A, scale 1:20 000.
- Bédard, J.H., Lauzière, K., Tremblay, A., Sangster, A., and Tellier, M.**  
1998: Evidence from Betts Cove ophiolite boninites for forearc seafloor-spreading; *Tectonophysics*, v. 284, p. 233–245.
- Beischer, G.**  
1988: Report on geological, geochemical, and geophysical surveys, Betts Cove project, May to November, 1987; unpublished company report, Newfoundland Department of Mines and Energy, Assessment File # 2E/13, p. 1–54.
- Beischer, G.A., Averill, S., Golightly, P., and Grant, R.W.**  
1988: Assessment report on geological, geochemical and geophysical exploration for the Betts Cove project for licence 1930e on claim block 1163, licence 2608 on claim blocks 3569 and 3574, licence 2609 on claim block 3573 and licence 2747 on claim blocks 3553-3554 in the Long Pond and Red Cliff Pond areas on the Baie Verte Peninsula, north-central Newfoundland; 4 reports, (Inco Gold Company; Consolidated Rambler Mines Limited; Overburden Drilling Management Limited; Maritec Limited; Eastern Geophysics Limited; Canadian Nickel Company Limited; Eastern Newfoundland Limited; Activation Laboratories Limited), Newfoundland and Labrador Geological Survey File 002E/13/0584, 465 p.
- Brenan, J.M., Shaw, H.F., and Ryerson, F.J.**  
1995: Experimental evidence for the origin of lead enrichment in convergent margin magmas; *Nature*, v. 378, p. 54–56.

- Cameron, W.E., Nisbet, E.G., and Dietrich, V.J.**  
1979: Boninites, komatiites and ophiolitic basalts; *Nature*, v. 280, p. 550–553.
- Cawood, P.A. and Dunning, G.R.**  
1993: Silurian age for movement on the Baie Verte line: implications for accretionary tectonics in the Northern Appalachians; *Geological Society of America, Abstracts with Programs*, v. 25, p. A422.
- Cawood, P.A. and Suhr, G.**  
1992: Generation and obduction of ophiolites: constraints from the Bay of Islands Complex, western Newfoundland; *Tectonics*, v. 11, p. 884–897.
- Cawood, P.A., Dunning, G.R., Lux, D., and Van Gool, J.A.M.**  
1994: Timing of peak metamorphism and deformation along the Appalachian margin of Laurentia in Newfoundland - Silurian, not Ordovician; *Geology*, v. 22, p. 399–402.
- Cawood, P.A., van Gool, J.A.M., and Dunning, G.R.**  
1995: Collisional tectonics along the Laurentian Margin of the Newfoundland Appalachians; *in Current Perspectives in the Appalachian-Caledonian Orogen*, (ed.) J.P. Hibbard, C.R. van Staal, and P.A. Cawood; *Geological Association of Canada, Special Paper 41*, p. 283–301.
- Church, W.R.**  
1977: The ophiolites of southern Québec: oceanic crust of Betts Cove type; *Canadian Journal of Earth Sciences*, v. 14, p. 1668–1673.  
1979: 'The ophiolites of southern Québec: oceanic crust of Betts Cove type' Reply to Upadhyay (1979); *Canadian Journal of Earth Sciences*, v. 16, p. 1306–1308.
- Church, W.R. and Riccio, L.**  
1974: The sheeted dike layer of the Betts Cove ophiolite does not represent spreading; *Discussion, Canadian Journal of Earth Sciences*, v. 11, p. 1499–1502.
- Coish, R.A.**  
1977a: Petrology of the mafic units of West Newfoundland ophiolites; Ph.D. thesis, University of Western Ontario, London, Ontario, 227 p.  
1977b: Ocean floor metamorphism in the Betts Cove ophiolite, Newfoundland; *Contributions to Mineralogy and Petrology*, v. 60, p. 255–270.  
1989: Boninitic lavas in Appalachian ophiolites: a review; *in Boninites and Related Rocks*, (ed.) A.J. Crawford; Unwyn Hyman, London, United Kingdom, p. 264–287.
- Coish, R.A. and Church, W.R.**  
1979: Igneous geochemistry of mafic rocks in the Betts Cove ophiolite, Newfoundland; *Earth and Planetary Science Letters*, v. 70, p. 29–39.
- Coish, R.A., Hickey, R., and Frey, F.A.**  
1982: Rare earth element geochemistry of the Betts Cove ophiolite, Newfoundland: complexities in ophiolite formation; *Geochimica et Cosmochimica Acta*, v. 46, p. 2117–2134.
- Cousineau, P.A. and Bédard, J.H.**  
1998: Infilling of a fore-arc basin from multiple sources: the Bobby Cove Formation, Snooks Arm Group, Newfoundland; *Geological Association of Canada–Mineralogical Association of Canada Meeting, Program with Abstracts*, v. 23, p. A39–40.  
2000: Sedimentation in a subaqueous arc/backarc setting: the Bobby Cove Formation, Snooks Arm Group, Newfoundland; *Precambrian Research*; v. 101, no. 2–4, p. 111–134.
- Coyle, M.**  
1990: Geology, geochemistry and geochronology of the Springdale Group, an Early Silurian caldera in central Newfoundland: Ph.D. thesis, Memorial University of Newfoundland, St. John's, Newfoundland, 390 p.
- Crawford, A.J., Falloon, T.J., and Green, D.H.**  
1989: Classification, petrogenesis and tectonic setting of boninites; *in Boninites and Related Rocks*, (ed.) A.J. Crawford; Unwyn Hyman, London, United Kingdom, p. 1–49.
- Dallmeyer, R.D.**  
1977:  $^{40}\text{Ar}/^{39}\text{Ar}$  age spectra of minerals from the Fleur de Lys terrane in northwest Newfoundland: their bearing on chronology of metamorphism within the Appalachian orotectonic zone; *Journal of Geology*, v. 85, p. 89–103.
- Dallmeyer, R.D. and Hibbard, J.P.**  
1984: Geochronology of the Baie Verte Peninsula, Newfoundland: implications for the tectonic evolution of the Humber and Dunnage zones of the Appalachians orogen; *Journal of Geology*, v. 92, p. 489–512.
- Dallmeyer, R.D. and Williams, H.**  
1975:  $^{40}\text{Ar}/^{39}\text{Ar}$  ages from the Bay of Island metamorphic aureole: their bearing on the timing of Ordovician ophiolite obduction; *Canadian Journal of Earth Sciences*, v. 12, p. 1685–1690.
- Dean, P.L. and Strong, D.F.**  
1975: Geology of King's Point map-area, Newfoundland; *Geological Survey of Canada, Open File 380*, scale 1:63 360.
- DeGrace, J.R., Kean, B.F., Hsu, E., and Green, T.**  
1976: Geology of the Nippers Harbour map area (2E/13), Newfoundland; Newfoundland Department of Mines and Energy, Mineral Development Division, Report 76-3, 73 p.
- Dewey, J.F.**  
1969: Evolution of the Appalachian/Caledonian Orogen; *Nature*, v. 22, p. 124–129.
- Donoghue, H.G., Adams, W.S., and Harpur, C.E.**  
1959: Tilt Cove operations of the Maritimes Mining Corporation Limited; *Canadian Institute of Mining and Metallurgy Bulletin, Proceedings*, v. 52, no. 563, p. 150–169.
- Dunning, G.R. and Krogh, T.E.**  
1985: Geochronology of ophiolites of the Newfoundland Appalachians; *Canadian Journal of Earth Sciences*, v. 22, p. 1659–1670.
- Dunning, G.R., O'Brien, S.J., Colman-Sadd, S.P., Blackwood, R.F., Dickson, W.L., O'Neill, P.P., and Krogh, T.E.**  
1990: Silurian orogeny in the Newfoundland Appalachians; *Journal of Geology*, v. 98, p. 895–913.
- Falloon, T.J. and Crawford, A.J.**  
1991: The petrogenesis of high-calcium boninite lavas dredged from the northern Tonga ridge; *Earth and Planetary Science Letters*, v. 102, p. 375–394.
- Falloon, T.J., Green, D.H., and McCulloch, M.T.**  
1989: Petrogenesis of high-Mg and associated lavas from the north Tonga trench; *in Boninites and Related Rocks*, (ed.) A.J. Crawford; Unwyn Hyman, London, United Kingdom, p. 357–395.
- Galley, A. and Koski, R.**  
1999: Setting and characteristics of ophiolite-hosted volcanogenic massive sulfide deposits; *in Volcanic-associated Massive Sulfide Deposits*, (ed.) M.D. Hannington and C.T. Barrie; *Reviews in Economic Geology*, v. 10, p. 215–236.
- Gill, J.B.**  
1981: *Orogenic Andesites and Plate Tectonics*; Springer, New York, New York, 390 p.
- Goodwin, L.B. and Williams, P.F.**  
1996: Deformation path partitioning within a transpressive shear zone, Marble Cove, Newfoundland; *Journal of Structural Geology*, v. 18, p. 975–990.
- Hall, R.P., Hughes, D.J., and Friend, C.R.L.**  
1985: Geochemical evolution and unusual pyroxene chemistry of the MD tholeiite dyke swarm from the Archaean Craton of southern west Greenland; *Journal of Petrology*, v. 26, p. 253–282.
- Harris, N.B.W., Inger, S., and Xu Ronghua**  
1990: Cretaceous plutonism in Central Tibet: an example of post-collisional magmatism?; *Journal of Volcanology and Geothermal Research*, v. 44, p. 21–32.
- Harris, R.A.**  
1992: Peri-collisional extension and the formation of Oman-type ophiolites in the Banda arc and Brooks Range; *in Ophiolites and their Oceanic Analogues*, (ed.) L.M. Parson, B.J. Murton, and P. Browning; *Geological Society of London, Special Volume 60*, p. 301–325.
- Hawkins, J.W., Bloomer, S.H., Evans, C.A., and Melchior, J.T.**  
1984: Evolution of intra-oceanic arc-trench system; *Tectonophysics*, v. 102, p. 175–205.
- Herzig, P.M. and Hannington, M.D.**  
1995: Polymetallic massive sulfides at the modern seafloor; a review; *Ore Geology Reviews*, v. 10, p. 95–115.
- Hibbard, J.P.**  
1982: Significance of the Baie Verte Flexure, Newfoundland; *Geological Society of America Bulletin*, v. 93, p. 790–797.  
1983: Geology of the Baie Verte Peninsula, Newfoundland; Newfoundland Department of Mines and Energy, Memoir 2, 279 p.
- Hibbard, J.P., St-Julien, P., and Trzcienski, W.E., Jr.**  
1995: Humber zone internal; *in Chapter 3 of Geology of the Appalachian/Caledonian Orogen in Canada and Greenland*, (co-ord.) H. Williams; *Geological Survey of Canada, Geology of Canada*, no. 6, p. 114–139 (*also* *Geological Society of America, The Geology of North America*, v. F-1).

- Hickey, R.L. and Frey, F.A.**  
1982: Geochemical characteristics of boninite-series volcanics: implications for their source; *Geochimica et Cosmochimica Acta*, v. 46, p. 2099–2115.
- Hooper, P.R. and Hawkesworth, C.J.**  
1993: Isotopic and geochemical constraints on the origin and evolution of the Columbia River basalt; *Journal of Petrology*, v. 34, p. 1203–1246.
- Hudson, K.A.**  
1988: Gold and base metal mineralization in the Nippers harbour ophiolite, Newfoundland; M.Sc. thesis, Memorial University of Newfoundland, St. John's, Newfoundland, 305 p.
- Hurley, T.D.**  
1982: Metallogeny of a volcanogenic gold deposit, Cape St.-John Group, Tilt Cove, Newfoundland; M.Sc. thesis, McMaster University, Hamilton, Ontario, 69 p.
- Hurley, T.D. and Crocket, J.H.**  
1985: A gold-sphalerite association in a volcanogenic base-metal-sulphide deposit near Tilt Cove, Newfoundland; *Canadian Mineralogist*, v. 23, p. 423–430.
- Inger, S.**  
1994: Magmagenesis associated with extension in orogenic belts: examples from the Himalaya and Tibet; *Tectonophysics*, v. 238, p. 183–197.
- Innocent, C., Briquieu, L., and Cabanis, B.**  
1994: Sr-Nd isotope and trace-element geochemistry of late Variscan volcanism in the Pyrenees: magmatism in post-orogenic extension?; *Tectonophysics*, v. 238, p. 161–181.
- Irvine, T.N. and Baragar, W.R.A.**  
1971: A guide to the chemical classification of the common volcanic rocks; *Canadian Journal of Earth Sciences*, v. 8, p. 523–548.
- Jamieson, R.A. and O'Bierne-Ryan, A.M.**  
1991: Decompression-induced growth of albite porphyroblasts, Fleur de Lys Supergroup, western Newfoundland; *Journal of Metamorphic Geology*, v. 9, p. 433–439.
- Jamieson, R.A., Sanderson, S.D., McDonald, L., and Goodwin, L.B.**  
1993: Silurian extension along the Humber-Dunnage boundary zone, Baie Verte Peninsula, Newfoundland; in *Late Orogenic Extension in Mountains Belts*, (ed.) M. Seranne and J. Malavieille; Abstract Volume, Bureau de Recherche en Géologie Minière, no. 219, p. 102.
- Jenner, G.A.**  
1977: Geochemistry of the Upper Snooks Arm Group, Newfoundland; M.Sc. thesis, University of Western Ontario, London, Ontario, 134 p.  
1981: Geochemistry of high-Mg andesites from Cape Vogel, Papua New Guinea; *Chemical Geology*, v. 33, p. 307–332.
- Jenner, G.A. and Fryer, B.J.**  
1980: Geochemistry of the upper Snooks Arm Group basalts, Burlington Peninsula, Newfoundland: evidence against formation in an island arc; *Canadian Journal of Earth Sciences*, v. 17, p. 888–900.
- Keppler, H.**  
1996: Constraints from partitioning experiments on the composition of subduction-zone fluids; *Nature*, v. 380, p. 237–240.
- Kerr, A.**  
1997: Space-time composition relationships among Appalachian-cycle plutonic suites in Newfoundland; in *The Nature of Magmatism in the Appalachian Orogen*, (ed.) A.K. Sinha, J.B. Whalen, and J.P. Hogan; Geological Society of America, Memoir 191, p. 193–220.
- Kessler, L.G., II and Bédard, J.H.**  
1998: Epiclastic volcanic debrites - evidence of flow transformations between avalanche and debris flow processes, middle Ordovician, Baie Verte Peninsula, Newfoundland; Geological Association of Canada–Mineralogical Association of Canada Meeting, Program with Abstracts, v. 23, p. A91.  
2000: Epiclastic volcanic debrites – evidence of flow transformations between avalanche and debris flow processes, Middle Ordovician, Baie Verte Peninsula, Newfoundland; *Precambrian Research*; v. 101, no. 2–4, p. 135–161.
- Kostopoulos, D.K. and Murton, B.J.**  
1992: Origin and distribution of components in boninite genesis: significance of the OIB component; in *Ophiolites and Their Modern Oceanic Analogues*, (ed.) L.M. Murton and P. Browning; Geological Society of London, Special Publication 60, p. 133–154.
- Lafliche, M.R., Camiré, G., and Jenner, G.A.**  
1998: Geochemistry of post-Acadian, Carboniferous continental intraplate basalts from the Maritimes Basin, Magdalen Islands, Québec, Canada; *Chemical Geology*, v. 148, p. 115–136.
- Large, R.R.**  
1992: Australian volcanic-hosted massive sulfide deposits; features, styles, and genetic models; *Economic Geology*, v. 87, p. 471–510.
- Lavigne, J.**  
1993: The geology and geochemistry of gold mineralization in the Betts Big Pond area, Newfoundland; M.Sc. thesis, University of Ottawa, Ottawa, Ontario, 216 p.
- Mattinson, J.M.**  
1975: Early Paleozoic ophiolite complexes of Newfoundland: isotopic ages of zircons; *Geology*, v. 3, p. 181–183.
- Miyashiro, A.**  
1973: The Troodos ophiolitic complex was probably formed in an island arc; *Earth and Planetary Science Letters*, v. 19, p. 218–224.
- Mullen, E.D.**  
1983: MnO/TiO<sub>2</sub>/P<sub>2</sub>O<sub>5</sub>: a minor element discriminant for basaltic rocks of oceanic environments and its implications for petrogenesis; *Earth and Planetary Science Letters*, v. 62, p. 53–62.
- Neale, E.R.W., Kean, B.F., and Upadhyay, H.D.**  
1975: Post-ophiolite unconformity, Tilt Cove-Betts Cove area, Newfoundland; *Canadian Journal of Earth Sciences*, v. 12, p. 880–886.
- Papezik, V.S.**  
1964: Nickel minerals at Tilt Cove, Notre Dame bay, Newfoundland; Geological Association of Canada, Proceedings, v. 15, pt. 2, p. 27–32.
- Pearce, J.A.**  
1975: Basalt geochemistry used to investigate past tectonic environments on Cyprus; *Tectonophysics*, v. 25, p. 41–67.
- Pearce, J.A. and Cann, J.R.**  
1973: Tectonic setting of basic volcanic rocks determined using trace element analyses; *Earth and Planetary Science Letters*, v. 19, p. 290–300.
- Pearce, J.A. and Norry, M.J.**  
1979: Petrogenetic implications of Ti, Zr, Y, and Nb variations in volcanic rocks; *Contributions to Mineralogy and Petrology*, v. 69, p. 33–47.
- Pearce, J.A. and Peate, D.W.**  
1995: Tectonic implications of the composition of volcanic arc magmas; *Annual Review of Earth and Planetary Sciences*, v. 23, p. 251–285.
- Pearce, J.A., Harris, N.B.W., and Tindle, A.G.**  
1984: Trace element discrimination diagrams for the tectonic interpretation of granitic rocks; *Journal of Petrology*, v. 25, p. 956–983.
- Pinet, N. and Tremblay, A.**  
1995: Is the Taconian Orogeny of southern Quebec the result of the Oman-type obduction?; *Geology*, v. 23, p. 121–124.
- Pringle, J.**  
1978: Rb-Sr ages of silicic igneous rocks and deformation, Burlington Peninsula, Newfoundland; *Canadian Journal of Earth Sciences*, v. 15, p. 293–300.
- Reston, T.J., Ruoff, O., McBride, J.H., Ranero, C.R., and White, R.S.**  
1996: Detachment and steep normal faulting in Atlantic oceanic crust west of Africa; *Geology*, v. 24, p. 811–814.
- Riccio, L.M.**  
1972: The Betts Cove ophiolite, Newfoundland; M.Sc. thesis, University of Western Ontario, London, Ontario, 91 p.
- Sangster, A.L., Lauzière, K., and Bédard, J.H.**  
1995: Mineral deposit studies in the Betts Cove ophiolite; in *Report of Activities 1995*; Newfoundland Department of Mines, p. 20–21.
- Sangster, A.L., Lavigne, J.G., Douma, S., and Hamilton, W.**  
1994: Geology, alteration and stable-isotope geochemistry of the Nugget Pond gold deposit; in *Report of Activities 1994*; Newfoundland Department of Mines, p. 34–37.
- Santaguida, F. and Hannington, M.D.**  
1996: Characteristics of gold mineralization in volcanogenic massive sulphide deposits of the Notre Dame Bay area, central Newfoundland; *Canadian Journal of Earth Sciences*, v. 33, p. 316–334.
- Saunders, C.M.**  
1985: Controls of mineralization in the Betts Cove ophiolite; M.Sc. thesis, Memorial University of Newfoundland, St. John's, Newfoundland, 200 p.

- 1990: A field guide to mineralization in the Betts Cove area; *in* Metallogenic Framework of Base and Precious Metal Deposits, Central and Western Newfoundland – Field Trip Guide, (ed.) H.S. Swinden, D.T.W. Evans, and B.F. Keen; Geological Survey of Canada, Open File 2156, p. 194–200.
- Saunders, C.M. and Strong, D.F.**  
1986: Alteration-zonation related to variations in water/rock ratio at the Betts Cove ophiolitic massive sulphide deposit, Newfoundland, Canada; *in* Metallogeny of Basic and Ultrabasic Rocks, (ed.) M.J. Gallagher, R.A. Ixer, G.R. Neary, and H.M. Prichard; London Institute of Mining Metallurgy, Conference Proceedings, p. 161–175.  
1988: Geological setting of mineralization at Tilt Cove, Betts Cove Ophiolite, Newfoundland; *in* The Volcanogenic Sulphide Districts of Central Newfoundland, (ed.) H.S. Swinden and B.F. Keen; Guidebook and Reference Manual, Mineral Deposits Division, Geological Association of Canada, p. 54–61.
- Schröeter, T.G.**  
1971: Geology of the Nippers Harbour area, Newfoundland; M.Sc. thesis, University of Western Ontario, London, Ontario, 88 p.
- Shervais, J.W.**  
1982: Ti-V plots and the petrogenesis of modern and ophiolitic lavas; *Earth and Planetary Science Letters*, v. 59, p. 101–118.
- Snelgrove, A.K.**  
1931: Geology and ore deposits of Betts Cove - Tilt Cove area, Notre Dame Bay, Newfoundland; *Canadian Mining and Metallurgical Bulletin*, v. XXIV (225–236), p. 478–519.
- Sobolev, A.V. and Danyushevsky, L.V.**  
1994: Petrology and geochemistry of boninites from the north termination of the Tonga trench: constraints on the generation conditions of primary high-Ca boninite magmas; *Journal of Petrology*, v. 35, p. 1183–1211.
- Squires, G.C.**  
1981: The distribution and genesis of the Tilt Cove sulphide deposits; B.Sc. thesis, Memorial University of Newfoundland, St. John's, Newfoundland, 115 p.
- Stanley, R.C. and Ratcliffe, N.M.**  
1985: Tectonic synthesis of the Taconian orogeny in western New England; *Geological Society of America Bulletin*, v. 96, p. 1227–1250.
- Stevens, R.K.**  
1970: Cambro-Ordovician flysch sedimentation and tectonics in west Newfoundland and their possible bearing on a proto-Atlantic ocean; *in* Flysch Sedimentation, (ed.) J. Lajoie; Geological Association of Canada, Special Paper 7, p. 165–177.
- Strong, D.F.**  
1984: Geological relationships of alteration and mineralization at Tilt Cove, Newfoundland; Newfoundland Department of Mines and Energy, Report 84-3, p. 81–90.
- Strong, D.F. and Coyle, M.**  
1987: Evolution of Taconic to Variscan fault styles and associated Acadian magmatism in west Newfoundland, with implications for driving mechanisms; *Geological Society of America, Abstracts with Programs*, v. 21, p. 69–70.
- Strong, D.F. and Saunders, C.M.**  
1988: Ophiolite sulphide mineralization at Tilt Cove, Newfoundland; controls by upper mantle and crustal processes; *Economic Geology*, v. 83, p. 239–255.
- Sun, S.-S. and McDonough, W.F.**  
1989: Chemical and isotopic systematics of oceanic basalts: implications for mantle compositions and processes; *in* Magmatism in the Ocean Basins, (ed.) A.D. Saunders and M.J. Norry; Geological Society of London, Special Publication 42, p. 313–345.
- Swinden, H.S., Jenner, G.A., Kean, B.F., and Evans, D.T.W.**  
1989: Volcanic rock geochemistry as a guide for massive sulphide exploration in central Newfoundland; *in* Current Research; Newfoundland Department of Mines and Energy, v. 89-1, p. 201–219.
- Swinden, H.S., Jenner, G.A., and Szybinski, Z.A.**  
1997: Magmatic and tectonic evolution of the Cambrian-Ordovician Laurentian margin of Iapetus: geochemical and isotopic constraints from the Notre Dame subzone, Newfoundland; *in* The Nature of Magmatism in the Appalachian Orogen, (ed.) A.K. Sinha, J.B. Whalen, and J.P. Hogan; Geological Society of America, Memoir 191, p. 337–364.
- Swinden, S., McBride, D.M., and Dubé, B.**  
1990: Preliminary geological and mineralogical notes on the Nugget Pond Gold Deposit, Baie Verte Peninsula, Newfoundland; *in* Current Research; Newfoundland Department Of Mines and Energy, Geological Survey Branch, Report 90-1, p. 201–215.
- Tatsumi, Y.**  
1989: Migration of fluid phases and genesis of basaltic magmas in subduction zones; *Journal of Geophysical Research*, v. 94, p. 4697–4707.
- Taylor, R.N., Nesbitt, R.W., Vidal, P., Harmon, R.S., Auvray, B., and Croudace, I.W.**  
1994: Mineralogy, chemistry, and genesis of the boninite series volcanics, Chichijima, Bonin Islands, Japan; *Journal of Petrology*, v. 35, p. 577–617.
- Thompson, R.N., Morrison, M.A., Hendry, G.L., and Parry, S.J.**  
1984: An assessment of the relative roles of crust and mantle in magma genesis: an elemental approach; *Philosophical Transactions of the Royal Society of London, Series A*, v. 310, p. 549–590.
- Tremblay, A., Bédard, J.H., and Lauzière, K.**  
1997: Structural history of the Betts Cove complex and cover rocks, Canadian Appalachians: from obduction to exhumation and folding of an Ordovician oceanic crust; *Journal of Geology*, v. 105, p. 701–716.
- Upadhyay, H.D.**  
1973: The Betts Cove ophiolite and related rocks of the Snooks Arm Group, Newfoundland; Ph.D. thesis, Memorial University of Newfoundland, St. John's, Newfoundland, 224 p.  
1979: 'The ophiolites of southern Québec: oceanic crust of Betts Cove type' Comment on Church (1977); *Canadian Journal of Earth Sciences*, v. 16, p. 1302–1306.  
1980: Ordovician komatiites and associated boninite-type magnesian lavas from Betts Cove, Newfoundland; *in* Komatiites, (ed.) N.T. Arndt and E.G. Nisbet; George Allen and Unwin, London, United Kingdom, p. 187–198.
- Upadhyay, H.D. and Strong, D.F.**  
1973: Geological setting of the Betts Cove copper deposits, Newfoundland: an example of ophiolite sulfide mineralization; *Economic Geology*, v. 68, p. 161–167.
- Varfalvy, V., Hébert, R., Bédard, J.H., and Lafèche, M.R.**  
1997: Occurrence of primitive boninitic intrusive magmas in upper mantle rocks of the North Arm Mountain massif, Bay of Islands, Newfoundland, Canada: evidence for an arc environment; *Canadian Mineralogist*, v. 35, p. 543–570.
- Weaver, J.S. and Langmuir, C.**  
1980: Calculation of phase equilibrium in mineral-melt systems; *Computers and Geosciences*, v. 16, p. 1–19.
- Williams, H.**  
1979: The Appalachian orogen in Canada; *Canadian Journal of Earth Sciences*, v. 16, p. 792–807.
- Williams, H., Colman-Sadd, S.P., and Swinden, H.S.**  
1988: Tectonostratigraphic subdivisions of Central Newfoundland; *in* Current Research, Part B; Geological Survey of Canada, Paper 88-1B, p. 91–98.
- Williams, S.H.**  
1992: Lower Ordovician (Arenig - Llanvirn) graptolites from the Notre Dame Subzone, central Newfoundland; *Canadian Journal of Earth Sciences*, v. 29, p. 1717–1733.

